Identification of Molecular Mechanisms Mediating TWIST-1 Regulation of Mesenchymal Stem Cell Proliferation and Differentiation

Chee Ho H'ng, B.Sc (Hons.)

Student ID: a1612377

Mesenchymal Stem Cell Group

South Australian Health & Medical Research Institute (SAHMRI)

&

The Discipline of Physiology

Adelaide Medical School

Faculty of Health Science

University of Adelaide

A thesis submitted to the University of Adelaide

For the degree of Doctor of Philosophy

September 2019

Table of Contents

DECLARATION

I certify that this work contains no material which has been accepted for the award of any other degree or diploma in my name, in any university or other tertiary institution and, to the best of my knowledge and belief, contains no material previously published or written by another person, except where due reference has been made in the text. In addition, I certify that no part of this work will, in the future, be used in a submission in my name, for any other degree or diploma in any university or other tertiary institution without the prior approval of the University of Adelaide and where applicable, any partner institution responsible for the joint-award of this degree.

I give permission for the digital version of my thesis to be made available on the web, via the University's digital research repository, the Library Search and also through web search engines, unless permission has been granted by the University to restrict access for a period of time.

Signed

Chee Ho H'ng
Date:

ACKNOWLEDGEMENTS

First, I would like to thank my supervisors Professor Stan Gronthos, Dr. Esther Camp and Professor Peter Anderson for your support, guidance, time, patience, motivation and encouragement throughout my Ph.D journey. This once in a lifetime opportunity has been by far the most challenging but most worthwhile experience of my life. Stan, Esther and Peter have always had faith in me. I very much appreciate Stan's honesty, professionalism, wisdom, humble and ability to connect related experts to help with my projects.

Enormous thanks must go to all the members in the Mesenchymal Stem Cell Laboratories for being such a great group of people who look out for one another and help each other succeed. I have received help and guidance from Dr. Agnes Arthur, Dr. Jim Cakouros, Sharon Paton and Clara Pribadi, and have developed friendships that I value greatly. I would like to especially thank Agnes for her help in many professional and personal advices. Agnes has helped me in migration assays, mice tissues collection and μCT analysis. Jim has helped in the ChIP analysis.

I would also like to thank all the members in the Myeloma Research Laboratories for their help in the laboratory. I would especially thank Dr. Stephen Fitter (Steve) and Dr. Duncan Hewett for their invaluable molecular expertise and advices in Western Blot, molecular cloning and infection techniques.

Many other people in SAHMRI have also assisted in this project. I would like to thank Dr. Randall Grose for helping with the cell sorting using FLOW cytometry, Mark Van Der Hoek for helping with the RNA-sequencing and Dr. Jim Breen for running the bioinformatics analysis and advices.

Finally, I would like to say a huge thank you to my family for always supporting and encouraging me to pursue what I love, unconditionally.

Thank you everyone, I am sure that I could not have done it without any of you.

ABBREVIATIONS

ACAN	aggrecan
ADIPOQ	adiponectin
ALP	alkaline phosphatase
bHLH	basic helix-loop-helix
BLAST	basic Local Alignment Search Tool
BM	bone marrow
BMD	bone mineral density
BMP	bone morphogenetic protein
BMSC	bone marrow stem/stromal cell
BrdU	5-brome-2-deoxyuridine
BSA	bovine serum albumin
BSP	bone sialoprotein
C/EBPα	CCAAT/enhancer binding protein alpha
CBC	cranial bone cells
CBFA1	core binding factor 1
cDNA	complimentary DNA
CFU	colony forming unit
CFU-F	colony-forming unit-fibroblast
ChIP	chromatin immunoprecipitation
CKLF	chemokine like factor
CMTM8	chemokine-like factor superfamily 8
CNN1	calponin 1
COL I	collagen type 1
COL II	collagen type 2
COL X	collagen type 10
CPSF3	cleavage and polyadenylation-specific factor 3
CTSK	cathepsin K
CXCR4	chemokine receptor 4
CYP26B1	cytochrome P450 family 26 subfamily B member 1

C-ROS-1	tyrosine kinase receptor C-ROS-1 oncogene
DAPI	4’,6-diamidino-2-phenylindole dihydrochloride
DMEM	Dulbecco’s modified eagle medium
DMSO	dimethyl sulfoxide
DNA	deoxyribonucleic acid
DNase	deoxyribonuclease
dNTP	deoxyribonucleotide triphosphate
DTT	dithiothreitol
ECM	extracellular matrix
EGF	epithelial growth factor
EGFR	epithelial growth factor receptor
EDTA	ethylenediaminetetra-acetic acid
EMT	epithelial-to-mesenchymal transition
ERK	extracellular signal-regulated kinase
EZH2	enhancer of zeste homolog 2
FABP4	fatty acid binding protein 4
FACS	fluorescence-activated cell sorting
FCS	foetal calf serum
FGF	fibroblast growth factor
FGFR	fibroblast growth factor receptor
GFP	green fluorescence protein
GPD1	glycerol-3-phosphate dehydrogenase 1
G0S2	G0/G1 Switch 2
HEK293T	human embryonic kidney 293 cell line
HeLa	human cervical cancer cell line
HEPES	4-(2-hydroxyethyl)-1-piperazineethanesulfonic acid
HepG2	human liver cancer cell line
HES4	Hes family bHLH transcription factor 4
HGF	hepatocyte growth factor
HOPX	homeodomain-only protein homeobox
IGF-1	insulin-like growth factor 1
IRES	internal ribosome entry site

kDa	kiloDalton
KRT19	keratin 19
MACS	magnetic cell sorting
MAPK	mitogen-activated protein kinase
mg/ mL/ mm/ mM	milligram/ millilitre/ millimetre/ millimolar
M	molar
mRNA	messenger ribonucleic acid
MSC	mesenchymal stem cells
MSX2	muscle segment homeobox 2
mTOR	mechanistic target of rapamycin kinase
MUC-18	CD146
ng/ nm	nanogram/ nanometre
OCN	osteocalcin
ONN	osteonectin
OPN	osteopontin
OSX	osterix
PBS	phosphate buffered saline
PCR	polymerase chain reaction
PC3	human prostate cancer cell line
PDGF	platelet-derived growth factor
PI3K	phosphoinositide 3 kinase
PLIN1	perilipin 1
PPARγ2	peroxisome proliferator-activated receptor gamma 2
RNA	ribonucleic acid
RO	reverse osmosis
RT-qPCR	reverse transcription-quantitative polymerase chain reaction
RUNX2	runt-related transcription factor
SCS	Saethre-Chotzen syndrome
SD	standard deviation
SDF-1	stromal derived factor 1
SDS-PAGE	sodium dodecyl sulfate polyacrylamide gel electrophoresis
SEM	standard error of mean

siRNA	small interfering ribonucleic acid
SLUG	Snail family transcriptional repressor 2
SMAD	SMAD protein
STRO-1	stromal precursor antigen-1
TGFβ	transforming growth factor beta
Tween20	polyethylene glycol sorbitan monolaurate
TWIST-1	Twist family basic helix-loop-helix transcription factor 1
VCAM-1	vascular cell adhesion molecule 1
VEGF	vascular endothelial growth factor
VIM	vimentin
WNT	wingless related protein
WT	wild type
w/v	weight per volume
α-MEM	alpha-modified Eagle's medium
μCT	micro-computed tomography
μg/ μL/ μm/ μM	microgram/ microliter/ micrometre/ micromolar

PUBLICATIONS

Scientific Manuscripts

1. Hng, C., E. Camp, P. Anderson, J. Breen, A. Zannettino, S. Gronthos. (2019). HOPX counteracts Twist-1/EZH2 regulation of BMSC cell fate determination via suppression of adipogenic associated genes. *Stem Cells*, n/a-n/a. (Under Review)

2. Hng, C., E. Camp, P. Anderson, A. Zannettino, S. Gronthos. (2019). CMTM8 is a suppressor of mesenchymal stem cell osteogenic differentiation and promoter of proliferation via EGFR signalling. *Stem Cells International*, n/a-n/a. (Under Review)

Conference Proceedings

1. 10th Annual Florey Postgraduate Research Conference, Adelaide, September 2016, Poster. **Awarded Florey Medical Research Foundation Award.**
2. 6th Australia and New Zealand Society for Cell and Developmental Biology Adelaide Meeting, Adelaide, November 2016, Oral presentation.
3. EMBL Australia Postgraduate Symposium, Adelaide, November 2016, Poster.
4. SAHMRI Research Showcase, Adelaide, November 2016, Poster.
5. ASMR SA Annual Scientific Meeting, Adelaide, June 2017, Oral presentation.
6. ANZBMS & IFMRS Joint Meeting, Brisbane, June 2017, Poster.
7. EMBL PhD Course, Melbourne, July 2017, Poster.
8. University of Adelaide 3minute Thesis, August 2017, Oral presentation.
9. 11th Annual Florey Higher Degree Research Conference, Adelaide, September 2017, Poster. **Awarded Florey Medical Research Foundation Award & Adelaide Medical School Award.**
10. ComBio Adelaide 2017, Adelaide, October 2017, Poster.

11. ANZORS-RSA Joint Conference 2017, Adelaide, October 2017, Oral presentation.
12. 2017 SAHMRI Research Showcase, Adelaide, October 2017, Poster.
13. Australia and New Zealand Society for Cell and Developmental Biology, Adelaide, November 2017, Poster.
14. ASMR SA annual Scientific Meeting, Adelaide, June 2018, Poster.
15. ISSCR International Society for Stem Cell Research, Melbourne, June 2018, Poster.
16. 8th ANZSCDB Adelaide Meeting, Adelaide, June 2018, Poster.
17. SAHMRI Showcase, Adelaide, October 2018, Poster.
18. 12th Annual Florey Postgraduate Research Conference, Adelaide, September 2018, Poster.
19. 13th Annual Florey Postgraduate Research Conference, Adelaide, September 2019, Poster.

ABSTRACT

Bone marrow-derived mesenchymal stem/ stromal cells (BMSC) are self-renewing, multipotent cells that can give rise to multiple lineages including osteoblasts (bone), chondrocytes (cartilage) and adipocytes (fat). Interestingly, various pathways that promote BMSC osteogenesis/chondrogenesis simultaneously suppress adipogenesis and vice versa. The basic Helix-Loop-Helix (bHLH) transcription factor, *TWIST-1* is highly expressed by BMSC and plays an important role in BMSC proliferation, lifespan, differentiation and commitment. Enforced expression of *TWIST-1* enhances proliferation potential and lifespan of BMSC. It also enhances the adipogenic potential of BMSC yet inhibits chondrogenesis and osteogenesis. However, the underlying mechanisms mediating TWIST-1 regulation of BMSC growth and differentiation are not fully understood.

In order to identify novel TWIST-1 gene targets involved in BMSC proliferation and osteogenic differentiation, previous studies from our laboratory have compared the gene expression profile of BMSC, which express either endogenous or enforced expression of *TWIST-1* during either normal growth conditions or osteogenic inductive conditions, using microarray analysis. Two novel differentially expressed genes were identified, *HOPX* and *CMTM8*, as being suppressed by TWIST-1. The aim of this thesis is to determine whether *HOPX* and *CMTM8* are novel targets of TWIST-1 in BMSC and whether they are involved in mediating the effects of TWIST-1 on cell proliferation and lineage commitment.

To assess the functional role of *HOPX* and *CMTM8* in the context of BMSC biology, expression of HOPX and CMTM8 were overexpressed using retroviral transduction and supressed using siRNA. The present thesis demonstrated that *HOPX* counteracts TWIST-1/

EZH2 regulation of BMSC cell fate determination via suppression of adipogenic genes such as *C/EBPα*, *ADIPOQ*, *FABP4*, *PLIN1* and *PLIN4*, while HOPX is also a promoter of BMSC proliferation. This thesis also reported that CMTM8 is a suppressor of BMSC osteogenic differentiation and promoter of proliferation and cell migration via the EGFR signalling pathway.

This thesis provides better understanding of the downstream molecular mechanisms of TWIST-1 in bone development and post-natal homeostasis and therefore, provides insight into possible future therapeutic strategies that will alter the function of TWIST-1 targets.

Chapter 1: Introduction

1.1 Overview

Multipotent bone marrow mesenchymal stromal/ stem cells (BMSC) are currently being assessed for their efficacy in a wide range of skeletal tissue engineering and regenerative medicine based clinical trials. However, the mode of action of BMSC in clinical trials is not fully understood with little consensus within the literature on the relative levels of contribution of paracrine effects stimulating host cells verses direct reconstitution of affected tissues by implanted BMSC. Therefore, a better understanding of the precise molecular mechanisms that direct BMSC growth and cell fate determination will help develop more potent preparations of BMSC for clinical use.

TWIST family genes have been shown to play an important role in early embryonic development and postnatal skeletal homeostasis [1-3]. However, the molecular mechanisms of how *TWIST* genes influence MSC self-renewal or commitment to a particular cell lineage have yet to be fully determined. This thesis examines two molecular mechanisms which mediate Twist-related protein 1 (TWIST-1) control of BMSC growth and differentiation, and provides new insight into the downstream gene target(s) of TWIST-1. This thesis lays the foundation for future work that could facilitate the development of more potent tissue engineering and regenerative medicine therapies, for different orthopaedic based disorders and diseases.

This introduction describes the basic biology of bone and skeleton, and the important roles of BMSC in bone remodelling, together with the molecular mechanisms that regulate the physiology of these cells. Specifically, it describes the functional role of TWIST-1 in BMSC proliferation, differentiation, migration and cell fate commitment as well as suggesting possible cellular processes regulated by TWIST-1.

1.2 Skeletal Development

1.2.1 Macroscopic organisation of skeletal system

Bone is a dynamic and rigid organ and has several functions including: provides mechanical support and protection for internal organs, produces white and red blood cells, acts as a storage for minerals and fats, and serves as muscle anchor sites to enable locomotion (reviewed in [4]). Human adult skeleton is composed of 206 bones can be categorised into two major groups based on gross anatomy: the long bones, comprising the humerus, femur and tibia, and the flat bones, such as the cranial bones, scapulae and the ribs.

Long bones can be divided into three segments: the epiphyses (proximal and distal), which make up the extremities of the bones; the diaphysis, cylindrical shaft between the proximal and distal ends of the bone; and the metaphysis, which is the intermediate region between the epiphyses and the diaphysis of the bone (Figure 1.1). Between the epiphysis and the metaphysis contains the epiphyseal plate (growth plate), which is a layer of hyaline cartilage in growing bone. The outer surface of the bone is covered with a fibrous membrane called the periosteum, which contains nerves, blood vessels and lymphatic vessels that nourish the bone. Underneath the fibrous sheet are dense layers of calcified bone, known as the cortical bone, which encases the haematopoietic bone marrow in the medullary cavity. The marrow of young animals contain higher numbers of haematopoietic stem cells and mesenchymal stem cells in contrast to marrow derived from ageing animals, where the marrow produces more adipocytes (yellow marrow), with lower incidences of different stem cell populations. The medullary cavity, metaphysis and epiphysis of long bones are filled with a meshwork of spongy calcified bone struts, known as trabecular bone. In general, the trabecular bone is more metabolically active than the cortical bone, while the later primarily serves as a mechanical support.

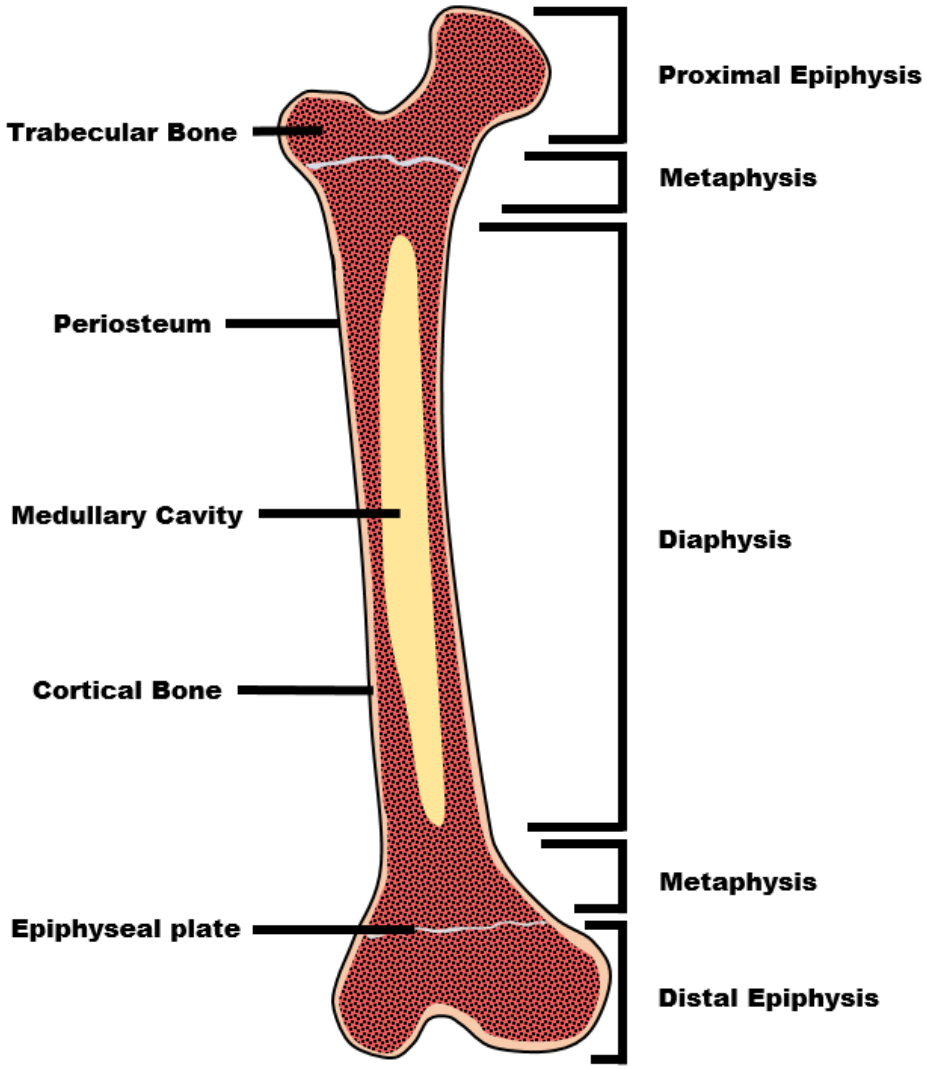

Figure 1.1: Basic anatomy of long bone. Schematic of human long bone depicting the different regions.

1.2.2 Bone matrix and composition

The mineralized extracellular matrix of the bone is mainly made up of type I collagen in the structure of fibrils and contains a minor proportion of serum-derived globular proteins, such as osteopontin, osteonectin and bone sialoprotein [5-14]. Within the mature bone are tightly bundled collagen fibres that arranged into layers (lamellae), which allow the construction of high density collagen in bone tissue. Moreover, bone contains inorganic mineral such as calcium and phosphate in the form of hydroxyapatite crystals [$Ca_{10}(PO_4)_6(OH)_2$] (reviewed in [15]). In the case of fracture healing, the collagen fibres in the bone form in a random oriented fashion which result in woven bone [16]. Woven bone is then progressively resorbed and replaced by more organised lamellar bone.

1.2.3 Cell types in bone tissues

Bone is composed of many different cell types including osteoprogenitors, osteoblasts, osteocytes and osteoclasts [17]. Osteoprogenitors are derived from multipotent mesenchymal stem cells, capable of differentiating into osteoblasts, the mature and non-proliferative cuboidal bone cells. Osteoblasts secrete osteoid (uncalcified bone matrix) that consists mainly of type I collagen and proteoglycans [18], and express alkaline phosphatase (ALP) required for mineralization of the osteoid. Once osteoblasts are surrounded by mineralized bone, they become osteocytes, which are terminally differentiated bone cells that regulate bone homeostasis by maintaining oxygen and mineral levels in the bone [19].

Many distinct morphologies and biomarkers of the different stages of bone cell differentiation have been identified. Morphologically, osteoblasts are larger and cuboidal cell while osteocytes appear to be smaller in size but have larger nuclei and multiple cytoplasmic extensions [20,

21]. Biochemically, runt-related transcription factor 2 (RUNX2) [22], Msh homeobox homolog 2 (MSX2) [23] and ALP [24-26] are commonly used early differentiation markers, while osteocalcin (OCN) and osteopontin (OPN) act as late differentiation markers of the mature osteoblast [26-29]. Other markers of the differentiation from osteoprogenitors to osteoblasts include fibroblast growth factor receptor I (FGFR1) and FGFR2 [30, 31], bone morphogenetic proteins (BMP) [32] and collagen I (COL I) [21].

Another cell type that is important in bone development and homeostasis is osteoclasts, derived from hematopoietic stem cells, which have a critical function in bone resorption [33]. Osteoclasts resorb the bone surface into its essential constituents via acid filled vesicles. Osteoporosis is a disease where there is overproduction of osteoclasts, leading to excess bone degradation resulting from the imbalance of bone homeostasis [34]. Thus, an imbalance between these cell types can lead to conditions of low bone mass such as osteoporosis.

1.2.4 Cartilage matrix and composition

Cartilage is an elastic and smooth connective tissue. It functions to cover and protects the ends of long bones at the joints such as elbows, ankles and knees. Moreover, cartilage acts as a template to provide structural support during bone formation via endochondral ossification. Cartilage is also an important structural component of other structures such as the nose, ear and rib cage, which exhibits a flexible property in contrast to the hard and stiff qualities of bone. However, cartilage has very limited repair capabilities due to the poor migration ability of chondrocytes and lack of oxygen and nutrient supply for the deposition of new matrix [35].

Chondrogenesis is the process where the cartilage is formed and is the earliest step of skeletogenesis. This process begins with the condensation a group of mesenchymal cells that further differentiate into chondroblasts and then chondrocytes [36]. Chondrocytes can be subdivided into non-hypertrophic and hypertrophic chondrocytes by their distinct morphologies, gene expression profiles and their specific functions. Non-hypertrophic chondrocytes include resting and proliferating chondrocytes. These chondrocytes are cartilage-forming cells as they express aggrecan (ACAN) and collagen II (COL II), the major components of the cartilaginous extracellular matrix required for cartilage template formation. At the same time, these group of chondrocytes regulate the rate of differentiation of hypertophic chondrocytes [37]. Once a cartilage template is formed, the innermost chondrocytes differentiate into pre-hypertrophic chondrocytes expressing low level of COL II. Pre-hypertrophic chondrocytes are located below the proliferating chondrocytes. This population of cells is larger than proliferating chondrocytes and begin to express RUNX2, a key factor of bone formation. Hypertrophic chondrocytes on the other hand are even larger cells that express vascular endothelial growth factor (VEGF) and collagen X (COL X) instead of COL II [38].

1.2.5 Bone formation - Intramembranous Ossification

Bone can form through two different mechanisms: intramembranous ossification and endochondral ossification. During intramembranous ossification, both the spongy and compact bones arise directly from sheets of condensed mesenchymal connective tissues. An ossification centre is primarily formed when a group of mesenchymal stem cells gather and commit to the osteogenic lineage, which then become osteoprogenitor cells. Osteoprogenitor cells then differentiate into early osteoblasts within the ossification centre. These osteoblasts secret osteoid and later trapped within the ossification centre and then differentiate into osteocytes

for further bone homeostasis. This event also stimulates the surrounding osteoprogenitor cells to differentiate into new osteoblasts allowing further bone formation [39].

1.2.6 Bone formation - Endochondral Ossification

Most of the bones in the body such as bony plates at the base of the skull and long bones form via endochondral ossification. In endochondral ossification (Figure 1.2), a hyaline cartilage template is initially formed, providing the structural support for the formation of bone. Primary ossification centre is then formed in the middle of the cartilage as described previously in Section 1.2.5, resulting in compact calcified matrix in the middle of the cartilage and spongy uncalcified matrix in the surrounding. As calcification occurs, the cartilage template is degraded. This allows the development of secondary ossification centres at each pole of the cartilage template, leading to formation of articular cartilage and epiphyseal plate that allow continuing growth of the bone [39].

1.2.7 Bone homeostasis - Remodelling

Bone is a dynamic tissue that is gradually remodelled over time, where complete replacement of the human skeleton occurs approximately every 10 years [40-42]. The remodelling and regenerating ability of bone is dependent on the balance between the different cell types. An average person reaches their peak bone mineral density (BMD) at around 30 years of age, and the BMD starts to decline after the peak, leading to bone loss conditions such as osteoporosis [43]. Therefore, understanding the precise stimuli responsible for the processes of every stages of this complex bone remodelling will help to control the process and possibly delay or prevent the effects of bone loss due to age, trauma and disease.

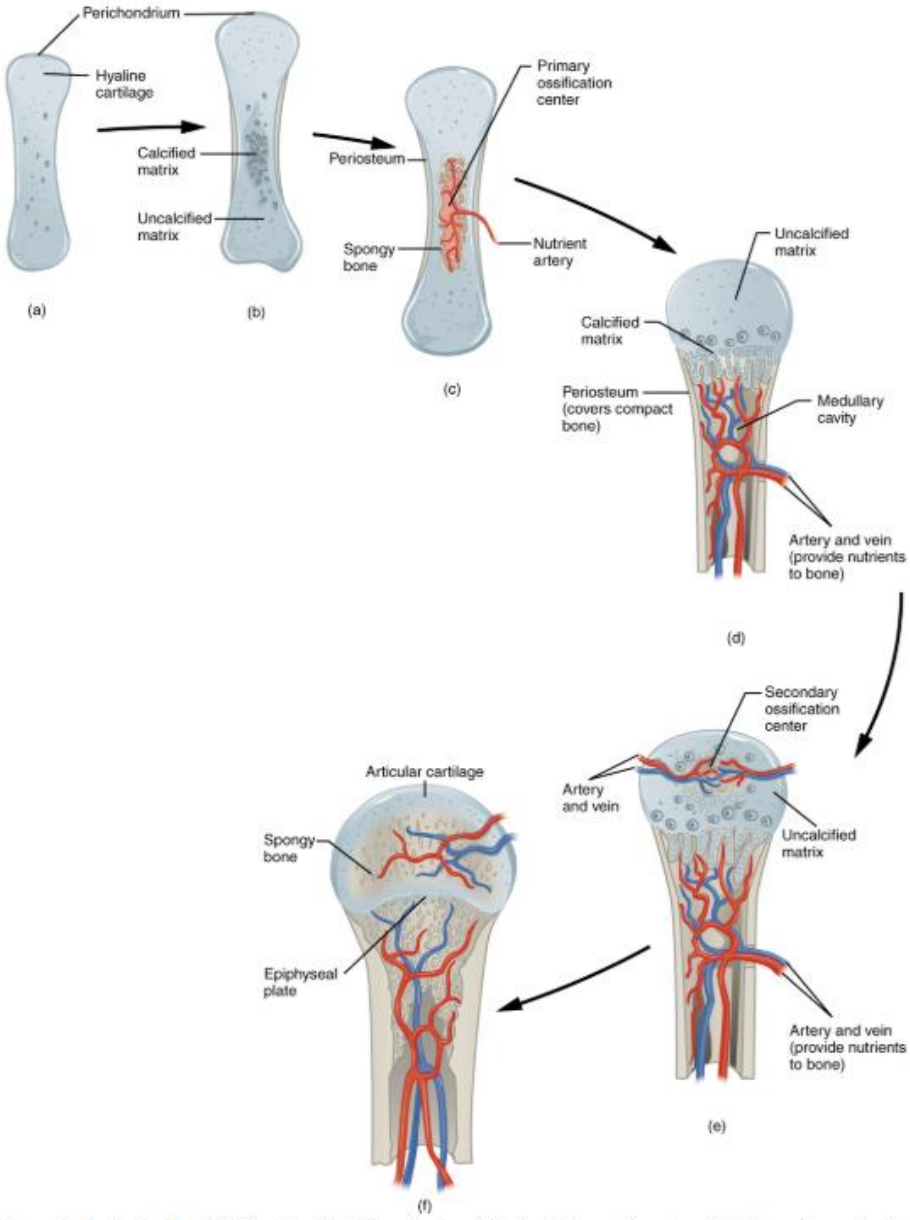

Figure 1.2: Endochondral Ossification. (a) Mesenchymal stem/ stromal cells condense and differentiate into chondrocytes. (b) Formation of the cartilage template of the future skeleton and the perichondrium. (c) Penetration of capillaries into cartilage template and transformation of perichondrium into periosteum. Primary ossification center start to develop. (d) Cartilage and chondrocytes expand at both ends of the bone. (e) Secondary ossification centers start to develop. (f) Chondrocytes remains at epiphyseal (growth) plate. Adapted from [39].

1.3 Mesenchymal Stem Cells

Friedenstein and colleagues first identified a population of non-hematopoietic stromal cells in the bone marrow of rodents, based on their capacity to form single-cell adherent colonies *in vitro* that resemble fibroblastic cells, called colony forming unit-fibroblasts (CFU-F) [44]. These stromal cells have subsequently been referred to as mesenchymal stem cells (MSC), due to their capacity for differentiation into multiple cell types, ability to recapitulate a bone marrow supporting organ *in vivo* (Figure 1.3) [44-48]. However, the methodologies for the isolation of primary BMSC have relied upon the rapid plastic-adhesion of BMSC, followed by their proliferation *in vitro* [44, 49-51]. Such methods resulted in the isolation of a heterogeneous population of marrow stromal cells, vascular smooth muscle cells and macrophages, comprised only of a small proportion of multipotent BMSC. Following the generation of antibody reagents that identified clonogenic BMSC in human bone marrow aspirates, it is now possible to isolate a more homogeneous population of adult human BMSC based on their co-expression of perivascular markers such as STRO-1, VCAM-1 (CD106) and MUC-18 (CD146) [46, 52-55]. This isolation protocol provides a means to isolate purified populations of BMSC for basic research and for their use in tissue engineering and regenerative medicine therapies.

The International Society for Cell Therapy later proposed minimum criteria to define MSC, which include (1) ability to adhere to plastic in standard culture conditions; (2) expression of the surface molecules CD73, CD90, CD105 in the absence of the hematopoietic markers CD11b, CD14, CD19, CD34, CD45, CD79a, and class II antigen HLA-DR; and (3) capability of differentiating into at least osteoblasts, adipocytes, and chondroblasts *in vitro* [56].

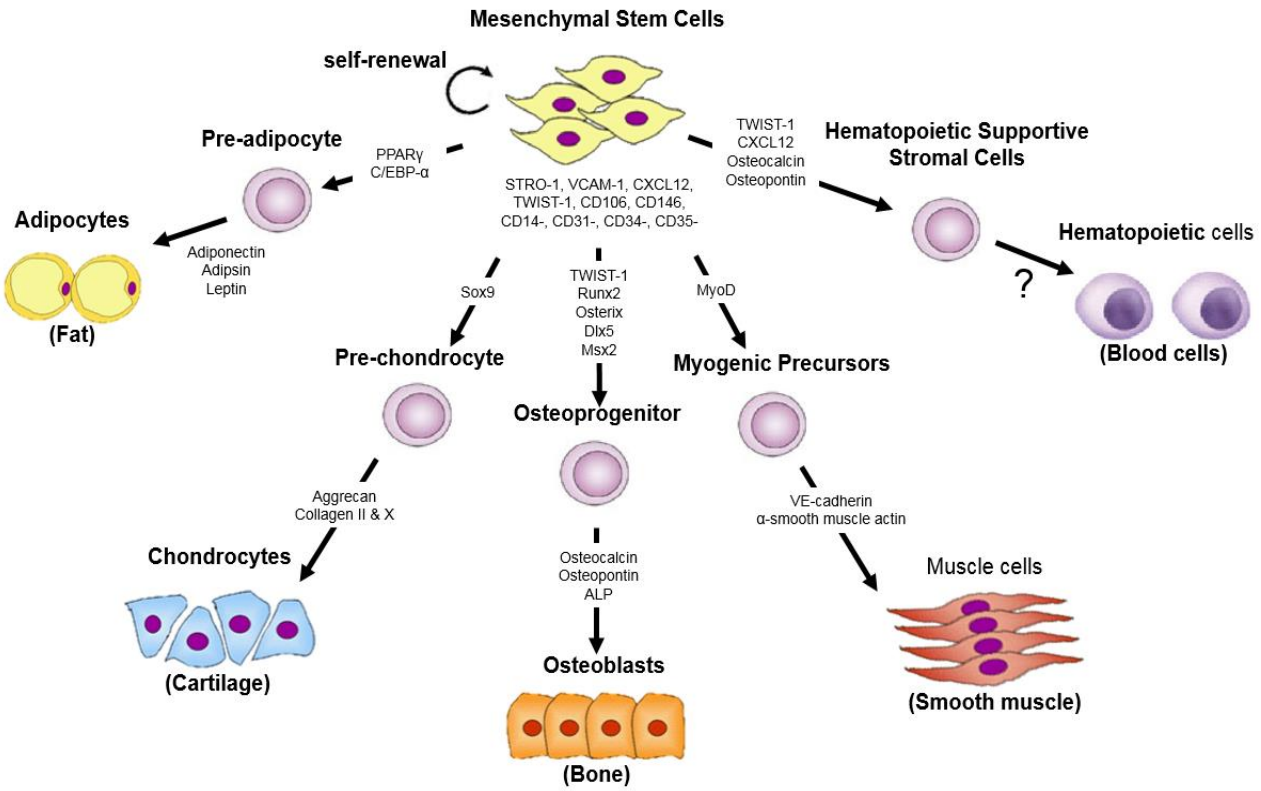

Figure 1.3: Multilineage potential of BMSC. Schematic diagram of signalling molecules and transcription factors involved in the regulation of BMSC differentiation.

However, these criteria were established only to standardize human MSC isolation as MSC from different species may express different surface markers [57]. Furthermore, the definition is lack of assessment of multidifferentiation and self-renewal capacity *in vivo*. Therefore, more recently MSC have typically been defined by their multipotency and self-renewal capability [46, 54, 55].

MSC-like populations have also been isolated from various human tissues, but have significantly diverse growth and differentiation capabilities, morphology and gene expression profiles [58]. These observations suggest that MSC-like populations from different tissues may be biologically distinct and exhibit unique self-renewal and multipotential capabilities. For example, MSC isolated from bone marrow [46, 50], umbilical cord blood [59], peripheral blood [60], adipose tissue [61], dental tissue [62, 63], synovial tissue [64] and lung tissue [65] exhibit different paracrine properties, growth and differentiation potential, but show similar surface marker expressions [66]. Therefore, MSC-like populations derived from different tissue sources makes it challenging to determine the most appropriate cell population for specific tissue engineering and regenerative medicine applications.

1.3.1 Bone marrow-derived mesenchymal stem cells migration

BMSC are one of the most common stem cell source used in cell therapy in regenerative medicine. During bone homeostasis or tissue healing, BMSC migrate from bone marrow to remodelling or injury sites through peripheral circulation [45, 67, 68]. Therefore, the efficacy of BMSC in bone remodelling and cell therapy depends on their homing ability [68, 69]. The migration of BMSC is regulated by complex mechanical and chemical factors in this trafficking process [70].

1.3.2 Chemical factors that regulate BMSC migration

Factors involved in BMSC migration such as cytokines, growth factors and chemokines have been reviewed in [70]. The stromal derived factor 1 (SDF-1)/chemokine receptor 4 (CXCR4) axis is critical for inducing BMSC migration and recruitment to injury sites. It has been shown that increased concentration of SDF-1 can upregulate CXCR4 expression and promotes BMSC migration and tissue regeneration in various tissues such as liver, brain, skeletal muscle and heart [71-75]. In additions, growth factors such as hepatocyte growth factor (HGF), insulin-like growth factor (IGF-1), transforming growth factor β1 (TGF-β1), vascular endothelial growth factor (VEGF), platelet-derived growth factor (PDGF) and basic fibroblast growth factor (bFGF) showed the ability to regulate BMSC migration.

HGF is a pleiotropic growth factor of mesenchymal origin that binds to its receptor, c-Met [76]. Activation of c-Met signalling can promote the proliferation, survival and migration of various cell populations including BMSC [77]. It was shown in rat and mouse systems that HGF increases BMSC migration via the Akt/FAK and PI3K pathways. [78, 79].

In addition, the PI3K signalling pathway has also been intergrated by IGF-1, where IGF-1 is a mitogen that can induce migration of multiple cell types [80, 81]. Studies have shown that overexpression of Igf-1 in rat BMSC improves cell survival and promotes cell recruitment via paracrine action of Sdf-1 [82]. Further investigation showed that IGF-1 increased the expression of SDF-1 receptor, CXCR4, which then increased BMSC migration via the PI3K signalling pathway [81].

TGF-β1 is a another growth factor that can increase BMSC recruitment and migration via regulating signalling pathways such as PI3K/AKT, FAK, ERK1/2, p38 and N-cadherin [83]. In mice myocardial tissues that experienced ischemia/reperfusion injuries, high expression of Tgf-β1 was found to enhance homing of BMSC to the injuries sites via modulation of Cxcr4 [84].

Nonetheless, VEGF is a growth factor that plays an important role in the growth and migration of various types of cells [85]. It has been shown that enforced expression of VEGF in human BMSC can increase expression of SDF-1α in infarcted hearts, resulting in increased migration of BMSC and cardiac stem cells to the affected sites [85]. Moreover, VEGF can signal through PDGF receptors and enhances BMSC proliferation and migration [86]. Studies have shown that PDGF is a highly potent growth factor that promotes BMSC migration, recruitment and tissue repair [87, 88]. Blocking of PDGF-dependent signalling pathways inhibits MSC migration and survival in colon cancer [89]. In addition, bFGF was found to promote BMSC migration through upregulation of αVβ3 integrin and thus activates the MEK/ERK pathway and PI3K/AKT pathway [90, 91].

1.3.3 Transcriptional regulation of osteoblast differentiation

Osteoblast development is promoted through the regulation of different transcription factors and growth factors (Figure 1.4). Master regulatory genes for osteoblast lineage commitment include *RUNX2*, osterix (*OSX*), distal-less homeobox 5 (*DLX5*) and *MSX2* [92-97]. RUNX2 (also known as CBFA1) is an early osteogenic marker essential for osteoblast differentiation, which activates various bone associated markers such as *OCN*, *OPN* and bone sialoprotein (*BSP*) [93]. *OSX* is one of the downstream targets of RUNX2, which is predominantly

expressed by osteogenic progenitors but is expressed at low levels by pre-hypertrophic chondrocytes [97]. In mice, *Osx* is expressed as early as the commitment of MSC to the osteoblast lineage, and its expression increases as osteoblast differentiation occurs [98]. Following initiation of the osteogenic differentiation via *Runx2* [93], other genes such as *Dlx5* and *Msx2* participate in the maintenance and regulation of osteoblast differentiation [94, 95].

1.3.4 Transcriptional regulation of chondrocytes differentiation

In vitro and *in vivo* studies have identified a number of transcription factors that play important roles in chondrocyte development, from their lineage commitment to their terminal maturation (Figure 1.5). SOX9 is a key transcription factor of chondrogenesis and is necessary for commitment of MSC towards the chondrogenic lineage [99, 100]. *SOX9* was reported to activate chondrogenic markers such as *ACAN*, *COL II* and *COL X* [101-105], and trigger the expression of *SOX5* and *SOX6* [99], which then interact with SOX9 to promote chondrocyte differentiation [106]. Loss-of-function mutation in *SOX9* results in early maturation of pre-hypertrophic chondrocytes into hypertrophic cells [99, 107]. On the other hand, overexpression of *SOX9* in the growth plate slows down chondrocyte maturation process [108]. Furthermore, *SOX9* also represses hypertrophic chondrocyte-specific genes such as *VEGFα* and *COL10a1* [109, 110]. Interestingly, *SOX9* has been demonstrated to interact directly with *RUNX2* and block its activity [111]. It was further shown that *SOX9* prevents the differentiation of chondrocytes into osteoblasts by suppressing both β-catenin signalling and *RUNX2* expression [112]. Together, these findings suggest that SOX9 plays an important role in chondrogenic lineage commitment and differentiation via regulating multiple chondrogenic genes.

1.3.5 Transcriptional regulation of adipocyte differentiation

Figure 1.6 shows the major transcription factors and growth factors that are required for each stage of adipocyte differentiation. Two identified master regulatory transcription factors of adipocyte differentiation, CCAAT/enhancer binding protein alpha (C/EBPα) and peroxisome proliferator-activated receptor gamma 2 (PPARγ2) have been demonstrated to activate adipocyte-specific genes. Transcription factors of the C/EBP family play an important role in adipocyte differentiation. It has been shown that *C/EBP-β* and *C/EBP-δ* are involved in the induction of adipocyte differentiation at an earlier stage than *C/EBPα* and *PPARγ2*, and that the promoter region of the *PPARγ2* gene contains binding sites for C/EBP [113, 114]. *C/EBPα* expression has also been observed before the expression of most adipogenic genes, and is required for the adipogenic induction [115, 116]. Moreover, C/EBPα and PPARγ2 have been shown to act cooperatively during adipocyte differentiation through activating each other's expression and therefore regulating the expression of other adipogenic genes [113]. As one of the most essential transcription factors for adipocyte differentiation, *PPARγ2* is expressed before most adipogenic genes [117]. Activation of *PPARγ2* leads to cell cycle arrest and subsequent activation of other adipogenic genes [118]. *PPARγ2* was found to promote adipogenesis and inhibit osteoblastogenesis [119, 120]. Reduced expression of *PPARγ2* was associated with reduced marrow adipogenesis, increased osteoblastogenesis *in vitro* as well as increased trabecular bone volume *in vivo* [121]. *In vitro* culture of $Ppar\gamma2^{+/-}$ mice BMSC showed increased expression of *Runx2* and *Osx*, resembling increased osteoblast formation [122]. These studies showed that C/EBPα and PPARγ2 are master regulatory transcription factors that act cooperatively to promote adipogenesis, where PPARγ2 also acts to inhibit osteogenesis.

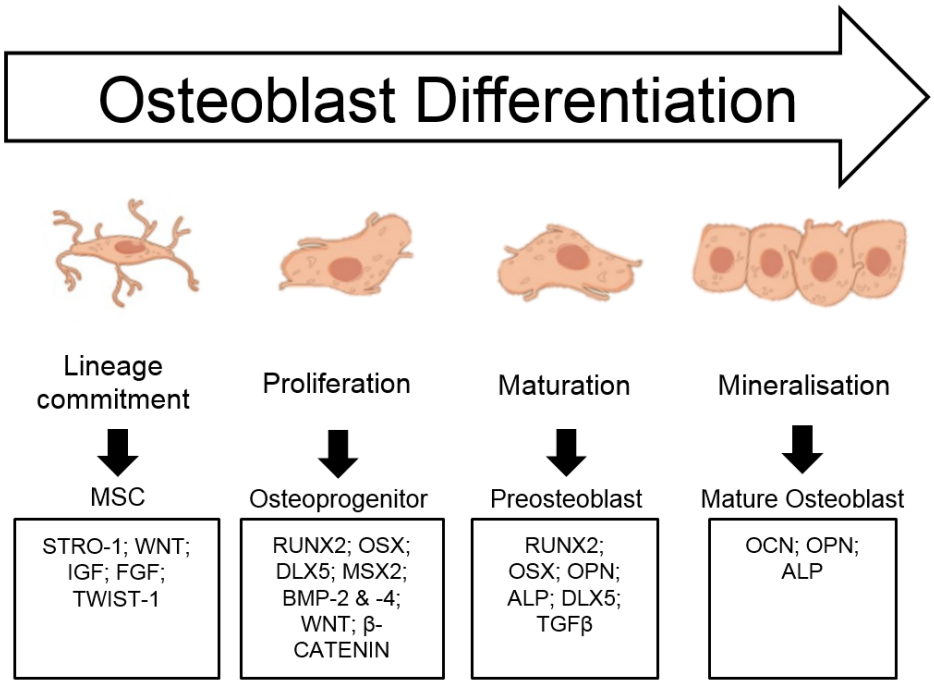

Figure 1.4: Osteoblast differentiation. The stem cell marker, STRO-1 and transcription factor, TWIST-1 inhibit BMSC differentiation and maintain BMSC in an immature and proliferative state. The transcription factors Runx2 and Osterix initiate BMSC differentiation down the osteoblast lineage. Osteocalcin, osteonectin and osteopontin are involved in the maturation of osteoblasts. Adapted from [123].

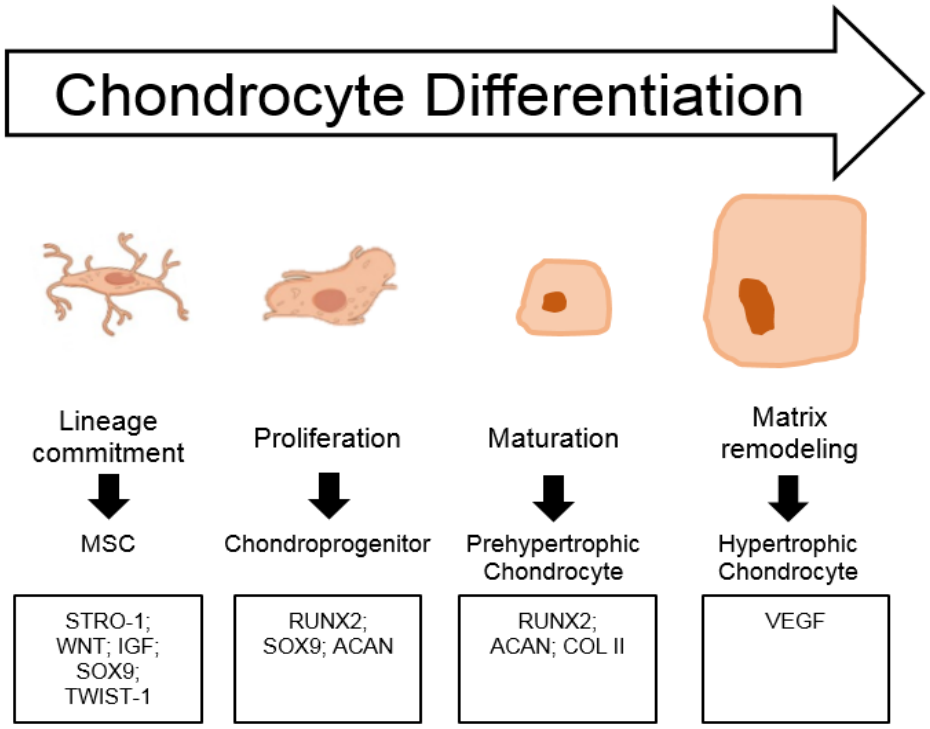

Figure 1.5: Chondrocyte differentiation. The transcription factor Sox9, together with drives chondrocyte differentiation and proliferation. Chondrocyte hypertrophy is driven by the transcription factor Runx2 and is negatively regulated by Sox9. Adapted from [124].

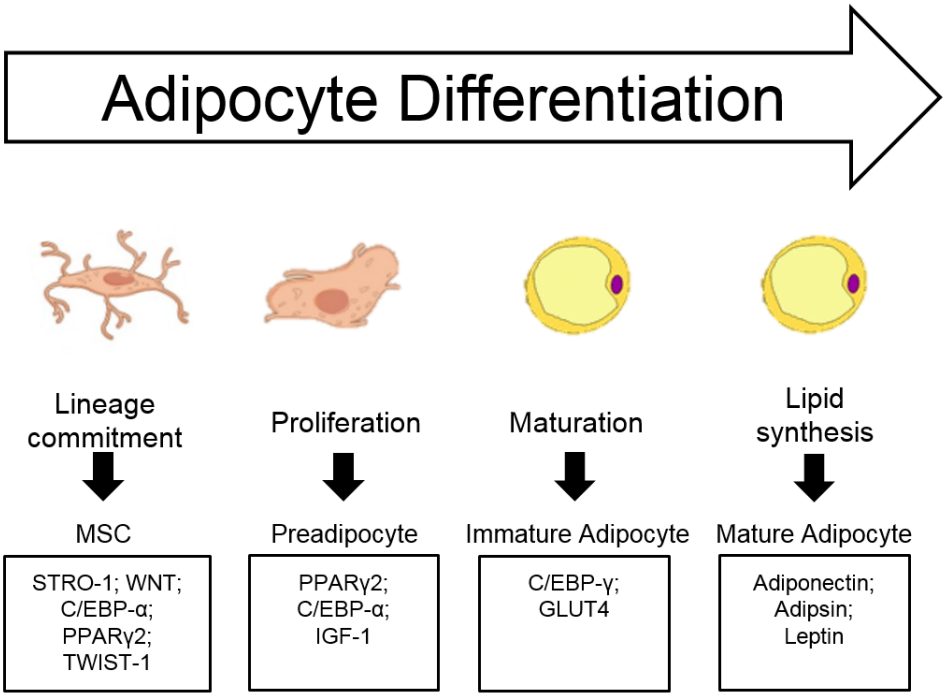

Figure 1.6: Adipocyte differentiation. The transcription factors C/EBPα and PPARγ initiate BMSC differentiation down the adipocyte lineage. Adiponectin, Adipsin and Leptin are involved in the maturation of adipocytes. Adapted from [125]

1.3.6 Crosstalk/ signalling interactions between BMSC osteogenesis, chondrogenesis and adipogenesis

In the bone marrow, the differentiation of BMSC into osteoblasts and adipocytes is competitively balanced. The commitment of BMSC to the adipogenic lineage may result in increased adipocyte formation and decreased osteoblast numbers as observed in age-related bone loss [126]. Numerous *in vitro* experiments performed on BMSC have revealed that factors that promote adipocyte formation inhibit osteoblastogenesis [127, 128], and conversely, factors that promote osteoblast formation inhibit adipogenesis [125]. This mainly occurs through the interaction between different signalling pathways, outlined below and the action of the transcription factor TWIST-1.

WNT (Wingless-related Integration Site) molecules are cysteine-rich glycoproteins that regulate cell migration, proliferation, differentiation via two distinct pathways: canonical via β-catenin and non-canonical/calcium [129]. Canonical WNT/β-catenin signalling pathway was shown to promote bone formation via promotion of stem cell self-renewal [130], promotion of osteoblast differentiation [131] and inhibition of adipogenesis [132] via suppressing *C/EBPα* and *PPARγ2* [133-137] (Figure 1.7).

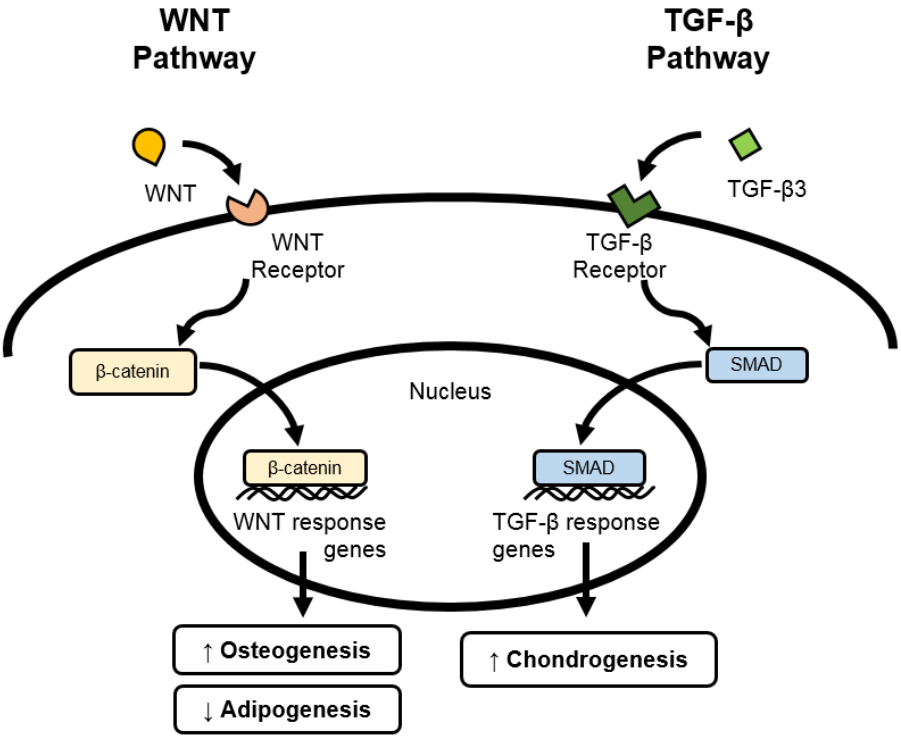

Figure 1.7: The canonical Wnt and TGF-β signalling pathway. Wnt ligand bind to the Wnt receptor on the cell surface and stimulates activation of β-catenin. Binding of β-catenin on to Wnt response genes results in upregulation of osteogenesis and downregulation of adipogenesis. TGF-β binds to its receptor on cell surface and activates SMAD proteins. Binding of SMAD protein on to TGF-β response genes results in upregulation of chondrogenesis. Adapted from [131, 132, 138].

TGF-β (transforming growth factor-beta) family members are involved in skeletal development and regulation of chondrocyte differentiation [50, 139, 140]. TGF-β cytokines serves various functions from embryogenesis to homeostasis, including proliferation and differentiation [141]. TGF-β has been found to stimulate expression of WNT and β-catenin and therefore promote osteo/chondrogenesis while inhibiting adipogenesis [138]. TGF-β3 promotes chondrogenic differentiation of MSC through intracellular cascades, such as SMAD proteins, JNK, p38, extracellular-signal regulated kinase (ERK1/2) and mitogen-activated protein (MAP) kinases [137, 139, 142] (Figure 1.7).

BMP (bone morphogenic protein) molecules are part of the TGF-β superfamily of growth factors that involved in the regulation of cell migration, apoptosis, proliferation, differentiation and also development and functions of tissues, including bone and cartilage [143]. BMP-2, -4, -6, -7 have been proven to play roles in osteo/adipogenic differentiation of MSC [144-150]. Chen et al. (1998) proposed that BMP affects cell fate determination of MSC via binding to different receptors, which then stimulate different downstream signalling cascades [151]. For example, binding of BMP to BMPR-1A activates adipogenic factors *PPARγ2* and *C/EBPα*, which promote adipocyte differentiation, whilst binding of BMP to BMPR-1B activates osteogenic factors *RUNX2* and *OSX*, which commit MSC into osteoblast lineage [151]. Furthermore, BMP effects on lineage commitment of MSC is dose-dependent with low level of BMP-2 favors adipocyte differentiation while high level of BMP-2 favors osteo/chondrogenic differentiation [152].

mTOR (mammalian target of rapamycin) molecules are a member of the phosphatidylinositol 3-kinase-related kinase (PI3K) protein family that primarily senses nutrient in mammalian

cells. mTOR can assemble into two distinct multiprotein complexes, termed mTORC1 and mTORC2 [153]. The mTORC1 signalling pathway has previously been reported to play an important role in osteoblast proliferation and differentiation [154, 155]. Inhibition of either the PI3K or mTOR signalling pathways in osteoprogenitor cells promote osteogenic differentiation in human embryonic stem cells and human and murine MSC [155-158]. Furthermore, the mTORC1 signalling pathway has also been shown to be involved in adipocyte differentiation by activating key adipogenic transcription factors, such as *PPARγ2* and *C/EBPα* [159, 160].

FGF (fibroblast growth factors) family members control MSC differentiation differently. FGF1, 2, 10 promote adipocytes differentiation [161-164]. However, FGF2 was also shown to promote proliferation and osteoblastogenic differentiation of BMSC [165-168]. Therefore, the impacts of FGF on adipo/osteoblastogenesis depends on the mode of signalling, nature of ligands and other extracellular stimuli. Moreover, adipocytes may affect bone homeostasis through secretion of adipokines and fatty acids with paracrine actions [169]. Other molecules shown to regulate MSC growth and differentiation include TWIST-1 [1].

1.4 TWIST-1 Regulation in BMSC

1.4.1 TWIST-1 is highly expressed by BMSC

TWIST-1 gene is mapped to 7q21.2 and encodes for a basis helix-loop-helix (bHLH) transcription factor that is important in skeletal and head mesodermal tissue development [170, 171]. This bHLH molecule acts as either a homo- or heterodimer with other bHLH molecules, and binds to a highly conserved E-box region (CANNTG) on the promoter region of genes [172]. Human BMSC express high levels of *TWIST-1*, yet expression is downregulated

following BMSC *ex vivo* expansion and maturation, correlating to a reduced lifespan potential [1, 46, 54, 173].

Isenmann et al. (2009) performed functional studies to determine the effect of TWIST-1 on BMSC proliferation and lifespan [1]. *TWIST-1* high expressing BMSC lines demonstrated a higher proliferation rate and lifespan compared with the vector control BMSC lines. Supportive studies demonstrated that overexpression of the *TWIST-1* can inhibit the senescence of BMSC, leading to increased cellular proliferation and extended lifespan [2] (Figure 1.8).

1.4.2 TWIST-1 regulates epithelial-to-mesenchymal transition (EMT) of cells

EMT is a critical process in embryogenesis and cancer metastasis, which is thought to be a hallmark of cancer stem cell and many progenitor cell populations [174]. Cells that undergo EMT lose their polarity and intracellular adhesion molecules, thereby enable them to migrate [174]. Other studies have highlighted the role of TWIST-1 as a master regulator of cell migration by promoting EMT during embryogenesis and cancer metastasis [175]. It was discovered that using mouse mammary tumour cell lines, increase *Twist-1* expression results in breast cancer invasion and metastasis; while suppression of *Twist-1* expression inhibits metastasis of carcinoma cell from mammary gland to the lung [176]. Furthermore, *Twist-1* has been shown to bind to the E-box in the promoter of *E-cadherin* (epithelial associated gene) and represses the transcription [176]. Cleavage of E-cadherin ectodomain create fragments capable of inducing EMT, invasion and proliferation of MCF-7 mammary carcinoma cells in a paracrine manner via the epithelial growth factor receptor (EGFR) signalling [177]. EGFR has also been implicated by prostate cancer bone metastasis [178].

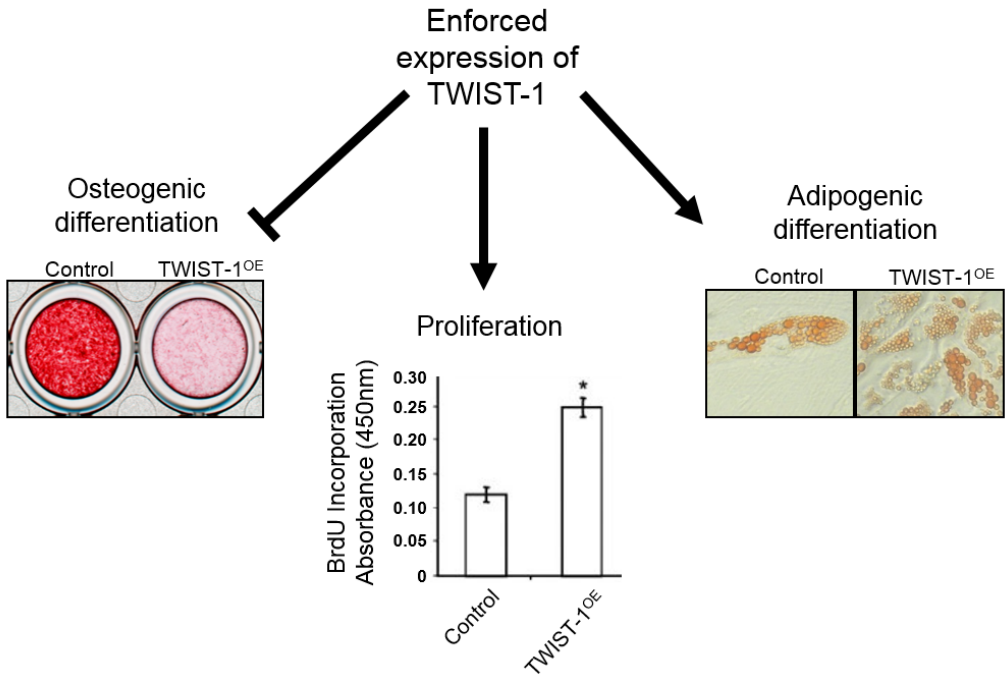

Figure 1.8: Functions of TWIST-1 in BMSC proliferation and differentiation. TWIST-1 overexpressing BMSC showed increased proliferation and adipogenic differentiation capacity, whilst decreased osteogenic differentiation potential. Adapted from [1].

Nuclear translocation of EGFR directly supress transcription of *miR-1*, where miR-1 is an upstream suppressor of *TWIST-1* [178]. Therefore, increased levels of nuclear EGFR leads to release of suppression on *TWIST-1* expression by miR-1, which then allows EMT and cell migration to occur. These studies demonstrated that TWIST-1 is a promoting factor of cell EMT and migration, possibly modulated by EGFR signalling pathway.

1.4.3 TWIST-1 regulated transcription factors and signalling pathways

TWIST-1 regulates a range of transcription factors and signalling pathways involved in osteogenic differentiation of BMSC (Figure 1.9) such as tyrosine kinase receptor C-ROS-1 oncogene (C-ROS-1) [3], enhancer of zeste homolog 2 (EZH2) [2], Hes family bHLH transcription factor 4 (HES4) [179], BMP [180], β-catenin [181], WNT [182], MSX2 [95], FGFR2, ERK1/2, PI3K [183] and RUNX2 [92]. TWIST-1 has been demonstrated to be a negative transcription factor in bone cell development [184, 185]. Furthermore, *Twist-1* heterozygous mice reveal increased expression of FGF2 and BMP signalling [186, 187].

1.4.4 The role of TWIST-1 in bone pathology

TWIST-1 family genes have been shown to play an important role in early embryonic development, however, the molecular mechanisms of how *TWIST-1* genes influence MSC commitment to a particular cell type or stay as multipotent stem cells has yet to be fully determined. Studies in mice showed that Twist-$1^{-/-}$ embryos are lethal but Twist-$1^{+/-}$ heterozygous embryos survive post birth and have craniofacial and limb deformities [170, 188-190].

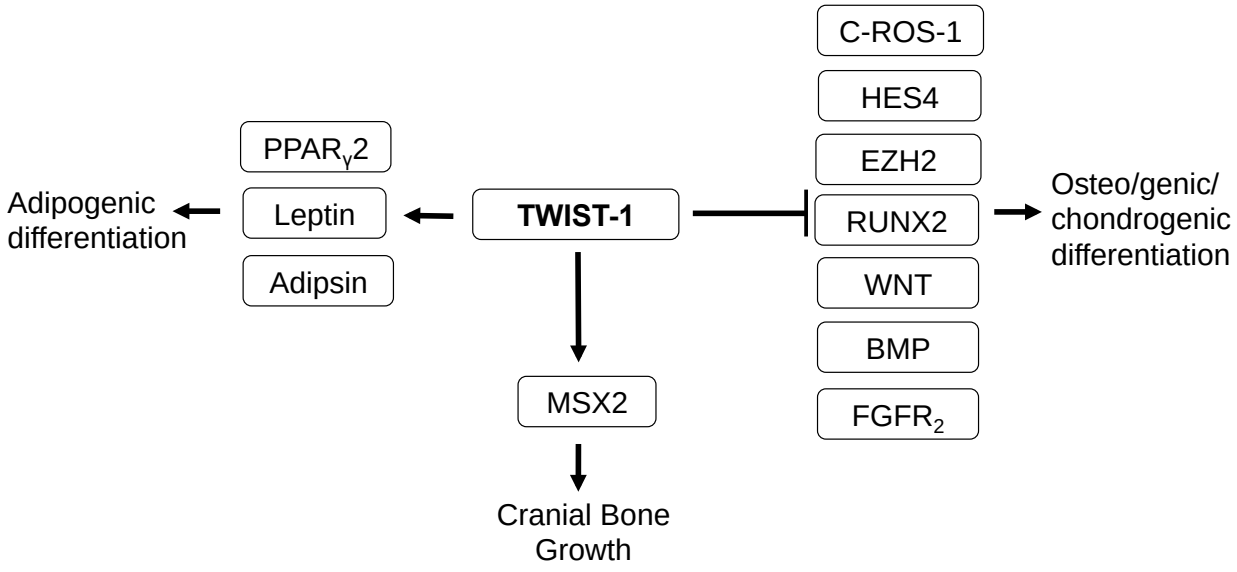

Figure 1.9: Factors regulated by TWIST-1. TWIST-1 regulates transcription factor MSX2 during cranial bone development. In BMSC, TWIST-1 negatively regulates a number of transcription factors including C-ROS-1, HES4, EZH2 and RUNX2; and other factors such as WNT, BMP and FGFR2, resulting in inhibition of BMSC osteogenic and chondrogenic differentiation. Moreover, TWIST-1 also positively regulates PPARγ2, Adipsin and Leptin and promotes BMSC adipogenic differentiation.

In humans, TWIST-1 haploinsufficiency leads to a bone disorder called Saethre-Chotzen Syndrome (SCS) which is characterized by craniofacial (premature suture fusion and asymmetrical face) (Figure 1.10) and limb anomalies (brachydactyly and cutaneous syndactyly) [191, 192]. It was demonstrated that cranial parietal bone cells derived from SCS patients have reduced TWIST-1 expression compared with normal cranial bone cells (CBC) and exhibit a profound capacity to generate mineralised nodules *in vitro* under osteogenic conditions [2]. In addition, it was reported that decreased level of *TWIST-1* in SCS cranial cells causes changes of gene expression which leads to a decrease in osteoprogenitor proliferation and increased osteogenesis, resulting in premature fusion [193].

In growth plate, studies have shown that TWIST-1 negatively regulates chondrogenesis [194]. It was found that *TWIST-1* expression is restricted to proliferating, immature chondrocytes within the growth plate during postnatal development and absent in hyperthophic chondrocytes. Further *in vivo* studies suggest that postnatal bone formation is inhibited in *Twist-1* overexpressing mice, characterised by shorten limbs at two-week age [195]. Moreover, abnormal growth plate structure and vascular invasion were also observed in these mice at various timepoints during postnatal development. These findings demonstrate that alteration of TWIST-1 expression can modulate growth plate organization and lead to abnormal postnatal longitudinal bone growth [195].

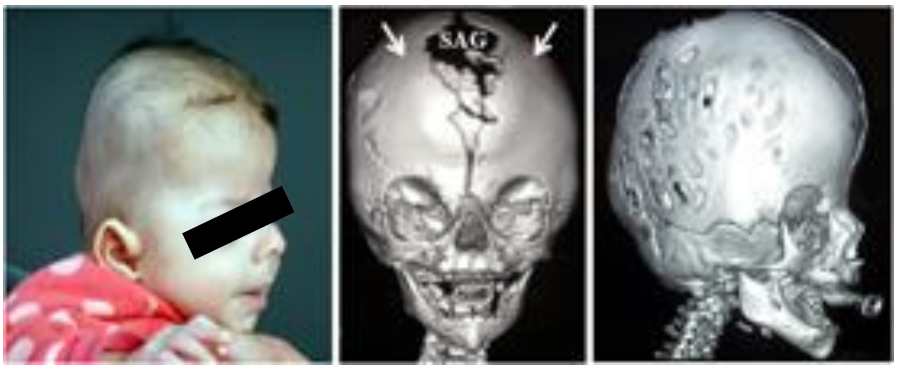

Figure 1.10: Patient with SCS. Frontal and side photo and CT scans of a 5 months old child with bulging forehead (provided by co-supervisor Prof. Anderson). Arrows indicate fused coronal suture on both sides of the skull. The sagittal suture is still unfused. Adapted from [3].

1.4.5 Association between TWIST-1 and EZH2 in BMSC functions

Previous studies have demonstrated an association between TWIST-1 and Enhancer of zeste homolog 2 (EZH2) in BMSC, where TWIST-1 increased EZH2 expression [2]. High levels of TWIST-1 expression in BMSC enhance recruitment of Ezh2 to silence the Ink4A/Arf locus (a promoter of p53), resulting in histone methylation (H3K27me3) along the locus to repress Ink4A/Arf activation, to inhibit cellular senescence and increase the lifespan of BMSC [2]. Further functional studies found that EZH2 regulates BMSC lineage specification, where high expression of EZH2 in BMSC promotes adipogenic differentiation and inhibits osteogenic differentiation [196]. Therefore, TWIST-1 regulation of EZH2 was exploited for its downstream molecular mechanisms during BMSC proliferation and differentiation.

1.5 Significance/ Contribution to the Discipline

Decreased levels of TWIST-1 affect the growth of both cranial (intramembranous ossification) and long bone (endochondral ossification). Many of the underlying mechanisms of how TWIST-1 regulates MSC division and differentiation still remain poorly understood. As a consequence, ineffective control of cell proliferation and lineage commitment remains a hurdle to be overcome to permit the clinical use of BMSC. Thus, understanding the downstream molecular mechanisms of TWIST-1 in bone development and post-natal homeostasis proposed in this study will provide insight into possible future therapeutic strategies that will alter the function of TWIST-1 targets.

1.6 Hypothesis

Our previous data demonstrated that there is a possible negative correlation between *TWIST-1* and the putative target genes, homeodomain-only protein homeobox (*HOPX*) and chemokine-like factor superfamily 8 (*CMTM8*). We therefore proposed that suppression of *TWIST-1* increases the levels of these genes, leading to increased bone formation and decreased adipogenesis in bone marrow stromal cell populations.

1.7 Aims

Aim 1: To identify putative TWIST-1 gene targets from preliminary microarray analysis using real-time PCR and chromatin immunoprecipitation techniques in human BMSC.

Aim 2: To assess the functional role of TWIST-1 gene targets during BMSC proliferation and cell fate determination.

Aim 3: To investigate the molecular mechanisms and signalling pathways which are altered by TWIST-1 gene targets during BMSC proliferation and fate determination.

Chapter 2: Materials & Methods

2.1 Table 2.1 Suppliers of Commonly Used Reagents

Reagent	Catalogue No.	Supplier
10x Tris/Glycine buffer	1610771	Bio-Rad
Acetic Acid glacial	AA009-2.5L-P	Chem Supply
Acetone	AA008-2.5L-P	Chem Supply
Acrylamide/BIS 30% 37.5:1 ratio 500mL	1610158	Bio-Rad
Agar Bacto	214010	BD (Beckton Dickinson)
Agarose	9010E	Scientifix
Alizarin Red S LR	AL080-100G	Chem Supply
Ammonium persulphate (APS)	A3678	Sigma Aldrich
Annexin V Alexa Fluor 488	A13201	Thermo Fisher
Annexin V Binding Buffer	422201	Australian Biosearch
Annexin V PE	640908	Australian Biosearch
Anti-Tubulin antibody	ab6160	Abcam
Bovine serum albumin	A9418-100G	Sigma Aldrich
Calcium chloride	CA01940500	Scharlau
Cell Proliferation ELISA, BrdU	11647229001	Sigma Aldrich
ChIP-Grade Protein G Magnetic Bead	CST.9006S	Genesearch eFreezer
Chloroform AR stabilized with Ethanol	CA038-2.5L	Chem Supply
CMTM8 Polyclonal Antibody	15039-1-AP	United Bioresearch
Complete EDTA free Protease Inhibitor cocktail tablets	4693132001	Sigma Aldrich

DAPI 10mg	D9542-10mg	Sigma Aldrich
DBL Dexamethasone Sodium Phosphate	163199	RAH Pharmacy
Difco LB Broth	240230	BD (Beckton Dickinson)
Dimethyl Sulfoxide (DMSO)	DA013-2.5L-P	Chem-Supply
Distilled water Ultrapure	10977015	Life Technologies
Dithiothreitol (DTT)	10197777001	Sigma Aldrich
DNASE1 amplification grade	18068015	Life Technologies
dNTP's mix (1mL of 10mM solution)	FISBIODN-10M/01	Adelab
Erlotinib 10mg	5083S	Genesearch efreezer
Ethanol 100% Undenatured	EA043-2.5L-P	Chem Supply
Ethanol 70% w/w (80%v/v)	AJA726-20L	Thermo Fisher
Ethanol Undenatured 80% v/v	EL156-20L-P	Chem Supply
Ethylenediaminetetraacetic acid (EDTA)	ED-500G	Sigma Aldrich
Faramount Aq mounting medium	S302580-2	Agilent Technologies
Foetal Bovine Serum 500mL Batch: F21701 (FCS)	AU-FBS/PG	CellSera
Formaldehyde, 40% (w/v)	FL010-10L-P	Chem Supply
Formalin, 10% neutral buffered	AJA2518-5L	Thermo Fisher
Glycerol (Glycerine)	GA010-2.5L-P	Chem Supply
Glycine	GA007-500G	Chem Supply
Haematoxylin	MHS1-100ML	Sigma Aldrich

Hanks' buffered saline solution (HBSS)	H9394-500ML	Sigma Aldrich
HEPES Solution 1 M, pH 7.0-7.6	H0887-100ML	Sigma Aldrich
Human HGF (HeK293)	100-39H-25	Lonza
Hydrochloric Acid 32%	HT020-500M	Chem Supply
Hydrogen Peroxide 30% H2O2	MERC1.07209.0500	BioStrategy
IgG2a: 200µg/mL	SANTSC-13119	bio-strategy (VWR)
KAPA2G Fast Genotyping Mix	KK5121	Sigma Aldrich
L-Ascorbic acid 2-phosphate	A8960-5G	Sigma Aldrich
L-Glutamine 200mM	G7513-100ml	Sigma Aldrich
LIPOFECTAMINE 3000	L3000015	Life Tech Supply Centre
LIPOFECTAMINE RNAIMAX	13778150	Life Technologies
Methanol	MA004-2.5L-P	Chem Supply
N,N,N,N-tetramethylethylenediamine (TEMED)	T9281-100ML	Sigma Aldrich
Negative control siRNA 5nmol	4390843	Life Technologies
Nonidet® P40 substitute	74385	FLUKA BioChemika
Oligo-dT	18418012	Life Technologies
Paraformaldehyde	P6148-500G	Sigma Aldrich
PBS	D8537-500ml	Sigma Aldrich
Penicillin/Streptomycin	P4333-100ML	Sigma Aldrich
pGem-Teasy Vector System	A1360	Promega eFreezer
Pico Green DNA Kit	P11496	Life Technologies

Precision Plus Protein Dual Color Standards	1610374	Bio-Rad
Propan-2-ol-AR (isoPropyl Alcohol)	PA013-2.5L-P	Chem Supply
Protein Assay Reagent A	5000113	Bio-Rad
Proteinase K	25530-015	Life Technologies
QIAquick PCR Purification Kit	28104	Qiagen
Rabbit IgG, poly - Isotype Ctrl (ChIP Grade)	ab171870	Abcam
Random Hexamers	RP-6	Geneworks
RC reagent I	5000117	Bio-Rad
RC reagent II	5000118	Bio-Rad
Recombinant human EGF	AF-100-15	Peprotech
Recombinant human HGF	100-39H-25	Lonza
Recombinant Human Insulin 100mg	91077C-100MG	Sigma Aldrich
Roche Glycogen 20mg/mL	10901393001	Sigma Aldrich
RT2 SYBR Green ROX qPCR Mastermix	330523	Qiagen
Senescence β-Galactosidase Staining Kit	9860S	Genesearch eFreezer
Sodium Acetate anhydrous (di sodium hydrogen)	SA005-500G	Chem Supply
Sodium azide	8591	Sigma Aldrich
Sodium bicarbonate	S6014-1KG	Sigma Aldrich
Sodium carbonate	SA099-500G	Chem Supply

Sodium chloride LR 2.5L	SL046-2.5KG	Chem Supply
Sodium dodecyl sulphate (SDS)	11667289001	Sigma Aldrich
Sodium fluoride	1614002-1G	Sigma Aldrich
Sodium hydroxide, pellets	SA178-500G	Chem Supply
Sodium hypochlorite 8-12.5%	ST044-5L	Chem Supply
Sodium phosphate	342483-500G	Sigma Aldrich
Sodium pyrophosphate	P8010-500G	Sigma Aldrich
Sodium pyruvate 100mM	S8636-100ml	Sigma Aldrich
Sodium pyruvate 25G powder	P5280-25G	Sigma Aldrich
Sodium vanadate	S6508	Sigma Aldrich
Standard Molecular Grade Agarose	9010E	Scientifix
STRO-1	39-8401	Thermo Fisher
SUPERSCRIPT IV 10,000 units	18090050	Life Tech Supply Centre
Tris (Sigma-7-9®)	T1378	Sigma Aldrich
TRIS ultra-pure 99.9%	TRIS01-1KG	Chemsupply
TritonX-100	X100-1L	Sigma Aldrich
TRIzol®	15596018	Life Tech Supply Centre
Trypan blue (0.4%)	T8154-100ML	Sigma Aldrich
Trypsin 10x	T4174-100ML	Sigma Aldrich
Tween 20	P1379-500ML	Sigma Aldrich
α-Modified Eagle's medium (α-MEM)	M4526-500ML	Sigma Aldrich
β-glycerophosphate	G9422-50G	Sigma Aldrich
β-mercaptoethanol	21985-023	Life Technologies

2.2 Solutions, Buffer and Media for Cell Culture

2.2.1 Alpha Modified Eagle's Medium (α-MEM)

α-MEM (Sigma-Aldrich, M4526-500ML) was supplemented with 10% (v/v) FCS (Cell Sera, AU-FBS/PG), 50U/mL Penicillin, 5μg/mL Streptomycin (Sigma Aldrich, P4333-100ML), 1mM Sodium Pyruvate (Sigma Aldrich, S8636-100ml), 100μM L-ascorbate-2-phosphate (Sigma Aldrich, A8960-5G), 2mM L-Glutamine (Sigma Aldrich, G7513-100ml) and 10mM HEPES (Sigma Aldrich, H0887-100ML). The medium was subsequently filter-sterilised through a 0.2μm bottle top filter and stored at 4°C.

2.2.2 High Glucose Dulbecco's Modified Eagle's Medium (DMEM)

High Glucose Dulbecco's Modified Eagle's Medium (Sigma-Aldrich, D6546-500ML) was supplemented with 10% (v/v) FCS (Cell Sera, AU-FBS/PG), 50U/mL Penicillin, 5μg/mL Streptomycin (Sigma Aldrich, P4333-100ML), 1mM Sodium Pyruvate (Sigma Aldrich, S8636-100ml), 100μM L-ascorbate-2-phosphate (Sigma Aldrich, A8960-5G), 2mM L-Glutamine (Sigma Aldrich, G7513-100ml) and 10mM HEPES (Sigma Aldrich, H0887-100ML). The medium was subsequently filter-sterilised through a 0.2μm bottle top filter and stored at 4°C.

2.2.3 Osteogenic Inducing Medium

α-MEM (Sigma-Aldrich, M4526-500ML) was supplemented with 5% (v/v) FCS (Cell Sera, AU-FBS/PG), 50U/mL Penicillin, 5μg/mL Streptomycin (Sigma Aldrich, P4333-100ML), 1mM Sodium Pyruvate (Sigma Aldrich, S8636-100ml), 100μM L-ascorbate-2-phosphate (Sigma Aldrich, A8960-5G), 2mM L-Glutamine (Sigma Aldrich, G7513-100ml), 10mM HEPES (Sigma Aldrich, H0887-100ML), 10^{-7}M dexamethasone phosphate (RAH Pharmacy, 163199) and 1.8mM inorganic phosphate, KH_2PO_4 (BDH Chemicals, UK).

2.2.4 Adipogenic Inducing Medium

α-MEM (Sigma-Aldrich, M4526-500ML) was supplemented with 5% (v/v) FCS (Cell Sera, AU-FBS/PG), 50U/mL Penicillin, 5μg/mL Streptomycin (Sigma Aldrich, P4333-100ML), 1mM Sodium Pyruvate (Sigma Aldrich, S8636-100ml), 100μM L-ascorbate-2-phosphate (Sigma Aldrich, A8960-5G), 2mM L-Glutamine (Sigma Aldrich, G7513-100ml), 10mM HEPES (Sigma Aldrich, H0887-100ML), 0.5μM hydrocortisone (Sigma-Aldrich, St. Louis, MO, USA), 60μM indomethacin (Sigma-Aldrich, St. Louis, MO, USA) and 10^{-7} M dexamethasone phosphate (RAH Pharmacy, 163199).

2.2.5 Table 2.2 Culture Media

Cell type	Abbreviation	Supplements
BMSC	α-MEM	α-MEM (Sigma-Aldrich, M4526-500ML)
CBC	+	10% FCS (Cell Sera, AU-FBS/PG)
	additives	50U/mL, 5μg/mL Penicillin, Streptomycin (Sigma Aldrich, P4333-100ML)
		1mM Sodium Pyruvate (Sigma Aldrich, S8636-100ml)
		100μM L-ascorbate-2-phosphate (Sigma Aldrich, A8960-5G)
		2mM L-Glutamine (Sigma Aldrich, G7513-100ml)
		10mM HEPES (Sigma Aldrich, H0887-100ML)
HEK293T	High glucose DMEM	High glucose DMEM (Sigma-Aldrich, D6546-500ML)
		10% FCS (Cell Sera, AU-FBS/PG)

	+ additives	50U/mL, 5µg/mL Penicillin, Streptomycin (Sigma Aldrich, P4333-100ML) 1mM Sodium Pyruvate (Sigma Aldrich, S8636-100ml) 100µM L-ascorbate-2-phosphate (Sigma Aldrich, A8960-5G) 2mM L-Glutamine (Sigma Aldrich, G7513-100ml) 10mM HEPES (Sigma Aldrich, H0887-100ML)
JM109	LB media	10g/L Tryptone Peptone (Becton Dickinson, Sparks, MD, USA) 5g/L Yeast Extract (Becton Dickinson, Sparks, MD, USA) 10g/L NaCl (Sigma Aldrich, Castle Hill, Aus)
BMSC CBC	Osteogenic media	α-MEM (Sigma-Aldrich, M4526-500ML) 5% FCS (Cell Sera, AU-FBS/PG) 50U/mL, 5µg/mL Penicillin, Streptomycin (Sigma Aldrich, P4333-100ML) 1mM Sodium Pyruvate (Sigma Aldrich, S8636-100ml) 100µM L-ascorbate-2-phosphate (Sigma Aldrich, A8960-5G) 2mM L-Glutamine (Sigma Aldrich, G7513-100ml) 10mM HEPES (Sigma Aldrich, H0887-100ML) 10^{-7} M dexamethasone phosphate (RAH Pharmacy, 163199) 1.8mM inorganic phosphate, KH_2PO_4 (BDH Chemicals, UK)

BMSC	Adipogenic media	α-MEM (Sigma-Aldrich, M4526-500ML) 5% FCS (Cell Sera, AU-FBS/PG) 50U/mL, 5μg/mL Penicillin, Streptomycin (Sigma Aldrich, P4333-100ML) 1mM Sodium Pyruvate (Sigma Aldrich, S8636-100ml) 100μM L-ascorbate-2-phosphate (Sigma Aldrich, A8960-5G) 2mM L-Glutamine (Sigma Aldrich, G7513-100ml) 10mM HEPES (Sigma Aldrich, H0887-100ML) 0.5μM hydrocortisone (Sigma-Aldrich, St. Louis, MO, USA) 60μM indomethacin (Sigma-Aldrich, St. Louis, MO, USA) 10^{-7} M dexamethasone phosphate (RAH Pharmacy, 163199)

2.2.6 Table 2.3 Cell Culture Buffers

Buffer Name	Components
1x PBS	MilliQ water (Media production unit, IMVS)
	10% Phosphate Buffered Saline, Ca^{+}/Mg^{+} free (Sigma-Aldrich, USA)
HHF Buffer	Hanks' Buffered Saline Solution (Sigma Aldrich, H9394-500ML)
	5% FCS (Cell Sera, AU-FBS/PG)
	50 U/mL, 5µg/mL Penicillin, Streptomyciin (Sigma-Aldrich, USA)
Blocking Buffer	HHF
	5% normal human serum (Red Cross, SA, Australia)
FACS Buffer	1x PBS
	3% FCS (Cell Sera, AU-FBS/PG)
	5mM EDTA
MACS Buffer	1x PBS
	1% BSA (SAFC, Lenexa, KS, USA)
	5mM EDTA (Merck, Kilsyth, VIC, Australia)
	0.01% sodium azide

2.2.7 Cell Culture Conditions

All cell culture procedures were conducted in a Class II laminar flow hood (Top Safe 1.2, Bio Air, Siziano, Italy). Cells cultured for expansion were maintained in MCO-18AIC Sanyo CO_2 incubators (Sanyo Oceania, North Ryde, NSW, Australia), at 37°C, 5% CO_2 in a humidified environment. Eppendorf 5810 centrifuge (Eppendorf South Pacific, North Ryde, NSW, Australia) was used for centrifugation of cell suspensions during expansion. The use of cells obtained from human subjects was approved by the Royal Adelaide Hospital ethics committee under protocol numbers 940911a and REC1033/06/2019.

2.2.8 Isolation of Mesenchymal Stem Cells Using Magnetic Activated Cell Sorting (MACS)

This MSC isolation method was based on the protocol described previously [197]. Following informed consent in accordance with procedures approved by the Human Ethics Committee of the Royal Adelaide Hospital, South Australia (protocol number 940911a), approximately 40mL of human bone marrow was aspirated from the posterior iliac crest of healthy young volunteers (18-35 years old). The samples were then diluted with an equal volume of blocking buffer (HHF supplemented with 5% (v/v) normal human serum), mixed well and strained through a 70μm cell strainer (Becton Dickinson Biosciences, San Jose, CA, USA). Lymphoprep density gradient separation was performed to isolate the mononuclear cells as described in section 2.2.9. Cells were then pooled and enumerated using a haemocytometer. Following enumeration, cells were resuspended in 500μL of STRO-1 supernatant per 5 x 10^7 cells and incubated on ice for one hour with occasional agitation. Cells were then washed twice in HHF wash buffer and resuspended in 0.5mL HHF containing biotinylated goat anti-mouse IgM (Southern Biotechnology Associates, Birmingham, UK) and incubated at 4°C for 45 minutes. The cells were then washed three times in MACS buffer (Ca^{2+} and Mn^{2+} free PBS

was supplemented with 1% BSA in PBS, 5mM EDTA and 0.01% sodium azide) before being resuspended in 450µL of MACS buffer to which 50µL of streptavidin microbeads (Miltenyi Biotec, Bergisch Gladbach, Germany) were added (10µL of microbeads/10^7 cells in 90µL MACS buffer). The mixture was incubated on ice for 15 minutes before being washed once in ice-cold MACS buffer and loaded onto the mini MACS column (Miltenyi Biotec, MS column). Cells reactive to STRO-1 antibody were bound to the magnetised matrix of the column. The column was washed three time with 500µL MACS buffer to remove any non-specifically bound STRO-1^- cells. The column was removed from the magnetic field and the STRO-1^+ cells were collected by flushing the column with 1mL of MACS buffer. The STRO-1^+ cells were then culture expanded as described in section 2.2.9.

2.2.9 Culture of Human BMSC

Following immunoselection with STRO-1, bone marrow cells were cultured in 75cm^2 tissues culture flasks at 30 x 10^3 cell per cm^2 in α-MEM + additives, at 37°C in a humidified environment supplemented with 5% CO_2. Cells were cultured to 80-90% confluence at which time; cells were harvested by enzymatic digestion with 0.05% trypsin (2.2.12) (SAFC, Lenexa, KS, USA) then used for experiments or reseeded (8 x 10^3 cell per cm^2) for further expansion.

2.2.10 Isolation of Human CBC

Human parietal bone calvarial cells were derived from the cranium of donors with informed consent by the Human Ethics Committee of the Women's and Children's Hospital, South Australia (Approval number REC1033/06/2019) as described in [198].

2.2.11 Culture of Human CBC

Human CBC were obtained by collagenase digestion and explant culture following the method described by [199]. Briefly, dissected suture CBC samples were minced into 1mm fragments and incubated in 0.25% collagenase for 2 hours at 37°C. Samples were centrifuged and supernatant removed. Following three washes in 1 x PBS, samples were plated at 5 bone fragments per well, in 12-well plates, and cultured in α-MEM + additives, at 37°C in a humidified environment supplemented with 5% CO_2. Cells were cultured to 80-90% confluence at which time; cells were harvested by enzymatic digestion with 0.05% trypsin (2.2.12) (SAFC, Lenexa, KS, USA) then used for experiments or reseeded (8 x 10^3 cell per cm^2) for further expansion.

2.2.12 Trypsin Digestion

Trypsin was used to detach cells from the surface of tissue culture flasks. Briefly, culture media was aspirated and cells were washed once with PBS or Hanks' solution to remove any remaining proteins. Enough 0.05% trypsin solution (SAFC, Lenexa, KS, USA) was added to cover the cells. Cells were incubated at 37°C for 3-5 minutes to enable enzymatic digestion of proteins bonding the cultured cells to the tissue culture flask.

2.2.13 Adherent Retroviral HEK293T Packaging Cell Line

Cells were cultured in T75 tissue culture flasks in high glucose DMEM + additives, at 37°C in a humidified environment supplemented with 5% CO_2. Cells were cultured to 80-90% confluence at which time; cells were harvested by enzymatic digestion with 0.05% trypsin (SAFC, Lenexa, KS, USA) then used for experiments or reseeded (8 x 10^3 cell per cm^2) for further expansion.

2.2.14 Cryopreservation of Cells

Cells were cryopreserved in FCS containing 10% (v/v) of dimethyl sulfoxide (DMSO; Chem Supply DA013-2.5L-P). Immediately prior to freezing, 1ml of pre-prepared ice cold FCS 20% DMSO solution was added drop wise to ~1 x 10^6 cells in 1mL of FCS on ice. Cell suspension were then transferred to 2mL ampoules and cryopreserved in a Mr. Frosty (C1562 Freezing Container, Nalgene, USA) placed into a -80°C freezer for at least 4 hours. The Mr. Frosty freezing container ensures the cells are cooled at the appropriate rate of 1°C per minute. Once at -80°C the ampoules were then transferred to the vapour phase of liquid nitrogen for extended storage at -196°C.

2.2.15 Thawing of Cryopreserved Cells

Cells were removed from liquid nitrogen (-196°C) and immediately thawed in a 37°C water bath. Once thawed, cell suspension in FCS 10% (v/v) of DMSO were immediately transferred to a 14mL polypropylene tube containing 11mL of appropriate growth media. This preparation was centrifuged at 1,400 x g for 5 minutes at 4°C. Cell pellets were then resuspended in 10mL of appropriate growth media and plated at a density of 8 x 10^3 cells/cm^2.

2.2.16 Counting Cells

Washed cells were resuspended in 1mL of appropriate media. From this cell suspension, 10µL was removed for counting. Depending on the estimated cell number, a dilution factor between two and ten was used to count cells. Cells were counted using trypan blue (Sigma Aldrich, Castle Hill, Australia). Trypan blue enters the cell membranes of dead cells and all cells that are not blue can be counted as live cells. To obtain an accurate cell number at 100 cells were counted using a haemocytomoter.

2.2.17 Table 2.4 Cytokines and Inhibitors Used In This Study

Cytokine	Source
Human Recombinant EGF	(Peprotech, AF-100-15)
Human Recombinant HGF	(Lonza, 100-39H-25)
Human Recombinant Insulin	(Sigma Aldrich, 91077C-100MG)
Erlotinib	(Genesearch, 5083s)

All cytokines were reconstituted according to manufacturer's instructions and diluted to the appropriate concentration in serum-free media or PBS as required and stored at -80°C.

2.3 Chromatin Immunoprecipitation

Human BMSC (1×10^6) from were cultured under growth, osteogenic or adipogenic inducing conditions for 7 days and chromatin immunoprecipitation (ChIP) performed using the Magna ChIP kit (Millipore Corporation, Billerica, MA, www.merckmillipore.com.au) in accordance with manufacturer's instructions. Briefly, when cells reached 80-90% confluence, 37% formaldehyde was added dropwise (final concentration 0.75%) for 10 minutes at room temperature to crosslink protein and DNA within the cells. After 10 minutes, glycine was added (final concentration 125mM) to the media and incubate for 5 minutes at room temperature to quench the formaldehyde and terminates the crosslink reaction. Cells were then centrifuged (1,000 x g, 4°C, 5 minutes) and washed twice with ice cold 1 x PBS. Cell pellets were scraped from each flask, transferred to 14mL propylene tubes and centrifuged (1,000 x g, 4°C, 5 minutes). Supernatant was removed and cells were resuspended in 400µl cells lysis buffer containing 1:10 dilution of protease inhibitor cocktail. Resuspended lysed cells were sonicated using a Bioruptor bath sonicator (Diagenode, Liège, Belgium) at 3 watts for 30 seconds in an

ice bath to obtain crosslinked DNA from ~200-500bp in length. Sonicated samples were centrifuged (8,000 x g, 4°C, 15 minutes) to remove any insoluble material, transferred to fresh microcentrifuge tubes and stored at -80°C.

When required, sheared crosslinked chromatin was thawed on ice and diluted with 600µl RIPA buffer containing 1:10 dilution of protease inhibitor cocktail. At this stage, 10µl of sample was removed to be used as an input control and stored at 4°C. Samples were pre-clear with 20µl protein G-conjugated magnetic beads (9006S, Cell Signalling, Danvers, Massachusetts, USA) at 4°C for 2 hours. A magnetic rack was used to separate magnetic bead/antibody/chromatin complex out of the solution and supernatant transferred to new microcentrifuge tubes. An anti-mouse TWIST-1 antibody (ab50887, 1µg, Abcam, Melbourne, Victoria), anti-rabbit EZH2 antibody (49-1043, 1µg, Life Technologies, Mulgrave, VIC, Australia) and anti-IgG control antibodies (normal mouse IgG and normal rabbit IgG, 1µg), were added to respective samples and incubate overnight at 4°C with constant rotation. Magnetic bead/antibody/chromatin complex were separated out of the solution and supernatant transferred to new microcentrifuge tubes. Magnetic bead/antibody/chromatin complex were washed three times in 1mL of Low Salt Immune Complex Wash Buffer and three times in High Salt Immune Complex Wash Buffer. Washed protein/DNA complexes were incubated at 65°C in 120µl ChIP elution buffer/1µl Proteinase K for 4 hours with shaking at 800rpm to reverse protein/DNA crosslinks and bonds between antibodies and magnetic beads. Samples were cooled to room temperature, magnetic beads were isolated and supernatant containing DNA transferred to a fresh microcentrifuge tube. DNA was purified using QIAquick PCR Purification Kit (28104, Qiagen, USA) in accordance with manufacturer's instructions. Immunoselected genomic DNA was then used in real-time PCR as previously described [2].

2.3.1 Table 2.5 ChIP primers

Gene	Accession No.	Fwd 5' -3'	Rev 5'-3'
EZH/CMTM8_S1	NM_178868.5	aggaaataacaccgggctct	tgatgtggtacctcgaatgc
EZH/CMTM8_S2	NM_178868.5	ctgggaagaaagggttgtga	cacgtggagatcaggtgaga
EZH/HOPX_S1	NM_001145459.1	tgctcatctgttggaaaacg	caactccccttcctccaaat
EZH/HOPX_S2	NM_001145459.1	tcccacagatgatctcacca	tgcatgcagagtgtgacaga
EZH/HOPX_S3	NM_001145459.1	aagcccacaggtggaagttt	gttccccgcaagacaagtta
GAPDH	NM_002046.7	tgtcagtgcgttccagtctc	aggaacaggagggaaaagga
POSTN	NM_006475.3	ctctggaaaggattgcagaat	agttgtgggagggaacactg
P14TSS	NM_000077.4	ggagcgatgtgatccgttatc	tgaaatcccaatcgtcttccac
TWIST/CMTM8_S1	NM_178868.5	ctcccaaagtgctgggatta	gcccaggagtttgtggttac
TWIST/CMTM8_S2	NM_178868.5	cacaaactcctgggcttga	cagtactgtgagaggccaagg
TWIST/CMTM8_S3	NM_178868.5	ggatatcaattgtcccagca	cagcatggtactggcataaga

2.3.2 Table 2.6 Antibodies Used in ChIP

Anti-rabbit EZH2	(49-1043, Life Technologies, Mulgrave, VIC, Australia)
Anti-mouse TWIST	(ab50887, Abcam, Melbourne, Australia),
Normal Mouse IgG	(12-371, Sigma Aldrich, St Louis, MO, USA),
Normal Rabbit IgG	(ab171870, Abcam, Melbourne, Australia)

2.3.3 Table 2.7 ChIP Buffers

Buffer Name	Components
Cell Lysis Buffer	50mM HEPES KOH pH7.5
	140mM NaCl
	1mM EDTA pH8
	1% Triton X-100
	0.1% Sodium Deoxycholate
	0.1% SDS
	1 x Protease Inhibitors
RIPA Buffer	50mM Tris-HCl pH8
	150mM NaCl
	2mM EDTA pH8
	1% NP40
	0.5% Sodium Deoxycholate
	0.1% SDS
	1 x Protease Inhibitors
Low Salt Immune Complex Wash Buffer	0.1% SDS
	1% Triton X-100
	2mM EDTA pH8

	150mM NaCl 20mM Tris-HCl pH8
High Salt Immune Complex Wash Buffer	0.1% SDS 1% Triton X-100 2mM EDTA pH8 500mM NaCl 20mM Tris-HCl pH8
Elution Buffer	1% SDS 100mM $NaHCO_3$

2.4 Molecular Biology Techniques

RNATechniques

2.4.1 Preparation of Total Cellular RNA

Total cellular RNA was extracted from 0.2–5 x 10^6 cells using the TRIzol® Method (Invitrogen, Australia). Briefly, cells were washed in 1 x PBS, and lysed in 1mL TRIzol® solution. The RNA was extracted by the addition of 1/5 volume of chloroform, mixed with vigorous shaking, and incubated for 3 minutes at RT. Samples were centrifuged at 12,000 x g for 5 minutes at 4°C to separate phases, and the aqueous phase (containing RNA) was carefully removed and transferred to a fresh RNase-free 1.5mL eppendorf tube. Total RNA was precipitated by the addition of 500µL isopropanol and 2µL ribonuclease (RNase)-free

glycogen, and incubated on ice for 10 minutes or overnight at 4°C. The RNA was pelleted by centrifugation at 12,000 x g for 15 minutes at 4°C, washed with 75% (v/v) ethanol before being centrifuged at 7,500 x g for 5 minutes at 4°C. The RNA was resuspended in 10µL RNase-free DEPC-treated Milli-Q water and heated to 60°C for approximately 10 minutes to facilitate solubilisation of RNA. The RNA was used immediately for cDNA synthesis or stored at -80°C until required.

2.4.2 Determination of RNA Concentration and Purity

The concentration of RNA in solution was determined by measuring the absorption at 260nm on a UV spectrophotometer (Nanodrop-8000, Thermo Fisher Scientific, USA), assuming that an A260 of 1.0 represents 40µg/mL of RNA. The purity of the RNA was determined by the ratio of A260:A280, where a ratio of >1.8 is considered to represent highly pure RNA. The A260:A280 were consistently in the range of 1.8-2.

2.4.3 Synthesis of Complementary DNA (cDNA)

Total cellular RNA was extracted from cell lines with TRIzol® as described in Section 2.4.1. Total RNA (1µg) was reverse transcribed into single-stranded cDNA using Superscript IV (Invitrogen, Australia) according to manufacturer's instructions. Briefly, 1µL oligo(dT), 1 µg total RNA, 1µL dNTP mix, 250ng/µL random hexanucleotide primers and distilled water to a total volume of 13µL was added to each microcentrifuge tube. This mixture was heated to 65°C for 5 minutes and then incubated on ice for at least 1 minute in order to denature the RNA. The heat denatured RNA was added to 4µL of 5x first strand buffer, 1µL of 0.1M DTT solution and 1µL Superscript IV enzyme (Invitrogen, Australia). The reaction mixture was incubated for 10 minutes at 23°C then 10 minutes at 45°C and finally at 80°C for 10 minutes. The cDNA

samples were then diluted 1:10 with RNase-free DEPC-treated water and either used immediately for PCR or frozen at –20°C.

2.4.4 Real-Time Polymerase Chain Reaction (PCR)

Real-Time PCR reactions were performed in a CFX Connect Real-Time PCR Detection System (Bio-Rad) according to the parameters outlined in Table 2.8. For each reaction, 2µL of cDNA (previously diluted 1:10 with RNase-free DEPC-treated water) was used in a reaction mixture containing 4.75µL RNase-free DEPC-treated water, 0.75µL forward and reverse primer (10µM working stock) and 7.5µL Sybr Green Mix (Qiagen, 330523).

2.4.5 Table 2.8 Cycling Parameters for Real-Time PCR

50°C - 2 min
95°C - 15 min (enzyme activation)
Cycling 95°C - 15 sec (denaturation)
60°C - 30 sec (primer annealing) 48-52 cycles
72°C - 10 sec (primer extension)
72°C - 30 sec (final extension)
Melt cycle stepwise increase in temperature from 65°C to 95°C with an increment of 0.5°C

2.4.6 Table 2.9. Real-time PCR Primers Used In This Study (Human)

Gene	Accession No.	Fwd 5'-3'	Rev 5'-3'
ADIPOQ	NM_009605.4	cctaagggagacatcggtga	gtaaagcgaatgggcatgtt
ADIPSIN	NM_001928.4	gacaccatcgaccacgac	ccacgtcgcagagagttc
AOC3	NM_003734.4	gtctttgtccccatggct	cacttgttgctgtggttgct
C/EBPα	NM_004364.4	gggcaaggccaagaagtc	ttgtcactggtcagctccag
C-MET	NM_001127500.3	acatccagtaccctgatgctacag	gtgggtttcagcactctggt
CMTM8	NM_178868.5	tgggcctgtgctttaacgg	gtatttccagcgtagcagatgg
CNN1	NM_001299.6	aggctccgtgaagaagatca	ccacgttcaccttgtttcct
COL4A1	NM_001845.6	ccattggtgacaaaggacaa	gaaagcctcggtctccttg
E-CAD	NM_004360.5	ggccaggaaatcacatccta	ctcaaaatcctccctgtcca
EZH2	NM_004456.4	actgctggcaccgtctgatg	cctgagaaataatctccccacag
FABP4	NM_001442.3	tactgggccaggaatttgac	gtggaagtgacgcctttcat
G0S2	NM_015714.4	ggaagatggtgaagctgtacg	cttgcttctggagagcctgt
GPD1	NM_005276.4	aaacgccactggcatatctc	tttggtgtctgcatcagctc
HOPX	NM_001145459.1	tcaacaaggtcgacaagcac	gtgacggatctgcactctga
KRT19	NM_002276.5	ctgaaggaagagctggccta	tcatattggcttcgcatgtc
OPN	NM_001040058.2	gcagacctgacatccagtacc	gatggccttgtatgcaccattc
PLIN1	NM_002666.5	ctctcgatacaccgtgcaga	tggtcctcatgatcctcctc
PLIN4	NM_001367868.2	ccttcggaaaagatggtgtc	taagtgcagaccgagtggtg
RUNX2	NM_001024630.4	gtggacgaggcaagagtttca	catcaagcttctgtctgtgcc
SLUG	NM_003068.5	catgccattgaagctgaaaa	ggtaatgtgtgggtccgaat
TWIST-1	NM_000474.4	tcttacgaggagctgcagacgca	atcttggagtccagctcgtcgct
VIMENTIN	NM_003380.5	gaaattgcaggaggagatgc	tcctggatttcctcttcgtg
β-ACTIN	NM_001101.3	gatcattgctcctcctgagc	gtcatagtccgcctagaagcat

2.5 Molecular Biology Buffers and Reagents

2.5.1 Diethyl Pyrocarbonate (DEPC)-Treated (RNase-free) Milli-Q Water

Milli-Q water for RNA and cDNA work was treated with 0.1% (v/v) DEPC (Sigma, USA), a potent inhibitor of RNases. The mixture was incubated overnight at RT, and then autoclaved to remove all traces of DEPC that might otherwise modify purine residues in RNA by carboxymethylation.

2.5.2 Luria Broth (L-Broth)

A broth containing 1% (w/v) Bacto-tryptone (Becton Dickinson, USA), 0.5% (w/v) yeast extract (Becton Dickinson, USA), and 1% (w/v) NaCl was prepared in Milli-Q water. The solution was pH adjusted to pH 7.0 with NaOH, and sterilised by autoclaving on a fluid cycle. The broth was stored at RT until required.

2.5.3 LB Agar

1.5% (w/v) Bacto-agar (Becton Dickinson, USA) was dissolved in L-broth, autoclaved on a fluid cycle and cooled with gentle mixing to prevent solidification. Ampicillin (100μg/mL) was added to the LB agar when cool enough to handle, and plates poured into 100mm bacterial-grade petri dishes. LB agar plates were stored at 4°C. 10g/L Tryptone Peptone (Becton Dickinson, Sparks, MD, USA), 5g/L Yeast Extract (Becton Dickinson, Sparks, MD, USA), 10g/L NaCl (Sigma Aldrich, Castle Hill, Aus).

2.5.4 SDS "Running Buffer" for Electrophoresis

A buffer comprising 0.3% (w/v) Tris-HCl, 1.44% (w/v) Glycine, 0.1% (w/v) SDS was prepared in water, then the solution was pH adjusted to pH 8.3 and stored at RT.

2.5.5 SDS-PAGE "Transfer Buffer" for Electrophoresis

A buffer comprising 0.3% (w/v) Tris-HCl, 1.44% (w/v) Glycine, 15% Methanol (v/v), and 0.1% SDS was prepared in water, pH adjusted to pH 8.3 and stored at 4°C. Each batch of transfer buffer was used twice and then discarded.

2.6 Retroviral Transfection and Infection Techniques

2.6.1 Cloning and Expression Vectors

(a) pRUFiG2-IRES-GFP (Figure 2.1) - a 6071 base pair MMLV-based retroviral vector was a kind gift from Mr Paul Moretti (Hanson Institute, South Australia). This vector was used to create the *HOPX*, and *CMTM8* over-expressing cell lines.

(i) pRUFiG2-IRES-GFP-HOPX - The HOPX coding region (NCBI Accession number: NM_001145459.1) was generated from cDNA synthesized from HOPX high expressing BMSC and cloned into pGem®-T Easy vector. HOPX coding region was then excised from pGem®-T Easy using BamHI and XhoI enzymatic digestion, blunt-ended using Klenow fragment and ligated into the pRUFiG2-IRES-GFP vector, which had been digested with BamHI and XhoI.

(ii) pRUFiG2-IRES-GFP-CMTM8 - The CMTM8 coding region (NCBI Accession number: NM_178868.5) was generated from cDNA synthesized from HOPX high expressing BMSC and cloned into pGem®-T Easy vector. CMTM8 coding region was then excised from pGem®-T Easy using BamHI and XhoI enzymatic digestion, blunt-ended using Klenow fragment and ligated into the pRUFiG2-IRES-GFP vector which had been digested with BamHI and XhoI.

DNA Techniques

2.6.2 Preparation of Chemically Competent DH5α Cells

A single colony was inoculated into 10mL L-Broth grown overnight in a 37°C shaking incubator. This starter culture was then used to inoculate 200mL L-Broth and was grown at 37°C, shaking until the culture reached $OD_{600} = 0.6$. The bacteria were incubated on ice for 30 minutes, then pelleted at 3,000 x g, 4°C for 5 minutes. The cells were then resuspended in 25mL ice-cold 0.1M $MgCl_2$ and pelleted again at 3,000 x g, 4°C for 5 minutes. Cells were resuspended in 8mL ice-cold 0.1M $CaCl_2$ + 15% glycerol and incubated on ice for 1 hour. Aliquots were frozen and stored at -80°C until required.

2.6.3 Transformation of Competent Cells

For transformation of ligations into competent E.coli, 10µL of the ligation reaction (Section 2.6.7) was added to 100µL competent cells, mixed gently and incubated on ice for 30 minutes. The cells were then heat-shocked at 42°C for 90 seconds and then placed back on ice for 5 minutes. After incubation, 200µL SOC medium was added to the cells and incubated for 30 minutes in a 37°C shaking incubator. Of this mixture, 100µL was plated onto L-Agar plates containing 100µg/mL Ampicillin and incubated at 37°C overnight. Transformed colonies were picked and used to inoculate L-broth for subsequent plasmid purification.

2.6.4 Preparation of Glycerol Stocks

Glycerol stock cultures of log phase bacterial cultures were prepared by the dilution of an overnight culture in an equal volume of 80% (v/v) glycerol and stored at -80°C for long term storage.

2.6.5 Purification of Plasmid DNA from Bacterial Cultures

2.6.5.1 Small Scale Plasmid DNA Extraction (Mini-Prep)

Mini-Prep DNA extractions were performed according to manufacturer's instructions using the Qiagen Plasmid Midi-prep kit (Qiagen, USA).

2.6.5.2 Medium Scale Plasmid DNA Extraction (Midi-Prep)

Midi-Prep DNA extractions were performed according to manufacturer's instructions using the Qiagen Plasmid Midi-prep kit (Qiagen, USA).

2.6.6 Manipulation of DNA Products

2.6.6.1 Quantitation of DNA

The concentration of DNA in solution was determined by measuring the absorption at 260nm on a UV spectrophotometer (Nanodrop-8000, Thermo Fisher Scientific, USA), assuming that an A260 of 1.0 represents 50μg/mL of DNA (1cm light path).

2.6.6.2 Restriction Digestion of DNA

Restriction digestion of DNA were performed by digesting 1μg of DNA with 10 units of restriction enzyme in the presence of 1x digestion buffer in a total reaction volume of 10μL. The reaction was incubated at 37°C for 1-2 hour.

2.6.7 DNA Ligation

Ligations were routinely carried out in a total volume of 10μL containing DNA insert:vector of 3:1 (molar ratio), 1x ligation buffer (50mM Tris HCl pH 7.8, 10mM MgCl2, 10mM DTT, 1mM ATP) and 2 units of T4 DNA ligase at RT for 2 hours.

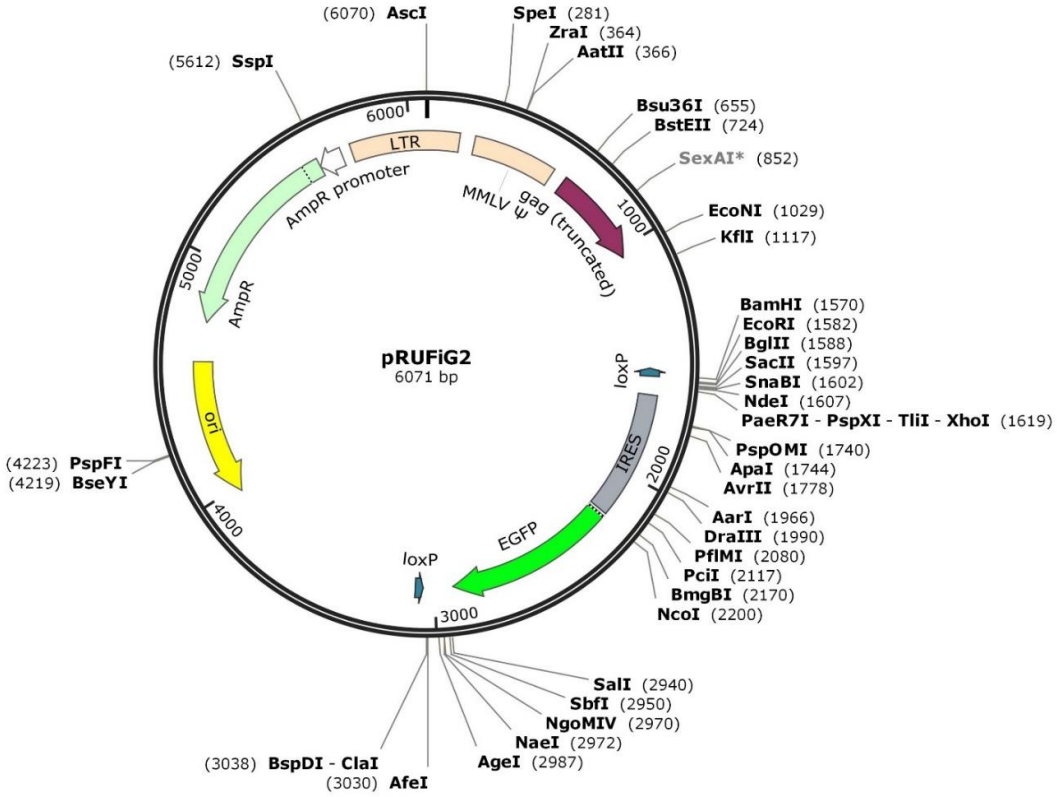

Figure 2.1 The pRUF-IRES-GFP Mammalian Expression Vector. This 6071bp retroviral vector was used to create the *HOPX* and *CMTM8* overexpressing BMSC.

2.6.8 DNA Sequencing

A PCR reaction using the conditions described below (table) was used to amplify target DNA. Following PCR, samples were transferred to a 1.5mL Eppendorf tube containing 80µL 75% isopropanol and 1µL Glycogen (29mg/mL). These samples were incubated for 15 minutes at room temperature away from light before DNA was pelleted by centrifugation at 16,000 x g for 15 minutes at room temperature. Supernatant was then aspirated and DNA pellets washed with 200µL 75% ethanol before being centrifuged at 16,000 x g for 2 minutes. Ethanol was aspirated and pellets allowed to dry for 10 minutes. Samples were then delivered to AGRS sequencing centre and stored at -20°C until analysed.

2.7 Transfection and Infection Techniques

2.7.1 Transfection of HEK293T Packaging Cell Line with GFP-Encoding Plasmids

Twenty four hours prior to transfection, 6cm tissue culture dishes were seeded with 2 x 10^6 HEK293T cells in a volume of 3mL of high glucose DMEM-10 (equating to approximately 50-60% confluence on the day of transfection) and incubated in a humidified environment at 37°C in the presence of 5% CO_2. At the time of transfection, the media was removed from the dishes and replaced with 2mL of high glucose DMEM. The following two mixtures were prepared for each 6cm tissue culture dish – Mix 1: 5µg retroviral GFP plasmid DNA and 5µg pEQPAM3 plasmid (encoding GAG, Pol and viral envelope protein) in 500µL serum-free DMEM; Mix 2: 13µL Lipofectamine 3000 (Invitrogen, USA) added drop-wise to 500µL serum-free DMEM. Mix 2 was incubated at RT for 5 minutes, then added drop-wise to Mix 1. This DNA/Lipofectamine mixture was incubated for a further 20 minutes at RT, at which point it was added drop-wise to the HEK293T cells. The cells were incubated in a humidified environment at 37°C in the presence of 5% CO_2 for 48 hours, and the efficiency of the transfection was assessed under a UV microscope (Olympus, Japan).

2.7.2 Viral Infection of Cells

At 48 hours post-transfection, the supernatant from the HEK293T cells (containing viral particles) was filtered through a 0.45μm low protein binding syringe filter (Nalgene, USA) to remove any cellular debris, diluted 1:1 with fresh media (in which the cells to be infected are grown) and 4μg/mL polybrene (Sigma, USA) was added immediately prior to its addition to the cells. The cells to be infected were plated at 2 x 10^5 cells/mL. Infection was repeated two times after every 24 hours. After three times of viral infection, the viral supernatant was removed, and the cells were cultured in their normal growth medium. GFP expression was assessed using a UV microscope (Olympus, Japan). The infected cells were then sorted for GFP expression by FACS, using a BD FACSAria™ Fusion flow cytometer (http://www.bdbiosciences.com).

2.8 siRNA Knockdown Transfections

BMSC were seeded at 2.2 x 10^4 cells per well (24-well plate) the day before siRNA knockdown was performed. Sequence specific siRNAs against *HOPX* and *CMTM8* (Ambion/Life Technologies, Mulgrave, VIC, Australia, http://www.lifetechnologies.com/) were used at 12pM to achieve a > 90% knockdown of transcript levels. The siRNA used in this study were: *HOPX* s39106, *HOPX* s39107, *CMTM8* s45676, *CMTM8* HSS135801 and Silencer® Select Negative Control #1 siRNA. The procedure was performed following manufacturer's instructions with a 72 hours incubation period before performing functional assays.

2.8.1 Table 2.10 siRNA Used In This Study

siRNA	Catalogue No.	Supplier
siHOPX	s39106, s39107, s39108	Life Technologies
siCMTM8	s45676, HSS135801	Life Technologies

2.9 Functional Analysis of *HOPX* and *CMTM8* overexpressing MSC

2.9.1 BrdU Proliferation assay

Proliferation (4 to 6 days) was performed as per the manufacturer's instructions using the Cell Proliferation ELIZA, BrdU kit (11647229001; Roche Diagnostics Corporation, Indianapolis, IN).

2.9.2 Senescence Assay

A Cell Signalling Technology's Senescence Assay Kit was used to measure the presence of senescence-associated β-galactosidase (Cell Signalling Technology, Boston, MA, USA). Growth media was removed and cells were rinsed once with 1 x PBS. Rinsed cells were fixed with 1mL of 1 x Fixative Solution and incubated at room temperature for 15 minutes. Following fixation, cells were rinsed twice with 1 x PBS before 1mL of β-galactosidase staining solution was added to each well and plates incubated at 37°C overnight in a dry-air incubator. Once stained, cells were enumerated manually.

2.9.3 Assessment of Osteogenic Differentiation Potential

In vitro mineralization assays were performed as previously described [46, 52]. Briefly, BMSC or CBC were seeded at 8 x 10^3 cells/cm^2 in 24 well plates and cultured in mineralization media for up to 28 days with media changes twice weekly. At 18-28 days the well were washed three

times in 1x PBS and fixed with 10% Neutral Buffered Formalin (NBF) (Thermo Fisher, AJA2518-5L) for 1 hour. Mineralized cultures were stained with 2% Alizarin Red S (Sigma Aldrich Inc., St Louis, MO, USA) in RO water. For quantitative assessment of mineral deposition, cells were seeded at 8 x 10^3 cells/cm^2 in 96 well plates and cultured in mineralization induction media for up to 28 days with media changes twice weekly. At 18-28 days the well were washed three times in 1 x PBS and the mineralized matrix dissolved in 100µL of 0.6M HCL (Merck, Kilsyth, VIC, Australia) for 1 hour at room temperature. The dissolved mineral solution was then transferred to 96 well microtitre plates and calcium levels were quantitated using the Arsenazo III (C7529-500 PT, PM Separations). Briefly, 4µL of each supernatant was transferred to a single well of a fresh microtitre plate. A calcium chloride (calcium/hosphorous combined standard (Sigma Aldrich, St Louis, MO, USA) standard curve was also established in triplicate. Arsenazo was added to each well at 200µL per well. The plates were shook to mix and incubated at room temperature for 1 minutes and the absorbance was read at 650nm on a microplate reader (iMark™ Microplate Absorbance Reader, BIO-RAD).

Following dissolution of the mineral with HCl, the wells were washed with 1x PBS and the cells were digested with 100µL of proteinase K (100µg/mL) (Invitrogen, Carlsbad, Canada) for 2-4 hours at 55°C. The cells were then triturated thoroughly to ensure complete disruption, 50µL volumes were transferred to a white 96 well microtitre plate (Costar, Corning, New York, NY, USA). DNA content per well was then quantified using the Pico Green assay as described in section 2.9.4.

2.9.4 Pico Green DNA Assay

Following digestion (2.9.3) 50µL of DNA standards (Table 2.3) were added to appropriate wells and 50µL of sample digests to appropriate wells. Pico Green stock was diluted 1:300 into 1x TE buffer. Diluted Pico Green (150µL) was added to all wells and the plate gently agitated to mix and protected from light (Quant-iT dsDNA Assay Kit, P11496, Invitrogen, Mulgrave, Victoria, Australia). The Plate was then read on the Victor^{TM} X4, PerkinElmer 2030 Multilabel Reader, under fluorescence settings with the following parameters.

2.9.5 Table 2.11 Microplate Pico Green Settings and High Molecular Weight DNA standards

Excitation filter:	485P
Emission filter:	520P
Gain:	1300
Optics:	3mm liquid light guides
Number of cycles:	1
Number of flashes:	10
Shake time:	10s on medium before reading cycle

Standards – High molecular weight DNA (Sigma, D4522, 5mg)

Prepare 10mg/mL stocks in sterile RO water and dilute standards to 5mg/mL, 2.5mg/mL, 1.25mg/mL, 0.625mg/mL, 0.312mg/mL and 0mg/mL.

2.9.6 Assessment of Adipogenic Differentiation Potential

Adipogenic assays were performed as previously described [46, 50]. BMSC were seeded at 8 x 10^3 cell/cm^2 in 24 well plates and cultured for 28 days in the presence of adipogenic media with media changes twice a week. At 28 days, the wells were washed three times with 1x PBS and cells fixed in 10% NBF for 1 hour at room temperature. Oil Red O staining solution was prepared by dissolving 0.5g of Oil Red O stain (MP Biomedicals, Solon, OH) in 100mL of isopropanol (Ajax Finechem, Taren Point, NSW, Australia) and further diluted 1.5:1 in RO water. Formation of lipid-laden fat cells was determined by Oil Red O staining. For quantitative assessment, overexpressing MSC were seeded at 8 x 10^3 cells/cm^3 in 96 well plates and were cultured for up to 28 days in the presence of adipogenic media with media changes twice a week. At the conclusion of the assay, wells were washed three times with 1x PBS, fixed in 10% Neutral Buffered Formalin for 1 hour at room temperature and stained with Nile Red and DAPI (4µg/mL) (Sigma Aldrich, Australia #N3013 and #D9542) before being imaged using an Olympus iX70 multi-wavelength inverted fluorescent microscope (Olympus, Tokyo, Japan) and enumerated manually.

2.9.7 Migration Assay

In vitro scratch assay: 3 x 10^4 cells were seeded into a 24-well plate to create a confluent monolayer. Cell monolayer was scraped in a straight line to create a ‘‘scratch’’ with a p200 pipet tip. Debris was removed by washing the cells once with 1 ml of the 1 x PBS and then replace with 1mL of normal growth medium. To obtain the same field during the image acquisition, markings were created to be used as reference points close to the scratch on the outer bottom of the plate with an ultrafine tip marker. Images were taken using phase contrast microscope and after initial scratch (T0). Cells were then incubated at 37 °C in 5% CO_2 for 16 hours. Images were taken again at post 16 hours incubation (T16) at the same spot using the

reference point. The area and length of uninvaded space within each well was measured using ImageJ at T0 and T16.

2.9.8 Flow Cytometric Analysis

Cells were prepared as a signal cell suspension using trypsin, cells were washed with HHF and past through a 70μM cell strainer, centrifuged at 1,400 rpm (Eppendorf, 5810R) for 5 minutes and resuspended in 10mL blocking buffer (5% horse serum, 10% BSA, 1% penicillin/ streptomycin, 5% FCS in HEPES media). A cell count was performed and cells were incubated with blocking buffer for 30 minutes on ice. Cells were separated into 5mL polypropylene tubes, corresponding to the antibodies being used. Samples were centrifuged (DiaCent-12) for 2 minutes; the blocking buffer was aspirated. Cells were resuspended in 200 μL of 20 μg/mL of purified primary antibody and incubated for 1 hour on ice, shaking. Samples were washed twice with HHF and then resuspended with the corresponding secondary antibody (1:50). Samples were incubated for 45 minutes on ice, washed twice in HHF, the supernatant was aspirated, samples were vortexed and resuspended in 500μL of FACS FIX. Samples were analysed with EPICS XL-MCL (Beckman Coulter, ADC) and EXPO32 software.

2.10 RNA-sequencing

BMSC with either empty vector and *HOPX* overexpressing vector were cultured at 2.5 x 10^4 cells in normal growth (Ctrl) or adipogenic (Adipo) inductive media for two weeks. RNA was isolated and purified using TRIzol® (Sigma-Aldrich Inc., Sydney, NSW, Australia) in accordance with manufacturer's instructions. 1μg of RNA was processed and sequenced by David Gunn Genomic Facility, SAHMRI, SA, Australia on the Illumina Nextseq 500 with a 75 cycle v2.5 High Output sequencing kit. Initial raw read processing was performed using an

in-house pipeline developed at SAHMRI. Raw 75bp single-end FASTQ reads were assessed for quality using FastQC [200] and results aggregated using R/Bioconductor package *ngsReports* [201]. Reads were then trimmed for sequence adapters using *AdapterRemoval* [202] and aligned to the human genome GRCh38/hg38 using the RNA-seq alignment algorithm *STAR* [203]. After alignment, mapped sequence reads were summarised to the GRCh38.p13 (NCBI: GCA_000001405.28) gene intervals using *featureCounts* [204], and count table transferred to the R statistical programming environment for expression analysis. Effect of sequence duplicates were also investigated using the function *MarkDuplicates* from the Picard tools package (http://broadinstitute.github.io/picard).

2.10.1 Differential gene expression and pathway analysis

Gene expression analyses were carried out in R using mostly Bioconductor packages *edgeR* [205, 206] and *limma* [207]. Gene counts were filtered for low expression counts by removing genes with less than 1 count per million (cpm) in more than two samples and then normalised by the method of trimmed mean of M-values [208]. Differential gene expression was carried out on log-CPM counts and precision weights available from the *voom* function in *limma* [209], with linear modelling and empirical Bayes moderation. Annotation of results were carried out using Ensembl annotations (http://grch37.ensembl.org) available in *biomaRt* [210], and expression results displayed in heatmaps using the *pheatmap* package [211].

2.11 Western Blotting Reagents

2.11.1 Blocking Solution

On the day of use, 1g membrane blocking agent (skim milk) was dissolved in 20mL TBS-Tween at room temperature with agitation.

2.11.2 Non-reducing Lysis Buffer

One protease inhibitor tablet was dissolved in 5.6mL RO water with agitation. Tris (200µL; 1M; pH7.5), 20µL EDTA (0.5M), 750µL sodium chloride (2M), 100µL Nonidet P40, 200µL sodium vanadate (100mM), 500µL sodium fluoride (0.5M), 100µL SDS (10% w/v), 400µL sodium pyrophosphate (250mM), 1250µL glycerol (80% v/v), 200µL sodium vanadate (0.5M) and 50µL phenylmethylsulfonyl fluoride (100mM) were then added and mixed thoroughly. The resulting solution of 1% Nonidet P40, 20mM Tris, 150mM sodium chloride, 1mM ethylenediaminetetraacetic acid, 25mM sodium fluoride, 10mM sodium phosphate, 2mM sodium vanadate and 0.5mM phenylmethylsulfonyl fluoride, supplemented with complete protease inhibitors, was stored in 1mL aliquots at -20°C for up to 3 months.

2.11.3 Polyacrylamide Gel (Stacking Gel)

RO water (5.42mL), 1.24mL 40% acrylamide, 0.66mL 2% bis-acrylamide, 2.52mL Tris-HCl (0.5M; pH6.8), 100µL SDS (10% w/v) and 50µL APS (10% w/v) were combined and were mixed by inversion. Immediately before use, 10µL TEMED was added and the solution was mixed carefully to avoid creating bubbles.

2.11.4 7.5% Polyacrylamide Gel (Separating Gel)

RO water (4.415mL), 1.875mL 40% acrylamide, 1.0mL 2% bis-acrylamide, 2.5mL Tris-HCl (1.5M; pH8.8), 150µL SDS (10% w/v) and 50µL APS (10% w/v) were combined and were mixed by inversion. Immediately before use, 10µL TEMED was added and the solution was mixed carefully to avoid creating bubbles.

2.11.5 13.6% Polyacrylamide Gel (Separating Gel)

RO water (2.127mL), 3.4mL 40% acrylamide, 1.813mL 2% bis-acrylamide, 2.5mL Tris-HCl (1.5M; pH8.8), 100µL SDS (10% w/v) and 50µL APS (10% w/v) were combined and were mixed by inversion. Immediately before use, 10µL TEMED was added and the solution was mixed carefully to avoid creating bubbles.

2.11.6 Reducing Loading Buffer, 5x

Glycerol (25mL), 25mL Tris (1.0M, pH6.8), 8g SDS, 400mg bromophenol blue, 8mL β-mercaptoethanol and 25mL RO water were mixed, the solution was filtered using a 0.45µm syringe filter and 2.5mL aliquots were stored at -20°C. Thawed aliquots were stored at 4°C until use. Cell lysates for Western blotting were diluted 1:4 in loading buffer for a final concentration of 50mM Tris, 1.6% SDS, 0.08% (w/v) bromophenol blue and 1.6% β-mercaptoethanol.

2.11.7 Running Buffer, 10x

Tris (30.3g), 144g glycine and 10g SDS were dissolved in RO water, the pH was adjusted to 8.3 and the volume was made up to 1L. The solution was stored at room temperature and was diluted 1:9 in RO water prior to use for a final concentration of 0.3% (w/v) Tris-HCl, 1.44% (w/v) glycine and 0.1% (w/v) SDS.

2.11.8 Tris-buffered Saline (TBS), 10x

Tris (24.2g) and 80g sodium chloride were dissolved in RO water, the pH was adjusted to 7.6 and the volume was made up to 1L. The solution was stored at room temperature and was diluted 1:9 in RO water before use.

2.11.9 1% Tween/TBS (TBS-Tween)

Tween 20 (1mL) was added to 100mL TBS (10x) and 899mL RO water and was carefully mixed to avoid bubbles. Solution was stored at room temperature until use.

2.11.10 TBS-Tween with 10% BSA

BSA (0.5g) was dissolved in 50mL TBS-Tween, with agitation. The solution was filtered using a 0.45μM syringe filter and was stored at 4°C. The solution was diluted 1:9 in TBS-Tween prior to use.

2.11.11 Transfer Buffer, 1x

Tris (12.104g) and 57.66g glycine were dissolved in 3L RO water, 0.6L methanol was added and the volume was made up to 4L. The solution was stored at 4°C and was used up to 2 times before discarding.

2.12 Protein Analysis

2.12.1 Preparation of Protein Lysates

Whole cell lysates were prepared on ice from 3×10^6 MSC. Cells were washed once with 10mL of ice cold PBS before 300μL of Lysis Buffer was added and cells were scraped off the dish using a cell scraper. Cell lysate was transferred to an Eppendorf tube and vortexed. This preparation was incubated on ice for approximately 30 minutes. Cell lysate was then centrifuged for 30 minutes at 16,000 x g at 4°C. Centrifugation was sufficient to separate out the nuclear proteins and other cellular debris which formed a pellet at the bottom of the tube. The supernatant was transferred to a new tube from which an aliquot was taken and protein

concentration quantitated using RC/DC protein assay kit (Bio-Rad Laboratories, Hercules, CA, USA) according to the manufacturer's instructions.

2.12.2 RCDC Protein Estimation

The protein concentration of all cell extracts was determined using the RCDC Protein Assay Kit (BioRad, USA) according to manufacturer's instructions. Serial dilutions of BSA (2mg/mL stock) were used to create a standard curve.

2.12.3 Preparation of Samples for SDS-PAGE

Cell lysates were thawed on ice and equivalent amounts of protein, as determined by RC/DC assay, were transferred to 1.5mL microfuge tubes. Appropriate volumes of 5 x reducing loading buffer were added and the samples were incubated for 5 minutes at 95°C on a heat block. The samples were cooled on ice, quickly centrifuged and the samples were loaded onto SDS-PAGE gels with a pre-stained protein marker (Bench-mark; catalogue number 10748-010; Invitrogen).

2.12.4 SDS-PAGE Gel Preparation

Spacer plates (1.5mm; catalogue number 1653312; Bio-Rad) and short plates (catalogue number 1653308; Bio-Rad) were assembled in a gel casting frame. Immediately following addition of TEMED, separating gel was poured until it was 2cm below the top of the short plate. The gel was then covered with water-saturated butanol to remove bubbles and was left for 15 minutes to set. When the gel was set, the butanol was poured off, the stacking gel was poured, a 10-well comb (1653365; Bio-Rad) was inserted and the gel was left to set for 15 minutes.

2.12.5 Loading and Running of SDS-PAGE Gels

The gels were assembled with the Mini-Protean® 3 (Bio-Rad) electrode assembly and clamping frame, the assembly was placed in a tank and the combs were removed. The inner chamber was filled with running buffer, ensuring the wells were well-rinsed with buffer. The tank was then half-filled with running buffer and the prepared samples and protein markers were loaded in appropriate wells. The lysates were run through the stacking gel at 20mA and were then resolved through the separating gel at 40mA.

2.12.6 Transfer of Protein to Polyvinylidene Difluoride (PVDF) Membranes

PVDF membrane (Hybond-P membrane, Amersham Biosciences, GE Healthcare, Little Chalfont, UK) was cut to size (6 x 9cm) and was pre-equilibrated in methanol for 5 minutes. The membrane, blotting paper and fibre pads were then soaked in transfer buffer until use. Following electrophoresis, the gel assembly was dismantled and the electrophoretic transfer cell (Mini Trans-Blot, Bio-Rad) was assembled, following the instructions of the manufacturer. Briefly, 2 sheets of blotting paper were placed on a fibre pad on the black side of the gel cassette holder and the gel was carefully placed on top. The pre-equilibrated membrane was laid over the gel, followed by 2 sheets of blotting paper, any air bubbles were expelled by rolling over the filter paper with a pipette and a final fibre pad was placed on top. The assembly was then placed in a tank with a cooling unit (cooled to -20°C), the tank was filled with transfer buffer and the protein transfer was carried out overnight at 30mA or for 2 hours at 200mA.

2.12.7 Protein Detection

Following Western blotting, the PVDF membrane was rinsed in TBS-Tween before being incubated for 1 hour in blocking buffer with agitation. The membrane was then probed with primary antibody (Table 2.12) diluted in blocking buffer overnight at 4°C with agitation. The

membranes were then washed 3 times for 5 minutes in TBS-Tween and the immunoreactive proteins were subsequently detected by incubation with alkaline-phosphatase-conjugated antibodies against rabbit immunoglobulin (Ig) (catalogue number AP182A; Chemicon, Melbourne, VIC) or mouse Ig (catalogue number AP322A; Chemicon), diluted 1:2000 in 1% BSA/TBS-Tween, for 1 hour at room temperature with agitation. The membranes were then washed 3 times for 5 minutes in TBS-Tween at room temperature with agitation.

The protein was then detected by imaging using LI-COR Odyssey CLX machine at 700nm and 800nm excitation. Quantitation was performed using Image Studio Lite Version 5.2 software. Where required, membranes were stripped of antibodies using a commercial stripping buffer (Western blot recycling kit; catalogue number 90100; Alpha Diagnostics, San Antonio, USA), following the instructions of the manufacturer. The blots were then rinsed in TBS-Tween and incubated for 1 hour in blocking buffer before reprobing with primary antibody.

2.12.8 Table 2.12 Primary Antibodies Used In Western Blot

Antibodies	Catalogue No.	Supplier
Anti-HOPX	11419-1-AP	United Bioresearch
Anti-HOPX	ab106251	Abcam
Anti-CMTM8	15039-1-AP	United Bioresearch
Anti-CMTM8	AV53386-100UL	Sigma Aldrich
PhosphoPlus EGFR (Tyr1065) kit	11862S	Genesearch
Anti-AKT	9272	Cell Signalling
Anti-Phospho-AKT (Ser473)	4051	Cell Signalling

2.13 Statistical Analysis

Data analysis was carried out using Microsoft GraphPad Prism 7 (GraphPad Software, LA Jolla, CA, http://www.graphpad.com/), which was used for the generation of graphs and statistical significance. Statistical differences (*) of $p<0.05$ between samples are shown based on Student's t-test and One-way ANOVA as indicated.

Chapter 3: Identification of TWIST-1 Target Molecules in the Regulation of BMSC Growth and Differentiation

3.1 Introduction

Studies of skeletal development have shown that *TWIST-1* expression correlates with bone cell immaturity where *TWIST-1* expression is downregulated as bone cells mature [187, 212, 213]. In addition, previous work from our laboratory showed that freshly isolated STRO1$^+$ BMSC express high levels of *TWIST-1*, which is downregulated rapidly when BMSC are expanded *ex vivo* [1]. Moreover, *TWIST-1* overexpressing BMSC have an increased proliferation rate, lifespan and adipogenic differentiation capacity, but decreased capacities for osteogenic and chondrogenic differentiation [1]. Other studies demonstrated that positive correlation between high levels of *TWIST-1* expression and high levels of STRO-1 expression, together with increased gene expression of the transcription factors, *Id-1* and *Id-2*, which are associated with cellular proliferation [214]. Furthermore, the enhanced capacity for adipogenic differentiation by *TWIST-1* overexpressing BMSC was accompanied by an increased in the expression of the adipogenic master regulator, PPARγ2 [1]. Interestingly, high levels of *TWIST-1* are associated with increased levels of osteogenic master regulators, *RUNX2* and *MSX2*, and decreased levels of late osteogenic differentiation markers, *OPN*, *OCN* and *BSP* [1]. These findings are supported by other studies that reported increased *RUNX2* expression is correlated with decreased expression of its target genes and reduction in osteoblast differentiation [215-217]. Overall, TWIST-1 appears to be a positive regulator of BMSC growth and an inhibitor of osteo/chondrogenic differentiation, which allows BMSC to differentiate along a default adipogenic pathway.

The aim of this study was to identify the downstream molecular mechanisms of TWIST-1 in BMSC cell lineage commitment. In order to identify novel TWIST-1 gene targets, *TWIST-1* overexpressing BMSC and controls were assessed in gene microarray studies [3]. Assessment of the data sets using Volcano plot analysis identified differentially expressed genes in vector

control BMSC during osteogenic differentiation (Figure 3.1A) and between vector control BMSC and *TWIST-1* overexpressing BMSC cultured under growth and osteogenic conditions (Figure 3.1B). A number of differentially expressed genes were identified, which appeared to be regulated by TWIST-1 during bone formation *in vitro* [3]. Expression of two genes, cytochrome P450 family 26 subfamily B member 1 (CYP26B1) and cathepsin K (CTSK) were found to be inhibited/repressed in BMSC during osteogenic differentiation. Conversely, these two genes were expressed at high levels in *TWIST-1* overexpressing BMSC during osteogenic differentiation when compared to control BMSC. CYP26B1 and CTSK have been shown to play a role in BMSC function [218-221]. Interestingly, the expression of the majority of differentially expressed genes was upregulated in BMSC during osteogenic differentiation but were found to be repressed in *TWIST-1* overexpressing BMSC during osteogenic differentiation since TWIST-1 inhibits the osteogenic potential of cells it is likely that these genes have a role in promoting osteogenesis. Differentially expressed genes were selected based on a P-value < 0.05 with a fold change of 2 fold (a log fold change (logFC) >=|1| or >=|-1|), then ranked according to fold change and plotted on a volcano plot, generated by plotting statistical significance over magnitude of fold change (F). The top 30 differentially expressed genes during osteogenic differentiation of *TWIST-1* overexpressing BMSC compared to vector only BMSC were selected based on the statistical significance and magnitude of fold change (Table 3.1). The microarray results obtained for the top 8 genes were validated using quantitative real-time PCR by our group (Figure 3.2A, 3.6A and data not shown). In order to select potential novel TWIST-1 target genes, a literature search was performed on published papers and publicly available databases for relationships between TWIST-1 and the top 8 genes described in Table 3.1.

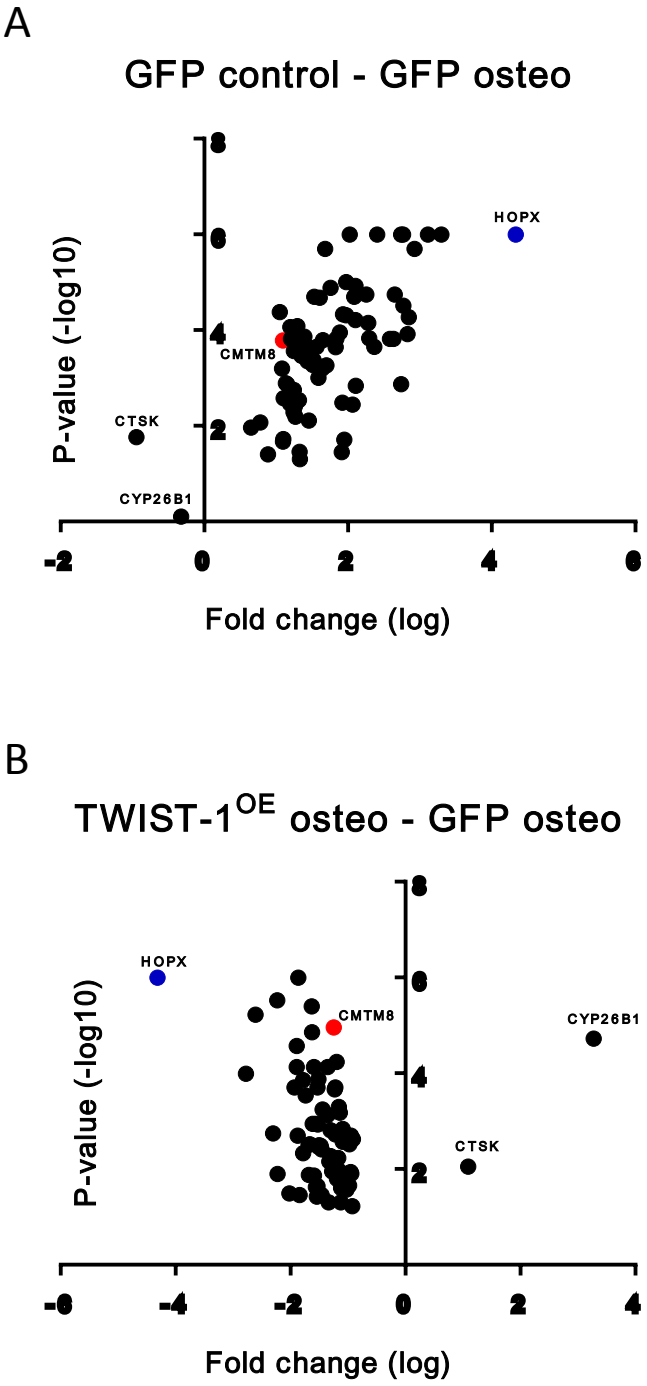

Figure 3.1. Volcano plot depicting statistical significance over magnitude of fold change for 79 differentially expressed genes. Volcano plot showing fold change of identified genes to their significance of the fold change between (A) BMSC cultured under growth and osteogenic conditions. (B) *TWIST-1* overexpressing BMSC and control BMSC during osteogenic differentiation.

Table 3.1. Top 30 differentially expressed genes during osteogenic differentiation of *TWIST-1* overexpressing BMSC compared to vector only BMSC. Rankings were calculated based on the statistical significance and magnitude of fold change.

Gene ID	Gene Name	Fold Change	-log10 of P-value
HOPX	HOP homeobox	-4.315	6
ROS1	ROS proto-oncogene 1, receptor tyrosine kinase	-1.866	6
ITGA5	integrin subunit alpha 5	-2.231	5.52
SCARA3	scavenger receptor class A member 3	-1.631	5.4
COL4A4	collagen type IV alpha 4 chain	-2.61	5.22
CMTM8	CKLF like MARVEL transmembrane domain containing 8	-1.25	4.96
KCNT2	potassium sodium-activated channel subfamily T member 2	-1.623	4.85
CYP26B1	cytochrome P450, family 26, subfamily b, polypeptide 1	3.273	4.72
NT5DC3	5'-nucleotidase domain containing 3	-1.891	4.57
DIAPH3	diaphanous related formin 3	-1.197	4.24
NPTX1	neuronal pentraxin 1	-1.889	4.13
CITED4	Cbp/p300 interacting transactivator with Glu/Asp rich carboxy-terminal domain 4	-1.594	4.13
PLCE1	phospholipase C epsilon 1	-1.353	4.13
SERPINA3	serpin family A member 3	-2.773	3.99
COL4A3	collagen type IV alpha 3 chain	-1.516	3.88
SEC14L2	SEC14 like lipid binding 2	-1.783	3.86
RERG	RAS like estrogen regulated growth inhibitor	-1.932	3.7
HHIP	hedgehog interacting protein	-1.532	3.7
SLC7A2	solute carrier family 7	-1.22	3.7
MT1E	metallothionein 1E	-1.23	3.66
ASPM	abnormal spindle microtubule assembly	-1.737	3.54
ALOX15B	arachidonate 15-lipoxygenase type B	-1.16	3.3
MT1M	metallothionein 1M	-1.439	3.24
CTNNB1	catenin beta 1	-1.141	3.18
GPAM	glycerol-3-phosphate acyltransferase, mitochondrial	-1.352	3.13
DLGAP5	DLG associated protein 5	-1.612	2.95
KIF20A	kinesin family member 20A	-1.559	2.95
NINJ2	ninjurin 2	-1.534	2.93
MTE	metallothionein E	-1.523	2.93
FAM83D	family with sequence similarity 83 member D	-1.089	2.84

3.1.1 Homeodomain only protein homeobox (HOPX)

HOPX is the smallest homeobox important in cardiogenesis [222]. Inhibition of *Hopx* in mouse and zebrafish results in disruption of cardiac development and lethality. *Hopx* is found to be expressed in cardiomyoblasts, which interacts physically with activated Smad4 and functions to coordinate local Bmp signals to inhibit Wnt pathway, promoting cardiomyogenesis [223]. Studies have shown that Twist-1 is a target of Wnt/β-catenin signalling pathway in mouse cranial mesenchyme [182]. TWIST-1 was also found to be required for cranial bone lineage commitment by maintaining WNT responsiveness [182]. Therefore, there may be a positive feedback circuit between TWIST-1 and WNT and that TWIST-1 negatively regulates HOPX, which may affect bone formation through WNT/BMP signalling pathway. However, little is known about the biological function of HOPX in BMSC and CBC during bone formation. Interestingly, previous studies have demonstrated an association between TWIST-1/ Enhancer of zeste homolog 2 (EZH2) and EZH2/ HOPX in BMSC, where TWIST-1 increased *EZH2* expression and EZH2 decreased *HOPX* expression [2, 224]. EZH2 is a histone methyltransferase that trimethylates the histone 3 lysine 27 (H3K27me3), which then leads to chromatin condensation and gene repression [225]. Therefore, HOPX may have a role in BMSC growth and differentiation.

3.1.2 Tyrosine Kinase Receptor C-ROS-1 oncogene (C-ROS-1)

C-ROS-1 is a transmembrane orphan tyrosine kinase receptor with no known ligand. Previous study from our laboratory have demonstrated that C-ROS-1 is expressed by BMSC and CBC and is a downstream target of TWIST-1 [3]. Furthermore, it has been demonstrated that C-ROS-1 signalling affects the PI3K/AKT/mTOR signalling cascade in BMSC [3]. Overall, this study has shown that C-ROS-1 is involved in BMSC fate switching between osteogenesis and adipogenesis, mediated via PI3K/AKT/mTORC1 signalling.

3.1.3 Integrin Subunit Alpha 5 (ITGA5)

Integrin is a family of transmembrane proteins that induce intracellular signals [226, 227]. The α5β1 integrin is a cell surface receptor for fibronectin that has been implicated in cell spreading, proliferation, differentiation, migration, and survival in different cell types [228-230]. Various studies have shown that ITGA5 is involved in osteogenic differentiation of BMSC [231-233]. It was reported that ITGA5 expression is upregulated during osteogenic differentiation of the human MSC. Moreover, enforced expression of ITGA5 results in increased osteogenic differentiation capacity *in vivo* and *in vitro*, which is mediated by ERK1/2-MAPK and PI3K signalling pathways [231].

3.1.4 Scavenger Receptor class A member 3 (SCARA3)

SCARA3 encodes a macrophage scavenger receptor-like protein of 606 amino acids [234]. It has a leucine zipper motif that overlaps with a transmembrane domain at its N-terminus, followed by two central coiled regions and a C-terminal collagen-like domain [234]. Additionally, an alternative splice variant of the SCARA3 gene encodes for a 466 amino acid protein identical to that described above, except that it possesses only a short C-terminal tail and lacks the collagen-like domain. It was found to be primarily secreted in myeloid cells and plays a role in microbial pattern recognition of innate immunity [234]. SCARA3 functions to protect cells by scavenging reactive oxygen species and harmful products of oxidation [235, 236]. Moreover, SCARA3 can bind endogenous ligands, such as extracellular matrix proteins (biglycan, decorin, denatured collagens) and modified LDLs (AcLDL, OxLDL) [237]. Functional studies have shown that SCARA3 controls lipid homeostasis which is critical in the osteoblast/adipocyte differentiation balance [237]. The shift in bone/fat marrow ratio towards fat might lead to decreased bone mineral density. Another study has shown that SCARA3 expression was downregulated in post-menopausal osteoporotic bone tissue, which may have

a prominent role in antibody clearance, phagocytosis, pathogen recognition and inflammatory response [238]. In addition, SCARA3 can interact with cleavage and polyadenylation-specific factor 3 (CPSF3), an enzyme necessary for polyadenylation of RNA. The binding of SCARA3 to CPSF3 subsequently alter subcellular distribution and induce cell death [239]. However, little is known about the underlying molecular mechanism of SCARA3, particularly during BMSC cell fate determination, and in the context of bone disorders involving an imbalance of bone/ fat ratio such as osteoporosis.

3.1.5 Collagen Type IV Alpha 4 Chain (COL4A4)

COL4A4 is a main structural component of basement membranes. Mutations in COL4A4 are associated with Alport syndrome (hereditary glomerulonephropathy). Studies have reported that *col4a4* expression is downregulated during early stage of osteoblast differentiation in the mouse MC3T3-E1 cell line, suggesting that *Col4a4* may have a role in preventing premature osteoblasts to enter maturation [240]. Therefore, COL4A4 has known functions in bone biology.

3.1.6 CKLF-like MARVEL transmembrane domain containing 8 (CMTM8)

Our previous studies have found that the CMTM8 is a putative downstream target of TWIST-1 in primary human BMSC [3]. Other studies of different cancer lines, HEK293T, human cervical carcinoma cell line (HeLa) and human prostate carcinoma cell line (PC3), reported that CMTM8, also known as CKLFSF8, suppresses the epidermal growth factor receptor (EGFR) signalling pathway by accelerating clearance of cell surface EGFR, resulted in a decrease in cell proliferation [241]. Another study showed that EGFR signalling suppresses osteoblast differentiation and inhibits expression of the osteoblastic transcription factors RUNX2 and OSTERIX, which may lead to the development of immature osteoblastic-like

cells characteristic of osteosarcoma [242]. The EGFR signalling pathway has also been shown to be important in maintaining osteoprogenitor populations in an undifferentiated stage [242]. In other tumor types such as hepatocellular carcinoma cells and immortalized breast epithelial cells, CMTM8 was reported to act as a tumour suppressor gene by suppressing the activity of the oncogenic protein, c-Met, and therefore leading to a decreased in EMT status of cells [243-245]. Given that CMTM8 has been known to be involved in several signalling pathways that mediate cell proliferation and differentiation in other systems, there is no information of the role of CMTM8 during BMSC growth and cell fate determination.

3.1.7 Potassium Sodium–Activated Channel Subfamily T Member 2 (KCNT2)

KCNT2, also known as SLO2.1 or SLICK, is a Na^+-activated K^+ channel found to be expressed in the nervous system, heart, kidney and brain [246-248]. However, little is known about the function of KCNT2, particularly during BMSC growth and cell fate determination.

3.1.8 Cytochrome P450 Family 26 Subfamily B Member 1 (CYP26B1)

CYP26B1 is an enzyme responsible in the degradation of excess intracellular retinoic acid (RA). Mutations in *CYP26B1* gene leads to severe skeletal anomalies such as joint synostosis, calvaria bone hypoplasia, advanced ageing of bone and angulated femora [249]. Vitamin A (retinol) has been known to be toxic to bone tissue as excessive dietary intake of vitamin A can result in reduced bone formation [219-221]. Therefore, CYP26B1 has known functions in bone biology.

3.1.9 Rationale of selecting HOPX and CMTM8

Two novel genes that were differentially expressed and appeared to have important roles in BMSC biology were *HOPX* and *CMTM8*. HOPX displayed the highest overall fold change and

P-value. Our previous work has shown relationships between TWIST-1/EZH2 and EZH2/HOPX during BMSC cell fate determination [224]. Furthermore, it has been reported that HOPX plays a dual-role in maintaining the balance of undifferentiated and differentiated cells [222, 250]. HOPX can promote or inhibit proliferation and differentiation of cells at different stages. However, the function of HOPX in BMSC growth and cell fate determination is novel. Therefore, HOPX was selected as one of the focus of this study.

Out of the top 8 genes that were assessed *C-ROS-1*, *ITGA5*, *COL4A4*, *CYP26B1* were excluded from this project due the reported roles in BSMC or bone biology. Therefore, out of the 8 only *HOPX*, *SCARA3*, *CMTM8* and *KCNT2* are presented as novel TWIST-1 targets with potential roles in BMSC proliferation and differentiation and were potential candidates for further exploration. However, using the transcription factor binding site predictor tool, no TWIST-1 binding sites have been identified near *SCARA3* promoter regions, while *CMTM8* contains three putative TWIST-1 binding sites in the intron 1; and *HOPX* contains EZH2 binding sites in its promoter regions. Therefore, due to time constraints HOPX and CMTM8 have been selected as the focus of Chapter 4 and 5, respectively, as *KCNT2* had the lowest fold change and P-value among these genes.

3.2 Results

3.2.1 Identification of TWIST-1 target genes during growth and osteogenic conditions

To identify novel TWIST-1 gene targets involved in BMSC proliferation and osteogenic differentiation, a microarray analysis was previously performed in our laboratory comparing the gene expression profile of BMSC, which express either endogenous or enforced expression of *TWIST-1* during growth or undergoing osteogenic differentiation. Figure 3.1 displays the volcano plot plotting the fold change (log) of gene expression against the P-value (-log10), demonstrating the differentially expressed genes in vector only BMSC cultured under either growth condition (Control) or osteogenic inductive condition (Osteo). It is clear that during BMSC osteogenesis, 79 genes were upregulated and 2 genes were downregulated. The two downregulated genes were CTSK and CYP26B1, both are known to be involved in bone remodelling and bone homeostasis [218-221]. Interestingly, when comparing *TWIST-1* overexpressing BMSC to vector control BMSC during osteogenesis, the 79 genes were downregulated, indicating an inverse relationship between *TWIST-1* and these genes (Figure 3.1B). A table was derived from the microarray analysis to show the top 30 genes with highest P-value and fold change (Table 3.1), when *TWIST-1* is overexpressed during osteogenesis. The microarray analysis provides insight into possible downstream targets of TWIST-1 in regulation of BMSC growth and osteogenesis. Based on the literature, a few novel candidate genes from Table 1 were selected for further functional confirmatory studies, including *HOPX* and *CMTM8*. Studies on C-ROS-1 in relation to TWIST-1 have been published by our laboratory [3].

3.2.2 HOPX expression in BMSC

HOPX showed the highest expression among the 79 upregulated genes in vector-control BMSC during osteogenesis, whilst it was expressed at the lowest level in *TWIST-1* overexpressing

cells, suggesting that HOPX may play important roles in BMSC growth and osteogenesis. To confirm the microarray, *HOPX* expression was determined in vector control and *TWIST-1* overexpressing BMSC during growth, osteogenic or adipogenic differentiation using real-time PCR. At day 21, *HOPX* gene expression levels were found to be upregulated during BMSC osteogenic (Figure 3.2A) and adipogenic (Figure 3.2B) differentiation, compared to growth condition in both vector and *TWIST-1* overexpressing BMSC. However, *HOPX* expression was downregulated in *TWIST-1* overexpressing BMSC compared to vector only BMSC in all conditions, showing a negative correlation between *TWIST-1* and *HOPX* in BMSC.

We next examine expression pattern of *HOPX* during growth, osteogenic and adipogenic inductive conditions (Figure 3.2C). Total RNA were collected at day 4, 7, 10, 14 and 21 of culture, and *HOPX* expression was assessed by real-time PCR. *HOPX* transcripts were expressed at low levels during growth conditions and increased gradually at a very low level throughout the timepoints assessed. During osteogenesis, *HOPX* was expressed at low levels at day 4 and its expression peaked at day 7 and remained above control levels over time. During adipogenesis, *HOPX* was expressed at low levels at day 4 and its expression gradually increased over time. This data validates the microarray analysis and suggests that HOPX is a potential factor involved in BMSC differentiation. Further studies of the functional role of HOPX in BMSC growth and differentiation are detailed in Chapter 4.

After confirming the expression of *HOPX* in BMSC, the question arose as to whether HOPX is expressed in human cranial bone cells (CBC), committed pre-osteoblasts with a high potential to form a mineralized extracellular matrix *in vitro* [3]. We analysed the expression of *HOPX* in human wild type CBC and in TWIST-1 haploinsufficient CBC derived from patients with Saethre-Chotzen Syndrome. *TWIST-1* haploinsufficient mutation in CBC results in

Figure 3.2. *HOPX* gene expression is upregulated during BMSC differentiation and is suppressed in *TWIST-1* overexpressing cells. (A) *TWIST-1* overexpressing ($TWIST^{OE}$) and vector only BMSC were cultured under Ctrl and Osteo conditions for 21 days. cDNA was prepared from RNA harvested from these donors and real-time PCR was performed to measure levels of *HOPX* relative to *β-actin*. (B) *HOPX* expression was measured for $TWIST^{OE}$ and Vector BMSC cultured under Ctrl and Adipo condition as described above. (C) BMSC were cultured under growth (Ctrl), osteogenic (Osteo) and adipogenic (Adipo) inducing conditions. cDNA was prepared from RNA harvested at day 4, 7, 10, 14 and 21. Real-time PCR was used to measure levels of *HOPX* expression relative to *β-actin*. Graphs represent mean ± S.E.M, One-way ANOVA $p<0.05$(*), n=3 donors. (D) Human CBC from 1 normal and 2 SCS patients were cultured under Ctrl and Osteo conditions for 21 days. cDNA was prepared from RNA harvested from these donors and real-time PCR was performed to measure levels of *HOPX* relative to *β-actin*. Graphs represent mean ± S.E.M, One-way ANOVA $p<0.05$(*).

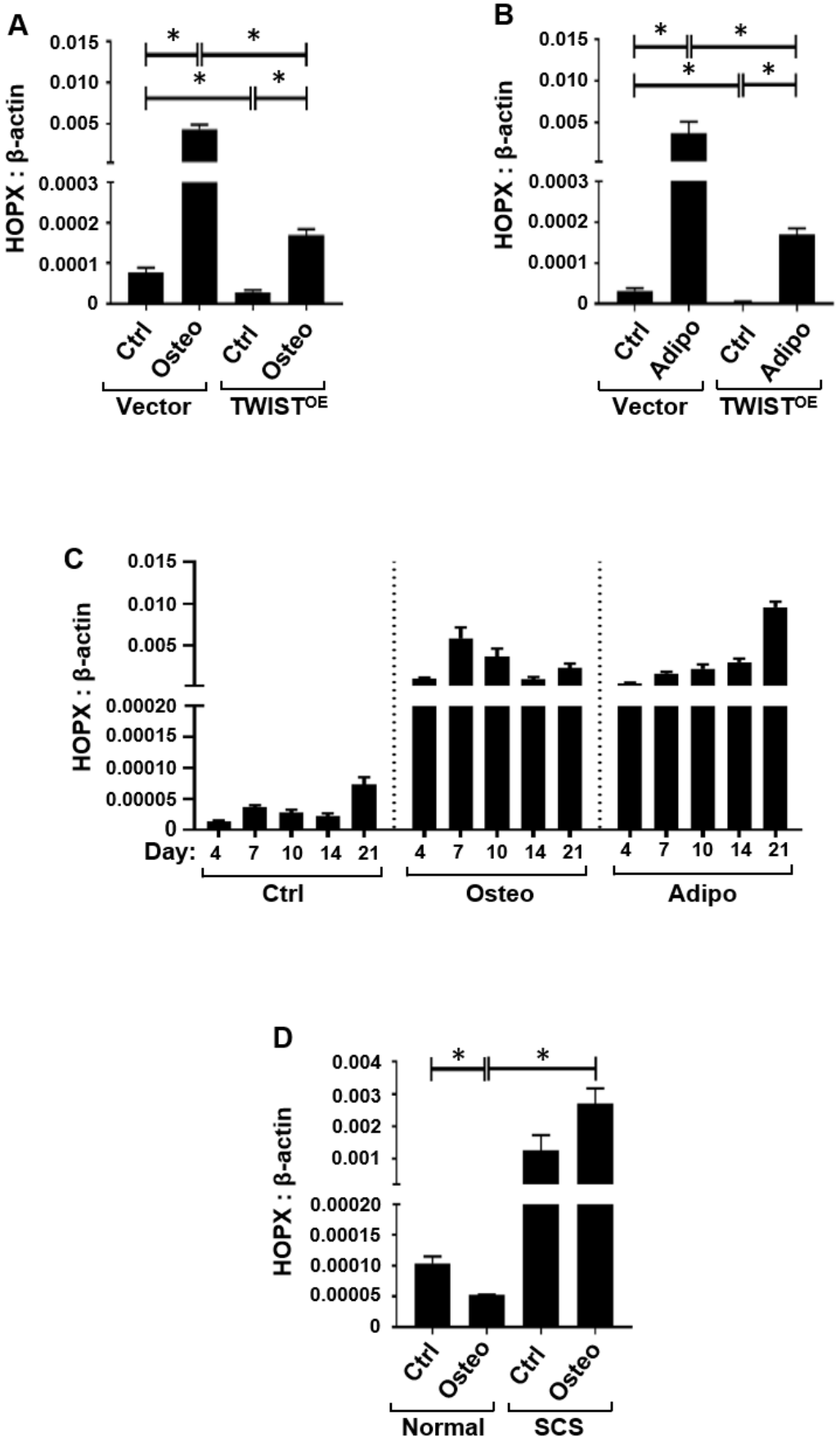
A
HOPX : β-actin
0.015
0.010
0.005
0.0003
0.0002
0.0001
0
Ctrl
Osteo
Ctrl
Osteo
Vector
TWIST^OE
B
HOPX : β-actin
Ctrl
Adipo
Ctrl
Adipo
Vector
TWIST^OE
C
HOPX : β-actin
0.00020
0.00015
0.00010
0.00005
Day: 4 7 10 14 21 4 7 10 14 21 4 7 10 14 21
Ctrl
Osteo
Adipo
D
HOPX : β-actin
0.004
0.003
0.002
0.001
Ctrl
Osteo
Ctrl
Osteo
Normal
SCS

decreased cell proliferation and increased osteogenesis. In the present study, CBC from un-affected donors and SCS patients were cultured under growth or osteogenic conditions. Total RNA was assessed by real-time PCR. Due to the low number of donors, only CBC from one un-affected and two SCS donors were used. Low levels of *HOPX* gene transcripts were observed in CBC with wild type levels of *TWIST-1* when cultured under growth or osteogenic inductive conditions (Figure 3.2D). Interestingly, SCS derived CBC exhibited increased *HOPX* gene expression levels during osteogenesis (Figure 3.2D). Thus, when the level of *TWIST-1* is reduced there is an increase in *HOPX* expression. This data supports the notion of a negative correlation between *TWIST-1* and *HOPX* in CBC. However, lower levels of HOPX transcripts were observed in normal CBC when cultured under osteogenic inductive conditions, in comparison to normal growth conditions, which contradict the findings from Figure 3.2A and 3.2B. This could be due to the fact that CBC are more committed pre-osteoblast. In addition to this, the osteogenic inductive media used contains dexamethaxone, which could also induce adipogenic differentiation of BMSC. Unlike BMSC, CBC do not undergo adipogenesis.

3.2.3 Regulation of HOPX by TWIST-1

TWIST-1 is known to regulate biological processes through binding to the E-box (CANNTG) on the promoter of target genes or by homo- or hetero-dimerization with other protein molecules, leading to activation or repression of transcription or protein functions [172, 251, 252]. To investigate whether TWIST-1 binds directly to the promoter of *HOPX*, *in silico* analyses were performed using the transcription factor binding site predictor, 'Gene Transcription Regulation Database' [253] and three putative TWIST-1 binding sites were found from 13,000kb to 16,500kb away from the 3' end of *HOPX* but not at the 5' end promoter region of HOPX (Figure 3.3). However, analyses did show the presence of binding sites for EZH2 at promoter regions of *HOPX*, where the promoter regions were search for using

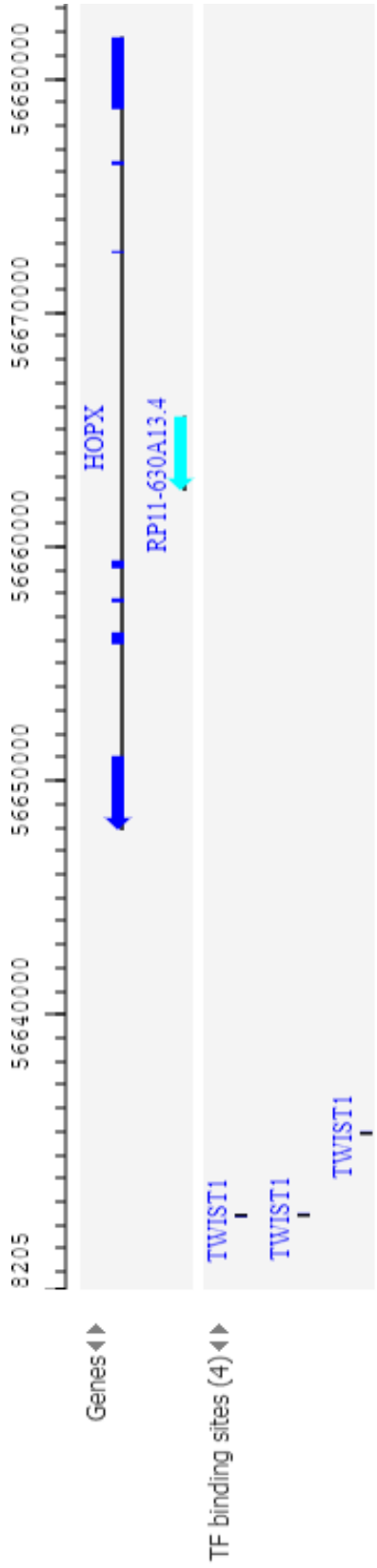

Figure 3.3. Schematic diagram of *in silico* analysis showing putative binding sites of TWIST-1 on the *HOPX* gene. Adapted from [253].

Figure 3.4. Schematic diagram of *in silico* analysis showing putative binding sites of EZH2 on the *HOPX* gene. S1, S2 and S3 indicate sites where ChIP analysis of EZH2 binding was performed. Adapted from [253].

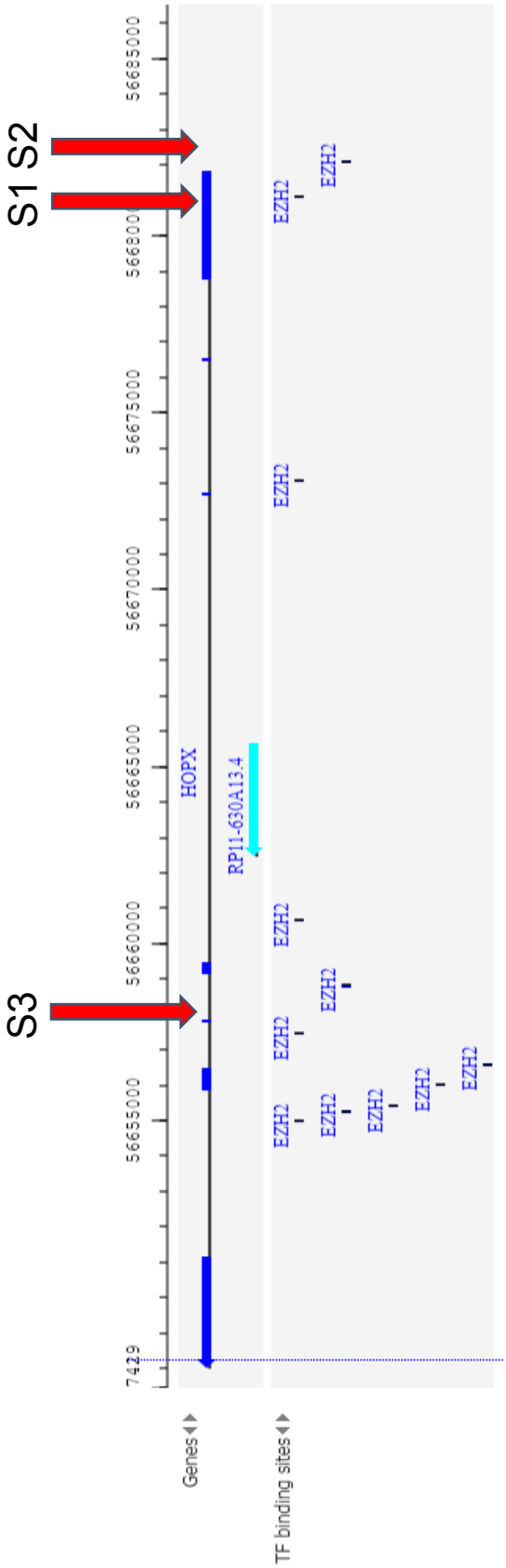
S1 S2
S3
56685000
56680000
56675000
56670000
56665000
56660000
56655000
7429
HOPX
RP11-630A13.4
EZH2
Genes
TF binding sites

'Eukaryotic Promoter Database, SIB' (Figure 3.4). EZH2 is a target of TWIST-1, thus the presence of putative EZH2 binding sites on the *HOPX* promoter suggests that TWIST-1 may regulate the expression of *HOPX* through the modulation of EZH2. EZH2 is a H3K27 methytransferase induced by TWIST-1 in BMSC and inhibits osteogenic differentiation and cellular senescence but increases adipogenesis [2, 196]. Therefore, it is possible that regulation of *HOPX* expression by TWIST-1 is through its interaction with EZH2. TWIST-1 positively regulates EZH2, which in turn binds to the promoter region of *HOPX* and negatively regulates its expression. ChIP analysis was subsequently employed to assess genomic DNA isolated from human BMSC under growth, osteogenic and adipogenic inducing conditions (Figure 3.5). ChIP analysis showed direct binding of EZH2 to one of these putative binding regions (S3) during growth conditions (Figure 3.5A-C), less enrichment of EZH2 was observed on all sites (S1, S2 and S3) during osteogenic inducing conditions (Figure 3.5D), and no enrichment of EZH2 was observed during adipogenic inducing conditions (Figure 3.5E). Decreased levels of *HOPX* was observed in *EZH2* overexpressing BMSC when compared to vector only BMSC (Figure 3.5F), suggesting that *HOPX* expression is directly regulated by EZH2.

3.2.4 CMTM8 expression in BMSC

CMTM8 showed a fold change of -1.25 (log) and a P-value of 4.96 (-log10) in *TWIST-1* overexpressing cells during osteogenesis when compared to vector only cells, suggesting that CMTM8 has a role in BMSC growth and osteogenesis. To confirm the microarray, *CMTM8* expression was determined in vector control and *TWIST-1* overexpressing BMSC during growth, osteogenic or adipogenic differentiation using real-time PCR. At day 21, *CMTM8* gene expression levels were found to be upregulated during BMSC osteogenic (Figure 3.6A) and adipogenic (Figure 3.6B) differentiation compared to growth condition in both and *TWIST-1* overexpressing BMSC. However, *CMTM8* expression was downregulated in *TWIST-1*

overexpressing BMSC compared to vector control BMSC in all conditions, showing a negative correlation between *TWIST*-1 and *CMTM8* in BMSC.

We next examined the expression pattern of *CMTM8* in BMSC during growth, osteogenic and adipogenic inductive conditions (Figure 3.6C). Total RNA was collected at day 4, 7, 10, 14 and 21 of culture, and *CMTM8* expression was assessed by real-time PCR. *CMTM8* transcripts were expressed at low levels during growth condition and increased gradually at a very low level throughout the time points assessed. During osteogenesis, *CMTM8* was expressed at low levels at day 4 followed by fluctuate expression over time and its expression peaked at day 21. During adipogenesis, *CMTM8* was expressed at low levels at day 4 and its expression gradually increased over time. This data validates the microarray analysis and suggests that CMTM8 is a potential factor involved in BMSC differentiation. Further studies of the functional role of CMTM8 in BMSC growth and differentiation are detailed in Chapter 5.

After confirming the expression of *CMTM8* in BMSC, the question arose whether *CMTM8* is expressed in human CBC. Human CBC from un-affected donors and SCS patients were cultured under growth or osteogenic conditions. Total RNA was assessed by real-time PCR. Low levels of *CMTM8* gene transcripts were observed in normal and SCS patient CBC when cultured under growth or osteogenic inductive conditions (Figure 3.6D). However, SCS patient CBC exhibited lower expression of *CMTM8* when compared to CBC from normal patient. This data contradicts the microarray data, which suggests a negative correlation between *TWIST-1* and *CMTM8* in CBC.

Figure 3.5. ChIP analysis of three putative EZH2 binding sites located on the *HOPX* promoter (site 1 (S1), site 2 (S2) and site 3 (S3)) using control antibody (IgG) or EZH2 antibody. (A-C) Fold enrichment was calculated by measuring the levels of enriched genomic DNA compared to the input genomic DNA of three independent BMSC donors cultured in growth conditions by PCR. Fold enrichment was calculated by measuring the levels of enriched genomic DNA compared to the input genomic DNA of two BMSC donors cultured in (D) osteogenic and (E) adipogenic inducing conditions by PCR. Graph represents mean ± S.E.M enriched genomic DNA of GAPDH (negative control), p14TSS (positive control) and S1, S2 and S3 of HOPX promoters. Fold enrichment results for HOPX, S1, S2 and S3 were compared to GAPDH (negative control). Graphs represent mean ± S.D., Student's t-test, $p<0.05$(*), n=2 donor. (F) *HOPX* expression was measured for $EZH2^{OE}$ and Vector BMSC cultured under growth conditions. Real-time PCR was used to measure levels of *HOPX* expression relative to *β-actin*. Graphs represent mean ± S.D., Student's t-test, $p<0.05$(*), n=1 donor.

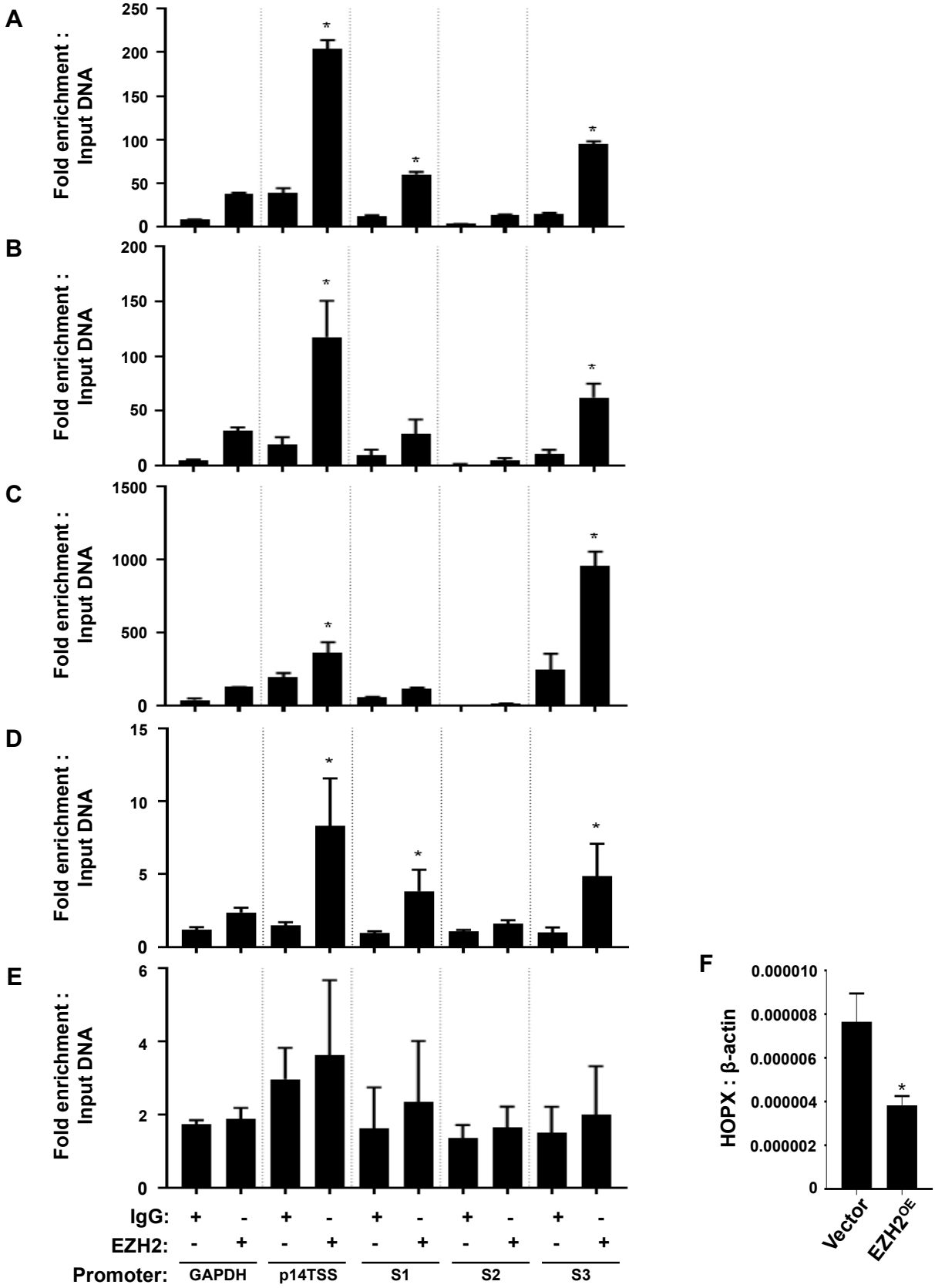
A
B
C
D
E
F
Fold enrichment : Input DNA
250
200
150
100
50
0
200
150
100
50
0
1500
1000
500
0
15
10
5
0
6
4
2
0
IgG: + - + - + - + - + -
EZH2: - + - + - + - + - +
Promoter: GAPDH p14TSS S1 S2 S3
HOPX : β-actin
0.000010
0.000008
0.000006
0.000004
0.000002
0
Vector
EZH2OE

Figure 3.6. *CMTM8* gene expression is upregulated during BMSC differentiation and is suppressed in *TWIST-1* overexpressing cells. (A) *TWIST-1* overexpressing ($TWIST^{OE}$) and Vector only BMSC were cultured under Ctrl and Osteo conditions for 21 days. cDNA was prepared from RNA harvested from these donors and real-time PCR was performed to measure levels of *CMTM8* relative to *β-actin*. (B) *CMTM8* expression was measured for $TWIST^{OE}$ and Vector BMSC cultured under Ctrl and Adipo condition as described above. (C) BMSC were cultured under growth (Ctrl), osteogenic (Osteo) and adipogenic (Adipo) inducing conditions. cDNA was prepared from RNA harvested at day 4, 7, 10, 14 and 21. Real-time PCR was used to measure levels of *CMTM8* expression relative to *β-actin*, n=3 donors. (D) Human CBC from 1 normal and 2 SCS patients were cultured under Ctrl and Osteo conditions for 21 days. cDNA was prepared from RNA harvested from these donors and real-time PCR was performed to measure levels of *CMTM8* relative to *β-actin*. Graphs represent mean ± S.E.M, One-way ANOVA $p<0.05$(*).

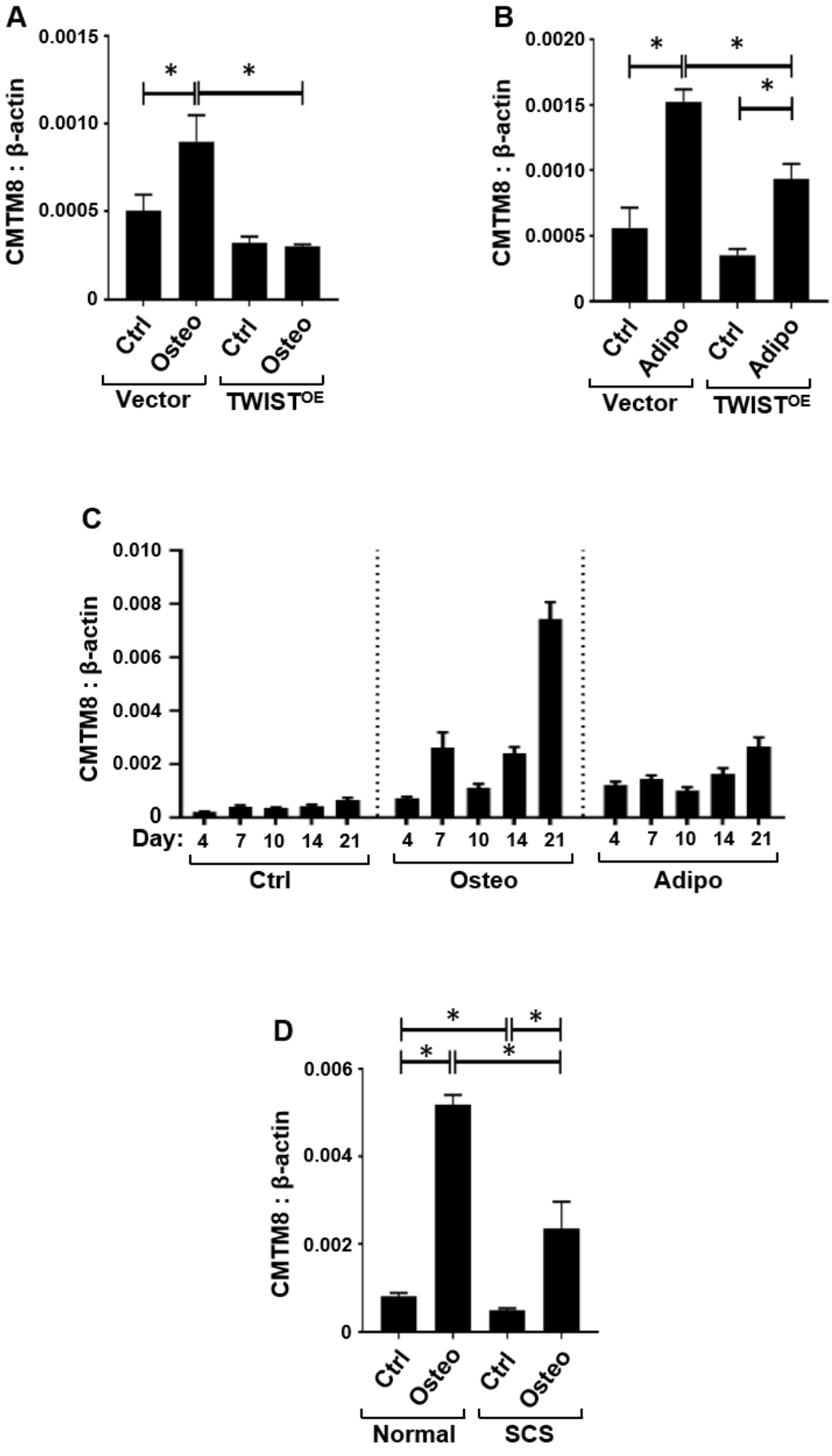
A
CMTM8 : β-actin
0.0015
0.0010
0.0005
0
*
*
Ctrl
Osteo
Ctrl
Osteo
Vector
TWIST^OE
B
CMTM8 : β-actin
0.0020
0.0015
0.0010
0.0005
0
*
*
*
Ctrl
Adipo
Ctrl
Adipo
Vector
TWIST^OE
C
CMTM8 : β-actin
0.010
0.008
0.006
0.004
0.002
0
Day: 4 7 10 14 21 4 7 10 14 21 4 7 10 14 21
Ctrl
Osteo
Adipo
D
CMTM8 : β-actin
0.006
0.004
0.002
0
*
*
*
*
Ctrl
Osteo
Ctrl
Osteo
Normal
SCS

3.2.5 Regulation of CMTM8 by TWIST-1

In silico analyses showed three putative TWIST-1 binding sites in the first intron of *CMTM8* at approximately 9,500kb to 11,000kb 3' away from the first exon of *CMTM8* (Figure 3.7). However, ChIP analysis was unsuccessful in showing direct binding of TWIST-1 to these putative binding regions (Figure 3.8). Interestingly, the *in silico* analyses demonstrated the presence of multiple putative EZH2 bindings sites along the 5' promoter region of *CMTM8* gene (Figure 3.9), suggesting EZH2 can directly bind to *CMTM8*. Unfortunately, ChIP analysis failed to showed direct binding of EZH2 to these putative binding regions (Figure 3.10A). However, decreased levels of *CMTM8* was observed in *EZH2* overexpressing BMSC when compared to vector only BMSC (Figure 3.10B), suggesting an alternate mechanism of regulation.

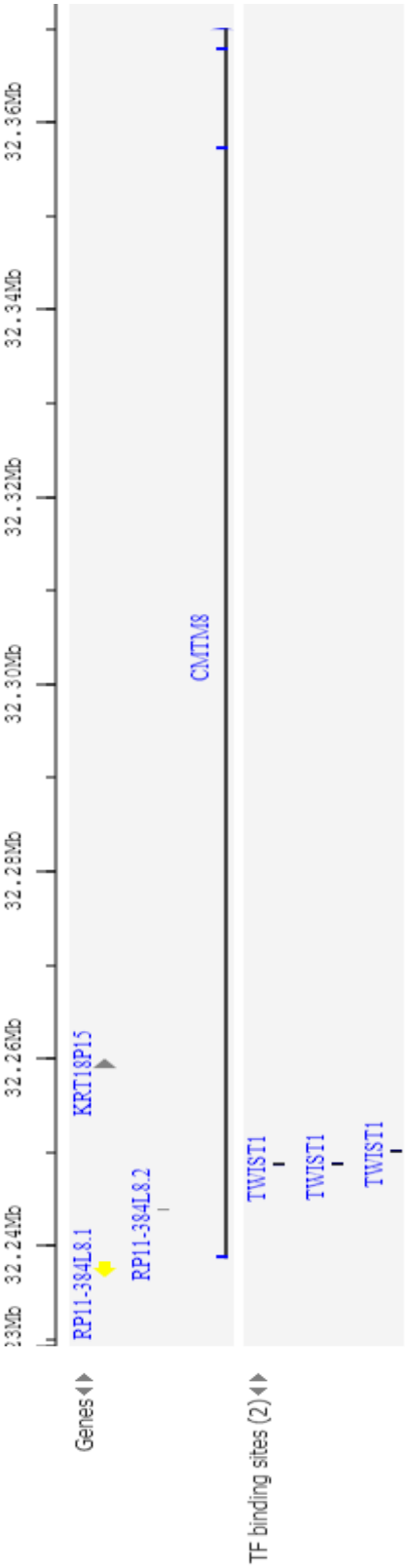

Figure 3.7. Schematic diagram of *in silico* analysis showing putative binding sites of TWIST-1 on the *CMTM8* promoter. Adapted from [253].

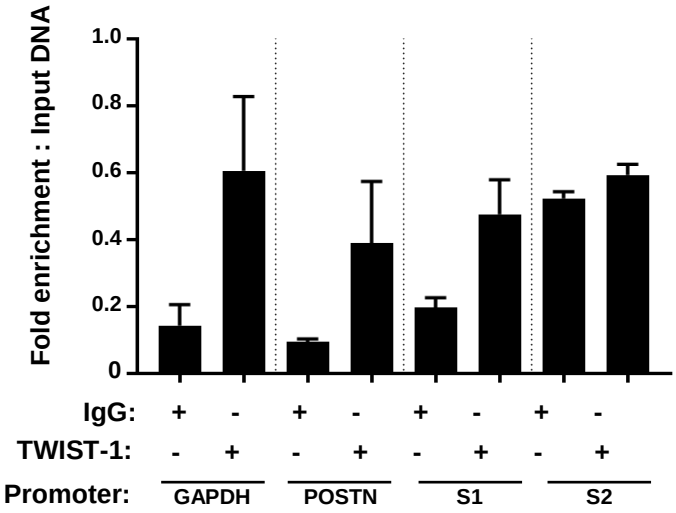

Figure 3.8. ChIP analysis of two putative TWIST-1 E-box binding sites located on the CMTM8 intron 1 (site 1 (S1) and site 2 (S2)) using control antibody (IgG) or TWIST-1 antibody. Fold enrichment was calculated by measuring the levels of enriched genomic DNA compared to the input genomic DNA of BMSC cultured in growth conditions by PCR. Fold enrichment results for CMTM8, S1 and S2 were compared to GAPDH (negative control). Graphs represent mean ± S.E.M, Student's t-test $p<0.05$(*), n=1 donors.

Figure 3.9. Schematic diagram of *in silico* analysis showing putative binding sites of EZH2 on the *CMTM8* promoter. S1 and S2 indicate sites where ChIP analysis of EZH2 binding was performed. Adapted from [253].

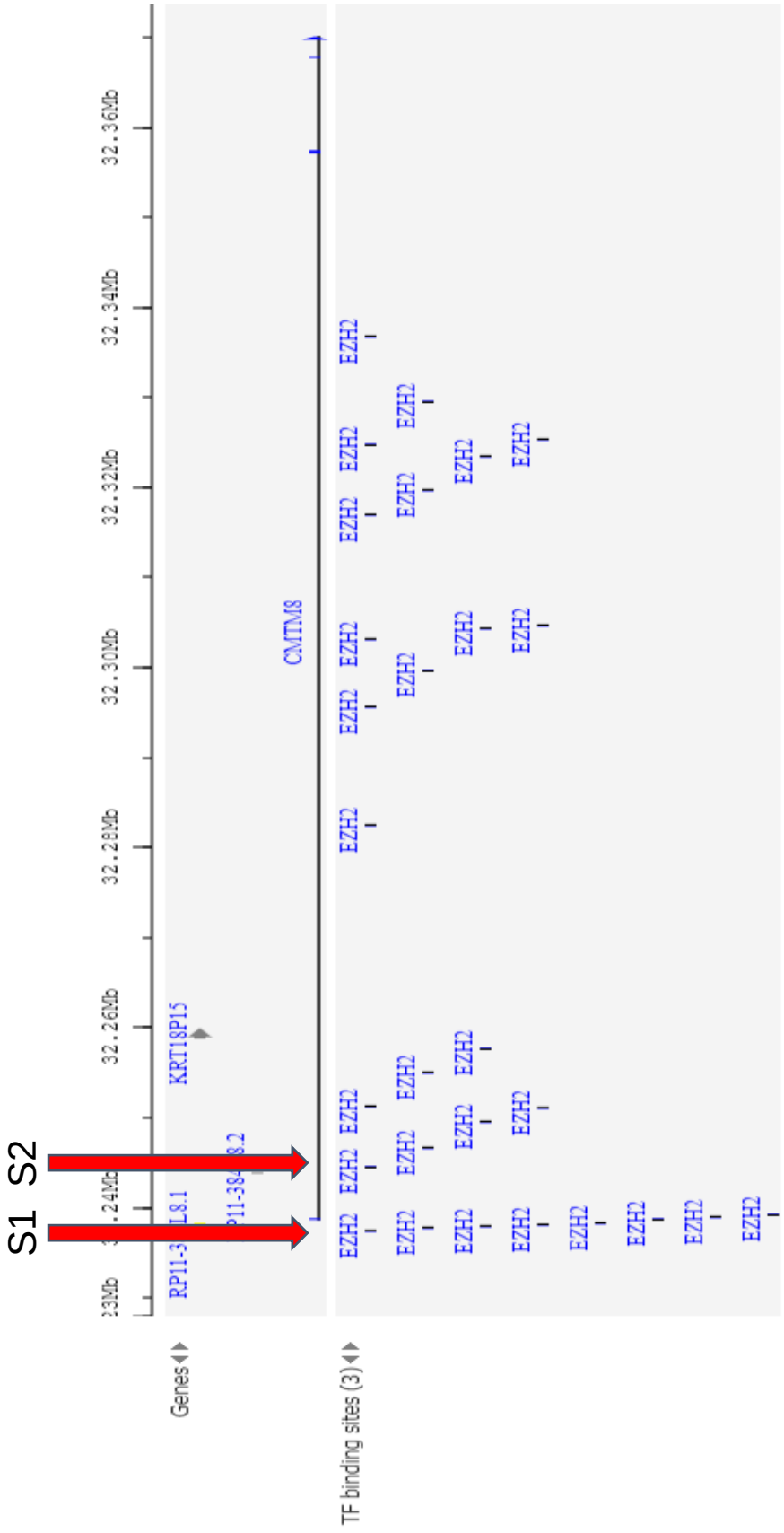
S1
S2
32.36Mb
32.34Mb
32.32Mb
32.30Mb
32.28Mb
32.26Mb
CMTM8
KRT18P15
RP11-3
L8.1
P11-38
8.2
EZH2
Genes
TF binding sites (3)

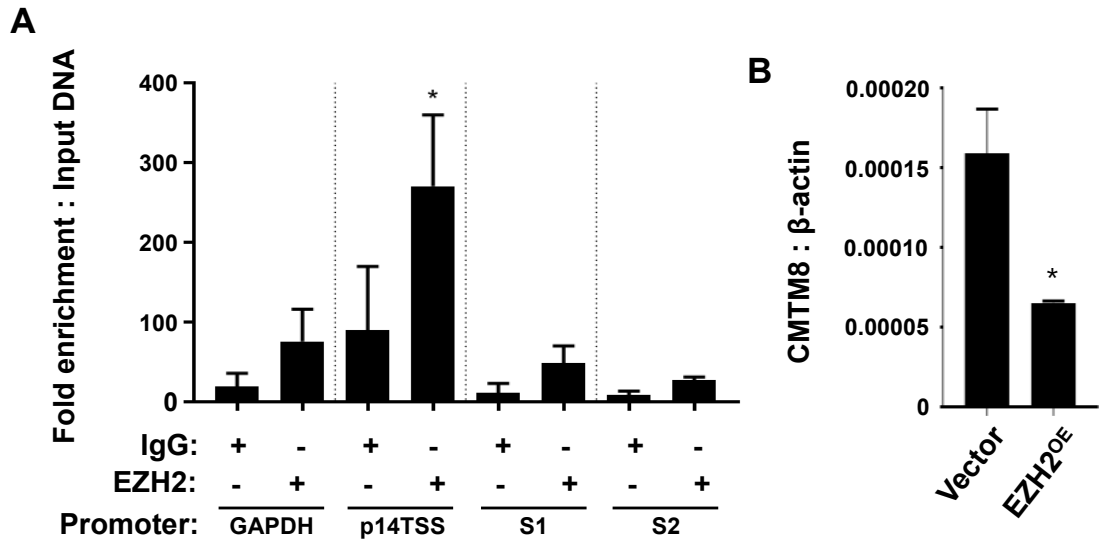

Figure 3.10. (A) ChIP analysis of two putative EZH2 binding sites located on the CMTM8 promoter and intron 1 (site 1 (S1) and site 2 (S2)) using control antibody (IgG) or EZH2 antibody. Fold enrichment was calculated by measuring the levels of enriched genomic DNA compared to the input genomic DNA of BMSC cultured in growth conditions by PCR. Fold enrichment results for CMTM8, S1 and S2 were compared to GAPDH (negative control). Graphs represent mean ± S.E.M, Student's t-test $p<0.05$(*), n=2 donors. (B) *CMTM8* expression was measured for $EZH2^{OE}$ and Vector BMSC cultured under growth conditions. Real-time PCR was used to measure levels of *CMTM8* expression relative to *β-actin*. Graphs represent mean ± S.D., student-t test, $p<0.05$(*), n=1 donor.

3.3 Discussion

In the present study, two candidate genes *HOPX* and *CMTM8*, with high fold change and P-values were selected for further study to identify any potential roles in human BMSC proliferation and differentiation. The *HOPX* gene was ranked with the highest fold change and P-value from the microarray analysis (Table 3.1). Our previous studies have demonstrated an association between TWIST-1/EZH2 and EZH2/HOPX in BMSC, where TWIST-1 increased *EZH2* expression and EZH2 decreased *HOPX* expression [2, 224]. EZH2 is a histone methyltransferase that trimethylates the histone 3 lysine 27 (H3K27me3), which then leads to chromatin condensation and gene repression [225]. In BMSC, TWIST-1 and EZH2 may act in association to inhibit *HOPX* expression to shutdown osteogenesis and cellular senescence, while allowing adipogenesis to occur [2, 196], suggesting that HOPX may play an important role during BMSC growth and differentiation. Microarray results were validated with real-time PCR, confirming an increased expression level of *HOPX* during both BMSC osteogenic and adipogenic differentiation and downregulation in the presence of enforced *TWIST-1* expression. In addition, our preliminary results found that BMSC expressed low level of *HOPX* during growth conditions, while *HOPX* expression levels increased dramatically during osteogenic and adipogenic differentiation, suggesting that HOPX is involved in BMSC differentiation.

SCS is autosomal-dominantly inherited and is induced by loss-of-function mutations of *TWIST-1* [192]. *TWIST-1* haploinsufficient mutation in CBC results in decreased cell proliferation and increased osteogenesis, leading to premature bone plate fusion in the developing skull (craniosynostosis). To begin to determine if HOPX plays a role in CBC osteogenic differentiation, *HOPX* gene expression was assessed in the CBC from un-affected human patient and SCS patients. Our data did not show an increase in *HOPX* transcript levels

during CBC osteogenic differentiation. However, a robust increase in *HOPX* transcript levels were observed in CBC from SCS patients. This suggests a negative correlation between *TWIST-1* and *HOPX* and that HOPX may be involved in BMSC and CBC differentiation.

TWIST-1 is known to regulate biological processes through binding to the E-box (CANNTG) on the promoter of target genes or by homo- or hetero-dimerization with other protein molecules, leading to activation or repression of transcription or protein functions [172, 251, 252]. To determine whether HOPX expression was directly regulated by TWIST-1, an *in silico* study was performed to identify putative E-box binding sites on the 5' region of the *HOPX* promoter. No E-box binding sites were identified however, the analysis did show the presence of putative EZH2 binding sites. ChIP analysis was subsequently employed to assess genomic DNA isolated from human BMSC cultured under osteogenic inducing conditions. ChIP analysis showed direct binding of EZH2 to these putative binding regions, suggesting that *HOPX* expression is directly regulated by EZH2. Furthermore, a negative correlation was observed between *EZH2* and *HOPX* expression. Thus, regulation of *HOPX* by TWIST-1 is likely mediated indirectly via the modulation of EZH2.

Another differentially expressed gene of interest with no known function in human BMSC was *CMTM8.* Previous studies have shown that CMTM8 plays an important role in cancer cell growth, survival and migration via regulation of EGFR and c-Met signalling pathway [241, 245]. EGFR and c-Met signalling have been known as crucial molecular mechanisms for cell expansion and motility. Both EGFR and c-Met belong to the tyrosine kinase receptor group. Ablation of EGFR pathway could lead to a decrease in cell proliferation and increased apoptosis [241]. Conversely, induced EGFR following EGF stimulation results in increased cell proliferation [241]. It has been shown that CMTM8 regulates EMT state of cells via c-Met

[245]. As a potential tumour suppressor gene, CMTM8 was thought to suppress cell metastasis by inhibiting c-Met signalling and the EMT changes.

Data from the microarray analysis was validated with real-time PCR, confirming increased expression levels of *CMTM8* during both BMSC osteogenic and adipogenic differentiation and downregulation in the presence of enforced *TWIST-1* expression. In addition, our preliminary results found that BMSC expressed low level of *CMTM8* during growth conditions, while *CMTM8* expression levels increased gradually across time during osteogenic and adipogenic differentiation, suggesting that CMTM8 is involved in BMSC differentiation. It is interesting to note that *CMTM8* expression levels were elevated at day 21 of BMSC osteogenic differentiation, suggesting a potential role of CMTM8 during late osteogenic differentiation. *CMTM8* gene expression was also assessed in CBC from SCS and from un-affected donors. Consistent with the BMSC data, *CMTM8* transcript levels were found to be upregulated during CBC osteogenic differentiation. However, in SCS patients, *CMTM8* transcript levels appeared to be significantly lower compared to that of normal control CBC. Overall, these preliminary studies suggest a negative correlation between *TWIST-1* and *CMTM8* only in BMSC and that CMTM8 may be involved in BMSC differentiation.

To determine what binding sites were present on the 5'region of the CMTM8 promoter, an *in silico* study was performed to identify putative E-box and EZH2 binding sites. Three putative TWIST-1 binding sites and multiple putative EZH2 binding sites were identified. However, ChIP analysis did not show binding of TWIST-1 or EZH2 on the promoter region of *CMTM8*, although a negative correlation between *EZH2* and *CMTM8* expression was observed. The negative correlation between *TWIST-1*, *EZH2* and *CMTM8* expression in BMSC may just be a

coincidence or *CMTM8* expression is mediated indirectly by TWIST-1 via the modulation of other molecules.

It is important to note that assessment of transcript levels of HOPX or CMTM8 showed insignificant donor-donor variability. In addition, expression levels of HOPX or CMTM8 were comparable between BMSC and CBC. The question arises as to whether the increased expressions of HOPX or CMTM8 overtime during differentiation inductive conditions is due to tissue culture artefact. To address this question, confirmatory experiments can be performed by replacing additives in our regular inductive media with differentiation inductive factor such as Bmp2 for osteogenic induction.

Chapter 4: HOPX Counteracts TWIST-1/ EZH2 Regulation of BMSC Cell Fate Determination via Suppression of Adipogenic Gene Pathways

4.1 Introduction

The homeodomain-only protein homeobox gene (*HOPX*), encodes HOPX which is the smallest known member of the homeodomain-containing protein family with the size of 8kDa [222, 250]. The human *HOPX* gene is located on chromosome 4 (4q11eq12) and contains seven exons, with only exons 1, 5, 6, and 7 contributing to transcription of the five mRNA transcript variants (National Center for Biotechnology Information; NCBI, data). Variant 1 encodes for a 91 amino acids protein (isoform a); Variants 2, 3 and 4 encode for a 73 amino acids protein (isoform b); and Variant 5 encodes for the longest isoform c protein with 112 amino acids (NCBI data) (Figure 4.1) [254]. In contrast, the mouse *Hopx* gene is located on chromosome 5 and encodes for three 73 amino acids variants (NCBI data). Human and murine *HOPX* sequences share 92% identity at the amino acid level. Unlike other typical homeobox proteins that bind to DNA and regulate their expression, HOPX does not bind directly to DNA. It has previously been described that HOPX binds to different protein partners and act as a co-factor to regulate molecular mechanisms by recruiting transcription factors to gene promoters [222, 250, 255]. Studies have demonstrated an association between TWIST-1/Enhancer of zeste homolog 2 (EZH2) and EZH2/HOPX in BMSC, where TWIST-1 increases *EZH2* expression and EZH2 decreases *HOPX* expression [2, 224]. EZH2 is a histone methyltransferase that trimethylates the histone 3 lysine 27 (H3K27me3), which then leads to chromatin condensation and gene repression [225]. In BMSC, TWIST-1 and EZH2 may act in association to inhibit *HOPX* expression to shutdown osteogenesis and cellular senescence, while allowing adipogenesis to occur [2, 196]. This suggests that HOPX may play an important role during BMSC growth and differentiation.

BMP and WNT signalling pathways have been reported to be integrated by HOPX during cell fate commitment of cardiomyoblasts [223]. It was shown *in vivo* using murine embryos that

Hopx physically interacts with activated Smad complex (Smad4 and phosphorylated Smad1/5/8) and represses Wnt responsive genes upon presence of Bmp4 [223]. Other studies have also identified HOPX-interacting partner such as histone deacetylase 2 (HDAC2), serum response factor (SRF) and enhancer of polycomb homolog 1 (EPC1) that is involved in cell proliferation and differentiation (Figure 4.2) [222, 250, 255-258]. Moreover, HOPX is also thought to act as a tumour suppressor gene, where its expression is suppressed in malignant tissues including; head and neck, breast, lung, oesophagus, colon/rectum, stomach, placenta, pancreas and uterus cancers [254, 258-267]. *Hopx* expression has been identified in many tissues including heart, liver, lung, brain, intestine and spleen, and is a critical protein in cardiac development [222, 250]. Various studies with conflicting data have reported that HOPX is a critical factor in maintaining the balance between cellular proliferation and differentiation by promoting or inhibiting different molecular pathways [222, 250, 268, 269]. Currently, no known function of HOPX has been identified during BMSC growth or differentiation. Using loss-of-function and gain-of-function studies, we have demonstrated that HOPX is a promoter of proliferation and an inhibitor of adipogenesis in human BMSC.

Figure 4.1. Gene structures of human *HOPX*. Seven exons (E1-E7) of the human *HOPX* gene are represented with different colours. Introns are displayed as black lines between each exon. Five different spliced variants (*HOPX-V1* to *HOPX-V5*) give rise to three isoforms: isoform a, b and c of 91, 73 and 112 amino acids, respectively. Adapted from [270].

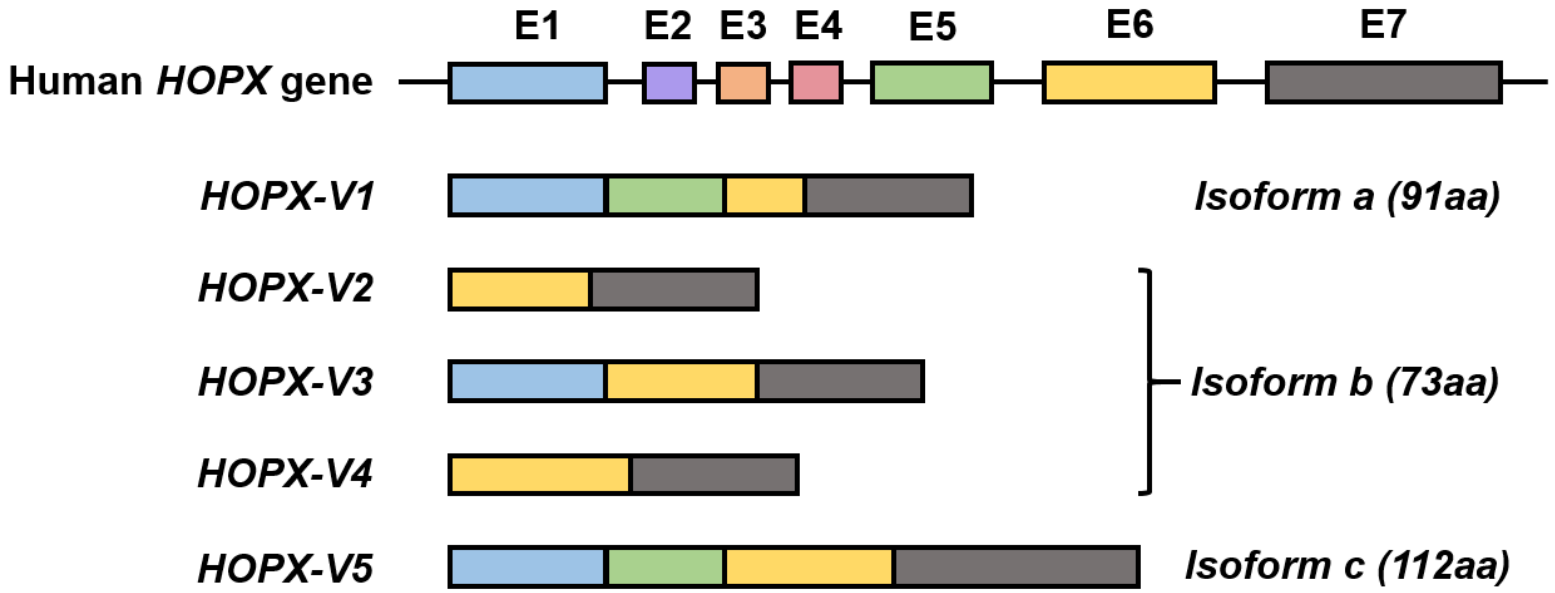
E1
E2
E3
E4
E5
E6
E7
Human HOPX gene
HOPX-V1
Isoform a (91aa)
HOPX-V2
HOPX-V3
Isoform b (73aa)
HOPX-V4
HOPX-V5
Isoform c (112aa)

Figure 4.2. Model illustrating interacting partners of HOPX. Direct interaction between HOPX and HDAC2 induces deacetylation of GATA4 and supresses gene transcription (left); Direct interaction between HOPX and SRF suppresses SRF transcriptional activity and modulation of growth related genes (middle); Direct interaction between HOPX and EPC1 induces transcription of differentiation related genes (right). Adapted from [258].

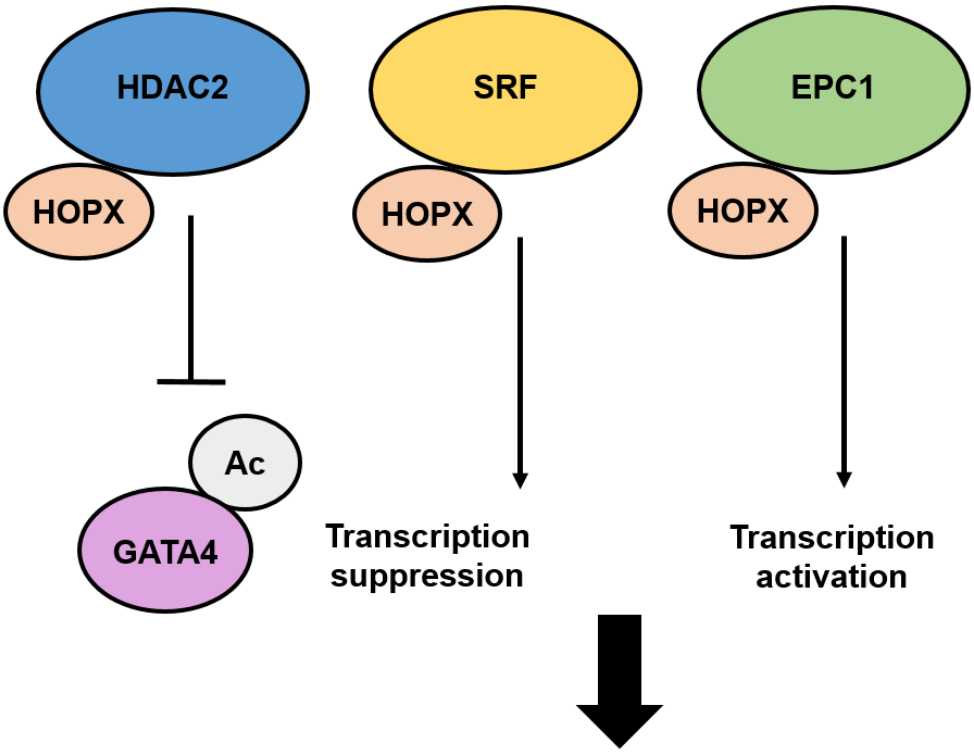

- **Differentiation**
- **Inhibition of proliferation, invasion, metastasis**

4.2 Results

4.2.1 Generation of *HOPX* overexpressing BMSC

Human *HOPX* overexpression vector constructs were generated to study the role of HOPX in the growth and differentiation of BMSC. The full length *HOPX* coding region (1.9 kb) was ligated into pRUF-IRES-GFP vector (6kb). Correct ligation and orientation of *HOPX* gene fragment was determined by Xho1 and BamH1 restriction digestion (Figure 4.3). pRUF-IRES-GFP-HOPX and pRUF-IRES-GFP were transformed into bacteria cultures, then purified DNA was sequenced to confirm the absence of mutations and correct orientation. Retroviral transduction was used to overexpress pRUF-IRES-GFP-HOPX and pRUF-IRES-GFP in BMSC. The level of transfection and infection efficiency was visualized by GFP expression using a fluorescent microscope (Figure 4.4). High GFP-positive BMSC were sorted using fluorescence activated cell sorting (FACS) (Figure 4.5) with transfection efficiency ranging from 12% - 40% for vector only BMSC and 16% - 30% for HOPX overexpressing BMSC and then cultured in normal growth media. The flow cytometry density plot (Figure 4.5) showed forward versus side scatter (FSC vs SSC) gating used to identify GFP positive cells based on size and granularity. No obvious changes in cell size distribution were observed between vector only and HOPX overexpressing cells. Sanger sequencing analysis confirmed correct sequences of *HOPX* inserts, as shown by pairwise alignment of the vector construct sequences to the consensus sequence from the NCBI website (Figure 4.6A). Purity of the vector constructs was assessed by visualizing the sequencing peaks using Chromas software (Technelysium Pty Ltd, South Brisbane, Australia) (Figure 4.6B).

4.2.2 Evaluation of *HOPX* overexpressing BMSC

Western blot analysis was performed to assess *HOPX* overexpression in four vector only BMSC and *HOPX* overexpressing BMSC donors at the protein level (Figure 4.7). However,

Figure 4.3. Restriction digest analysis on pRUF-IRES-GFP-HOPX vector ligation. 1% agarose gel electrophoresis separation of pRUF-IRES-GFP-HOPX vector DNA digested with Xho1 and BamH1 restriction enzymes. Lane 1 represents 1kb Plus DNA ladder. Lane 2, 3 and 4 represents pRUF-IRES-GFP-HOPX vector treated with BamH1, Xho1 and BamH1/ Xho1, respectively.

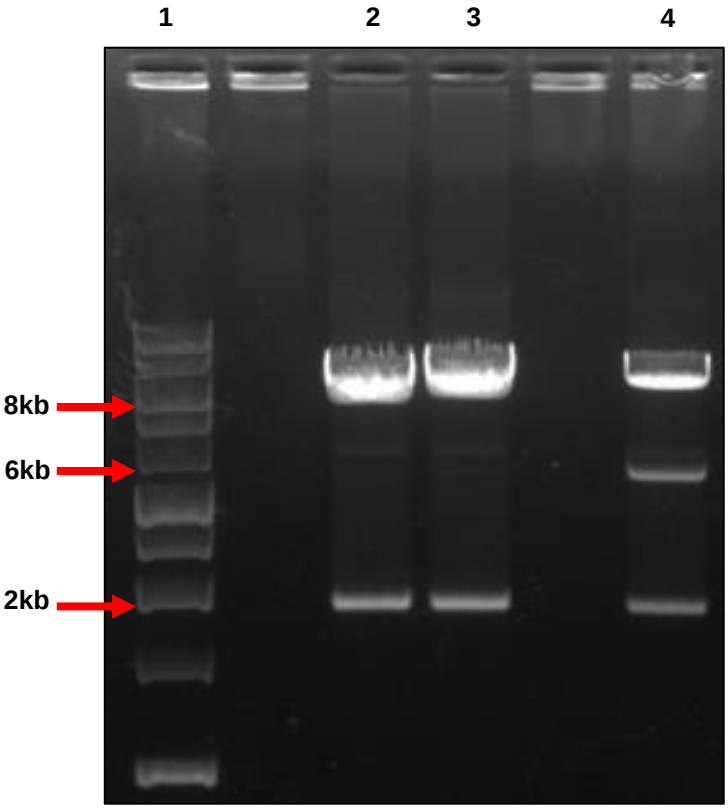
1
2
3
4
8kb
6kb
2kb

Figure 4.4. Enforced expression of pRUF-IRES-GFP-HOPX expressing cells. A representative micrograph showing GFP positive transfected HEK293T cells (Scale bar = 100μm) and BMSC (Scale bar = 200μm) when excited by UV light.

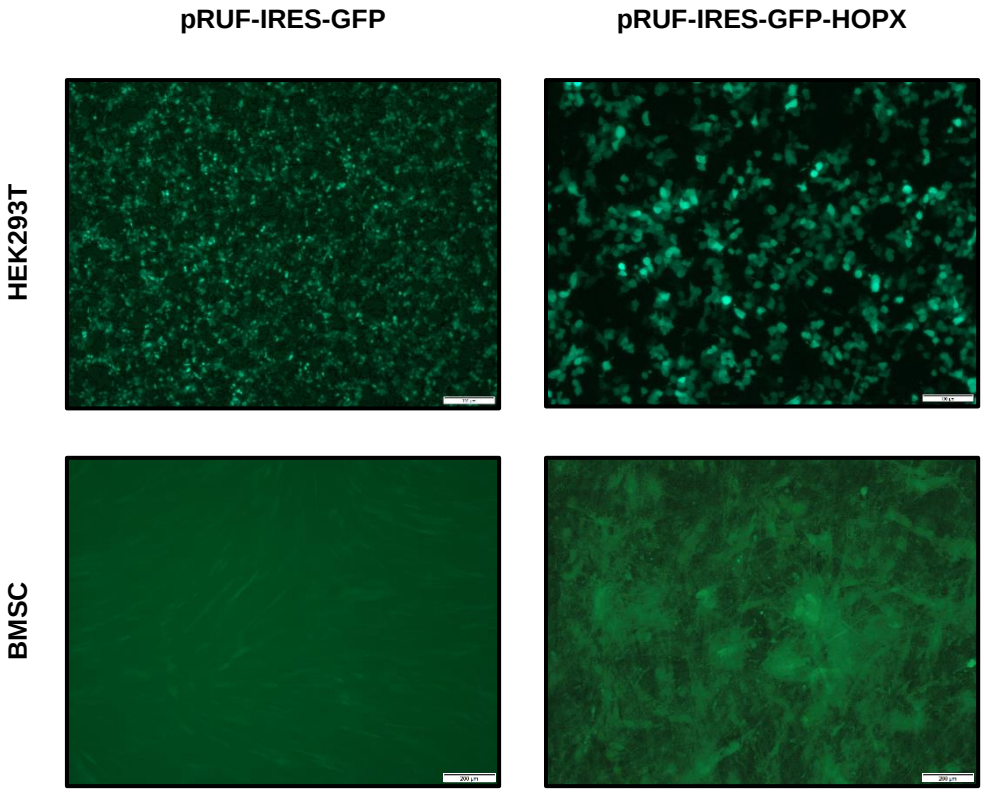
pRUF-IRES-GFP
pRUF-IRES-GFP-HOPX
HEK293T
BMSC

Figure 4.5. GFP positive BMSC selected with FACS. Representative flow cytometry density plot analyses showing GFP positive cell population (vector only & *HOPX* overexpressing BMSC) selected with uninfected cells as the gating control.

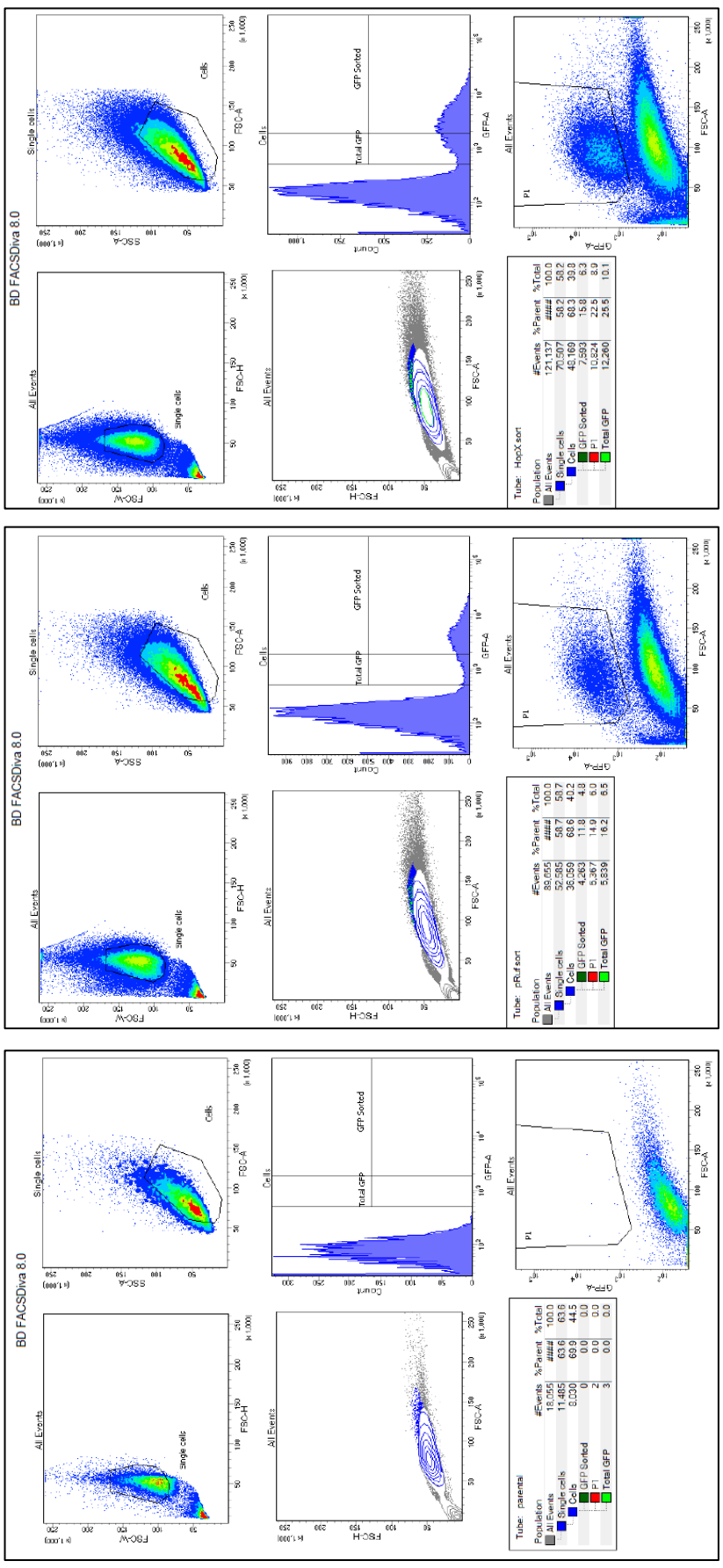
Gating Parental
Vector only BMSC
HOPX overexpressing BMSC
BD FACSDiva 8.0
Tube: parental
Tube: pRufsort
Tube: HopX sort
Population
#Events
%Parent
%Total
All Events
Single cells
Cells
GFP Sorted
P1
Total GFP
Single cells
All Events
Cells
Total GFP
GFP Sorted
P1
FSC-A
FSC-H
SSC-A
FSC-W
GFP-A
Count

Figure 4.6. Confirmation of correct *HOPX* sequence insert in the pRUF-IRES-GFP vector. (A) Sanger sequencing was performed on pRUF-IRES-GFP-HOPX vector using the Pairwise Sequence Alignment Tool. (B) The purity of the vector sequence was confirmed by visualizing the amplified peaks from Sanger sequencing using Chromas Software.

A

```
  1 atgtcggcggagaccgcgagcggccccacagaggaccaggtggaaatcct     50
    ||||||||||||||||||||||||||||||||||||||||||||||||||
  1 ATGTCGGCGGAGACCGCGAGCGGCCCCACAGAGGACCAGGTGGAAATCCT     50

 51 ggagtacaacttcaacaaggtcgacaagcacccggattccaccacgctgt    100
    ||||||||||||||||||||||||||||||||||||||||||||||||||
 51 GGAGTACAACTTCAACAAGGTCGACAAGCACCCGGATTCCACCACGCTGT    100

101 gcctcatcgcggccgaggcaggcctttccgaggaggagacccagaaatgg    150
    ||||||||||||||||||||||||||||||||||||||||||||||||||
101 GCCTCATCGCGGCCGAGGCAGGCCTTTCCGAGGAGGAGACCCAGAAATGG    150

151 tttaagcagcgcctggcaaagtggcggcgctcagaaggcctgccctcaga    200
    ||||||||||||||||||||||||||||||||||||||||||||||||||
151 TTTAAGCAGCGCCTGGCAAAGTGGCGGCGCTCAGAAGGCCTGCCCTCAGA    200

201 gtgcagatccgtcacagactaa     222 <-- CMTM8 consensus sequence (NCBI)
    ||||||||||||||||||||||
201 GTGCAGATCCGTCACAGACTAA     222 <-- CMTM8 vector construct sequence
```

B

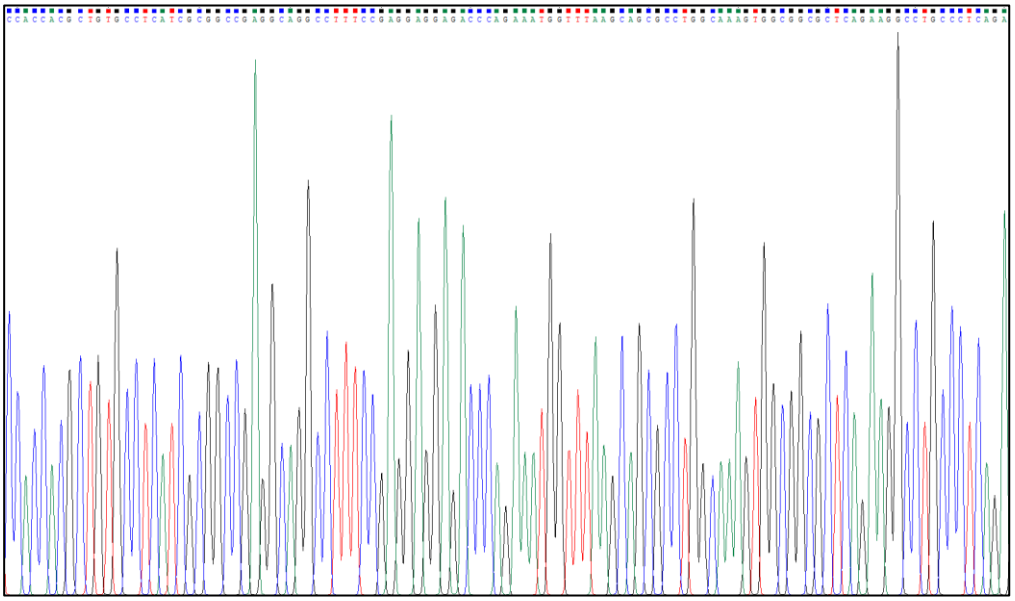

Figure 4.7. Western blot analysis to confirm expression of HOPX by pRUF-IRES-GFP-HOPX vector infected BMSC. Protein expression of HOPX was assessed by Western blot analysis using two different antibodies against HOPX: anti-HOPX-1 & anti-HOPX-2. Western blot to detect Tubulin (50kDa) was used as a loading control.

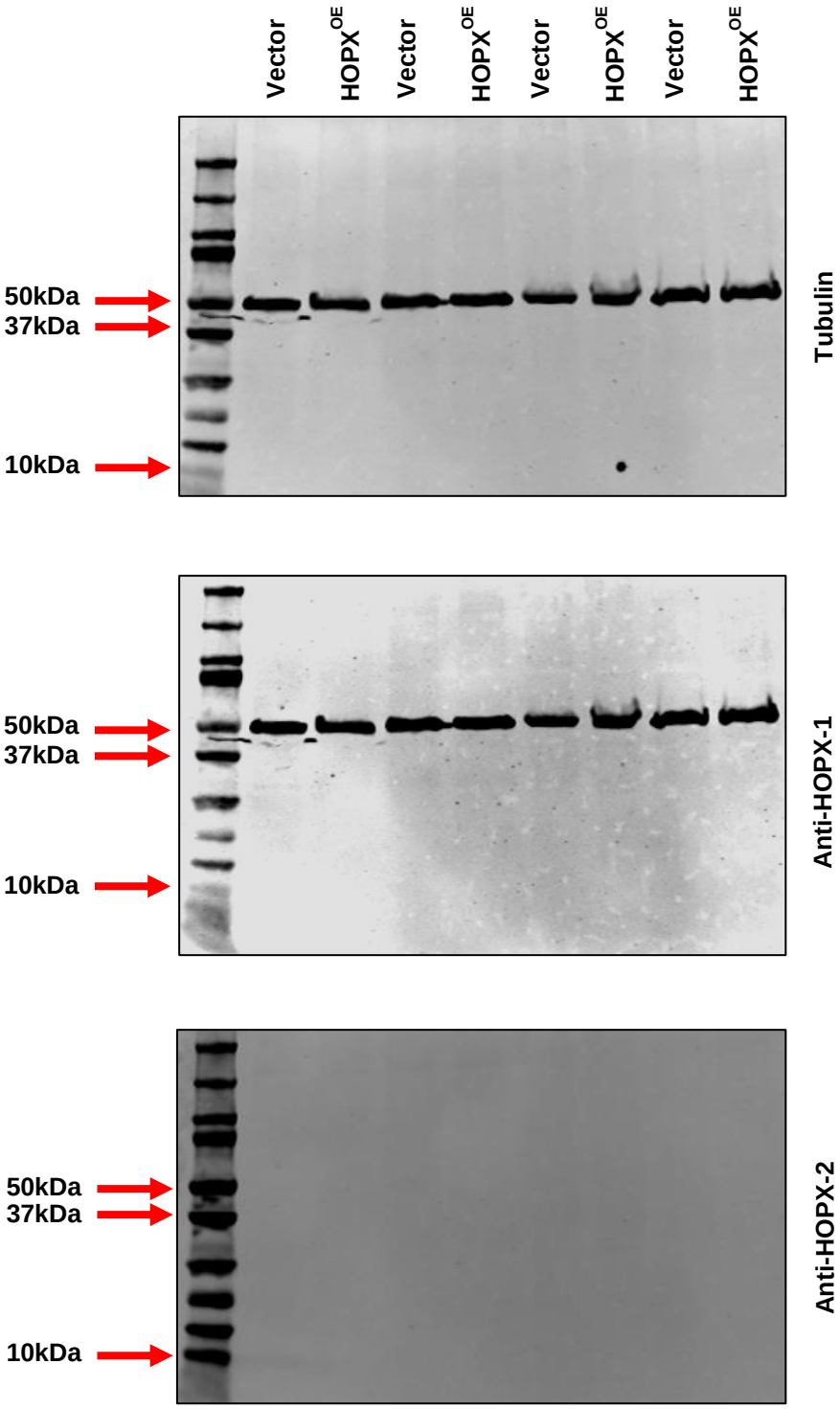
Vector
HOPX^OE
Vector
HOPX^OE
Vector
HOPX^OE
Vector
HOPX^OE
50kDa
37kDa
10kDa
Tubulin
50kDa
37kDa
10kDa
Anti-HOPX-1
50kDa
37kDa
10kDa
Anti-HOPX-2

no HOPX protein expression was detected using two different antibodies (over the concentrations of 1:200 and 1:1000) against HOPX: anti-HOPX-1 and anti-HOPX-2 (HOPX expected molecular weight is 8kDa), in comparison to the loading control, Tubulin. Nevertheless, when expression of *HOPX* transcript was determine in cells using real-time PCR, there was differential expression of *HOPX* in vector only BMSC compared to *HOPX* overexpressing BMSC. Interestingly, expression levels of *HOPX* transcripts in three pRUF-IRES-GFP-HOPX human BMSC donors were found to be approximately 100 fold higher compared with vector only control pRUF-IRES-GFP BMSC (Figure 4.8A).

4.2.3 HOPX is a promoter of BMSC proliferation

In order to determine if HOPX regulates BMSC growth, cell proliferation was assessed in *HOPX* overexpressing and vector control BMSC by analysis of BrdU incorporation. The data showed a significant increase in the proliferation rates of BMSC following enforced expression of *HOPX* (Figure 4.8B). To further confirm that HOPX regulates BMSC proliferation, *HOPX* expression was knocked down using two independent siRNA molecules targeting *HOPX* transcripts (Figure 4.8C). Knockdown of *HOPX* in BMSC resulted in a significant decreased in proliferation rates (Figure 4.8D). These data suggest that HOPX is a positive regulator of BMSC proliferation.

4.2.4 HOPX is an inhibitor of BMSC adipogenesis

To establish the role of HOPX during human BMSC adipogenic differentiation *in vitro*, *HOPX* overexpressing retroviral constructs or empty vector alone infected BMSC were cultured in control growth or adipogenic inductive media (Figure 4.9A). Overexpression of *HOPX* resulted in decreased Nile red-positive (Figure 4.9B, Ci, Cii) and Oil-red O positive (Figure 4.9Ciii,Civ) lipid producing adipocytes compared with empty vector control cells. Quantitative assessment

Figure 4.8. HOPX promotes BMSC proliferation. (A) cDNA was prepared from RNA harvested from *HOPX* overexpressing ($HOPX^{OE}$) and vector only BMSC. Real-time PCR was used to measure levels of *HOPX* relative to *β-actin*, n=5 donors. (B) $HOPX^{OE}$ and vector BMSC were incubated for 4 days and BrdU assay was performed, n=4 donors. (C) cDNA was prepared from RNA harvested from BMSC treated with scramble siRNA (siScram) or siRNA targeting *HOPX* (siHOPX1 & siHOPX2). Real-time PCR was used to measure levels of *HOPX* relative to *β-actin*, n=4 donors. (D) siScram, siHOPX1 (n=4 donors) and siHOPX2 (n=3 donors) BMSC were incubated for 6 days and BrdU assays performed. Graphs represent mean ± S.E.M, Student's t-test $p<0.05$(*).

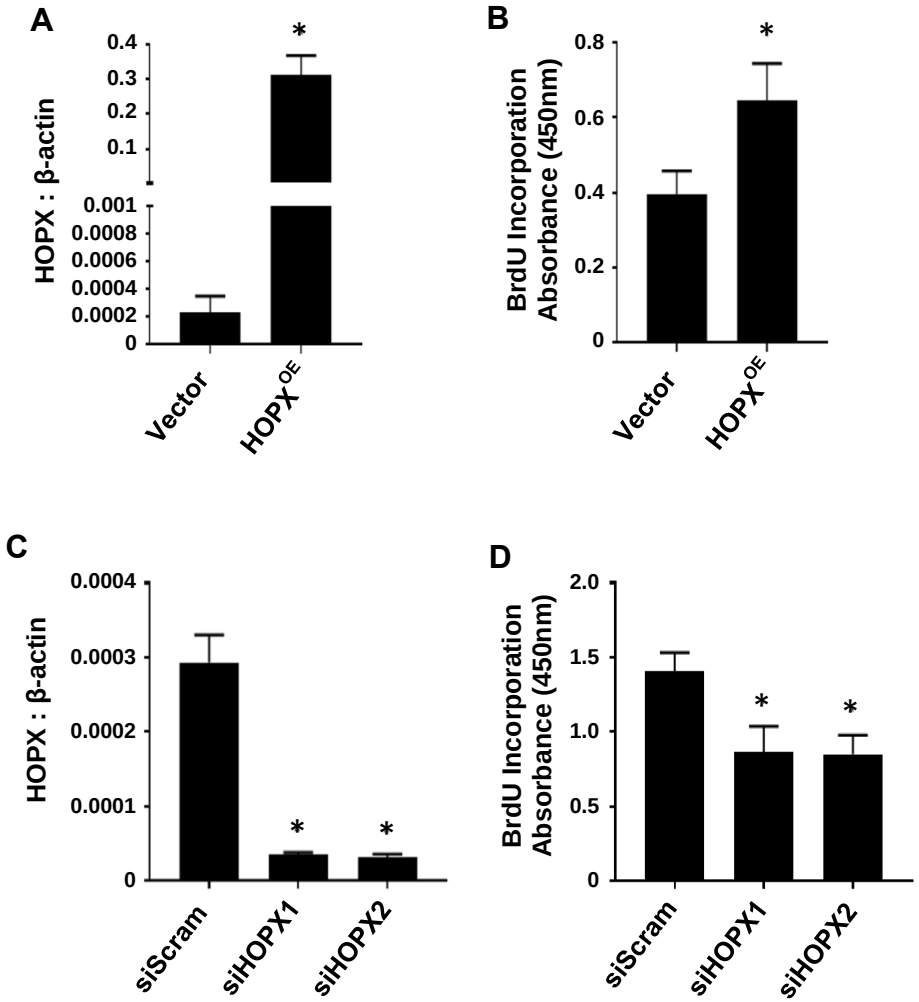
A
HOPX : β-actin
0.4
0.3
0.2
0.1
0.001
0.0008
0.0006
0.0004
0.0002
0
*
Vector
HOPX^OE
B
BrdU Incorporation
Absorbance (450nm)
0.8
0.6
0.4
0.2
0
*
Vector
HOPX^OE
C
HOPX : β-actin
0.0004
0.0003
0.0002
0.0001
0
*
*
siScram
siHOPX1
siHOPX2
D
BrdU Incorporation
Absorbance (450nm)
2.0
1.5
1.0
0.5
0
*
*
siScram
siHOPX1
siHOPX2

Figure 4.9. Enforced expression of *HOPX* inhibits BMSC adipogenesis. (A) *HOPX* overexpressing ($HOPX^{OE}$) and vector only BMSC were cultured in either control (Ctrl) or adipogenic (Adipo) inducing conditions for 3 weeks and *HOPX* expression levels were determined relative to *β-actin* using real-time PCR, n=6 donors. Graphs represent mean ± S.E.M, One-way ANOVA $p<0.05$(*). (B) Lipid-containing $HOPX^{OE}$ and vector only BMSC stained with Nile red and DAPI were quantified, n=3 donors. Graph represents mean ± S.E.M, Student's t-test $p<0.05$(*). (C) Representative images of lipid-containing (I) Vector BMSC and (II) $HOPX^{OE}$ BMSC stained with Nile red and DAPI. (C) Representative images of lipid-containing (III) Vector BMSC and (IV) $HOPX^{OE}$ BMSC stained with Oil Red O. Total RNA was harvested at 7-14 days (n=6 donors) post induction from $HOPX^{OE}$ and Vector BMSC. Real-time PCR was performed to measure levels of (D) *HOPX*, (E) *C/EBPα* and (F) *ADIPSIN* relative to *β-actin*. Graphs represent mean ± S.E.M, Student's t-test $p<0.05$(*). (Scale bar = 200μm)

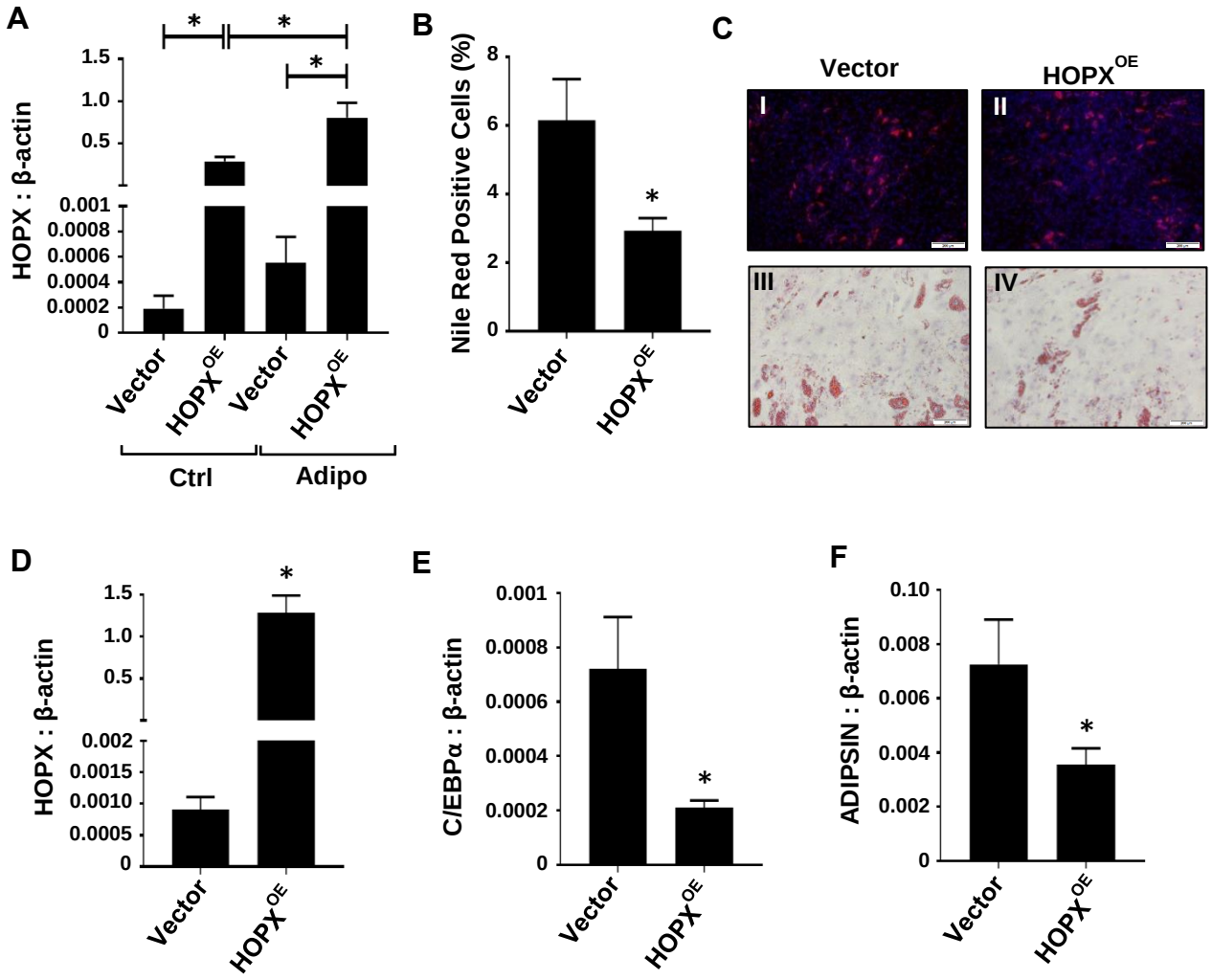
A
HOPX : β-actin
1.5
1.0
0.5
0.001
0.0008
0.0006
0.0004
0.0002
0
Vector
HOPX^OE
Vector
HOPX^OE
Ctrl
Adipo
B
Nile Red Positive Cells (%)
8
6
4
2
0
Vector
HOPX^OE
C
Vector
HOPX^OE
I
II
III
IV
D
HOPX : β-actin
1.5
1.0
0.5
0.002
0.0015
0.0010
0.0005
0
Vector
HOPX^OE
E
C/EBPα : β-actin
0.001
0.0008
0.0006
0.0004
0.0002
0
Vector
HOPX^OE
F
ADIPSIN : β-actin
0.10
0.008
0.006
0.004
0.002
0
Vector
HOPX^OE

from multiple BMSC lines showed a significant reduction of lipid-containing adipocytes in *HOPX* overexpressing BMSC cultured compared with vector controls (Figure 4.9C). Changes in adipogenic gene transcription patterns were assessed using real-time PCR, following adipogenic induction. The data demonstrated that *HOPX* overexpressing BMSC (Figure 4.9D) exhibited decreased levels of key adipogenic marker genes, *C/EBPα* (Figure 4.9E) and *ADIPSIN* (Figure 4.9F) expression levels when compared to vector only BMSC, under adipogenic inductive conditions.

To verify these findings, siRNA-mediated knockdown using two independent siRNA targeting *HOPX* transcripts in BMSC was performed (Figure 4.10A). The data showed a dramatic increase in Nile red-positive (Figure 4.10B, C, D) and Oil-red-O positive lipid forming adipocytes (Figure 4.10E) following adipogenic induction, compared with BMSC treated with control scramble siRNA (Figure 4.10B-E). Furthermore, siRNA knockdown of *HOPX* resulted in an increase in *C/EBPα* (Figure 4.10F) and *ADIPSIN* (Figure 4.10G) transcript expression compared with scramble siRNA-treated cells following adipogenic induction. Future experiments could examine other early adipogenic marker genes such as *PPARγ2*, and late adipogenic markers such as *ADIPONECTIN* and *LEPTIN*. Overall, these studies demonstrate that HOPX is a repressor of adipogenesis.

To determine the function of HOPX in BMSC osteogenic differentiation, *HOPX* overexpressing BMSC or vector control BMSC were cultured under control or osteogenic inductive media (Figure 4.11A). Measurements of extracellular calcium levels found no difference between *HOPX* overexpressing BMSC and vector control BMSC (Figure 4.11B). Similarly, mineralized deposits were stained with Alizarin Red after three weeks under osteogenic growth conditions with no observable differences (Figure 4.11C). In accord with

Figure 4.10. Suppression of *HOPX* expression promotes BMSC adipogenesis. (A) siScram, siHOPX1 and siHOPX2 BMSC were cultured in adipogenic (Adipo) inductive conditions for 3 weeks and *HOPX* expression levels were determined relative to *β-actin* using real-time PCR, n=8 donors. (B) Lipid-containing cells treated with siScram or siHOPX1 were stained with Nile red and DAPI, then quantified, n=3 donors. Graph represents mean ± S.E.M, Student's t-test $p<0.05$(*). (C) Lipid-containing cells treated with siScram or siHOPX2 were stained with Nile red and DAPI, then quantified, n=4 donors. (D) Representative images of lipid-containing siScram, siHOPX1 and siHOPX2 BMSC stained with Nile red and DAPI. (E) Representative images of lipid-containing siScram, siHOPX1 and siHOPX2 BMSC stained with Oil Red O. Total RNA was harvested at 7-14 days post induction from BMSC treated with siScram or siHOPX, n=4 donors. Real-time PCR was performed to measure levels of (F) *C/EBPα*, (G) *ADIPSIN* relative to *β-actin*. Graphs represent mean ± S.E.M, Student's t-test $p<0.05$(*). (Scale bar = 200μm)

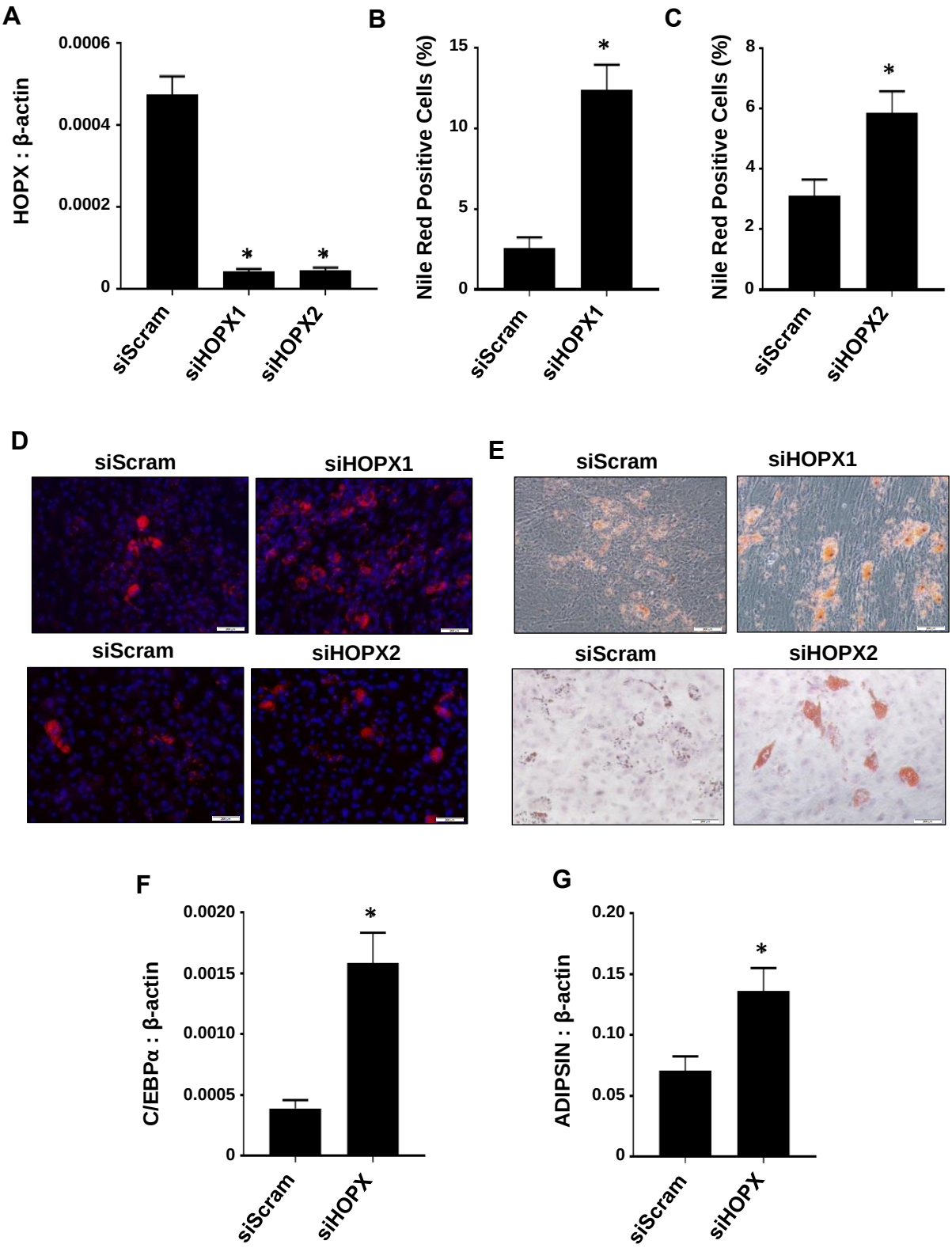
A
HOPX : β-actin
0.0006
0.0004
0.0002
0
*
*
siScram
siHOPX1
siHOPX2
B
Nile Red Positive Cells (%)
15
10
5
0
*
siScram
siHOPX1
C
Nile Red Positive Cells (%)
8
6
4
2
0
*
siScram
siHOPX2
D
siScram
siHOPX1
siScram
siHOPX2
E
siScram
siHOPX1
siScram
siHOPX2
F
C/EBPα : β-actin
0.0020
0.0015
0.0010
0.0005
0
*
siScram
siHOPX
G
ADIPSIN : β-actin
0.20
0.15
0.10
0.05
0
*
siScram
siHOPX

Figure 4.11. Enforced expression of *HOPX* does not affect BMSC osteogenic differentiation. (A) *HOPX* overexpressing ($HOPX^{OE}$) and vector only (Vector) BMSC were cultured in either control (Ctrl) or osteogenic inductive (Osteo) conditions and *HOPX* expression levels were determined relative to *β-actin* using real-time PCR, n=6 donors. Graphs represent mean ± S.E.M, One-way ANOVA $p<0.05$(*). (B) Extracellular calcium levels were quantitated and normalized to total DNA content per well, n=3 donors. Graph represents mean ± S.E.M, Student's t-test $p<0.05$(*). (C) Vector control and $HOPX^{OE}$ BMSC stained with Alizarin red. Total RNA was harvested at 7-14 days post induction (n=6 donors) from Vector and $HOPX^{OE}$ BMSC. Real-time PCR was used to measure levels of (D) *HOPX*, (E) *RUNX2*, (F) *OPN* relative to *β-actin*. Graphs represent mean ± S.E.M, Student's t-test $p<0.05$(*). (Scale bar = 200μm)

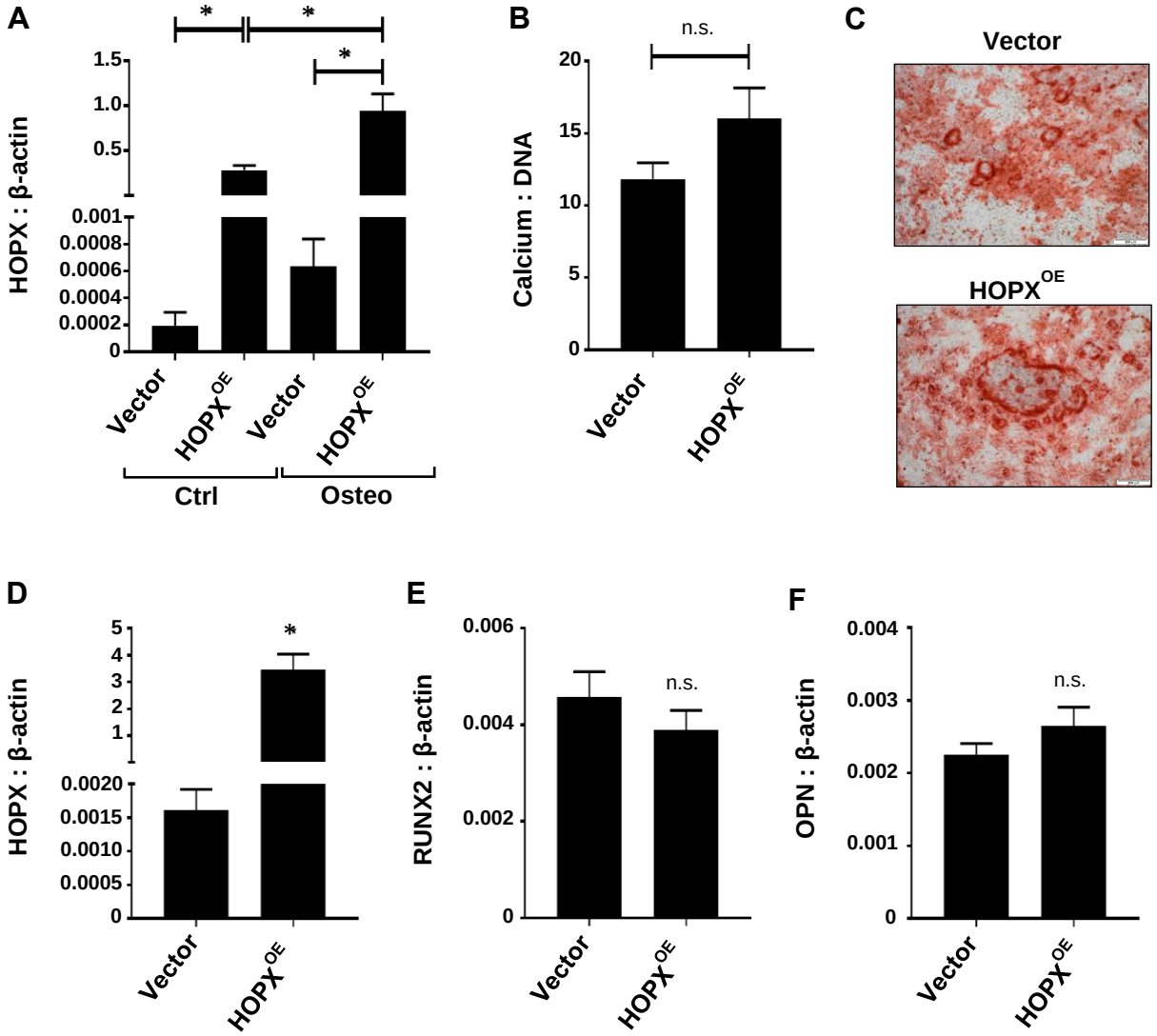
A
B
C
D
E
F
HOPX : β-actin
Calcium : DNA
RUNX2 : β-actin
OPN : β-actin
n.s.
Vector
HOPX^OE
Ctrl
Osteo

these findings, *HOPX* overexpressing BMSC (Figure 4.11D) showed no significant difference in the transcript levels of the osteogenic master regulator, *RUNX2* (Figure 4.11E) and the mature bone marker, *OPN* (Figure 4.11F), compared to the vector control cells.

Confirmatory studies employing siRNA-mediated knockdown of *HOPX* in BMSC (Figure 4.12A) found no significant differences in the levels of Alizarin positive mineral and extracellular calcium levels compared with scramble siRNA-treated BMSC (Figure 4.12B-E). These findings demonstrate that HOPX has no direct effect on the osteogenic capacity of BMSC.

4.2.5 HOPX inhibits BMSC adipogenic differentiation via suppression of genes associated with adipogenesis

Parallel studies were performed to determine the potential mechanisms of HOPX action during BMSC adipogenic differentiation. Total RNA was collected from *HOPX* overexpressing and vector control BMSC cultured for two weeks under adipogenic inductive conditions, then processed for RNA-sequencing to identify novel HOPX-regulated genes during BMSC adipogenic commitment. Due to the variable gene expression patterns between different individuals (n=3 donors), the P-value significance was excluded as a criteria to select for differentially expressed genes (DE). Therefore, the top 50 DE (Figure 4.13) were selected based on the fold change (a log fold change (logFC) >= |1| or >=|-1|). To validate the RNA-sequencing results, confirmatory real-time PCR was performed on a number of genes that appeared to change expression in *HOPX* overexpressing BMSC under adipogenic conditions. *HOPX* transcripts were found to be elevated in *HOPX* overexpressing BMSC compared to vector control BMSC and which were relatively higher during adipogenesis compared to normal growth condition for the respective population. From the transcriptional expression

heat map (Figure 4.13), we observed a number of genes that were upregulated during adipogenesis but suppressed in *HOPX* overexpressing cells. Table 4.1 indicates the functional role of these genes following Gene Ontology (GO) enrichment analysis, with 188 genes involved in EMT, 185 genes in adipogenesis and 127 genes in fatty acid metabolism. Table 4.2 detailed the functions of genes selected from the heatmap that are involved in fat/lipid metabolism or adipogenesis. The differential gene expression levels of representative upregulated genes, *HOPX*, *ADIPOQ*, *AOC3*, *FABP4*, *G0S2*, *GPD1*, *PLIN1* and *PLIN4* were confirmed by real-time PCR (Figure 4.14A-H). Other genes were found to be downregulated during adipogenesis and promoted by HOPX expression such as *CNN1* (Figure 4.14I). The RNA-sequencing analysis provides insight into putative targets of HOPX during BMSC adipogenesis.

Figure 4.12. Suppression of *HOPX* does not affect BMSC osteogenic differentiation. (A) siScram, siHOPX1 and siHOPX2 BMSC were incubated in control (Ctrl) or osteogenic inductive (Osteo) conditions for 3 weeks, and HOPX expression levels were determined relative to *β-actin* using real-time PCR, n=8 donors. Extracellular calcium levels were quantitated in siScram, (B) siHOPX1 and (C) siHOPX2 BMSC and normalized to total DNA content per well, n=4 donors. (D-E) siScram, siHOPX1 and siHOPX2 BMSC were stained with Alizarin red. Representative of one donor is shown. Graphs represent mean ± S.E.M, Student's t-test $p<0.05$ (*), n.s. represents non-significant. (Scale bar = 200μm)

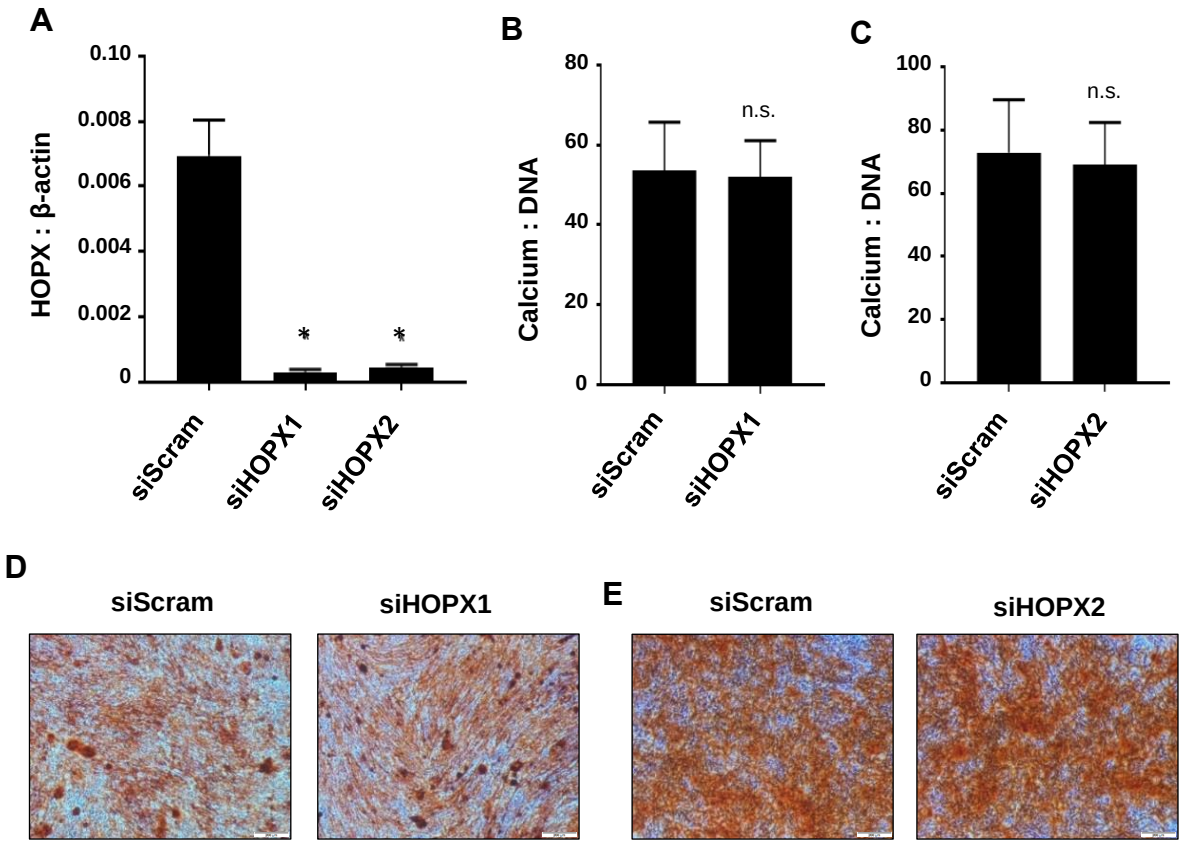
A
HOPX : β-actin
0.10
0.008
0.006
0.004
0.002
0
*
*
siScram
siHOPX1
siHOPX2
B
Calcium : DNA
80
60
40
20
0
n.s.
siScram
siHOPX1
C
Calcium : DNA
100
80
60
40
20
0
n.s.
siScram
siHOPX2
D
siScram
siHOPX1
E
siScram
siHOPX2

Figure 4.13. Potential mechanisms of HOPX regulation of BMSC adipogenesis. *HOPX* overexpressing ($HOPX^{OE}$) and vector only BMSC were cultured in either control (Ctrl) or adipogenic inductive (Adipo) conditions for 2 weeks. Total RNA was collected and assessed by RNA-seq analysis, n=3 donors per condition. The heat map depicts the top 50 differentially expressed genes (DE) selected based on fold expression as shown.

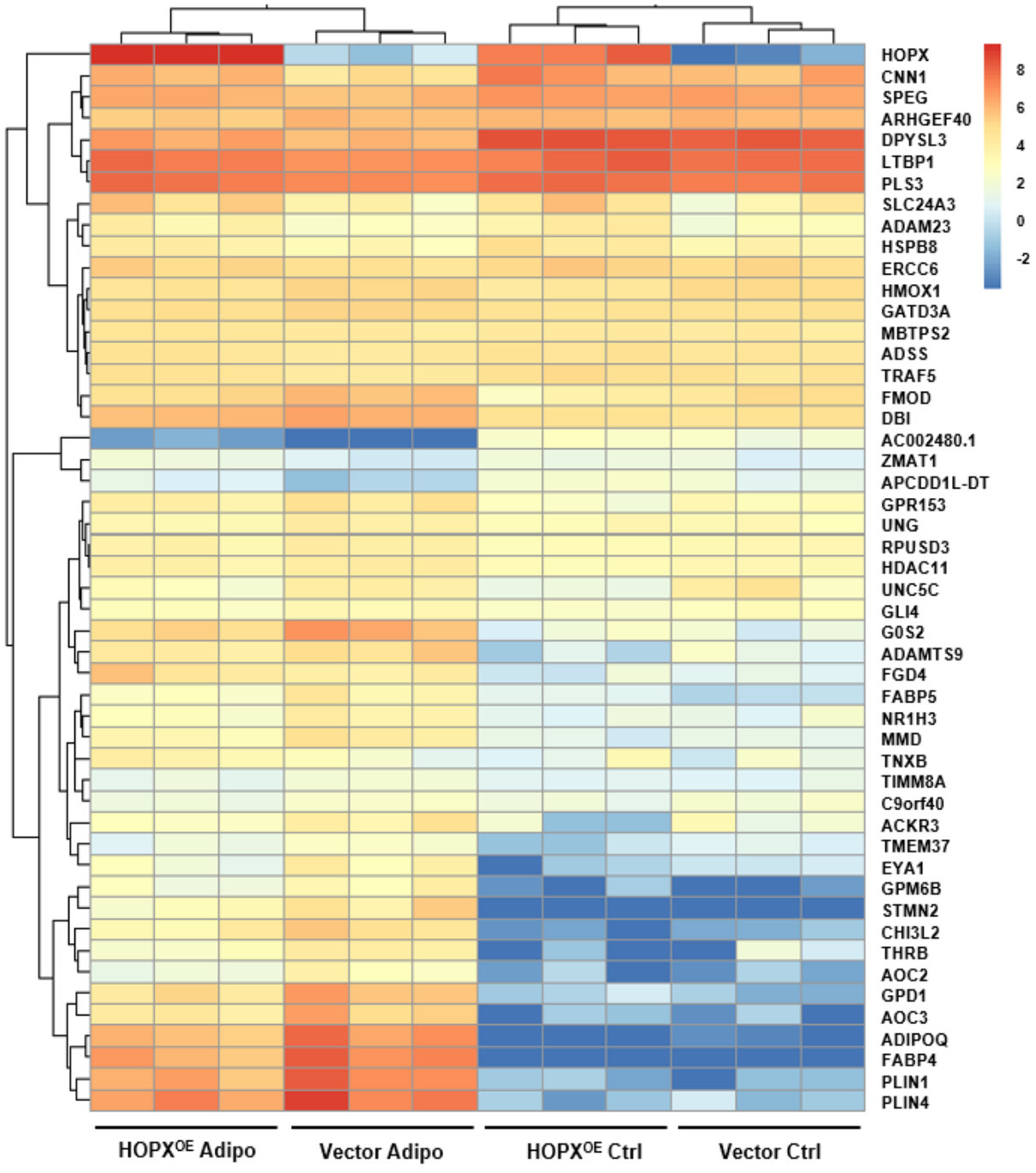
HOPX
CNN1
SPEG
ARHGEF40
DPYSL3
LTBP1
PLS3
SLC24A3
ADAM23
HSPB8
ERCC6
HMOX1
GATD3A
MBTPS2
ADSS
TRAF5
FMOD
DBI
AC002480.1
ZMAT1
APCDD1L-DT
GPR153
UNG
RPUSD3
HDAC11
UNC5C
GLI4
G0S2
ADAMTS9
FGD4
FABP5
NR1H3
MMD
TNXB
TIMM8A
C9orf40
ACKR3
TMEM37
EYA1
GPM6B
STMN2
CHI3L2
THRB
AOC2
GPD1
AOC3
ADIPOQ
FABP4
PLIN1
PLIN4
8
6
4
2
0
-2
HOPX^OE Adipo
Vector Adipo
HOPX^OE Ctrl
Vector Ctrl

Figure 4.14. Confirmation of RNA-seq data. Real-time PCR was performed to measure levels of (A) *HOPX*, (B) *ADIPOQ*, (C) *AOC3*, (D) *FABP4*, (E) *G0S2*, (F) *GPD1*, (G) *PLIN1*, (H) *PLIN4*, (I) *CNN1* relative to *β-actin*. Graphs represent mean ± S.E.M, One-way ANOVA $p<0.05$(*), n=2 donors.

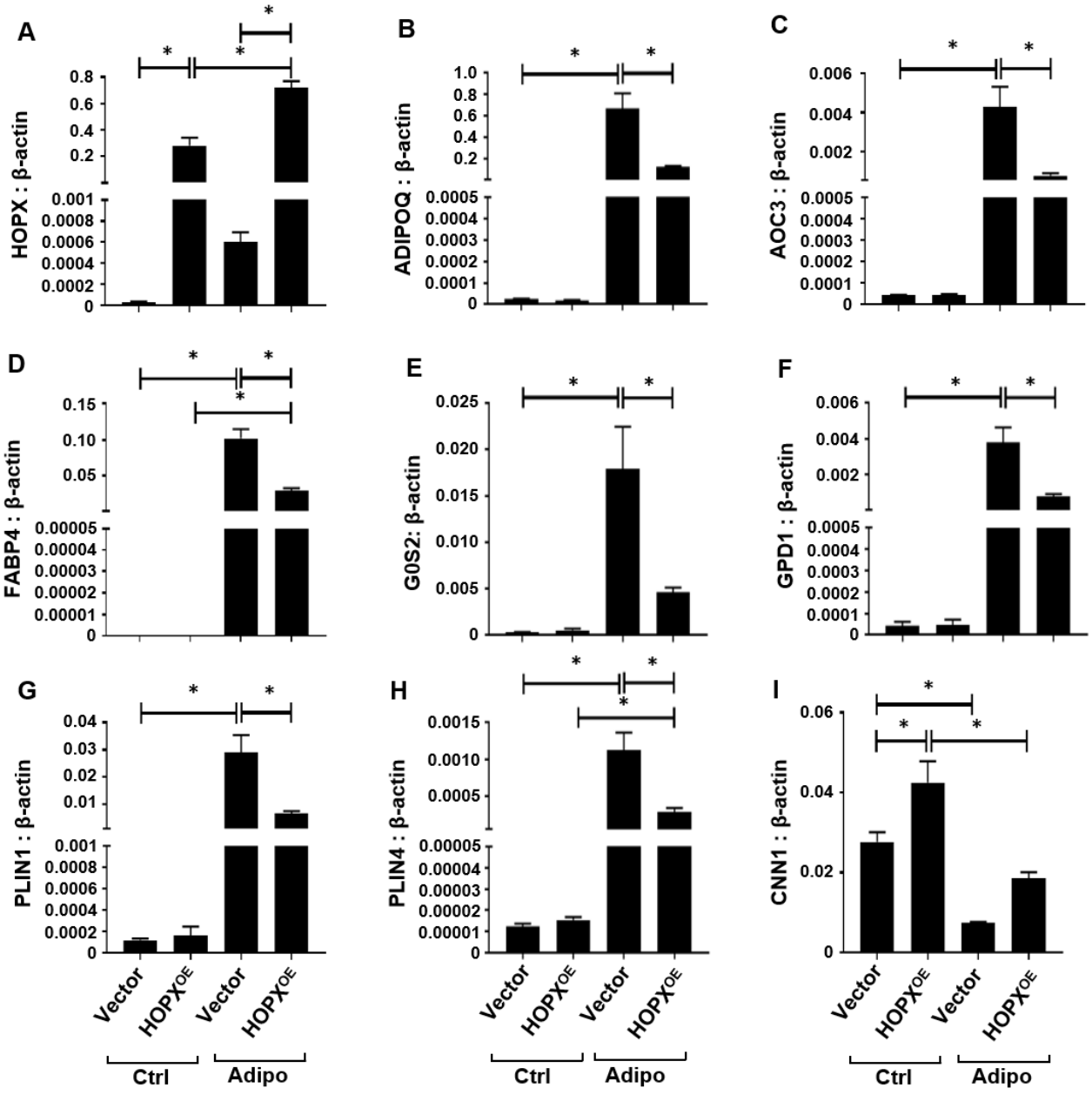
A
HOPX : β-actin
B
ADIPOQ : β-actin
C
AOC3 : β-actin
D
FABP4 : β-actin
E
G0S2: β-actin
F
GPD1 : β-actin
G
PLIN1 : β-actin
H
PLIN4 : β-actin
I
CNN1 : β-actin
Vector
HOPXOE
Vector
HOPXOE
Ctrl
Adipo

Table 4.1. Gene ontology annotations of differentially expressed genes from RNA-seq analysis of *HOPX* overexpressing and Vector only BMSC cultured under normal growth or adipogenic conditions.

Gene Ontology	No. Genes	Direction	P-value	FDR
Epithelial Mesenchymal Transition	188	Down	6.01E-09	3.00E-07
Adipogenesis	185	Up	3.55E-07	8.88E-06
Hypoxia	161	Down	6.56E-05	0.001069
Bile acid metabolism	67	Up	8.55E-05	0.001069
Fatty acid metabolism	127	Up	1.96E-04	0.001964
Xenobiotic_metabolism	131	Up	4.19E-04	0.003494
Angiogenesis	23	Down	7.99E-04	0.00571
Glycolysis	157	Down	0.001059	0.006621

Table 4.2. Genes from RNA-seq that are involved in fat/ lipid metabolism or adipogenesis.

Gene	Functions
ADAM23	• Receptor of LGI3: LGI3 binds to ADAM23 and supresses adipogenesis • LGI3 negatively regulates adiponectin
FMOD	• Regulates mesenchymal stem cell fate during skeletal aging • Decreases bone mass & increases bone marrow adiposity
PLS3	• Genetic variants in the PLS3 gene are associated with osteoporotic fractures in postmenopausal Chinese women • Plastin 3 influences bone homeostasis through regulation of osteoclast activity
HDAC11	• Suppresses osteoclast differentiation • Regulates metabolism and obesity • Loss of HDAC11 activates the adiponectin-AdipoR-AMPK pathway in the liver
UNC5C	• Repressed by Rhox5 • Rhox5 interacts with GATA, which is a binding partner of HOPX
G0S2	• Promotes abdominal fat deposition • Target of PPARγ • Knockdown G0S2 attenuate lipid accumulation
ADAMTS9	• Regulates cell growth and metastasis • Cartilage degradation: adiponectin increases ADAMTS9 expression
FABP5	• Involved in PPAR signalling • Promotes lipolysis of lipid droplets • Promotes BMSC proliferation
NR1H3	• Regulation of cholesterol homeostasis, regulating cholesterol uptake • Promotes fatty acids synthesis • PPARγ and adipogenesis
TNX	• Promoter of osteogenesis, inhibit osteoclast • Adipogenesis
GPD1	• PPARγ regulated gene • Triglyceride biosynthesis
AOC3	• Development of adiposity • Adipogenesis
ADIPOQ	• Adipogenesis
FABP4	• Promotes adipogenesis • Transports fatty acid • Association with FABP5 and AdipoQ
PLIN1	• Adipogenesis • Osteoporosis • Specific marker for liposarcoma • Promotes proliferation and migration in liposarcoma
PLIN4	• Triacylglycerol packaging into adipocytes. • Coat protein involved in the biogenesis of lipid droplets

4.3 Discussion

The bHLH transcription factor, TWIST-1 is an inhibitor of BMSC osteogenesis, whilst promoting adipogenesis and proliferation of BMSC [1]. The H3K27 methytransferase, EZH2, was found to be induced by TWIST-1 in BMSC and inhibits osteogenesis and cellular senescence but increases adipogenesis [2, 196]. Following studies of global ChIPseq analyses, EZH2 was found to regulate HOPX expression during BMSC osteogenic and adipogenic differentiation [224], suggesting a potential role of HOPX in regulating BMSC lineage specification.

HOPX is the smallest known member of the homeodomain-only containing protein family [222, 250]. Most homeodomains are 60 amino acids, while HOPX is only 73 amino acids composed of three α-helices arranged around a hydrophobic core. Protein structural studies have demonstrated that HOPX is unable to bind to DNA, suggesting that HOPX functions through protein-protein interaction with partner proteins. A number of HOPX partner proteins have been identified, including Hdac1, Hdac2, MTA 1/2/3, MBD3 and Rbbp4/7 [223]. *HOPX* has been shown to be a key factor in cardiac development, where it regulates cell proliferation and differentiation at different stages during murine cardiac development [222, 250]. The dual role of Hopx in the developing heart correlates with its action downstream of the Nkx2.5, where it controls myocyte proliferation and expansion through regulation of the serum response factors [271-273] and Hdac recruitment [222, 250, 256, 274]. Furthermore, Hopx and Hdac2 physically interact to mediate Gata4 deacetylation, and therefore co-ordinately regulate embryonic cardiomyocytes proliferation [255]. HOPX is widely expressed in diverse tissues, where it is critically involved in the regulation of proliferation and differentiation. BMSC express low level of *HOPX* when cultured *in vitro* yet expression is increased during osteogenesis and adipogenesis [224]. Studies of homozygous mutations of the *Hopx* gene (loss

of function mutations) in mouse showed partial penetrant embryonic lethality due to heart deformation during embryo development. However, those that survived display no gross deformities. *Hopx* heterozygous mutated mice are viable and comparable to wild type mice [222, 250]. This suggests that Hopx is critical for cardiac development. On the other hand, the incomplete penetrance of *HOPX* mutation indicates that there are other compensatory mechanisms that rescues part of the phenotype. However, no bone or fat-associated phenotypes have been observed in *Hopx* knockout studies. Our *in vitro* studies suggest that HOPX mediates postnatal BMSC proliferation and lineage determination.

In the present study, human BMSC were found to have low *HOPX* expression during normal growth cultures, coinciding with our previous studies [224]. However, when BMSC are induced under osteogenic or adipogenic conditions, *HOPX* expression was dramatically upregulated. HOPX expression showed a negative correlation with *TWIST-1* expression, however we found no evidence of TWIST-1 directly regulating the expression of *HOPX*. Our previous studies have shown that TWIST-1 can increase the lifespan and the proliferation of human BMSC *in vitro* as well as promote stemness by maintaining a more immature stem cell phenotype [1, 46, 54, 173]. Moreover, TWIST-1 was found to induce expression and recruitment of the epigenetic regulator, EZH2, to the Ink4A locus to increase the lifespan and prevent cellular senescence of BMSC [2]. Given that EZH2 regulates *HOPX* expression [224], it is likely that the affects of TWIST-1 on *HOPX* are mediated via EZH2 activity.

Functional studies using siRNA-mediated knockdown of *HOPX* did not affect BMSC osteogenesis but did alter the cellular proliferation and adipogenic potential of the cells. Our studies have shown that siRNA-mediated *HOPX* knockdown in human BMSC decreased proliferation and increased adipogenic potential of these cells. This was demonstrated by an

increase of lipid formation and increased expression of early adipogenic marker *C/EBPα* and mature marker *ADIPSIN*, when compared to the siRNA scramble controls. Conversely, these results were confirmed by enforced expression of *HOPX* in BMSC using retroviral transduction. *HOPX* overexpressing BMSC demonstrated decreased lipid formation and decreased expression of adipogenic associated markers. These findings suggest that HOPX is a novel molecular inhibitor of BMSC adipogenesis and may have implications in the regulation of fat metabolism. It also indicates that HOPX could act in a negative feedback loop to counter balance the levels of *TWIST-1*. Therefore, HOPX may function to inhibit the effects TWIST-1 on BMSC growth and differentiation [1, 2]. In fact, in our study, knockdown of *HOPX* had a greater effect on BMSC differentiation than overexpression. Furthermore, *HOPX* overexpression or knockdown studies failed to demonstrate any effects on the osteogenic potential of BMSC. This is likely because HOPX acts by inhibiting adipogenesis via suppression of *C/EBPα* by potentially binding to adipogenic suppressor proteins that act on its promoter as a complex, therefore, the differentiation pathway needs to be activated for *RUNX2* to be expressed and then HOPX can promote its recruitment. Given that both TWIST-1 and EZH2 inhibit BMSC osteogenic differentiation but allow adipogenesis to proceed [1, 196], implicates HOPX as a potential counter balance to regulate BMSC adipogenesis. Our findings open up further research into the role of the homeobox family members in BMSC biology and their complex interactions with other transcription regulators such as basic HLH factors.

HOPX is known to repress transcription by direct interaction with co-repressors such as HDAC2 which consequently inactivate GATA6/WNT7 pathway important in development and differentiation [255]. However, conflicting data in the literature demonstrate the duo-functions of HOPX in promoting and inhibiting proliferation and differentiation at different developmental stages, suggesting the importance of HOPX in maintaining the balance between

growth and differentiation in various tissues based on *in vitro* and *in vivo* systems [222, 250]. Our data suggests that in humans, HOPX is likely to play a role in fat metabolism. The suppressive effect of HOPX on C/EBPα- and ADIPSIN-mediated transcriptions also explains how adipogenesis can be inhibited. Intriguingly, BMSC osteogenesis appeared to be unaffected by HOPX, suggesting that the observed HOPX upregulation in osteogenic cultures is probably due to similar media supplements that also act to induce adipogenesis.

In bone marrow, the differentiation of MSC into osteoblasts and adipocytes is competitively balanced. The commitment of BMSC to the adipogenic lineage may result in increased adipocyte formation and decreased osteoblast numbers as observed in age-related bone loss [126]. Numerous *in vitro* experiments performed on BMSC have revealed various factors that promote adipocyte formation inhibit osteogenesis, and conversely, many factors that promote osteoblast formation inhibit adipogenesis [127, 128]. This occurs through the interaction between different signalling pathways such as WNT, BMP, TGF-β, Notch, mTOR [131-133, 138, 143, 152, 155, 160]. Of major importance is which signalling cues act on HOPX to regulate differentiation and stem cell renewal. Previous findings implicate the Bmp/Wnt signalling pathways in regulating Hopx family members [223]. Inhibition of Hopx in mouse and zebrafish results in disruption of cardiac development and lethality. Hopx is found to be expressed in cardiomyoblasts, which interacts physically with activated Smad4 and functions to coordinate local Bmp signals to inhibit Wnt pathway, promoting cardiomyogenesis [223]. However, little is known about the biological function of HOPX in BMSC during postnatal skeletal development and homeostasis.

In order to identify novel HOPX target genes during BMSC adipogenesis, RNA-seq analysis was performed on *HOPX* overexpressing and vector control BMSC cultured under normal

growth or adipogenic inductive condition for two weeks. Differentially expressed genes were identified between normal growth and adipogenic inductive conditions. Survey of the literature identified 188 genes involved in EMT, 185 genes in adipogenesis and 127 genes in fatty acid metabolism. To identify possible signalling or molecular pathways involved in HOPX signalling, gene ontology (GO) enrichment analysis was performed. A heatmap was constructed according to the fold change of gene expression between *HOPX* overexpressing and vector control BMSC cultured under either normal growth or adipogenic conditions. Many of the top 50 differentially expressed genes were found to be associated with adipogenesis such as *ADIPOQ*, *FABP4*, *PLIN1* and *PLIN4*, which generally showed a negative correlation with *HOPX* expression. RNA-seq analysis was validated using real-time PCR, which were found to be consistent between different *HOPX* overexpressing BMSC lines.

Adiponectin (ADIPOQ) is a cytokine secreted in various tissues including BMSC [275]. Adiponectin signals through its cell surface receptors adipoR1 (adiponectin receptor 1) and adipoR2 (adiponectin receptor 2) and can acts in either endocrine, paracrine or autocrine pathway [276, 277]. Upon ligand binding, distinct signalling pathways are initiated across tissues including PPARα, mTOR, AMPK [278-280]. On the other hand, the downstream signalling of adipoR1 can stimulate oxidative phosphorylation, which subsequently increase cell differentiation via suppression of the Wnt inhibitor, sclerostin [281, 282]. Therefore, suppression of *ADIPOQ* by HOPX leads to termination of various pro-adipogenic signalling pathways and results in decreased adipogenic potential of BMSC.

Interestingly, calponin 1 (*CNN1*) gene expression was increased in *HOPX* overexpressing BMSC (logFC = 1.52) compared to vector control BMSC, suggesting that *CNN1* is positively regulated by HOPX. CNN1 is an actin binding protein (ABP) that regulates the dynamics of actin cytoskeleton by direct/indirect participating in the assembly/disassembly of actin

filament, which in turn regulates the cell contraction and movement [283]. CNN1 has been shown to play a role in bone homeostasis, where high expression of CNN1 leads to delayed bone formation and decreased bone mass [284-286]. Cnn1 is known to interact directly with activated or inactivated Smad1/5/8 protein and inhibit Bmp2-Smad1/5/8 signalling [287]. Although the function of CNN1 in the regulation of fat metabolism is unknown, it is involved in the Bmp/Smad pathway, which is a critical pathway in the crosstalk between BMSC osteogenesis and adipogenesis. Therefore, CNN1 is a potential candidate to be further studied in BMSC adipogenesis as a possible regulator of TWIST-1/EZH2/HOPX function in cell fate determination.

Collectively, our findings suggest that HOPX promotes human BMSC proliferation and inhibits adipogenesis, and this is the first ever finding showing the importance of the HOPX in human BMSC self-renewal and cell fate determination as a possible counter balance to TWIST-1/EZH2 function. This study lays the foundation for further research into the role of the homeobox family members in BMSC biology and their complex interactions with basic HLH factors.

Chapter 5: CMTM8 Suppresses Osteogenic Differentiation of Human BMSC but Promotes Proliferation and Migration via the EGFR Signalling Pathway

5.1 Introduction

Using microarray analyses of human BMSC lines grown in culture media and osteogenic inducing media, our group recently identified the chemokine-like factor superfamily 8 (CLKLSF8) gene as a possible downstream target of TWIST-1. Microarray data and real-time PCR data have demonstrated that CLKLSF8 expression increases in human BMSC during osteogenic differentiation but is suppressed in *TWIST-1* overexpressing human BMSC during proliferation and osteogenic differentiation *in vitro* [3]. CLKLSF8, was renamed chemokine-like factor (CKLF)-like MARVEL transmembrane domain containing 8 (CMTM8) and belongs to the chemokine-like factor superfamily (CKLFSF). The CKLFSK consists of nine member molecules, CKLF and CMTM1-8 [288, 289]. CMTM1 links the CKLFSF family with chemokine molecules and CMTM8 links it with member of the transmembrane 4 super family (TM4SF). The characteristics of CMTM2-7 are intermediate between CMTM1 and CMTM8, where CMTM2 is structurally more closely related to chemokine molecules while CMTM7 is more closely related to transmembrane proteins [289]. The human *CMTM8* gene is located on chromosome 3 (3p22.3) and is transcribed into two mRNA transcripts variants (NCBI data). Variant 1 encodes for a 173 amino acids protein and variants 2 encodes for a 115 amino acids protein, lacking exon 2 (NCBI data) (Figure 5.1). In contrast, the mouse *Cmtm8* gene is located on chromosome 9 and encodes for a 173 amino acids protein (NCBI data). Human and murine CMTM8 sequences share 92.5% identity at the amino acid level. CMTM8 protein contains four putative transmembrane regions, however due to the lack of the CCG motif, it is not a typical tetraspanin [290]. Moreover, it contains a MAL-related protein for vesicle trafficking and membrane link domain (MARVEL) domain, suggesting that CMTM8 might play a role in membrane protein trafficking and apposition events [291]. The CMTM8 molecules also contains two tyrosine-based internalization consensus sequences, YXXØ, which can bind directly to the adaptor protein 2 that plays a role in budding from the plasma membrane [292].

Figure 5.1. Gene structures of human *CMTM8*. Four exons (Exon 1-Exon 4) of the human *CMTM8* gene are represented with different colours. Introns are displayed as black lines between each exon. Two different spliced variants (*CMTM8-V1* & *CMTM8-V2*) encodes for 173 and 115 amino acid proteins, respectively.

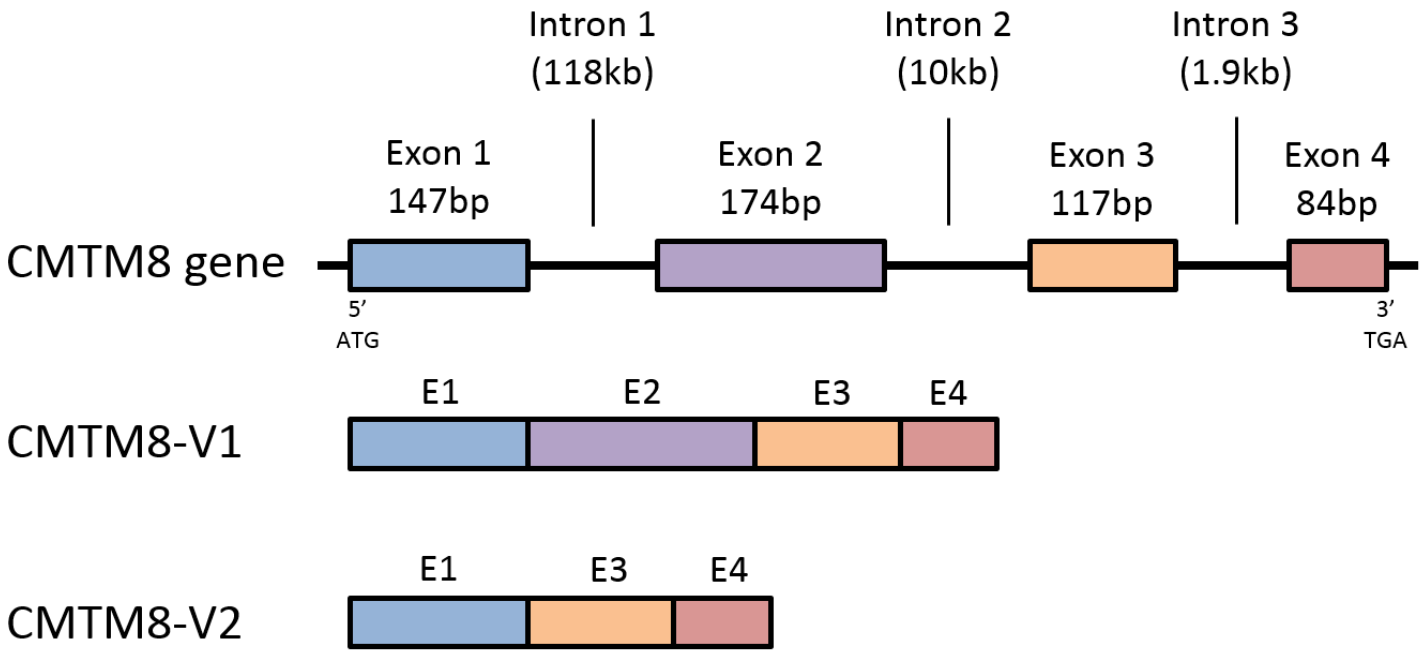
Intron 1
(118kb)
Intron 2
(10kb)
Intron 3
(1.9kb)
Exon 1
147bp
Exon 2
174bp
Exon 3
117bp
Exon 4
84bp
CMTM8 gene
5'
ATG
3'
TGA
E1
E2
E3
E4
CMTM8-V1
E1
E3
E4
CMTM8-V2

Other studies have demonstrated that CMTM8 enhances the ligand-induced internalization of epidermal growth factor receptor (EGFR) from the cell surface, attenuating EGFR-mediated signalling [241], leading to decreased proliferation in HEK293T, HeLa and PC3 cell lines. It has also been reported that the CMTM8-induced absence of EGFR-mediated signalling triggers HEK293T, HeLa and PC3 cell lines to undergo apoptosis via caspase-dependent and -independent pathways, as demonstrated by decreased levels of Bad-S112 phosphorylation [293]. In addition, CMTM8 may be unregulated in tumours, acting as a tumour suppressor gene with important roles in the male reproductive, hematopoietic and immune systems [294]. CMTM8 was found to be a suppressor of EMT-like phenotypes in HepG2 and MCF-10A immortalized human breast epithelial cells via c-Met/ERK signalling [245]. EMT is a hallmark of cell migration and cancer cell metastasis. This suggests that CMTM8 could have an effect on BMSC migration.

Currently, no known function of CMTM8 has been described during BMSC growth, migration and differentiation. The present study aimed to determine whether CMTM8 is a potential mediator of BMSC proliferation, migration and differentiation, using gene knockdown and gain-of-function studies.

5.2 Results

5.2.1 Generation of *CMTM8* overexpressing BMSC

Human *CMTM8* overexpression vector constructs were generated in order to study the role of CMTM8 in the growth and differentiation of BMSC. The full length *CMTM8* coding region (1.2 kb) was ligated into pRUF-IRES-GFP vector (6kb) construct. Correct ligation of *CMTM8* gene fragment was determined by Xho1 and BamH1 restriction digestion (Figure 5.2). pRUF-IRES-GFP-CMTM8 and pRUF-IRES-GFP were transformed into bacteria cultures, then purified DNA was sequenced to confirm the absence of mutations and correct orientation. Retroviral transduction was used to overexpress pRUF-IRES-GFP-CMTM8 and pRUF-IRES-GFP in BMSC. The level of transfection and infection efficiency was observed by visualization of GFP expression using a fluorescent microscope (Figure 5.3). The population of high GFP-positive BMSC were sorted using FACS (Figure 5.4) with transfection efficiency ranging from 40% - 64% for vector only BMSC and 40% - 80% for CMTM8 overexpressing BMSC and then culture expanded in normal growth media. From the forward versus side scatter (FSC vs SSC) gating of the flow cytometry density plot (Figure 5.4), no obvious changes in the size distribution of cells were observed between vector only and CMTM8 overexpressing cells. Sanger sequencing analysis was performed to confirm correct sequences of *CMTM8* inserts, as shown by the pairwise alignment of the vector construct sequences to the consensus sequence obtained from the NCBI website (Figure 5.5A). Purity of the vector constructs was assessed by visualizing the sequencing peaks using Chromas software (Technelysium Pty Ltd, South Brisbane, Australia) (Figure 5.5B).

5.2.2 Evaluation of CMTM8 overexpressing BMSC

Human *CMTM8* overexpression vector constructs were generated in order to study the role of CMTM8 in the growth and differentiation of BMSC. To confirm *CMTM8* overexpression in

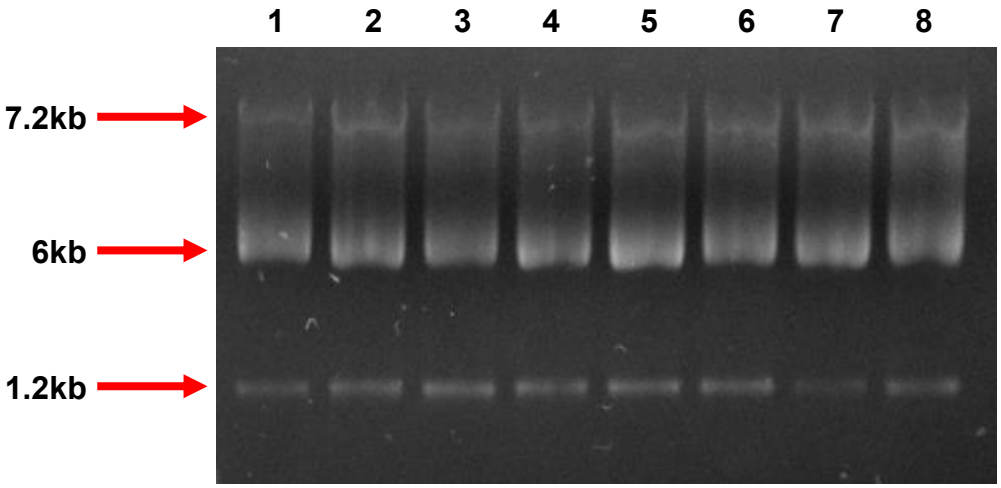

Figure 5.2. Restriction digest analysis on pRUF-IRES-GFP-CMTM8 vector ligation. 1% agarose gel electrophoresis separation of pRUF-IRES-GFP-CMTM8 vector DNA digested with Xho1 and BamH1 restriction enzymes. Lane 1-8 represents individual bacteria clone transformed with pRUF-IRES-GFP-CMTM8.

Figure 5.3. Enforced expression of pRUF-IRES-GFP-CMTM8 expressing cells. Representative micrographs showing vector only and *CMTM8* overexpressing BMSC; stained with DAPI/ Phalloidin (Scale bar = 100μm), GFP positive (Scale bar = 200μm), unstained BMSC (Scale bar = 200μm) and GFP positive HEK293T cells (Scale bar = 100μm) when excited by UV light.

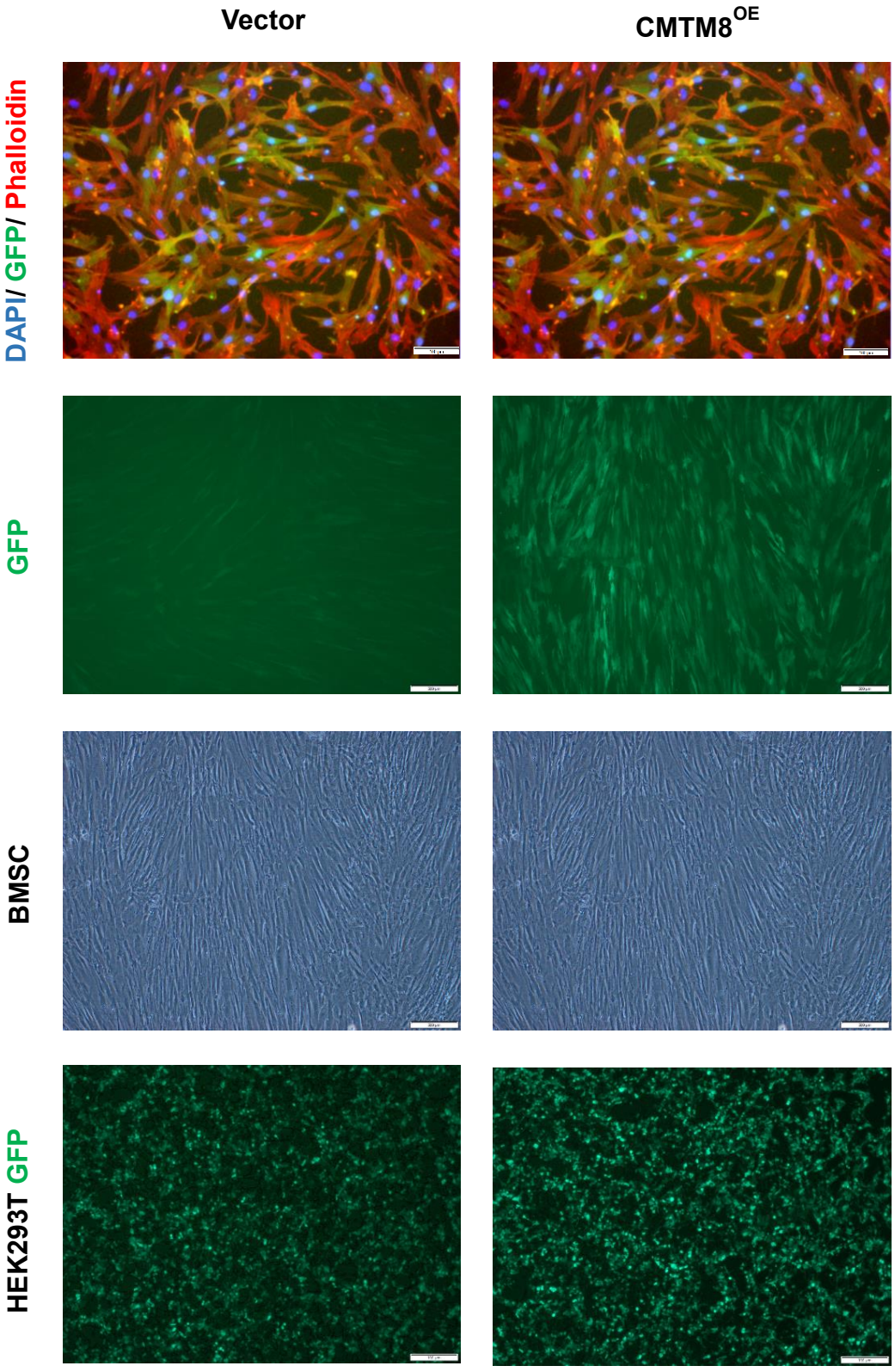
Vector
CMTM8OE
DAPI/ GFP/ Phalloidin
GFP
BMSC
HEK293T GFP

Figure 5.4. GFP positive BMSC selected with FACS. Representative flow cytometry density plot analyses showing GFP positive cell population selected with uninfected cells as the gating control.

Gating Parental | **Vector only BMSC** | ***CMTM8* overexpressing BMSC**

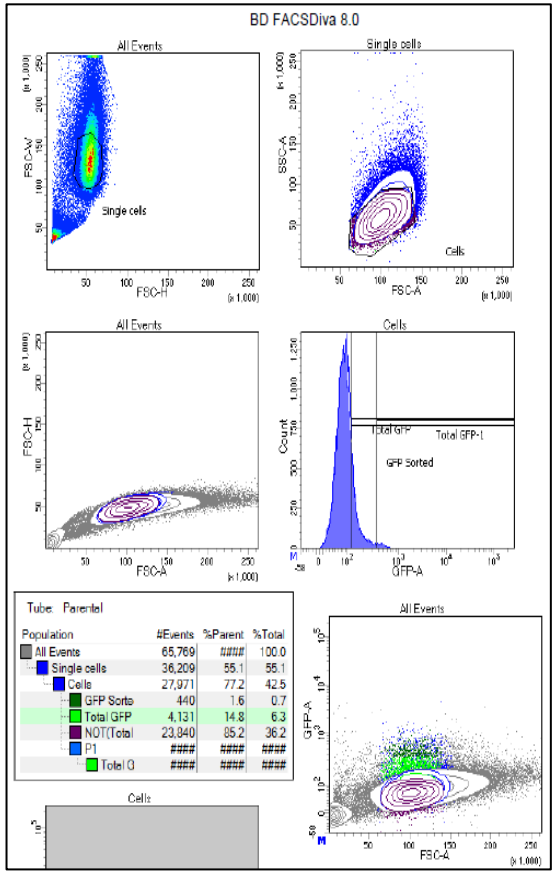

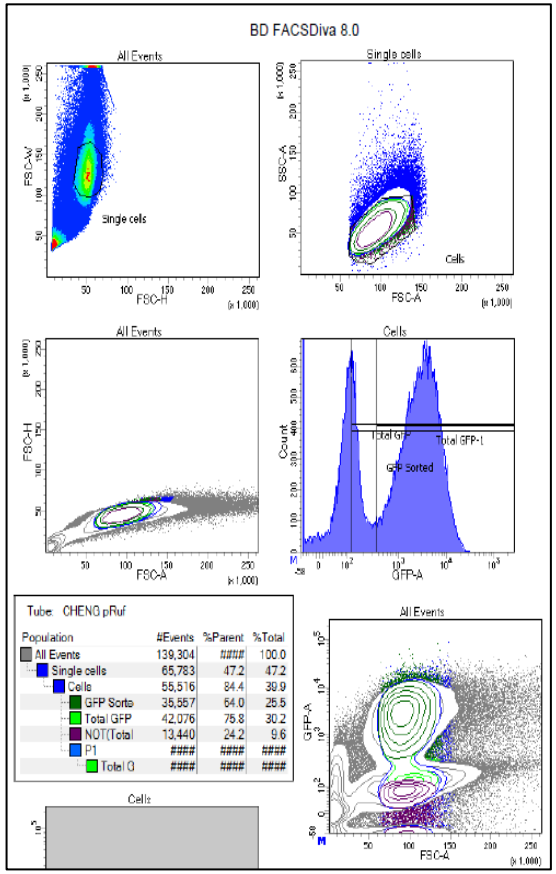

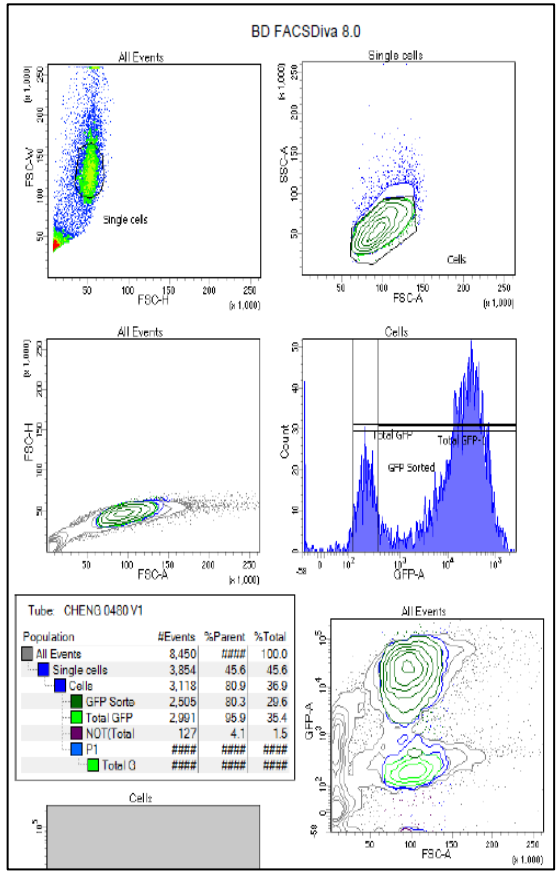

Figure 5.5. Confirmation of correct *CMTM8* sequence insert in the pRUF-IRES-GFP vector. (A) Sanger sequencing was performed on pRUF-IRES-GFP-CMTM8 vector using the Pairwise Sequence Alignment Tool. (B) The purity of the vector sequence was confirmed by visualizing the amplified peaks from Sanger sequencing using Chromas Software.

A

```
  1 atggaggagccgcagcgcgcccgctcgcacacagtcaccaccaccgccag   50
    ||||||||||||||||||||||||||||||||||||||||||||||||||
  1 ATGGAGGAGCCGCAGCGCGCCCGCTCGCACACAGTCACCACCACCGCCAG   50

 51 ctccttcgcagagaacttctccaccagcagcagcagcttcgcctacgacc  100
    ||||||||||||||||||||||||||||||||||||||||||||||||||
 51 CTCCTTCGCAGAGAACTTCTCCACCAGCAGCAGCAGCTTCGCCTACGACC  100

101 gggagttcctccgcaccctgcccggcttcctcatcgtggccgagatcgtt  150
    ||||||||||||||||||||||||||||||||||||||||||||||||||
101 GGGAGTTCCTCCGCACCCTGCCCGGCTTCCTCATCGTGGCCGAGATCGTT  150

151 ctggggctgctggtatggacgcttattgctggaactgagtacttccgggt  200
    ||||||||||||||||||||||||||||||||||||||||||||||||||
151 CTGGGGCTGCTGGTATGGACGCTTATTGCTGGAACTGAGTACTTCCGGGT  200

201 ccccgcatttggctgggtcatgtttgtagctgtattttactgggtcctca  250
    ||||||||||||||||||||||||||||||||||||||||||||||||||
201 CCCCGCATTTGGCTGGGTCATGTTTGTAGCTGTATTTTACTGGGTCCTCA  250

251 ccgtcttcttcctcattatctacataacaatgacctacaccaggattccc  300
    ||||||||||||||||||||||||||||||||||||||||||||||||||
251 CCGTCTTCTTCCTCATTATCTACATAACAATGACCTACACCAGGATTCCC  300

301 caggtgccctggacaacagtgggcctgtgctttaacggcagtgccttcgt  350
    ||||||||||||||||||||||||||||||||||||||||||||||||||
301 CAGGTGCCCTGGACAACAGTGGGCCTGTGCTTTAACGGCAGTGCCTTCGT  350

351 cttgtacctctctgccgctgttgtagatgcatcttccgtctcccctgaga  400
    ||||||||||||||||||||||||||||||||||||||||||||||||||
351 CTTGTACCTCTCTGCCGCTGTTGTAGATGCATCTTCCGTCTCCCCTGAGA  400

401 gggacagtcacaacttcaacagctgggcggcctcatcgttctttgccttc  450
    ||||||||||||||||||||||||||||||||||||||||||||||||||
401 GGGACAGTCACAACTTCAACAGCTGGGCGGCCTCATCGTTCTTTGCCTTC  450

451 ctggtcaccatctgctacgctggaaatacatatttcagttttatagcatg  500
    ||||||||||||||||||||||||||||||||||||||||||||||||||
451 CTGGTCACCATCTGCTACGCTGGAAATACATATTTCAGTTTTATAGCATG  500

501 gagatccaggaccatacag    519 ← CMTM8 consensus sequence (NCBI)
    ||||||||||||||||||||
501 GAGATCCAGGACCATACAG    519 ← CMTM8 vector construct sequence
```

B

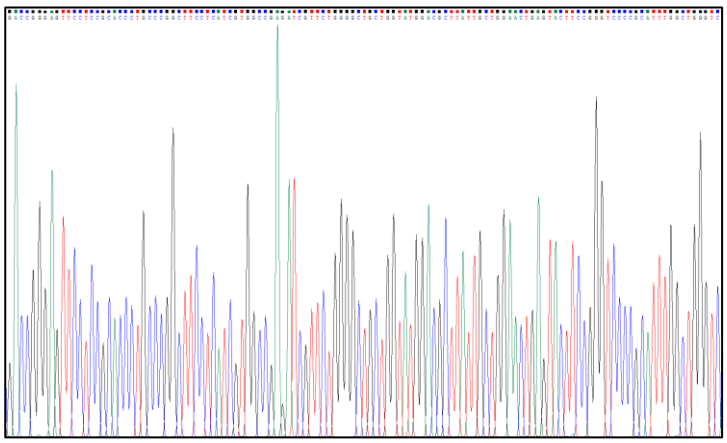

Figure 5.6. Western blot analysis to detect expression of CMTM8 by infected BMSC. Protein expression of CMTM8 was assessed by Western blot analysis using two different antibodies against CMTM8: anti-CMTM8-1 & anti-CMTM8-2. Molecular weight of CMTM8 is 20kDa. . Western blot to detect Tubulin (50kDa) was used as a loading control.

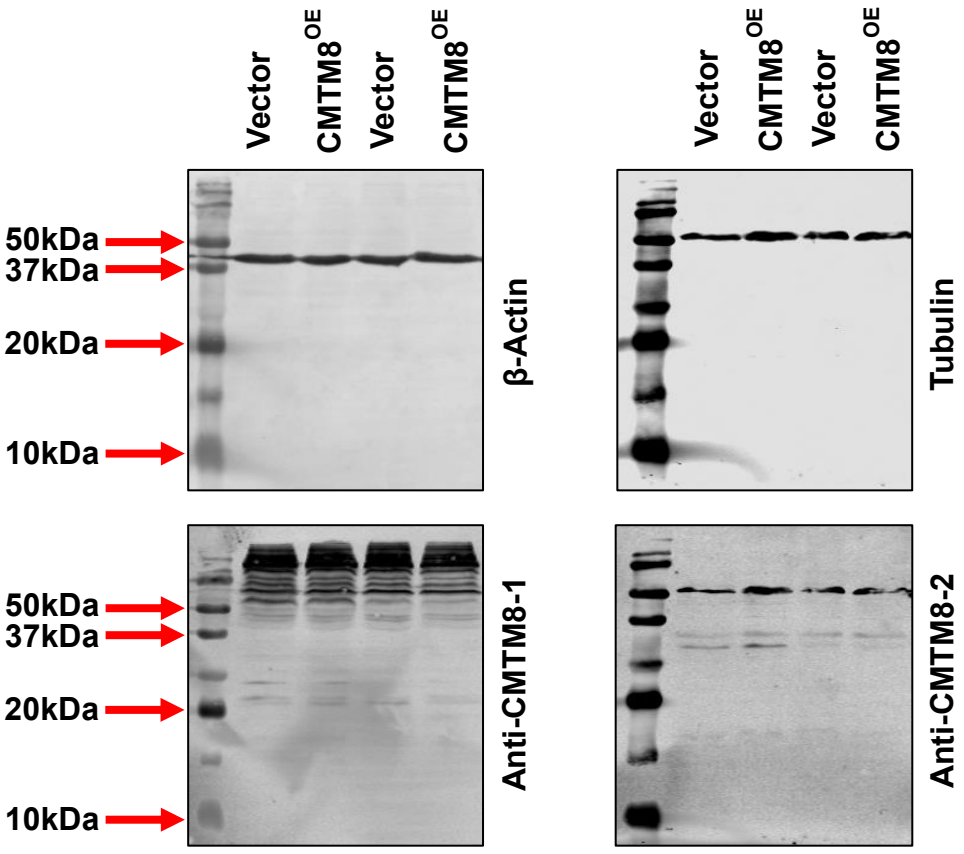
Vector
CMTM8OE
Vector
CMTM8OE
50kDa
37kDa
20kDa
10kDa
β-Actin
Tubulin
Anti-CMTM8-1
Anti-CMTM8-2

the infected cells, Western blot analysis was performed to assess the *CMTM8* expression of four vector only BMSC and CMTM8 overexpressing BMSC donors at the protein level (Figure 5.6). However, no CMTM8 protein of the expected 20kDa was detected using two different antibodies (over the concentration range of 1:200, 1:500 and 1:1000) against CMTM8: anti-CMTM8-1 and anti-CMTM8-2. Immunohistochemistry was then employed as another method to detect levels of CMTM8 in vector only and *CMTM8* overexpressing BMSC *in vitro.* Immunocytochemistry analysis was performed in order to visualize protein expression of CMTM8. Both populations of cells were GFP positive, demonstrating successful transcription of the infected vectors (Figure 5.7). The positive control for perivascular cells/ BMSC, α-SMA [46, 55] was detected in both populations. CMTM8 levels were assessed using two different antibodies against CMTM8: anti-CMTM8-1 and anti-CMTM8-2. As shown in Figure 5.7, no difference was observed in the intensity of fluorescence between vector only and *CMTM8* overexpressing BMSC, where staining appeared to be non-specific.

Although specific detection of CMTM8 was unsuccessful with the antibodies used, when expression of *CMTM8* transcript was determined in cells using real-time PCR, there was differential expression of *CMTM8* in vector only BMSC compared to *CMTM8* overexpressing BMSC. Expression levels of *CMTM8* transcripts in three pRUF-IRES-GFP-CMTM8 human BMSC donors were found to be approximately 1,000 fold higher compared with vector only control pRUF-IRES-GFP BMSC (Figure 5.8A).

5.2.3 CMTM8 is a promoter of BMSC proliferation

The role of CMTM8 during BMSC proliferation was assessed by performing overexpression and knockdown studies followed by analysis of BrdU incorporation. The data showed that *CMTM8* overexpressing BMSC (Figure 5.8A), exhibited an increased proliferation rate with

Figure 5.7. Immunocytochemistry staining of vector only and *CMTM8* overexpressing BMSC. Vector only and *CMTM8* overexpressing BMSC were stained with anti-CMTM8-1 (1:200, scale bar = 100μm) & anti-CMTM8-2 (1:200, scale bar = 100μm), with negative control (no antibody, scale bar = 200μm) & positive control (anti-α-SMA, scale bar = 100μm).

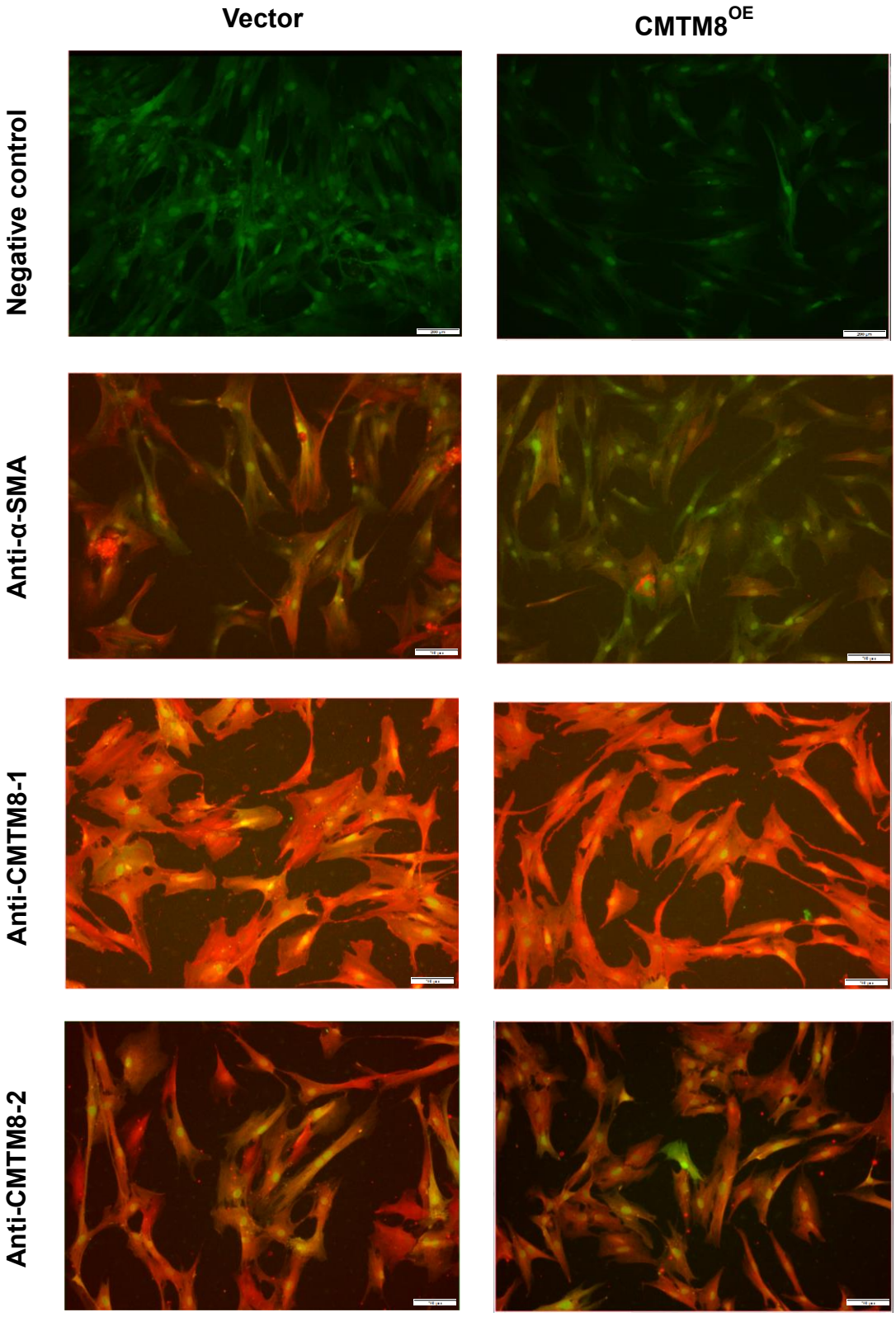
Vector
CMTM8OE
Negative control
Anti-α-SMA
Anti-CMTM8-1
Anti-CMTM8-2

Figure 5.8. CMTM8 promotes BMSC proliferation. (A) Empty vector transduced BMSC or *CMTM8* overexpressing BMSC were cultured under normal growth, real-time PCR was performed to examine levels of *CMTM8*. Graph represents mean ± S.E.M, Student's t-test $p<0.05$(*), n=3. (B) Vector-only or CMTM8 overexpressing BMSC were incubated for 3-5 days and BrdU assays were performed Graph represents mean ± S.E.M, Student's t-test $p<0.05$(*), n=5. (C) Representative images of vector-only BMSC and *CMTM8* overexpressing BMSC cultures were taken using Olympus light microscope at 20 X magnification. (D) Normal BMSC were treated with either negative siRNA (siScram) or siRNA to CMTM8 (siCMTM8_1 & siCMTM8_2), real-time PCR was performed to examine levels of *CMTM8*, Graph represents mean ± S.E.M, Student's t-test $p<0.05$(*), n=3. (E) BMSC treated with siScram/ siCMTM_1/ siCMTM-2 were incubated for 3-5 days and BrdU assays were performed, n=6. (F) Representative images of cells treated with siScram and siCMTM8_1, were taken using Olympus light microscope at 20 X magnification. (Scale bar = 200μm)

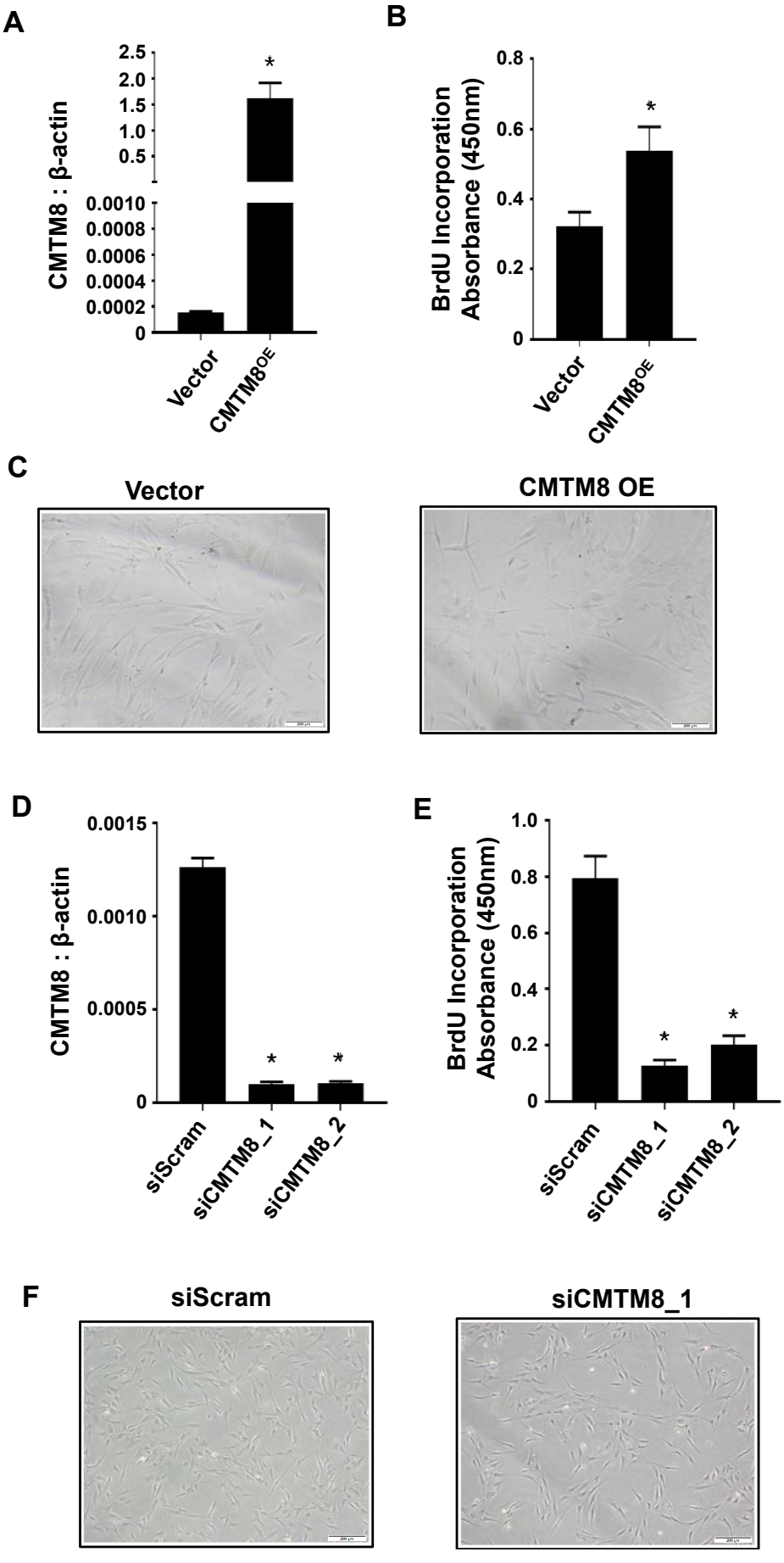
A
CMTM8 : β-actin
2.5
2.0
1.5
1.0
0.5
0.0010
0.0008
0.0006
0.0004
0.0002
0
*
Vector
CMTM8OE
B
BrdU Incorporation
Absorbance (450nm)
0.8
0.6
0.4
0.2
0
*
Vector
CMTM8OE
C
Vector
CMTM8 OE
D
CMTM8 : β-actin
0.0015
0.0010
0.0005
0
*
*
siScram
siCMTM8_1
siCMTM8_2
E
BrdU Incorporation
Absorbance (450nm)
1.0
0.8
0.6
0.4
0.2
0
*
*
siScram
siCMTM8_1
siCMTM8_2
F
siScram
siCMTM8_1

no observable effects on cell morphology (Figure 5.8B, C). The notion that CMTM8 is a promoter of BMSC proliferation was supported in experiments demonstrating that following siRNA mediated knockdown of *CMTM8* gene expression (Figure 5.8D), BMSC proliferation rates were significantly reduced with no effect on cell morphology (Figure 5.8E, F).

To investigate whether the reduced proliferation rate observed in *CMTM8* knockdown BMSC was attributed to apoptosis, BMSC were stained with AnnexinV and 7AAD (Figure 5.9). Flow cytometric analysis found that *CMTM8* knockdown resulted in no difference in the number of live AnnexinV$^-$/ 7AAD$^-$ cells, early apoptotic AnnexinV$^+$/ 7AAD$^-$ or late apoptotic AnnexinV$^+$/ 7AAD$^+$ cells (Figure 5.9A, B).

5.2.4 CMTM8 promotes BMSC proliferation via activation of EGFR

Previous studies from our laboratory have reported the mitogenic effect of EGF on BMSC [295]. The present study examined whether the effect of CMTM8 on BMSC proliferation was mediated via the EGFR pathway. Studies revealed that the mitogenic effect of EGF on BMSC was enhanced in *CMTM8* overexpressing BMSC compared to vector only control BMSC (Figure 5.10A). In parallel studies, siRNA mediated knockdown of *CMTM8* exhibited a suppressed proliferative response in the presence of EGF (Figure 5.10B).

Previous studies have reported that CMTM8 facilitates the internalization of EGFR into cytoplasm, where EGFR is phosphorylated [241]. To investigate whether the CMTM8 affects BMSC proliferation through EGFR signalling, siRNA-*CMTM8* transfected BMSC and control siScram transfected BMSC were stimulated with EGF and assessed by Western Blot (Figure 5.10C). The levels of total EGFR were not significantly different between *CMTM8* knockdown and control BMSC in the presence or absence of EGF (Figure 5.10Ci). However, when cells

were treated with EGF, there was an increase in the levels of phosphorylated EGFR in all cells at 10 minutes and 30 minutes post EGF stimulation. Nevertheless, levels of phosphorylated EGFR were reduced in siCMTM8 transfected cells at 10 minutes post EGF stimulation, when compared to siScram control transfected cells (Figure 5.10 Cii, D-F). At 30 minutes post EGF stimulation, reduced levels of phosphorylated EGFR in siCMTM8 transfected cells were still observed, compared to control, but only in cells from two out of the three donors (Figure 5.10 Cii, D-F). Assessment of ERK1/2, a major downstream effector of EGFR, found that total ERK1/2 levels were not significantly different between *CMTM8* knockdown and control BMSC in the presence or absence of EGF (Figure 5.10 Ci). When cells were treated with EGF, there was an increase in the levels of phosphorylated ERK1/2 post EGF stimulation in all cells. Levels of phosphorylated ERK1/2 were found to be reduced in siCMTM8 transfected cells at 10 minutes post EGF stimulation when compared to siScram control transfected cells (Figure 5.10 Cii,G-I). At 30 minutes post EGF stimulation, reduced levels of phosphorylated ERK1/2 in siCMTM8 transfected cells were still observed, compared to control, but only in cells from the two donors which also demonstrated a decrease in protein levels of phosphorylated EGFR (Figure 5.10 Cii, G-I). Assessment of another downstream effector of EGFR, AKT did not detect any expression of total or phosphorylated AKT.

Figure 5.9. CMTM8 does not affect BMSC apoptosis. siScram and siCMTM8 treated BMSC were stained with AnnexinV and 7AAD and scanned with flow cytometry. (A) Flow cytometry density plot of siScam, siCMTM8_1, siCMTM8_2 treated BMSC. (B) Percentage of live cells stained with $AnnexinV^{-}/ 7AAD^{-}$, early apoptotic cells stained with $AnnexinV^{+}/ 7AAD^{-}$, late apoptotic cells stained with $Annexin^{+}/ 7AAD^{+}$, necrotic cells stained with $AnnexinV^{-}/ 7AAD^{+}$. Graphs represent mean ± S.E.M, Student's t-test $p<0.05$(*), n=3 donors.

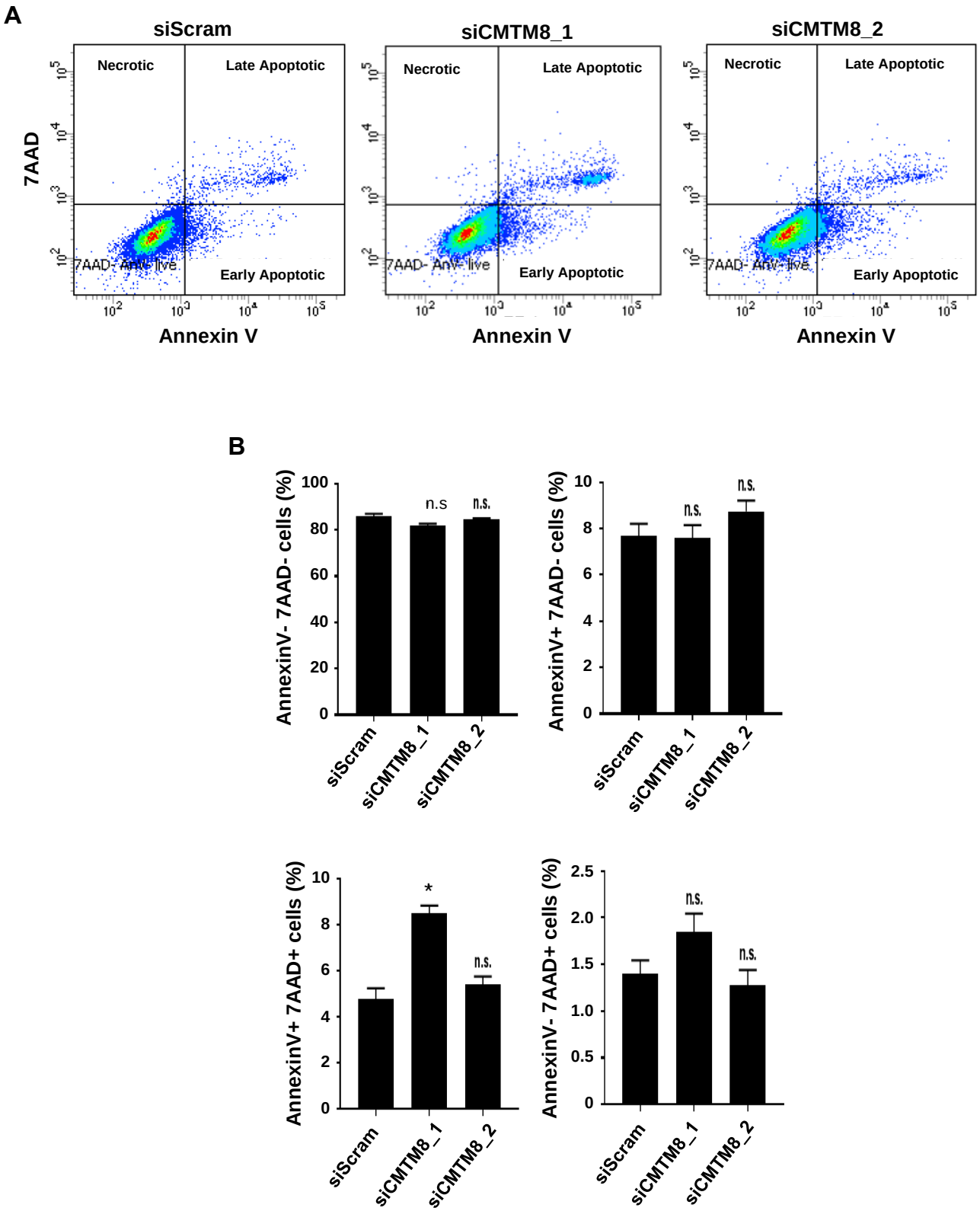
A
siScram
siCMTM8_1
siCMTM8_2
Necrotic
Late Apoptotic
7AAD- Anv- live
Early Apoptotic
7AAD
Annexin V
B
AnnexinV- 7AAD- cells (%)
AnnexinV+ 7AAD- cells (%)
AnnexinV+ 7AAD+ cells (%)
AnnexinV- 7AAD+ cells (%)
n.s
n.s.
*
siScram
siCMTM8_1
siCMTM8_2

Figure 5.10. CMTM8 promotes BMSC proliferation via activation of EGFR Signalling. (A) Vector-only and *CMTM8* overexpressing BMSC were also treated with 20ng/mL EGF for 3-5 days before BrdU assay was performed. (B) siScram or siCMTM8 treated BMSC were incubated with 20ng/mL EGF for 3-5 days and BrdU assay was performed. (A, B) Graphs represent mean ± S.E.M, One-way ANOVA $p<0.05$(*), n=3 donors. (C) Representative Western Blot. Cell lysates were collected from vector-only BMSC and *CMTM8* overexpressing BMSC treated with 20ng/mL EGF for 10 and 30 minutes or without EGF. Western Blot was performed to examine the total and phosphorylated form of EGFR, ERK1/2 and AKT using β-actin as the loading control. The intensity of bands were measured by normalizing (D-F) Phosphorylated EGFR to Total EGFR, (G-I) Phosphorylated ERK1/2 to Total ERK1/2.

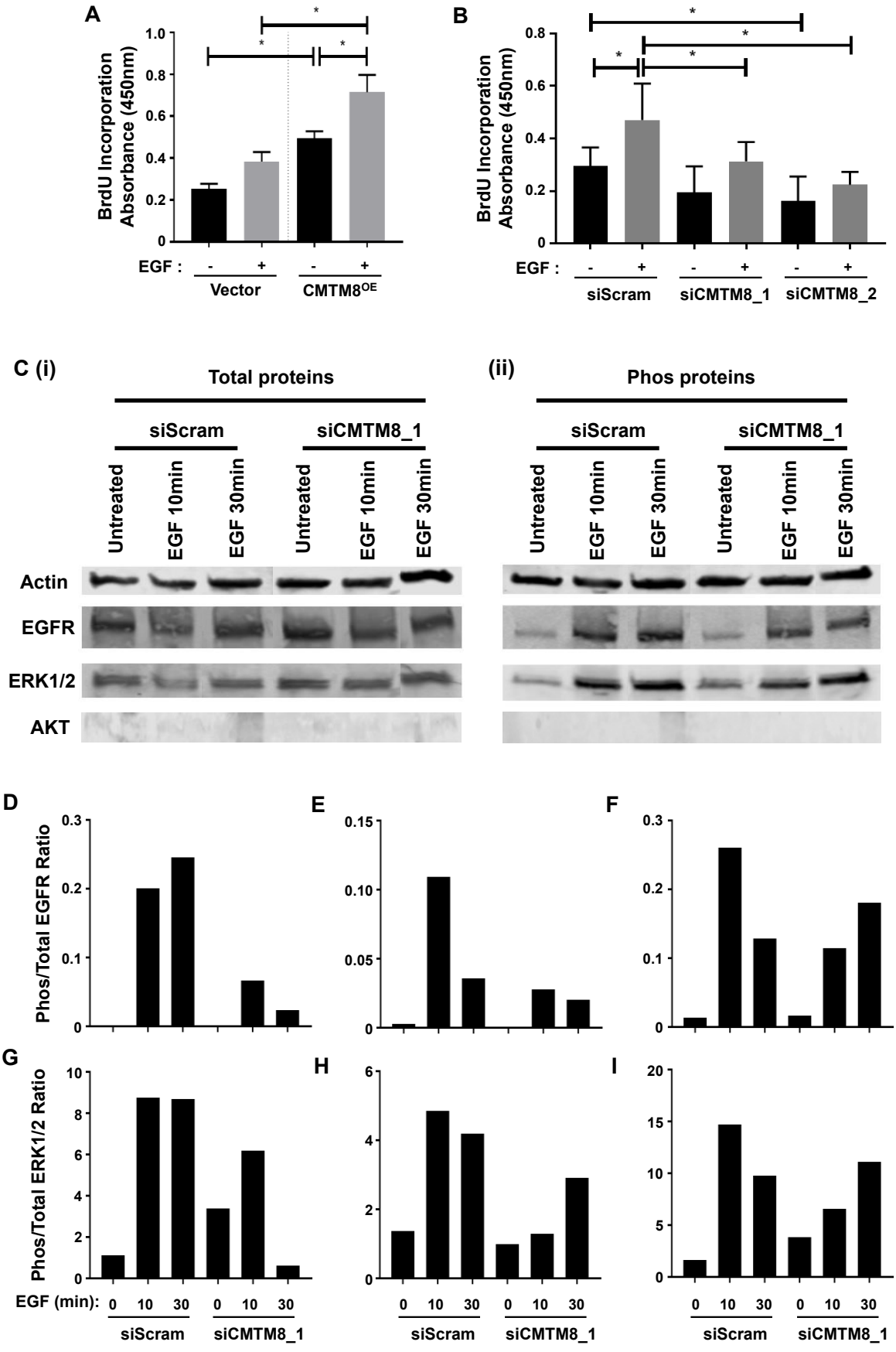
A
BrdU Incorporation Absorbance (450nm)
1.0
0.8
0.6
0.4
0.2
0
EGF : - + - +
Vector
CMTM8OE
B
BrdU Incorporation Absorbance (450nm)
0.8
0.6
0.4
0.2
0
EGF : - + - + - +
siScram
siCMTM8_1
siCMTM8_2
C (i)
Total proteins
siScram
siCMTM8_1
Untreated
EGF 10min
EGF 30min
Untreated
EGF 10min
EGF 30min
Actin
EGFR
ERK1/2
AKT
(ii)
Phos proteins
siScram
siCMTM8_1
Untreated
EGF 10min
EGF 30min
Untreated
EGF 10min
EGF 30min
D
Phos/Total EGFR Ratio
0.3
0.2
0.1
0
E
0.15
0.10
0.05
0
F
0.3
0.2
0.1
0
G
Phos/Total ERK1/2 Ratio
10
8
6
4
2
0
H
6
4
2
0
I
20
15
10
5
0
EGF (min): 0 10 30 0 10 30
siScram
siCMTM8_1
0 10 30 0 10 30
siScram
siCMTM8_1
0 10 30 0 10 30
siScram
siCMTM8_1

To further investigate the effect of CMTM8 on EGF-mediated proliferation, we treated vector-only BMSC (Figure 5.11A) and *CMTM8* overexpression BMSC (Figure 5.11B) with the EGFR inhibitor, Erlotinib and assessed for BrdU incorporation. Our results showed that both populations treated with EGF increased their proliferation rates compared to control DMSO treated cells. However, both cell populations displayed a dose-depended inhibition of cell proliferation in the presence of Erlotinib when compared with their respective DMSO control cells (Figure 5.11A, B). Further comparisons found that *CMTM8* overexpressing BMSC showed more resistance to Erlotinib at higher drug concentrations at 2μM and above (Figure 5.11C). Knock down of CMTM8 results in a decrease in EGFR signalling and CMTM8 overexpression results in less sensitivity to Erlotinib. These results suggest that CMTM8 promotes BMSC proliferation most likely via the activation of EGFR signalling.

5.2.5 CMTM8 promotes BMSC migration

Studies have shown that CMTM8 can inhibits EMT-like changes in HepG2 hepatocellular carcinoma cells [245], where EMT is a hallmark of cancer cell metastasis and cell migration. In the present study, overexpression of *CMTM8* did not result in changes in the expression of important EMT associated gene markers (Figure 5.12). We then performed functional experiments to examine whether CMTM8 has a role in BMSC migration with the use of an *in vitro* scratch assay. Images of migrating *CMTM8* overexpressing and vector only BMSC were compared between 0 hours and 16 hours (Figure 5.13A) and quantitated for area of occupation and migrating length. The data showed that *CMTM8* overexpressing BMSC had an increase in length (Figure 5.13B) and area (Figure 5.13C) of invading cells after 16 hours of incubation, compared to vector only BMSC. To confirm this finding, scratch assays were performed using *CMTM8* knockdown and control BMSC (Figure 5.13D). The *CMTM8* knockdown BMSC exhibited a decrease in the length (Figure 5.13E) and area (Figure 5.13F) invaded after 16 hours

incubation, compared to siRNA scramble control BMSC. These data suggest that *CMTM8* is a promoter of cell migration.

5.2.6 CMTM8 inhibits BMSC osteogenic differentiation

To assess the role of CMTM8 in human BMSC differentiation, functional studies were performed using *CMTM8* overexpressing BMSC or empty vector alone infected BMSC from two donors, cultured in osteogenic induction media (Figure 5.14A). The data showed that *CMTM8* overexpression resulted in a decrease in Alizarin red stained mineral deposits (Figure 5.14B) and extracellular calcium levels (Figure 5.14C), following osteogenic induction, compared with vector only BMSC. The CMTM8 mediated suppression of BMSC osteogenic differentiation was further supported by the decreased expression of the osteogenic markers *RUNX2* and *OPN,* in *CMTM8* overexpressing BMSC compared to vector only BMSC (Figure 5.14D, E).

To verify these findings, siRNA-*CMTM8* transfected BMSC were cultured in osteogenic differentiation media (Figure 5.14F). Suppression of *CMTM8* resulted in increased Alizarin red staining (Figure 5.14G) and extracellular calcium levels (Figure 5.14H), compared with siScram transfected cells. Enhanced BMSC osteogenic differentiation was further supported by the upregulation of osteogenic markers *RUNX2* and *OPN* expression (Figure 5.14I, J) compared to expression in siScram transfected cells. Overall, these studies demonstrated that CMTM8 represses BMSC osteogenic differentiation.

Figure 5.11. CMTM8 resists anti-proliferation effect of Erlotinib. (A) vector-only BMSC and (B) *CMTM8* overexpression BMSC were treated with either DMSO control, 20ng/mL EGF, 1μm Erlotinib with 20ng/mL EGF, 2μm Erlotinib with 20ng/mL EGF, 3μm Erlotinib with 20ng/mL EGF, or 6μm Erlotinib with 20ng/mL EGF for 3 days and BrdU assays were performed. Graphs represent mean ± S.E.M, Student's t-test $p<0.05$(*), n=3 donors. (C) Data from (A) and (B) were combined to visualize the difference between vector-only and *CMTM8* overexpressing BMSC. Graphs represent mean ± S.E.M, One-way ANOVA $p<0.05$(*), n=4 donors.

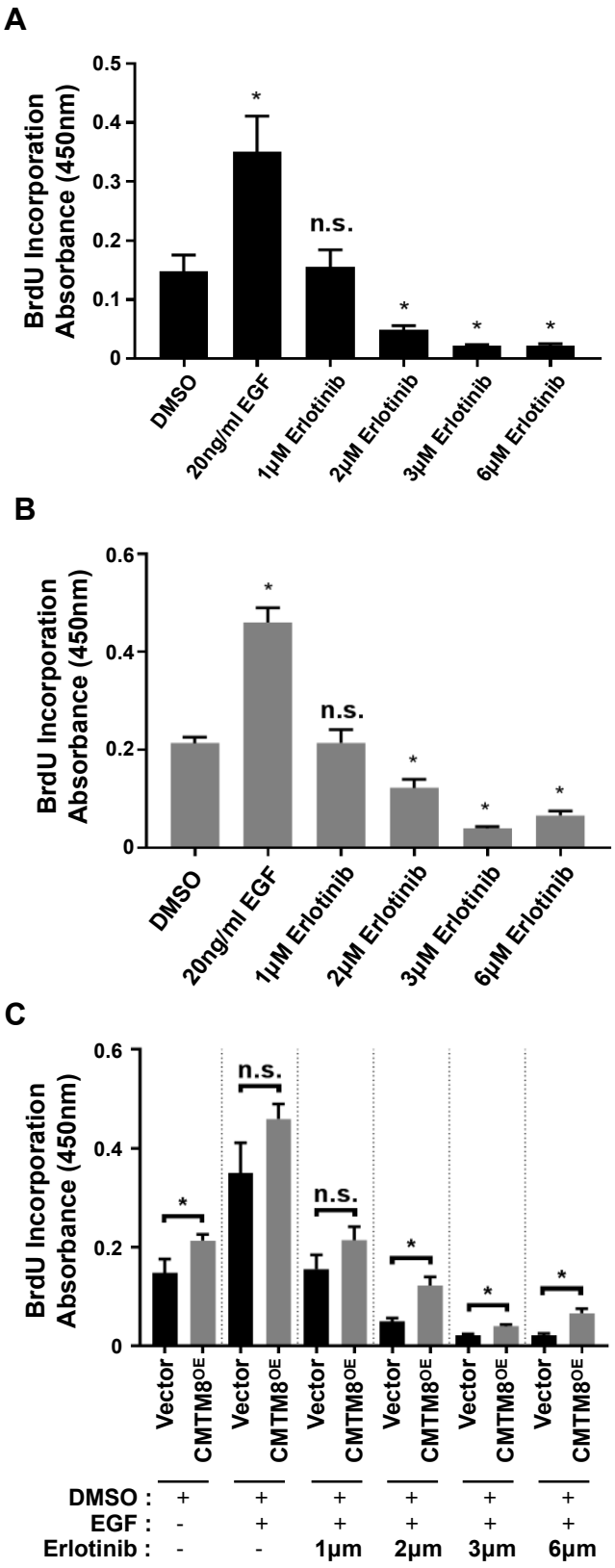
A
BrdU Incorporation
Absorbance (450nm)
0.5
0.4
0.3
0.2
0.1
0
*
n.s.
*
*
*
DMSO
20ng/ml EGF
1μM Erlotinib
2μM Erlotinib
3μM Erlotinib
6μM Erlotinib
B
BrdU Incorporation
Absorbance (450nm)
0.6
0.4
0.2
0
*
n.s.
*
*
*
DMSO
20ng/ml EGF
1μM Erlotinib
2μM Erlotinib
3μM Erlotinib
6μM Erlotinib
C
BrdU Incorporation
Absorbance (450nm)
0.6
0.4
0.2
0
*
n.s.
n.s.
*
*
*
Vector
CMTM8OE
DMSO :
EGF :
Erlotinib :
+
-
1μm
2μm
3μm
6μm

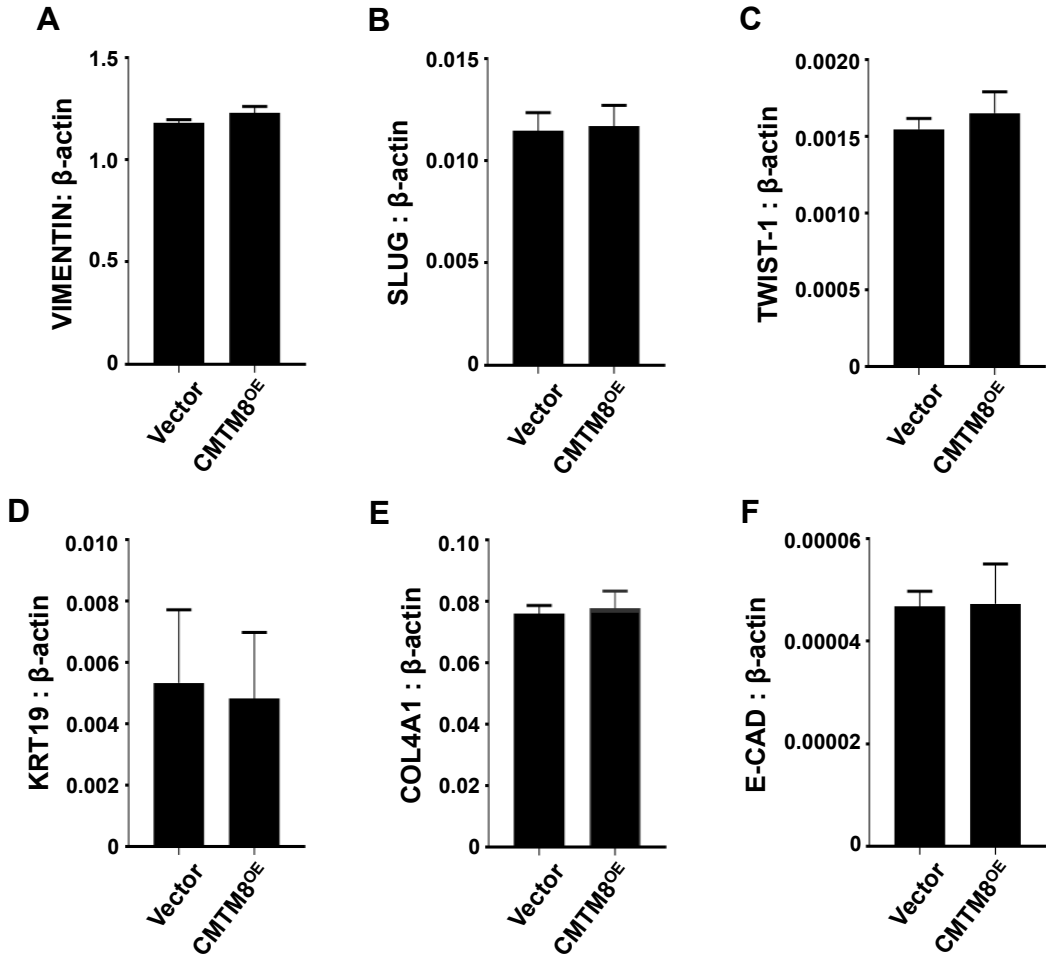

Figure 5.12. CMTM8 does not affect expression of EMT marker genes. Vector-only and *CMTM8* overexpressing BMSC were cultured in normal conditions expression levels of EMT markers: **(A)** *VIMENTIN*, **(B)** *SLUG*, **(C)** *TWIST-1*, **(D)** *KRT19*, **(E)** *COL4A1* and **(F)** E-*CAD* were determined relative to *β-actin* using real-time PC. Graphs represent mean ± S.E.M, Student's t-test $p<0.05$(*), n=3 donors.

Figure 5.13. CMTM8 promotes BMSC migration. BMSC were seeded into 24-well plate and *in vitro* scratch assays were performed. Images were taken and area and length invaded by cells were measured at 0 hour and 16 hours post incubation. Measurements were analysed relative to value obtained at 0 hour. (A) Representative images showing the area invaded by vector-only and *CMTM8* overexpressing cells with different treatments at 0 hour (T0) and 16 hours (T16). (B) Length invaded by vector-only and *CMTM8* overexpressing cells, n=5. (C) Area invaded by vector-only and *CMTM8* overexpressing cells, n=5. (B, C) Graphs represent mean ± S.E.M, Student's t-test $p<0.05$(*). (D) Representative images showing the area invaded by siScram and siCMTM8 treated cells with different treatments at 0 hour and 16 hours. (E) Length invaded by siScram and siCMTM8 treated cells, n=6. (F) Area invaded by siScram and siCMTM8 treated cells, n=6. (E, F) Graphs represent mean ± S.E.M, Student's t-test $p<0.05$(*), n represents number of donors.

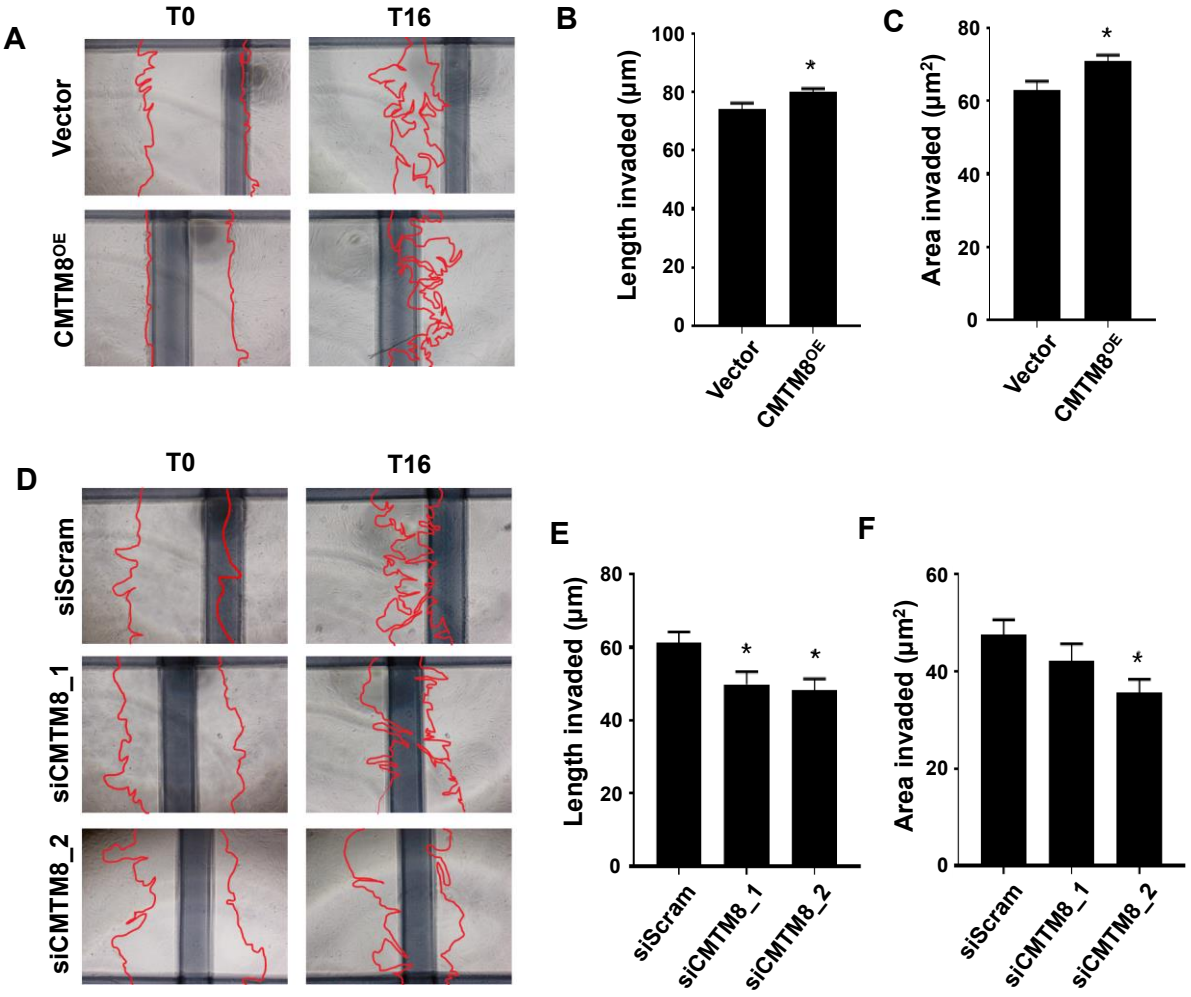
A
T0
T16
Vector
CMTM8OE
B
Length invaded (µm)
100
80
60
40
20
0
*
Vector
CMTM8OE
C
Area invaded (µm2)
80
60
40
20
0
*
Vector
CMTM8OE
D
T0
T16
siScram
siCMTM8_1
siCMTM8_2
E
Length invaded (µm)
80
60
40
20
0
*
*
siScram
siCMTM8_1
siCMTM8_2
F
Area invaded (µm2)
60
40
20
0
*
siScram
siCMTM8_1
siCMTM8_2

Figure 5.14. CMTM8 inhibits BMSC osteogenesis. (A) Vector-only and *CMTM8* overexpressing BMSC were cultured in osteogenic (Osteo) inductive conditions for 3 weeks and *CMTM8* expression levels were determined relative to *β-actin* using real-time PCR, n=8 donors. (B) Representative image of Alizarin Red that stained the mineral deposited by vector only and *CMTM8* overexpressing BMSC (C) Extracellular calcium levels of vector-only and *CMTM8* overexpressing BMSC were quantified, n=4 donors. Real-time PCR was performed to measure levels of (D, E) *RUNX2* and *OPN* relative to *β-actin* of two donors. (A, C, D, E) Graph represents mean ± S.E.M, Student's t-test $p<0.05$(*). (F) siScram, siCMTM8_1 BMSC were cultured in osteogenic (Osteo) inductive conditions for 3 weeks and *CMTM8* expression levels were determined relative to *β-actin* using real-time PCR, n=8 donors. (G) Representative image of Alizarin Red that stained the mineral deposited by siScram and siCMTM8_1 treated BMSC. (H) Extracellular calcium levels of cells treated with siScram or siCMTM8_1 were quantified, n=4 donors. Real-time PCR was performed to measure levels of (I, J) *RUNX2* and *OPN* relative to *β-actin* of two donors. (F, H, I, J) Graphs represent mean ± S.E.M, Student's t-test $p<0.05$(*). (Scale bar = 200μm)

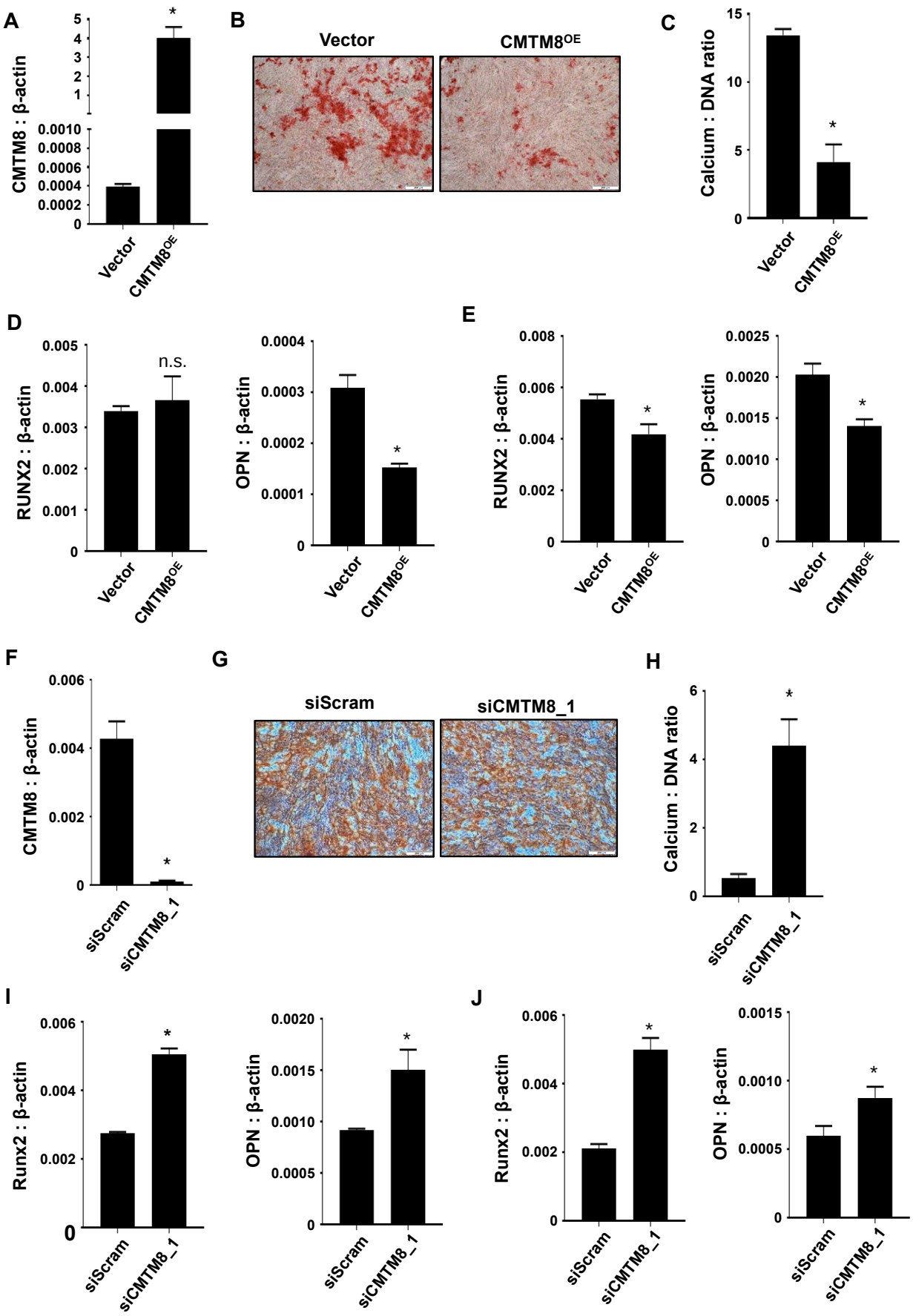
A
CMTM8 : β-actin
Vector
CMTM8OE
B
Vector
CMTM8OE
C
Calcium : DNA ratio
D
RUNX2 : β-actin
n.s.
OPN : β-actin
E
RUNX2 : β-actin
OPN : β-actin
F
CMTM8 : β-actin
siScram
siCMTM8_1
G
siScram
siCMTM8_1
H
Calcium : DNA ratio
I
Runx2 : β-actin
OPN : β-actin
J
Runx2 : β-actin
OPN : β-actin

5.2.7 CMTM8 has no effect on BMSC adipogenic differentiation

To determine the function of CMTM8 in BMSC adipogenic differentiation, *CMTM8* overexpressing BMSC or vector control BMSC were cultured under growth or adipogenic inductive media (Figure 5.15A). Measurements of number of lipid-containing adipocytes using Nile red staining found no difference between *HOPX* overexpressing BMSC and vector control BMSC (Figure 5.15Bi, C). Similarly, lipid droplets were stained with Oil Red O after three weeks under adipogenic growth conditions with no observable differences (Figure 5.15Bii). In accord with these findings, *CMTM8* overexpressing BMSC showed no significant difference in the transcript levels of the adipogenic master regulator, *C/EBPα* (Figure 5.15D) and the mature fat marker, *ADIPSIN* (Figure 5.15E), compared to the vector control cells. Confirmatory studies employing siRNA-mediated knockdown of *CMTM8* in BMSC (Figure 5.15F) found no significant differences in the number of nile red positive lipid-containing adipocytes compared with scramble siRNA-treated BMSC (Figure 5.15Gi-J). Similarly, lipid droplets were stained with Oil Red O after three weeks under adipogenic growth conditions with no observable differences (Figure 5.15Gii). Overall, these findings demonstrate that CMTM8 has no direct effect on the adipogenic capacity of BMSC.

Figure 5.15. CMTM8 does not affect BMSC adipogenic differentiation. (A) *CMTM8* overexpressing ($CMTM8^{OE}$) and vector only (Vector) BMSC were cultured in adipogenic inductive conditions and *CMTM8* expression levels were determined relative to *β-actin* using real-time PCR, n=3 donors. Graphs represent mean ± S.E.M, One-way ANOVA $p<0.05$(*). (B) Representative images of lipid-containing Vector BMSC and $CMTM8^{OE}$ BMSC stained with (i) Nile Red and (ii) Oil Red O. (C) Lipid-containing cells stained with Nile red and DAPI were quantified, n=3 donors. Graph represents mean ± S.E.M, Student's t-test $p<0.05$(*). Total RNA was harvested at 7-14 days post induction (n=3 donors) from Vector and $CMTM8^{OE}$ BMSC. Real-time PCR was used to measure levels of (D) *C/EBPα* and (E) *ADIPSIN* in relative to *β-actin*. Graphs represent mean ± S.E.M, Student's t-test $p<0.05$(*) (F) siScram and siCMTM8_1 treated BMSC were incubated in adipogenic inductive conditions for 3 weeks, and *CMTM8* expression levels were determined relative to *β-actin* using real-time PCR, n=4 donors. Graph represents mean ± S.E.M, Student's t-test $p<0.05$(*). (G) Representative images of lipid-containing siScram and siCMTM8_1 infected BMSC stained with (i) Nile Red and (ii) Oil Red O. (H) Lipid-containing cells stained with Nile red and DAPI were quantified, n=4 donors. Total RNA was harvested at 7-14 days post induction (n=4 donors) from siScram and siCMTM8_1 infected BMSC. Real-time PCR was used to measure levels of (I) *C/EBPα* and (J) *ADIPSIN* in relative to *β-actin*. Graphs represent mean ± S.E.M, Student's t-test $p<0.05$ (*), n.s. represents non-significant. (Scale bar = 200μm)

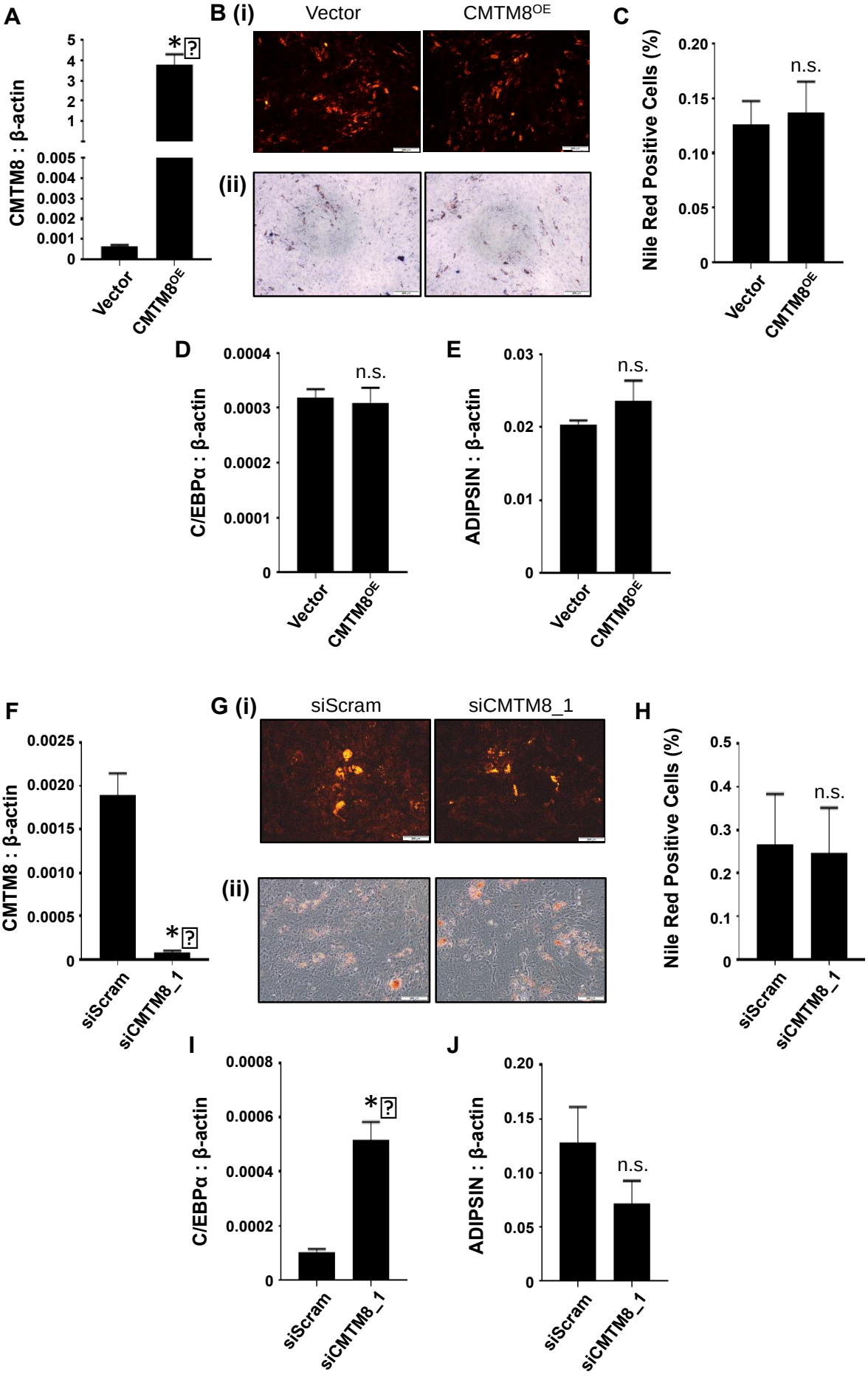
A
CMTM8 : β-actin
5
4
3
2
1
0.005
0.004
0.003
0.002
0.001
0
*?
Vector
CMTM8OE
B (i)
Vector
CMTM8OE
(ii)
C
Nile Red Positive Cells (%)
0.20
0.15
0.10
0.05
0
n.s.
Vector
CMTM8OE
D
C/EBPα : β-actin
0.0004
0.0003
0.0002
0.0001
0
n.s.
Vector
CMTM8OE
E
ADIPSIN : β-actin
0.03
0.02
0.01
0
n.s.
Vector
CMTM8OE
F
CMTM8 : β-actin
0.0025
0.0020
0.0015
0.0010
0.0005
0
*?
siScram
siCMTM8_1
G (i)
siScram
siCMTM8_1
(ii)
H
Nile Red Positive Cells (%)
0.5
0.4
0.3
0.2
0.1
0
n.s.
siScram
siCMTM8_1
I
C/EBPα : β-actin
0.0008
0.0006
0.0004
0.0002
0
*?
siScram
siCMTM8_1
J
ADIPSIN : β-actin
0.20
0.15
0.10
0.05
0
n.s.
siScram
siCMTM8_1

5.3 Discussion

The present study identified a new role for CMTM8 in regulating BMSC growth and differentiation. CMTM8 encodes a 173 amino acids protein consists of four putative transmembrane regions which is structurally similar to the transmembrane 4 super family (TM4SF11) [241]. In addition, CMTM8 contains a predicted MARVEL domain, suggesting a role in membrane protein sorting and trafficking, and membrane apposition events such as transportation of vesicle biogenesis, neurotransmitter secretion and polarized membrane trafficking [241, 291]. Moreover, in the cytosolic loop domain of CMTM8, there are 2 internalization consensus sequence YXXØ (Ø is a bulky hydrophobic residue), which can bind directly to the adaptor protein 2 (AP2) μ_2 subunit [241, 296]. Therefore, CMTM8 is a factor similar to a transmembrane protein but equipped with domains for extra functions.

Functional studies using siRNA-mediated knockdown or retroviral mediated overexpression of *CMTM8* demonstrated that CMTM8 promotes cellular proliferation and migration whilst inhibiting osteogenic differentiation. Interestingly, the effect of *CMTM8* overexpression on BMSC proliferation was not as dramatic as in the knockdown studies. Reports in the literature have demonstrated the ability of CMTM8 to induce apoptosis via caspase-dependent and –independent pathways [293]. Furthermore, CMTM8 overexpression has previously been reported to lead to decreased levels of Bad-S112 phosphorylation and induced apoptosis in cancer cell lines such as HeLa, PC3 and human breast adenocarcinoma cell line (MCF-7) [293]. In the present study, AnnexinV and 7AAD staining determined that the decrease in proliferation due to *CMTM8* knockdown was not due to the cells undergoing apoptosis. Therefore, CMTM8 appears to have a reverse function in promoting postnatal stem cell growth in contrast to cancer cell lines.

Other studies have reported that enforced expression of *CMTM8* facilitated ligand-induced internalization of EGFR from the cell surface, and therefore silencing EGFR-mediated signalling [241]. Corresponding to CMTM8, a typical tetraspanin, CD82 comprised of a YXXØ motif has been shown to regulates EGFR internalization in epithelial cells [297]. Therefore, with two YXXØ motifs and one MARVEL domain, CMTM8 is to accelerate the internalization of EGFR [241]. It was also shown that enforced expression of *CMTM8* inhibited cell proliferation, whilst suppression of CMTM8 promoted cell proliferation, following EGF stimulation of HEK293T, PC3 and HeLa cell lines. [241]. EGF stimulation induced activation of its receptor, EGFR and led to phosphorylation of its downstream component proteins, ERK1/2. However, after the initial intense ERK1/2 phosphorylation, phosphorylation decreased dramatically in *CMTM8* overexpressing cancer cell lines following EGF treatments [241]. On the other hand, siCMTM8 treated cells showed a slow and steady decrease in ERK1/2 phosphorylation. These studies suggest a negative effect of CMTM8 on EGF-induced signalling [241]. Most of the internalized EGFR are directed for lysosomal degradation and therefore desensitization of the EGFR signalling. However, there are also studies reporting that the endocytosed EGF–EGFR complex preserves its capability to generate signalling cascade from endosomes [298-300]. Therefore, the biological significance of compartment-restricted signalling in the context of the EGFR system remains unclear.

Our previous studies have demonstrated that EGF is a potent mitogen for human colony forming BMSC [295]. In our study western blot analysis demonstrated that EGF treatments did not alter that the expression of total EGFR, but did increase the levels of phosphorylated EGFR following stimulation with EGF. Interestingly, siRNA mediated knockdown of *CMTM8* in BMSC resulted in lower levels of phosphorylated EGFR compared to control, suggesting that CMTM8 promotes EGFR phosphorylation. We then assessed levels of ERK1/2, a major

downstream effector of EGFR, and found that total ERK1/2 levels were not altered but phosphorylated ERK1/2 levels were decreased following CMTM8 knockdown when compared to control. These data indicate that CMTM8 regulates total EGFR/ phosphorylated EGFR ratios in BMSC, in the presence of EGF to promote cell proliferation via the EGFR signalling pathway. In addition, no total or phosphorylated AKT was observed in siScram and siCMTM8 treated BMSC (Figure 5.10C), indicating that CMTM8 regulates EGFR/ ERK1/2 signalling but not EGFR/ AKT in BMSC. Confirmatory studies investigated the effect of CMTM8 on EGF-mediated proliferation, following treatment with the EGFR inhibitor, Erlotinib. The data showed that *CMTM8* overexpressing and vector control BMSC displayed a dose dependent decrease in proliferation in the presence of Erlotinib. Interestingly, when comparing the proliferation rates between vector-only BMSC and *CMTM8* overexpressing BMSC, the later showed higher proliferation rates when treated with Erlotinib at 2μm and above, suggesting that *CMTM8* overexpressing cells have the ability to resist the anti-proliferation effect of Erlotinib.

As a tumour suppressor gene, CMTM8 was reported to inhibit the EMT potential of the HepG2 and MCF-10A cells via c-Met signalling [245], which is an important feature of cell migration, metastasis and invasion. The tyrosine kinase receptor, c-Met resides transmembrane and on the cell surface activated by its ligand, HGF [76, 301-303]. Previous studies have demonstrated that downregulation of *CMTM8* result in EMT-like morphological changes that can be blocked by suppressing MEK and ERK2 in HepG2 and MCF-10A cell lines [245]. In addition, the protein expression levels of c-Met and HGF-induced c-Met/ERK signalling were increased when CMTM8 expression was downregulated in HepG2 and MCF-10A cell lines. It was also confirmed by CMTM8 overexpressing HepG2 and MCF-10A cells where HGF-induced c-MET/ERK signalling was inhibited and cell migration rate was reduced [245]. Together, these

findings suggest that CMTM8 functions as a negative regulator of HGF/c-MET signalling to ERK in HepG2 and MCF-10A cell lines, which then leads to decreased EMT-like changes. However, in the present study, siCMTM8 treated BMSC showed a decreased migration potential. In parallel studies, *CMTM8* overexpressing cells showed increased BMSC migration, suggesting that CMTM8 is a promoter of BMSC migration. However, examination of the expression levels of EMT associated mesenchymal (*VIMENTIN*, *SLUG*, *TWIST-1*) and epithelial (*KRT19*, *COL4A1* and *E-CAD)* genes did not show any significant differences, suggesting that CMTM8 does not promote BMSC migration through regulating the expression of EMT genes. As a transmembrane protein, CMTM8 could affect the cell-cell communication and the sensitivity towards stimulants, which could then effect the migration of cells. The different responses observed in EMT capacity between BMSC and other cell types by alteration of CMTM8 expression could be due to the differences between cell types from morphology to molecular and to functional levels. BMSC are primary cells while HepG2 and MCF-10A are modified cell lines. Moreover, in the present study, it is possible that CMTM8 regulates BMSC migration through EGFR signalling and has no effect on c-Met signalling. This could explain the different outcome observed between the present study and other studies that showed decreased EMT-like changes by CMTM8.

To date, studies have focused on the functional role of CMTM8 in proliferation, migration and apoptosis of different cancer lines [243, 245, 293, 304-309]. However, the effect of CMTM8 on BMSC cell fate determination has yet to be explored. Work presented in this thesis shows that *CMTM8* knockdown in BMSC resulted in an enhanced capacity for osteogenesis. Consistent with the loss-of-function studies, *CMTM8* overexpressing BMSC demonstrated decreased osteogenic differentiation potential. Collectively, these findings suggest that CMTM8 is a novel molecular inhibitor of BMSC osteogenic differentiation. Interestingly,

CMTM8 was found to have no affect on BMSC adipogenic differentiation. Therefore, CMTM8 appears to act as a switch to block BMSC differentiation in order to allow for cellular proliferation and migration to occur.

Chapter 6: General Discussions

6.1 Discussion

To date, there is strong evidence in the literature describing the critical role of BMSC in skeletal tissue development and homeostasis [52, 310-312]. The molecular factors modulating BMSC proliferation, differentiation and cell fate commitment involve complex interactions driven by transcription factors and epigenetic modifiers [1, 138, 313-319]. The Twist family of proteins have been identified in MSC proliferation, differentiation and cell fate commitment, where their association in bone development, fracture repair and disease have been reported [1, 320, 321]. Patients with mutations in *TWIST-1* gene display Saethre-Chotzen Syndrome, characterized by premature fusion of the sutures in the skull and other skeletal deformities such as shortened limbs and polydactyly [189, 193, 322]. Furthermore, studies have shown an association between TWIST-1/ TWIST-2 and osteoporosis, where heterozygous *TWIST-1* patients displayed higher bone mineral density values in the femoral neck and proximal femoral sites [321]. Previous works from our laboratory has identified possible functional roles of TWIST-1/ TWIST-2 in osteoporotic bone using ovariectomy induced osteoporotic murine model. The study showed that inhibition of TWIST-1 expression results in maintenance of bone mass following ovariectomy. Moreover, it has been shown that enforced expression of *TWIST-1* in BMSC resulted in enhanced BMSC proliferation and adipogenic differentiation, whilst decreased osteogenic/ chondrogenic differentiation and senescence [1, 2].

As TWIST-1 has been shown to be a critical regulator of BMSC function including growth, survival, lifespan and cell fate determination, the question arises as to what are the downstream molecular mechanisms of TWIST-1 mediating these processes. A limited number of studies have identified TWIST-1 target genes such as *EZH2*, *HES4*, *C-ROS-1*, *RUNX2*, *PPARγ2* [1-3, 179]. Moreover, it has been reported that TWIST-1 mediates these complex processes via

different signalling pathways, including Wnt, Bmp, TGFβ and FGF2 [129-133, 135, 136, 138-141, 143, 145, 148, 150, 161-164, 166, 168]. However, the precise downstream molecular mechanisms of TWIST-1 action during BMSC proliferation and cell fate determination have yet to be determined. This thesis focused on identifying potentially novel TWIST-1 target genes and examined the roles of these genes during the process of BMSC proliferation, migration and cell fate commitment.

Previous work from our laboratory has shown that enforced expression of *TWIST-1* in MSC extends their lifespan *in vitro* and maintains the cells in an immature state by inhibiting cellular senescence in association with epigenetic factors such as EZH2 [1, 48]. To determine possible gene targets of TWIST-1 in BMSC osteogenic differentiation, a microarray analysis to determine which genes were differentially expressed in *TWIST-1* overexpressing BMSC was also performed [3]. Microarray analysis identified a number of differentially expressed genes when TWIST-1 expression was enforced during BMSC osteogenesis. One of the differentially expressed gene was receptor tyrosine kinase proto-oncogene 1, *C-ROS-1*. TWIST-1 was found to directly bind to the proximal *C-ROS-1* promoter region and negatively regulate *C-ROS-1* expression, leading to decreased BMSC osteogenesis and increased adipogenesis via the PI3K/AKT/mTORC1 signalling pathway [3]. To further investigate the downstream effectors of TWIST-1, a few genes of interest that are novel in BMSC growth and cell fate determination were identified, including *HOPX*, *CMTM8* and *SCARA3*. However, using the transcription factor binding site predictor tool, no TWIST-1 binding sites have been identified near *SCARA3* promoter regions, while *CMTM8* contains three putative TWIST-1 binding sites in the intron 1; and *HOPX* contains TWIST-1 downstream effector, EZH2 binding sites in its promoter regions. Therefore, HOPX and CMTM8 were selected for further evaluation in this thesis.

The findings of this study demonstrated that *HOPX* and *CMTM8* are upregulated during BMSC osteogenic differentiation but are downregulated when *TWIST-1* is overexpressed. The question arises as to whether TWIST-1 interacts directly or indirectly with *HOPX* or *CMTM8*. This was addressed in Chapter 3 using ChIP analysis. The data generated from these studies failed to confirm direct interactions between TWIST-1 and *HOPX* or *CMTM8*. However, the interactions between *HOPX* and the TWIST-1 downstream effector, EZH2 were confirmed using ChIP analysis. This study also confirmed a negative correlation between *TWIST-1* and *HOPX*, supported by data showing higher levels of *TWIST-1* expression and lower levels of *HOPX* expression during normal growth conditions and higher *HOPX* expression levels during differentiation. ChIP analaysis was also used to confirm putative EZH2 binding sites along the *CMTM8* promoter but failed to show direct interaction between the two molecules, suggesting that TWIST-1 may regulated the expression of *CMTM8* indirectly through other mechanisms. CMTM8 was reportedly found to present as cell surface antigen. In future experiments, it is worth examining the expression levels of other cell surface antigens affected by TWIST-1, such as C-ROS-1 and ITGA5. This may help identify novel potency markers of BMSC proliferation or differentiation following ex vivo expansion.

The second aspect of this thesis focused on identifying the role of HOPX and CMTM8 in BMSC proliferation and differentiation potential. In this thesis, retroviral transduction was employed to transduce *HOPX* and *CMTM8* vector constructs into human BMSC. The expression vector constructs contained a GFP reporter gene that indicated successful transduction and allowed the purification of infected BMSC by FACS, therefore avoiding the antibiotic selection method, which is often associated with cellular toxicity [323]. Confirmation of enforced *HOPX* and *CMTM8* expression at the mRNA level was confirmed by real-time

PCR analysis. However, confirmation of the enforced *HOPX* and *CMTM8* expression at the protein level using Western blot analysis was unsuccessful using different commercially available antibodies at different concentrations. While retroviral transduction offers a relatively efficient mode of genetically modifying BMSC, the initial infection efficiencies prior to selection by FACS varied between 10% and 70%. Therefore, the selected cells are a heterogeneous population of BMSC. This may explain the different properties between the donors analysed given that the transduction efficiency varied between populations. The use of multiple, independent assays (such as Alizarin Red, Calcium production and analysis of expression levels of osteogenic markers) helped confirm observations and reduce the effects of variation between different *HOPX* and *CMTM8* overexpressing lines. In general, the observations made when multiple assays were used gave further confidence of low experimental error when similar results were generated using BMSC derived from the same donor.

The studies presented in this thesis are the first to show direct binding of EZH2 on the *HOPX* promoter by ChIP analysis, creating an association between TWIST-1/ EZH2/ HOPX. Assessment of *HOPX* expression levels in *EZH2* overexpressing BMSC revealed a negative correlation between *EZH2* and *HOPX*, supporting the notion that TWIST-1 induces *EZH2* and EZH2 suppresses *HOPX*. In addition, this thesis examined the functional role of HOPX in human BMSC proliferation and differentiation. Consistent with functional analyses, the *in vitro* data presented herein, showed that enforced expression of *HOPX* promoted BMSC proliferation. Notably, complementary studies in which *HOPX* was transiently knocked down in BMSC using two different siRNA molecules, resulted in decreased cell proliferation. Moreover, HOPX was shown to be an inhibitor of BMSC adipogenic differentiation. Although

the molecular mechanisms and signalling pathways activated/ repressed by HOPX-mediated cell proliferation remains to be fully elucidated, pathway analysis from transcriptomic data suggested that *HOPX* inhibits adipogenic associated genes such as *ADIPOQ*, *FABP4*, *PLIN1* and *PLIN4*. It is known that TWIST-1 and EZH2 inhibit BMSC osteogenic differentiation, promote adipogenesis and maintain BMSC in an immature state [1, 2]. Since EZH2 negatively regulates *HOPX*, the inhibitory effect by HOPX on BMSC adipogenic differentiation is consistent with the previous studies (Figure 6.1). However, HOPX was found to be a promoter of BMSC proliferation, which is contradictory to the effects of TWIST-1 and EZH2. One possible explanation could be the effect on BMSC proliferation by HOPX is not mediated through TWIST-1/EZH2. This explanation could also be true during BMSC osteogenesis, where no significant role of HOPX was observed. Future efforts will attempt to decipher the binding partners of HOPX, the genome wide binding sites of HOPX protein complexes and the role of putative HOPX targets in human BMSC growth and lineage determination.

A limited number of studies have been published investigating the role of CMTM8 primarily in cancer biology [243, 245, 293, 294, 304, 305, 308, 309], but no study has examined its role in BMSC biology. Studies using other cell types including HeLa, PC3, HepG2 and HEK293T cell lines have reported the association of CMTM8 in cellular proliferation, apoptosis and cancer cell metastasis. This thesis failed to show direct binding of TWIST-1 and EZH2 on the *CMTM8* promoter by ChIP analysis. However, assessment of *CMTM8* expression levels in *TWIST-1* and *EZH2* overexpressing BMSC revealed a negative correlation between *TWIST-1* and *EZH2* on *CMTM8*, suggesting that *TWIST-1* and *EZH2* may suppress *CMTM8* expression via indirect mechanisms. The reason that no enrichment of TWIST-1 or EZH2 binding could be limited by the coverage of the predictor tool and promoter regions assessed by real-time

PCR. Three putative TWIST-1 binding sites were identified in the first intron of CMTM8 using the GTRD transcription binding site prediction tool. Different prediction tools could be used in the future to identify more putative TWIST-1 binding sites. Multiple putative EZH2 binding sites were found in the 5' region of CMTM8 transcription start sites spanning around 20kb distant. In this study, only two putative EZH2 binding sites were assessed. Therefore, future studies will continue to examine binding of EZH2 on the other putative sites.

In Chapter 5, the novel role of CMTM8 in BMSC proliferation, differentiation and migration was investigated by employing *CMTM8* overexpressing BMSC and siRNA-mediated transient knockdown of *CMTM8 in vitro*. Given that there is a negative correlation between *TWIST-1/EZH2 and CMTM8*, CMTM8 was initially thought to be a potential inhibitor of proliferation/ migration and/ or a promotor of BMSC osteogenesis. However, the present thesis showed, for the first time, that CMTM8 is a promoter of BMSC proliferation and migration via modulating EGFR signalling, whilst inhibiting osteogenic differentiation. It has been reported that CMTM8 accelerates the internalization of EGFR from the cell membrane but does not lead to degradation of the EGFR [241]. Therefore, the fate of internalized EGFR is unknown, where it could be destined for lysosomal degradation and inactivation of the receptor signalling or it could enter the nucleus and maintains its signalling [298-300]. One study has reported the regulation of TWIST-1 by EGFR signalling pathway in prostate cancer cell lines, where translocation of EGFR into the nucleus results in enhanced TWIST-1 activities [178]. Interestingly, Western blot analysis from this thesis showed that when CMTM8 is suppressed, the levels of phosphorylated (active form) EGFR decreased, suggesting that CMTM8 activates EGFR signalling in BMSC. Therefore, from these studies, we speculate that CMTM8 activates EGFR signalling, which in turn activates TWIST-1 expression and consequently increases

EZH2 expression. A negative feedback loop is then formed between EZH2 and CMTM8 where EZH2 negatively regulates CMTM8 (Figure 6.2). This signalling pathway could explain the results observed in this thesis and other studies. A similar role of CMTM8 *in vivo* is yet to be investigated. This study provides insight into new strategies in controlling the fate of BMSC by regulating the expression of *CMTM8*. Future efforts will attempt to confirm the relationship between EZH2 and CMTM8; and to decipher the binding partner proteins or downstream signalling pathways of CMTM8 action and the role of putative CMTM8 targets in human BMSC growth and lineage determination. Moreover, many growth factors exert mitogenic effects on mesenchymal stem cells. Most notably, FGF2 is one of the most abundantly secreted factors during BMSC growth and regulated by TWIST-1. Future experiments could look into identifying the link between TWIST-1/CMTM8/FGF2 pathways**.**

Questions arise as to how HOPX and CMTM8 mediate the effects of TWIST-1 on the function of BMSC. Given that there is a negative correlation between HOPX or CMTM8 expression and TWIST-1 expression, HOPX or CMTM8 would be predicted to have opposite effects on BMSC to that of TWIST-1. However, in our studies, HOPX or CMTM8 did not show complete opposing effects to TWIST-1. For example, TWIST-1 and CMTM8 both inhibit BMSC osteogenesis. It is important to note that, as a critical factor of bone development and post natal homeostasis, TWIST-1 mediates BMSC growth and differentiation via direct regulation of osteogenic inductive gene such as binding to RUNX2 and inhibits its expression; and indirect regulation such as mediating expression of CMTM8. This study demonstrates the possible existence of a negative feedback loop between TWIST-1 and CMTM8 (Figure 6.2). Moreover, as a transcription factor, TWIST-1 modulates BMSC function via the regulation of a diverse array of gene targets and signalling pathways. Among the TWIST-1 targeted genes/pathways,

there are activating and inhibiting regulators for more precise controls of cell growth and differentiation. Therefore, the inhibition effect of TWIST-1 on BMSC osteogenic differentiation is the overall effect of an array of signalling pathways, while the effects of CMTM8 on BMSC osteogenesis exclude many TWIST-1 targeted genes/pathways.

This study confirmed that both HOPX and CMTM8 act as promoters of BMSC proliferation. Interestingly, TWIST-1 was also reported as a promoter of BMSC proliferation [1]. Given that there is a negative correlation, one possible explanation for this is that HOPX and CMTM8 act through different mechanisms in the absence of TWIST-1 in BMSC. This can be further examined by assessing the expression of cell cycle genes and cell cycle signalling molecules in the *HOPX and CMTM8* overexpressing and siRNA knock down BMSC.

The gap in knowledge of the molecular mechanisms underlying the differentiation of human mesenchymal stem cells into different cell lineages hinders the application of MSC for cell-based therapy. In this study, we identified a critical role of HOPX in inhibiting the molecular program that leads to BMSC adipogenic differentiation, while CMTM8 inhibits the osteogenic differentiation. These findings provide novel mechanistic insights into proliferation and lineage specification of BMSC. This information could be exploited in future studies to manipulate mesenchymal stem cells using small peptide or chemical inhibitors/ activators for optimising their potential in regenerative medicine and cell-based therapy.

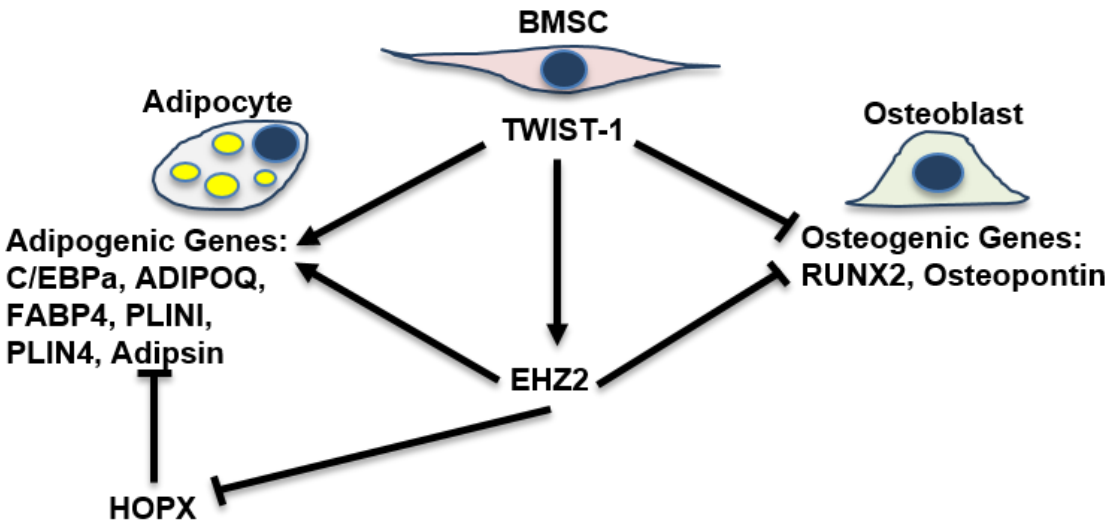

Figure 6.1 Model for HOPX modulation of BMSC adipogenesis. HOPX mediates the regulation of TWIST-1 and EZH2 via suppressing of adipogenic genes such as *C/EBPα*, *ADIPOQ*, *FABP4*, *PLIN1* and *PLIN4*.

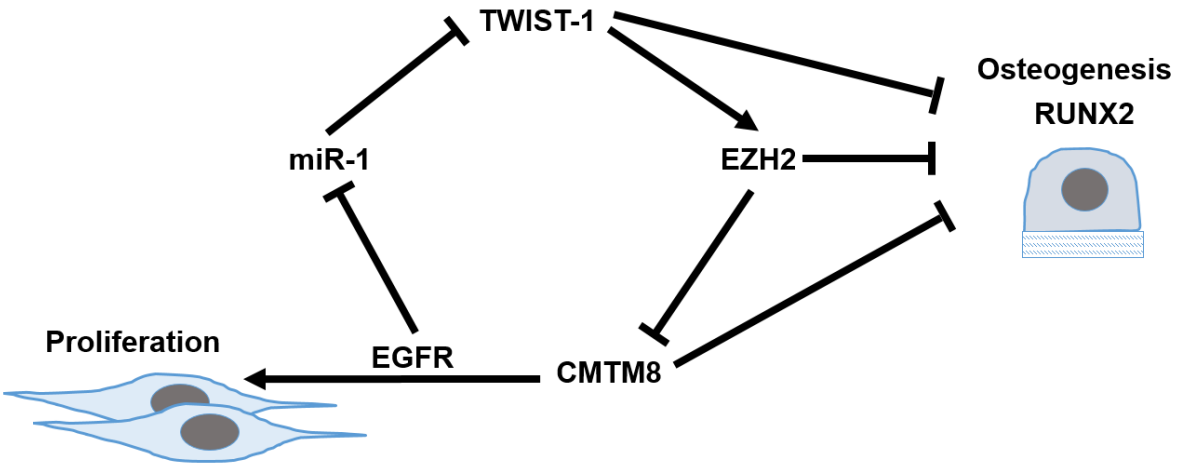

Figure 6.2 Model for CMTM8 modulation of TWIST-1 signalling. *CMTM8* activates EGFR signalling, where EGFR promotes BMSC proliferation, while represses expression of TWIST-1 inhibitor, miR-1, allowing transcription of *TWIST-1*. TWIST-1 then induces expression of *EZH2*, where both TWIST-1 and EZH2 are inhibitors of BMSC osteogenic differentiation. However, EZH2 simultaneously acts in a negative feedback loop to suppress *CMTM8* expression, which is also an inhibitor of BMSC osteogenesis. The overall effects of CMTM8 are promoting BMSC proliferation and inhibiting osteogenesis.

6.2 Future Directions

6.2.1 Does HOPX plays a role in BMSC migration and adhesion?

TWIST-1 has been shown as an EMT marker and promotes cell migration [170, 178, 324]. TWIST-1 contributes to cancer cells invasion and metastasis [178]. Other studies have reported a positive correlation between TWIST-1 and EZH2 expression, while E-cadherin (epithelial marker) expression showed a negative correlation with both TWIST-1 and EZH2 in prostate cancer cells [325]. Since TWIST-1 was shown to promote *EZH2* expression [2, 224], where EZH2 inhibits *HOPX* expression, it is interesting to investigate if HOPX can mediate the effect of TWIST-1 during BMSC migration and adhesion. One strategy is to perform wound healing assays and transwell migration assays using siRNA-mediated *HOPX* knockdown or *HOPX* overexpressing BMSC to assess the effect of HOPX in BMSC migration and adhesion, respectively. In this thesis, wound healing assays have been performed in siRNA-mediated *CMTM8* knockdown or *CMTM8* overexpressing BMSC, and showed that CMTM8 is a promoter of cell migration. To assess the effect of CMTM8 in BMSC adhesion, transwell migration assays can be performed.

After confirming the effects of HOPX and CMTM8 in BMSC migration and adhesion, it is important to identify the downstream molecular pathways of both molecules in these processes. HOPX or CMTM8 siRNA-mediated knockdown or overexpressing BMSC can be stimulated with different factors known to promote BMSC migration such as EGF, HGF, PDGF, SDF-1 and IGF-1; or treated with chemical inhibitors to these factors to inhibit BMSC migration, followed by assessment of migration capacity using would healing assay.

6.2.2 Generation of conditional knockout HOPX$^{-/-}$ homozygous mice.

The present study has been limited to *in vitro* analyses. It is important to determine whether HOPX plays a similar role in BMSC proliferation and cell fate determination *in vivo*. Although it has been shown that HOPX$^{-/-}$ homozygous mice display cardiac defects and 10% lethality rate [222, 250], no phenotype of the skeletal system/ body size/ weight of the mice have been described. To date no HOPX floxed mouse has been reported. CRISPR-Cas9 genome editing technique could be used to generate Loxp sites on the HOPX alleles [326, 327] . Therefore, future studies could lead to the generation of conditional knockout HOPX$^{-/-}$ homozygous mice specifically in the mesenchymal stem/ progenitor cells as we have previously reported for *EZH2* affecting bone/ cartilage and adipose tissues, using HOPX floxed mice mated with the Cre-driver Prrx1 [328].

6.2.3 Does HOPX inhibits marrow fat formation in osteoporotic skeletal system?

Osteoporosis is characterised by reduced bone mass and increased marrow fat formation. In the present thesis, an association between TWIST-1/EZH2/HOPX was reported. Given that TWIST-1 and EZH2 are inhibitors of BMSC osteogenesis and promoters of adipogenesis [1, 2, 48, 196] while HOPX is an inhibitor of BMSC adipogenesis, we speculate that HOPX may delay the onset of osteoporosis. Analysis of skeletal parameters of HOPX$^{-/-}$ homozygous conditional knockout mice from 6.2.2 could help address this issue using an ovariectomy or sham surgery mouse model [328, 329] and compared with wild type animals.

6.2.4 Proteomic and epigenomic analysis in different disease models.

Our future efforts will attempt to decipher the proteomic profile of HOPX such as binding partners of HOPX, the genome wide binding sites of HOPX protein complexes and the role of

putative HOPX targets in human BMSC, osteoporotic-induced mice model and high fat diet mice model, since HOPX was found to be an inhibitor of adipogenesis. Moreover, HOPX has been shown to be hypermethylated in its promoter CpG island in pancreatic cancer cells and other cancer cell types [265]. Therefore, quantitative-methylation-specific PCR (Q-MSP) can be carried out to quantitate the value of methylation on the *HOPX* promoter during growth or differentiation. This will provide the methylation profile on the *HOPX* promoter during these processes and provide better understanding of the epigenetic regulation of *HOPX* under normal physiological or pathological conditions, which could facilitate development of possible future therapeutic strategies that will alter the function of HOPX.

6.2.5 Generation of CMTM8$^{-/-}$ homozygous mice.

To date, no CMTM8$^{-/-}$ homozygous mouse strains have been reported. To demonstrate the role of CMTM8 during BMSC proliferation and cell fate determination *in vivo*, CRISPR-Cas9 genome editing technique could be used to generate Loxp sites on the CMTM8 alleles [326, 327] as described in 6.2.2. Therefore, future studies could lead to the generation of conditional knockout CMTM8$^{-/-}$ homozygous mice specifically in the mesenchymal stem/ progenitor cells as described in 6.2.3 for assessing the role of CMTM8 *in vivo*.

Chapter 7: References

1. Isenmann, S., et al., *TWIST family of basic helix-loop-helix transcription factors mediate human mesenchymal stem cell growth and commitment.* Stem Cells, 2009. **27**(10): p. 2457-68.
2. Cakouros, D., et al., *Twist-1 induces Ezh2 recruitment regulating histone methylation along the Ink4A/Arf locus in mesenchymal stem cells.* Mol Cell Biol, 2012. **32**(8): p. 1433-41.
3. Camp, E., et al., *Tyrosine kinase receptor c-ros-oncogene 1 mediates TWIST-1 regulation of human mesenchymal stem cell lineage commitment.* Bone, 2016.
4. Blair, H.C., M. Zaidi, and P.H. Schlesinger, *Mechanisms balancing skeletal matrix synthesis and degradation.* Biochem J, 2002. **364**(Pt 2): p. 329-41.
5. Eastoe, J.E. and B. Eastoe, *The organic constituents of mammalian compact bone.* Biochem J, 1954. **57**(3): p. 453-9.
6. Herring, G.M., *Comparison of Bovine Bone Sialoprotein and Serum Orosomucoid.* Nature, 1964. **201**: p. 709.
7. Andrews, A.T., G.M. Herring, and P.W. Kent, *Some studies on the composition of bovine cortical-bone sialoprotein.* Biochem J, 1967. **104**(3): p. 705-15.
8. Triffitt, J.T. and M. Owen, *Studies on bone matrix glycoproteins. Incorporation of (1-14C)glucosamine and plasma (14C)glycoprotein into rabbit cortical bone.* Biochem J, 1973. **136**(1): p. 125-34.
9. Ashton, B.A., J.T. Triffitt, and G.M. Herring, *Isolation and partial characterization of a glycoprotein from bovine cortical bone.* Eur J Biochem, 1974. **45**(2): p. 525-33.
10. Triffitt, J.T., *Plasma proteins present in human cortical bone: enrichment of the alpha2HS-glycoprotein.* Calcif Tissue Res, 1976. **22**(1): p. 27-33.
11. Triffitt, J.T., et al., *Origin of plasma alpha2HS-glycoprotein and its accumulation in bone.* Nature, 1976. **262**(5565): p. 226-7.

12. Termine, J.D., et al., *Osteonectin, a bone-specific protein linking mineral to collagen.* Cell, 1981. **26**(1 Pt 1): p. 99-105.

13. Horton, W.A., et al., *Immunohistochemistry of types I and II collagen in undecalcified skeletal tissues.* J Histochem Cytochem, 1983. **31**(3): p. 417-25.

14. Oldberg, A., A. Franzen, and D. Heinegard, *Cloning and sequence analysis of rat bone sialoprotein (osteopontin) cDNA reveals an Arg-Gly-Asp cell-binding sequence.* Proc Natl Acad Sci U S A, 1986. **83**(23): p. 8819-23.

15. Clarke, B., *Normal bone anatomy and physiology.* Clin J Am Soc Nephrol, 2008. **3 Suppl 3**: p. S131-9.

16. Dudley, H.R. and D. Spiro, *The Fine Structure of Bone Cells.* J Biophys Biochem Cytol, 1961. **11**(3): p. 627-49.

17. Sherwood, T.F., et al., *Cranial base growth and morphology in second-trimester normal human fetuses and fetuses with cleft lip.* Cleft Palate Craniofac J, 2001. **38**(6): p. 587-96.

18. Plotkin, L.I., et al., *Mechanical stimulation prevents osteocyte apoptosis: requirement of integrins, Src kinases, and ERKs.* Am J Physiol Cell Physiol, 2005. **289**(3): p. C633-43.

19. Barragan-Adjemian, C., et al., *Mechanism by which MLO-A5 late osteoblasts/early osteocytes mineralize in culture: similarities with mineralization of lamellar bone.* Calcif Tissue Int, 2006. **79**(5): p. 340-53.

20. Sommerfeldt, D.W. and C.T. Rubin, *Biology of bone and how it orchestrates the form and function of the skeleton.* Eur Spine J, 2001. **10 Suppl 2**: p. S86-95.

21. Gupta, R.R., et al., *Induction of an osteocyte-like phenotype by fibroblast growth factor-2.* Biochem Biophys Res Commun, 2010. **402**(2): p. 258-64.

22. Nacamuli, R.P., et al., *Markers of osteoblast differentiation in fusing and nonfusing cranial sutures.* Plast Reconstr Surg, 2003. **112**(5): p. 1328-35.

23. Alappat, S., Z.Y. Zhang, and Y.P. Chen, *Msx homeobox gene family and craniofacial development.* Cell Res, 2003. **13**(6): p. 429-42.

24. Ducy, P., *Cbfa1: a molecular switch in osteoblast biology.* Dev Dyn, 2000. **219**(4): p. 461-71.

25. Napoli, J.L., *Retinoic acid biosynthesis and metabolism.* FASEB J, 1996. **10**(9): p. 993-1001.

26. Yamaguchi, A., T. Komori, and T. Suda, *Regulation of osteoblast differentiation mediated by bone morphogenetic proteins, hedgehogs, and Cbfa1.* Endocr Rev, 2000. **21**(4): p. 393-411.

27. Desbois, C. and G. Karsenty, *Osteocalcin cluster: implications for functional studies.* J Cell Biochem, 1995. **57**(3): p. 379-83.

28. Garcia, T., et al., *Behavior of osteoblast, adipocyte, and myoblast markers in genome-wide expression analysis of mouse calvaria primary osteoblasts in vitro.* Bone, 2002. **31**(1): p. 205-11.

29. Morike, M., et al., *Expression of osteoblastic markers in cultured human bone and fracture callus cells.* J Mol Med (Berl), 1995. **73**(11): p. 571-5.

30. Iseki, S., A.O. Wilkie, and G.M. Morriss-Kay, *Fgfr1 and Fgfr2 have distinct differentiation- and proliferation-related roles in the developing mouse skull vault.* Development, 1999. **126**(24): p. 5611-20.

31. Liu, F., L. Malaval, and J.E. Aubin, *Global amplification polymerase chain reaction reveals novel transitional stages during osteoprogenitor differentiation.* J Cell Sci, 2003. **116**(Pt 9): p. 1787-96.

32. Yamamoto, N., K. Furuya, and K. Hanada, *Progressive development of the osteoblast phenotype during differentiation of osteoprogenitor cells derived from fetal rat calvaria: model for in vitro bone formation.* Biol Pharm Bull, 2002. **25**(4): p. 509-15.

33. Li, Z., K. Kong, and W. Qi, *Osteoclast and its roles in calcium metabolism and bone development and remodeling.* Biochem Biophys Res Commun, 2006. **343**(2): p. 345-50.

34. Krane, S.M., *Identifying genes that regulate bone remodeling as potential therapeutic targets.* J Exp Med, 2005. **201**(6): p. 841-3.

35. Gawlitta, D., et al., *Modulating endochondral ossification of multipotent stromal cells for bone regeneration.* Tissue Eng Part B Rev, 2010. **16**(4): p. 385-95.

36. Karsenty, G. and E.F. Wagner, *Reaching a genetic and molecular understanding of skeletal development.* Dev Cell, 2002. **2**(4): p. 389-406.

37. Horton, W.A., *In vitro chondrogenesis in human chondrodysplasias.* Am J Med Genet, 1993. **45**(2): p. 179-82.

38. Linsenmayer, T.F., et al., *Collagen types IX and X in the developing chick tibiotarsus: analyses of mRNAs and proteins.* Development, 1991. **111**(1): p. 191-6.

39. OpenStax, *Bone Formation and Development*. 4 ed. 2013: OpenStax, Openstax Anatomy and Physiology.

40. Manolagas, S.C., *Cell number versus cell vigor--what really matters to a regenerating skeleton?* Endocrinology, 1999. **140**(10): p. 4377-81.

41. Alman, B.A., S.P. Kelley, and D. Nam, *Heal thyself: using endogenous regeneration to repair bone.* Tissue Eng Part B Rev, 2011. **17**(6): p. 431-6.

42. Parfitt, A.M., *The two faces of growth: benefits and risks to bone integrity.* Osteoporos Int, 1994. **4**(6): p. 382-98.

43. Feng, X. and J.M. McDonald, *Disorders of bone remodeling.* Annu Rev Pathol, 2011. **6**: p. 121-45.

44. Friedenstein, A.J., R.K. Chailakhjan, and K.S. Lalykina, *The development of fibroblast colonies in monolayer cultures of guinea-pig bone marrow and spleen cells.* Cell Tissue Kinet, 1970. **3**(4): p. 393-403.

45. Sacchetti, B., et al., *Self-renewing osteoprogenitors in bone marrow sinusoids can organize a hematopoietic microenvironment.* Cell, 2007. **131**(2): p. 324-36.

46. Gronthos, S., et al., *Molecular and cellular characterisation of highly purified stromal stem cells derived from human bone marrow.* J Cell Sci, 2003. **116**(Pt 9): p. 1827-35.

47. Friedenstein, A.J., J.F. Gorskaja, and N.N. Kulagina, *Fibroblast precursors in normal and irradiated mouse hematopoietic organs.* Exp Hematol, 1976. **4**(5): p. 267-74.

48. Cakouros, D., et al., *Twist-ing cell fate: mechanistic insights into the role of twist in lineage specification/differentiation and tumorigenesis.* J Cell Biochem, 2010. **110**(6): p. 1288-98.

49. Castro-Malaspina, H., et al., *Characterization of human bone marrow fibroblast colony-forming cells (CFU-F) and their progeny.* Blood, 1980. **56**(2): p. 289-301.

50. Pittenger, M.F., et al., *Multilineage potential of adult human mesenchymal stem cells.* Science, 1999. **284**(5411): p. 143-7.

51. Kuznetsov, S.A., et al., *Single-colony derived strains of human marrow stromal fibroblasts form bone after transplantation in vivo.* J Bone Miner Res, 1997. **12**(9): p. 1335-47.

52. Gronthos, S., et al., *The STRO-1+ fraction of adult human bone marrow contains the osteogenic precursors.* Blood, 1994. **84**(12): p. 4164-73.

53. Simmons, P.J. and B. Torok-Storb, *Identification of stromal cell precursors in human bone marrow by a novel monoclonal antibody, STRO-1.* Blood, 1991. **78**(1): p. 55-62.

54. Zannettino, A.C., et al., *Human mulipotential mesenchymal/stromal stem cells are derived from a discrete subpopulation of STRO-1bright/CD34 /CD45(-)/glycophorin-A-bone marrow cells.* Haematologica, 2007. **92**(12): p. 1707-8.

55. Shi, S. and S. Gronthos, *Perivascular niche of postnatal mesenchymal stem cells in human bone marrow and dental pulp.* J Bone Miner Res, 2003. **18**(4): p. 696-704.

56. Dominici, M., et al., *Minimal criteria for defining multipotent mesenchymal stromal cells. The International Society for Cellular Therapy position statement.* Cytotherapy, 2006. **8**(4): p. 315-7.

57. Peister, A., et al., *Adult stem cells from bone marrow (MSCs) isolated from different strains of inbred mice vary in surface epitopes, rates of proliferation, and differentiation potential.* Blood, 2004. **103**(5): p. 1662-8.

58. Nombela-Arrieta, C., J. Ritz, and L.E. Silberstein, *The elusive nature and function of mesenchymal stem cells.* Nat Rev Mol Cell Biol, 2011. **12**(2): p. 126-31.

59. Erices, A., P. Conget, and J.J. Minguell, *Mesenchymal progenitor cells in human umbilical cord blood.* Br J Haematol, 2000. **109**(1): p. 235-42.

60. Kuznetsov, S.A., et al., *Circulating skeletal stem cells.* J Cell Biol, 2001. **153**(5): p. 1133-40.

61. Gronthos, S., et al., *Surface protein characterization of human adipose tissue-derived stromal cells.* J Cell Physiol, 2001. **189**(1): p. 54-63.

62. Gronthos, S., et al., *Postnatal human dental pulp stem cells (DPSCs) in vitro and in vivo.* Proc Natl Acad Sci U S A, 2000. **97**(25): p. 13625-30.

63. Seo, B.M., et al., *Investigation of multipotent postnatal stem cells from human periodontal ligament.* Lancet, 2004. **364**(9429): p. 149-55.

64. De Bari, C., et al., *Multipotent mesenchymal stem cells from adult human synovial membrane.* Arthritis Rheum, 2001. **44**(8): p. 1928-42.

65. Sabatini, F., et al., *Human bronchial fibroblasts exhibit a mesenchymal stem cell phenotype and multilineage differentiating potentialities.* Lab Invest, 2005. **85**(8): p. 962-71.

66. Baksh, D., R. Yao, and R.S. Tuan, *Comparison of proliferative and multilineage differentiation potential of human mesenchymal stem cells derived from umbilical cord and bone marrow.* Stem Cells, 2007. **25**(6): p. 1384-92.

67. Funari, A., et al., *Human Sinusoidal Subendothelial Cells Regulate Homing and Invasion of Circulating Metastatic Prostate Cancer Cells to Bone Marrow.* Cancers (Basel), 2019. **11**(6).

68. Su, P., et al., *Mesenchymal Stem Cell Migration during Bone Formation and Bone Diseases Therapy.* Int J Mol Sci, 2018. **19**(8).

69. Lin, W., et al., *Mesenchymal stem cells homing to improve bone healing.* J Orthop Translat, 2017. **9**: p. 19-27.

70. Fu, X., et al., *Mesenchymal Stem Cell Migration and Tissue Repair.* Cells, 2019. **8**(8).

71. Xiao Ling, K., et al., *Stromal Derived Factor-1/CXCR4 Axis Involved in Bone Marrow Mesenchymal Stem Cells Recruitment to Injured Liver.* Stem Cells Int, 2016. **2016**: p. 8906945.

72. Deng, Q.J., X.F. Xu, and J. Ren, *Effects of SDF-1/CXCR4 on the Repair of Traumatic Brain Injury in Rats by Mediating Bone Marrow Derived Mesenchymal Stem Cells.* Cell Mol Neurobiol, 2018. **38**(2): p. 467-477.

73. Kowalski, K., et al., *Stem cells migration during skeletal muscle regeneration - the role of Sdf-1/Cxcr4 and Sdf-1/Cxcr7 axis.* Cell Adh Migr, 2017. **11**(4): p. 384-398.

74. Pillarisetti, K. and S.K. Gupta, *Cloning and relative expression analysis of rat stromal cell derived factor-1 (SDF-1)1: SDF-1 alpha mRNA is selectively induced in rat model of myocardial infarction.* Inflammation, 2001. **25**(5): p. 293-300.

75. Askari, A.T., et al., *Effect of stromal-cell-derived factor 1 on stem-cell homing and tissue regeneration in ischaemic cardiomyopathy.* Lancet, 2003. **362**(9385): p. 697-703.

76. Ponzetto, C., et al., *A multifunctional docking site mediates signaling and transformation by the hepatocyte growth factor/scatter factor receptor family.* Cell, 1994. **77**(2): p. 261-71.

77. Forte, G., et al., *Hepatocyte growth factor effects on mesenchymal stem cells: proliferation, migration, and differentiation.* Stem Cells, 2006. **24**(1): p. 23-33.

78. Zhu, A., et al., *MiR-221 and miR-26b Regulate Chemotactic Migration of MSCs Toward HGF Through Activation of Akt and FAK.* J Cell Biochem, 2016. **117**(6): p. 1370-83.

79. Parr, C. and A.Y. Ali, *Boswellia frereana suppresses HGF-mediated breast cancer cell invasion and migration through inhibition of c-Met signalling.* J Transl Med, 2018. **16**(1): p. 281.

80. Mytilinaiou, M., et al., *IGF-I regulates HT1080 fibrosarcoma cell migration through a syndecan-2/Erk/ezrin signaling axis.* Exp Cell Res, 2017. **361**(1): p. 9-18.

81. Li, Y., et al., *Insulin-like growth factor 1 enhances the migratory capacity of mesenchymal stem cells.* Biochem Biophys Res Commun, 2007. **356**(3): p. 780-4.

82. Huang, B., et al., *Myocardial transfection of hypoxia-inducible factor-1alpha and co-transplantation of mesenchymal stem cells enhance cardiac repair in rats with experimental myocardial infarction.* Stem Cell Res Ther, 2014. **5**(1): p. 22.

83. Dubon, M.J., et al., *Transforming growth factor beta induces bone marrow mesenchymal stem cell migration via noncanonical signals and N-cadherin.* J Cell Physiol, 2018. **233**(1): p. 201-213.

84. Zhang, S.J., et al., *Effect of TGF-beta1/SDF-1/CXCR4 signal on BM-MSCs homing in rat heart of ischemia/perfusion injury.* Eur Rev Med Pharmacol Sci, 2016. **20**(5): p. 899-905.

85. Langer, H.F., et al., *Platelet derived bFGF mediates vascular integrative mechanisms of mesenchymal stem cells in vitro.* J Mol Cell Cardiol, 2009. **47**(2): p. 315-25.

86. Ball, S.G., C.A. Shuttleworth, and C.M. Kielty, *Vascular endothelial growth factor can signal through platelet-derived growth factor receptors.* J Cell Biol, 2007. **177**(3): p. 489-500.

87. Mishima, Y. and M. Lotz, *Chemotaxis of human articular chondrocytes and mesenchymal stem cells.* J Orthop Res, 2008. **26**(10): p. 1407-12.

88. Nedeau, A.E., et al., *A CXCL5- and bFGF-dependent effect of PDGF-B-activated fibroblasts in promoting trafficking and differentiation of bone marrow-derived mesenchymal stem cells.* Exp Cell Res, 2008. **314**(11-12): p. 2176-86.

89. Shinagawa, K., et al., *Stroma-directed imatinib therapy impairs the tumor-promoting effect of bone marrow-derived mesenchymal stem cells in an orthotopic transplantation model of colon cancer.* Int J Cancer, 2013. **132**(4): p. 813-23.

90. Wang, X., et al., *Concomitant Retrograde Coronary Venous Infusion of Basic Fibroblast Growth Factor Enhances Engraftment and Differentiation of Bone Marrow Mesenchymal Stem Cells for Cardiac Repair after Myocardial Infarction.* Theranostics, 2015. **5**(9): p. 995-1006.

91. Schmidt, A., et al., *Basic fibroblast growth factor controls migration in human mesenchymal stem cells.* Stem Cells, 2006. **24**(7): p. 1750-8.

92. Bialek, P., et al., *A twist code determines the onset of osteoblast differentiation.* Dev Cell, 2004. **6**(3): p. 423-35.

93. Ducy, P., et al., *Osf2/Cbfa1: a transcriptional activator of osteoblast differentiation.* Cell, 1997. **89**(5): p. 747-54.

94. Harris, S.E., et al., *Transcriptional regulation of BMP-2 activated genes in osteoblasts using gene expression microarray analysis: role of Dlx2 and Dlx5 transcription factors.* Front Biosci, 2003. **8**: p. s1249-65.

95. Ishii, M., et al., *Msx2 and Twist cooperatively control the development of the neural crest-derived skeletogenic mesenchyme of the murine skull vault.* Development, 2003. **130**(24): p. 6131-42.

96. Lee, M.S., et al., *TWIST, a basic helix-loop-helix transcription factor, can regulate the human osteogenic lineage.* J Cell Biochem, 1999. **75**(4): p. 566-77.

97. Nakashima, K., et al., *The novel zinc finger-containing transcription factor osterix is required for osteoblast differentiation and bone formation.* Cell, 2002. **108**(1): p. 17-29.

98. Zhang, C., et al., *Inhibition of Wnt signaling by the osteoblast-specific transcription factor Osterix.* Proc Natl Acad Sci U S A, 2008. **105**(19): p. 6936-41.

99. Akiyama, H., et al., *The transcription factor Sox9 has essential roles in successive steps of the chondrocyte differentiation pathway and is required for expression of Sox5 and Sox6.* Genes Dev, 2002. **16**(21): p. 2813-28.

100. Bi, W., et al., *Sox9 is required for cartilage formation.* Nat Genet, 1999. **22**(1): p. 85-9.

101. Bell, D.M., et al., *SOX9 directly regulates the type-II collagen gene.* Nat Genet, 1997. **16**(2): p. 174-8.

102. Lefebvre, V., et al., *SOX9 is a potent activator of the chondrocyte-specific enhancer of the pro alpha1(II) collagen gene.* Mol Cell Biol, 1997. **17**(4): p. 2336-46.

103. Lefebvre, V., P. Li, and B. de Crombrugghe, *A new long form of Sox5 (L-Sox5), Sox6 and Sox9 are coexpressed in chondrogenesis and cooperatively activate the type II collagen gene.* EMBO J, 1998. **17**(19): p. 5718-33.

104. Ng, L.J., et al., *SOX9 binds DNA, activates transcription, and coexpresses with type II collagen during chondrogenesis in the mouse.* Dev Biol, 1997. **183**(1): p. 108-21.

105. Zhou, G., et al., *Three high mobility group-like sequences within a 48-base pair enhancer of the Col2a1 gene are required for cartilage-specific expression in vivo.* J Biol Chem, 1998. **273**(24): p. 14989-97.

106. Smits, P., et al., *The transcription factors L-Sox5 and Sox6 are essential for cartilage formation.* Dev Cell, 2001. **1**(2): p. 277-90.

107. Bi, W., et al., *Haploinsufficiency of Sox9 results in defective cartilage primordia and premature skeletal mineralization.* Proc Natl Acad Sci U S A, 2001. **98**(12): p. 6698-703.

108. Akiyama, H., et al., *Interactions between Sox9 and beta-catenin control chondrocyte differentiation.* Genes Dev, 2004. **18**(9): p. 1072-87.

109. Hattori, T., et al., *SOX9 is a major negative regulator of cartilage vascularization, bone marrow formation and endochondral ossification.* Development, 2010. **137**(6): p. 901-11.

110. Leung, V.Y., et al., *SOX9 governs differentiation stage-specific gene expression in growth plate chondrocytes via direct concomitant transactivation and repression.* PLoS Genet, 2011. **7**(11): p. e1002356.

111. Zhou, G., et al., *Dominance of SOX9 function over RUNX2 during skeletogenesis.* Proc Natl Acad Sci U S A, 2006. **103**(50): p. 19004-9.

112. Dy, P., et al., *Sox9 directs hypertrophic maturation and blocks osteoblast differentiation of growth plate chondrocytes.* Dev Cell, 2012. **22**(3): p. 597-609.

113. Mandrup, S. and M.D. Lane, *Regulating adipogenesis.* J Biol Chem, 1997. **272**(9): p. 5367-70.

114. Zhu, Y., et al., *Structural organization of mouse peroxisome proliferator-activated receptor gamma (mPPAR gamma) gene: alternative promoter use and different splicing yield two mPPAR gamma isoforms.* Proc Natl Acad Sci U S A, 1995. **92**(17): p. 7921-5.

115. Lin, F.T. and M.D. Lane, *Antisense CCAAT/enhancer-binding protein RNA suppresses coordinate gene expression and triglyceride accumulation during differentiation of 3T3-L1 preadipocytes.* Genes Dev, 1992. **6**(4): p. 533-44.

116. Rosen, E.D. and B.M. Spiegelman, *Molecular regulation of adipogenesis.* Annu Rev Cell Dev Biol, 2000. **16**: p. 145-71.

117. Gregoire, F.M., C.M. Smas, and H.S. Sul, *Understanding adipocyte differentiation.* Physiol Rev, 1998. **78**(3): p. 783-809.

118. Fajas, L., J.C. Fruchart, and J. Auwerx, *Transcriptional control of adipogenesis.* Curr Opin Cell Biol, 1998. **10**(2): p. 165-73.

119. Lazarenko, O.P., et al., *Netoglitazone is a PPAR-gamma ligand with selective effects on bone and fat.* Bone, 2006. **38**(1): p. 74-84.

120. Lecka-Czernik, B., et al., *Divergent effects of selective peroxisome proliferator-activated receptor-gamma 2 ligands on adipocyte versus osteoblast differentiation.* Endocrinology, 2002. **143**(6): p. 2376-84.

121. Akune, T., et al., *PPARgamma insufficiency enhances osteogenesis through osteoblast formation from bone marrow progenitors.* J Clin Invest, 2004. **113**(6): p. 846-55.

122. Moerman, E.J., et al., *Aging activates adipogenic and suppresses osteogenic programs in mesenchymal marrow stroma/stem cells: the role of PPAR-gamma2 transcription factor and TGF-beta/BMP signaling pathways.* Aging Cell, 2004. **3**(6): p. 379-89.

123. Karsenty, G., H.M. Kronenberg, and C. Settembre, *Genetic control of bone formation.* Annu Rev Cell Dev Biol, 2009. **25**: p. 629-48.

124. Baek, W.Y., et al., *Positive regulation of adult bone formation by osteoblast-specific transcription factor osterix.* J Bone Miner Res, 2009. **24**(6): p. 1055-65.

125. Gimble, J.M., et al., *Bone morphogenetic proteins inhibit adipocyte differentiation by bone marrow stromal cells.* J Cell Biochem, 1995. **58**(3): p. 393-402.

126. Duque, G., *Bone and fat connection in aging bone.* Curr Opin Rheumatol, 2008. **20**(4): p. 429-34.

127. Beresford, J.N., et al., *Evidence for an inverse relationship between the differentiation of adipocytic and osteogenic cells in rat marrow stromal cell cultures.* J Cell Sci, 1992. **102 (Pt 2)**: p. 341-51.

128. Dorheim, M.A., et al., *Osteoblastic gene expression during adipogenesis in hematopoietic supporting murine bone marrow stromal cells.* J Cell Physiol, 1993. **154**(2): p. 317-28.

129. Pandur, P., D. Maurus, and M. Kuhl, *Increasingly complex: new players enter the Wnt signaling network.* Bioessays, 2002. **24**(10): p. 881-4.

130. Reya, T. and H. Clevers, *Wnt signalling in stem cells and cancer.* Nature, 2005. **434**(7035): p. 843-50.

131. Kato, M., et al., *Cbfa1-independent decrease in osteoblast proliferation, osteopenia, and persistent embryonic eye vascularization in mice deficient in Lrp5, a Wnt coreceptor.* J Cell Biol, 2002. **157**(2): p. 303-14.

132. Krishnan, V., H.U. Bryant, and O.A. Macdougald, *Regulation of bone mass by Wnt signaling.* J Clin Invest, 2006. **116**(5): p. 1202-9.

133. Bennett, C.N., et al., *Regulation of Wnt signaling during adipogenesis.* J Biol Chem, 2002. **277**(34): p. 30998-1004.

134. Liu, J. and S.R. Farmer, *Regulating the balance between peroxisome proliferator-activated receptor gamma and beta-catenin signaling during adipogenesis. A glycogen synthase kinase 3beta phosphorylation-defective mutant of beta-catenin inhibits expression of a subset of adipogenic genes.* J Biol Chem, 2004. **279**(43): p. 45020-7.

135. Moldes, M., et al., *Peroxisome-proliferator-activated receptor gamma suppresses Wnt/beta-catenin signalling during adipogenesis.* Biochem J, 2003. **376**(Pt 3): p. 607-13.

136. Ross, S.E., et al., *Inhibition of adipogenesis by Wnt signaling.* Science, 2000. **289**(5481): p. 950-3.

137. Williams, A.R. and J.M. Hare, *Mesenchymal stem cells: biology, pathophysiology, translational findings, and therapeutic implications for cardiac disease.* Circ Res, 2011. **109**(8): p. 923-40.

138. Zhou, S., K. Eid, and J. Glowacki, *Cooperation between TGF-beta and Wnt pathways during chondrocyte and adipocyte differentiation of human marrow stromal cells.* J Bone Miner Res, 2004. **19**(3): p. 463-70.

139. Augello, A. and C. De Bari, *The regulation of differentiation in mesenchymal stem cells.* Hum Gene Ther, 2010. **21**(10): p. 1226-38.

140. Mackay, A.M., et al., *Chondrogenic differentiation of cultured human mesenchymal stem cells from marrow.* Tissue Eng, 1998. **4**(4): p. 415-28.

141. Li, T.S., et al., *TGF-beta induces the differentiation of bone marrow stem cells into immature cardiomyocytes.* Biochem Biophys Res Commun, 2008. **366**(4): p. 1074-80.

142. Arita, N.A., D. Pelaez, and H.S. Cheung, *Activation of the extracellular signal-regulated kinases 1 and 2 (ERK1/2) is needed for the TGFbeta-induced chondrogenic and osteogenic differentiation of mesenchymal stem cells.* Biochem Biophys Res Commun, 2011. **405**(4): p. 564-9.

143. Chen, D., M. Zhao, and G.R. Mundy, *Bone morphogenetic proteins.* Growth Factors, 2004. **22**(4): p. 233-41.

144. Asahina, I., T.K. Sampath, and P.V. Hauschka, *Human osteogenic protein-1 induces chondroblastic, osteoblastic, and/or adipocytic differentiation of clonal murine target cells.* Exp Cell Res, 1996. **222**(1): p. 38-47.

145. Bowers, R.R. and M.D. Lane, *A role for bone morphogenetic protein-4 in adipocyte development.* Cell Cycle, 2007. **6**(4): p. 385-9.

146. Date, T., et al., *Bone morphogenetic protein-2 induces differentiation of multipotent C3H10T1/2 cells into osteoblasts, chondrocytes, and adipocytes in vivo and in vitro.* J Orthop Sci, 2004. **9**(5): p. 503-8.

147. Friedman, M.S., M.W. Long, and K.D. Hankenson, *Osteogenic differentiation of human mesenchymal stem cells is regulated by bone morphogenetic protein-6.* J Cell Biochem, 2006. **98**(3): p. 538-54.

148. Lavery, K., et al., *BMP-2/4 and BMP-6/7 differentially utilize cell surface receptors to induce osteoblastic differentiation of human bone marrow-derived mesenchymal stem cells.* J Biol Chem, 2008. **283**(30): p. 20948-58.

149. Maliakal, J.C., et al., *Osteogenic protein-1 (BMP-7) inhibits cell proliferation and stimulates the expression of markers characteristic of osteoblast phenotype in rat osteosarcoma (17/2.8) cells.* Growth Factors, 1994. **11**(3): p. 227-34.

150. Neumann, K., et al., *BMP7 promotes adipogenic but not osteo-/chondrogenic differentiation of adult human bone marrow-derived stem cells in high-density micro-mass culture.* J Cell Biochem, 2007. **102**(3): p. 626-37.

151. Chen, D., et al., *Differential roles for bone morphogenetic protein (BMP) receptor type IB and IA in differentiation and specification of mesenchymal precursor cells to osteoblast and adipocyte lineages.* J Cell Biol, 1998. **142**(1): p. 295-305.

152. Wang, E.A., et al., *Bone morphogenetic protein-2 causes commitment and differentiation in C3H10T1/2 and 3T3 cells.* Growth Factors, 1993. **9**(1): p. 57-71.

153. Guertin, D.A. and D.M. Sabatini, *Defining the role of mTOR in cancer.* Cancer Cell, 2007. **12**(1): p. 9-22.

154. Singha, U.K., et al., *Rapamycin inhibits osteoblast proliferation and differentiation in MC3T3-E1 cells and primary mouse bone marrow stromal cells.* J Cell Biochem, 2008. **103**(2): p. 434-46.

155. Lee, K.W., et al., *Rapamycin promotes the osteoblastic differentiation of human embryonic stem cells by blocking the mTOR pathway and stimulating the BMP/Smad pathway.* Stem Cells Dev, 2010. **19**(4): p. 557-68.

156. Vinals, F., et al., *Inhibition of PI3K/p70 S6K and p38 MAPK cascades increases osteoblastic differentiation induced by BMP-2.* FEBS Lett, 2002. **510**(1-2): p. 99-104.

157. Martin, S.K., et al., *NVP-BEZ235, a dual pan class I PI3 kinase and mTOR inhibitor, promotes osteogenic differentiation in human mesenchymal stromal cells.* J Bone Miner Res, 2010. **25**(10): p. 2126-37.

158. Huang, B., et al., *mTORC1 Prevents Preosteoblast Differentiation through the Notch Signaling Pathway.* PLoS Genet, 2015. **11**(8): p. e1005426.

159. Kim, J.E. and J. Chen, *regulation of peroxisome proliferator-activated receptor-gamma activity by mammalian target of rapamycin and amino acids in adipogenesis.* Diabetes, 2004. **53**(11): p. 2748-56.

160. Zhang, H.H., et al., *Insulin stimulates adipogenesis through the Akt-TSC2-mTORC1 pathway.* PLoS One, 2009. **4**(7): p. e6189.

161. Hutley, L., et al., *Fibroblast growth factor 1: a key regulator of human adipogenesis.* Diabetes, 2004. **53**(12): p. 3097-106.

162. Neubauer, M., et al., *Basic fibroblast growth factor enhances PPARgamma ligand-induced adipogenesis of mesenchymal stem cells.* FEBS Lett, 2004. **577**(1-2): p. 277-83.

163. Neubauer, M., et al., *Adipose tissue engineering based on mesenchymal stem cells and basic fibroblast growth factor in vitro.* Tissue Eng, 2005. **11**(11-12): p. 1840-51.

164. Sakaue, H., et al., *Requirement of fibroblast growth factor 10 in development of white adipose tissue.* Genes Dev, 2002. **16**(8): p. 908-12.

165. Dupree, M.A., et al., *Fibroblast growth factor 2 induced proliferation in osteoblasts and bone marrow stromal cells: a whole cell model.* Biophys J, 2006. **91**(8): p. 3097-112.

166. Hanada, K., J.E. Dennis, and A.I. Caplan, *Stimulatory effects of basic fibroblast growth factor and bone morphogenetic protein-2 on osteogenic differentiation of rat bone marrow-derived mesenchymal stem cells.* J Bone Miner Res, 1997. **12**(10): p. 1606-14.

167. Martin, I., et al., *Fibroblast growth factor-2 supports ex vivo expansion and maintenance of osteogenic precursors from human bone marrow.* Endocrinology, 1997. **138**(10): p. 4456-62.

168. Pitaru, S., et al., *Effect of basic fibroblast growth factor on the growth and differentiation of adult stromal bone marrow cells: enhanced development of mineralized bone-like tissue in culture.* J Bone Miner Res, 1993. **8**(8): p. 919-29.

169. Karsenty, G., *Convergence between bone and energy homeostases: leptin regulation of bone mass.* Cell Metab, 2006. **4**(5): p. 341-8.

170. Chen, Z.F. and R.R. Behringer, *twist is required in head mesenchyme for cranial neural tube morphogenesis.* Genes Dev, 1995. **9**(6): p. 686-99.

171. Wang, S.M., et al., *Cloning of the human twist gene: its expression is retained in adult mesodermally-derived tissues.* Gene, 1997. **187**(1): p. 83-92.

172. Murre, C., et al., *Interactions between heterologous helix-loop-helix proteins generate complexes that bind specifically to a common DNA sequence.* Cell, 1989. **58**(3): p. 537-44.

173. Menicanin, D., et al., *Identification of a common gene expression signature associated with immature clonal mesenchymal cell populations derived from bone marrow and dental tissues.* Stem Cells Dev, 2010. **19**(10): p. 1501-10.

174. Celia-Terrassa, T., et al., *Epithelial-mesenchymal transition can suppress major attributes of human epithelial tumor-initiating cells.* J Clin Invest, 2012. **122**(5): p. 1849-68.

175. Qin, Q., et al., *Normal and disease-related biological functions of Twist1 and underlying molecular mechanisms.* Cell Res, 2012. **22**(1): p. 90-106.

176. Yang, J., et al., *Twist, a master regulator of morphogenesis, plays an essential role in tumor metastasis.* Cell, 2004. **117**(7): p. 927-39.

177. David, J.M. and A.K. Rajasekaran, *Dishonorable discharge: the oncogenic roles of cleaved E-cadherin fragments.* Cancer Res, 2012. **72**(12): p. 2917-23.

178. Chang, Y.S., et al., *EGF Receptor Promotes Prostate Cancer Bone Metastasis by Downregulating miR-1 and Activating TWIST1*. Cancer Res, 2015. **75**(15): p. 3077-86.

179. Cakouros, D., et al., *Novel basic helix-loop-helix transcription factor hes4 antagonizes the function of twist-1 to regulate lineage commitment of bone marrow stromal/stem cells.* Stem Cells Dev, 2015. **24**(11): p. 1297-308.

180. Hayashi, M., et al., *Comparative roles of Twist-1 and Id1 in transcriptional regulation by BMP signaling.* J Cell Sci, 2007. **120**(Pt 8): p. 1350-7.

181. Goodnough, L.H., et al., *Twist1 mediates repression of chondrogenesis by beta-catenin to promote cranial bone progenitor specification.* Development, 2012. **139**(23): p. 4428-38.

182. Goodnough, L.H., G.J. Dinuoscio, and R.P. Atit, *Twist1 contributes to cranial bone initiation and dermal condensation by maintaining Wnt signaling responsiveness.* Dev Dyn, 2016. **245**(2): p. 144-56.

183. Miraoui, H., et al., *Molecular silencing of Twist1 enhances osteogenic differentiation of murine mesenchymal stem cells: implication of FGFR2 signaling.* J Cell Biochem, 2010. **110**(5): p. 1147-54.

184. Glackin, C.A., E.J. Murray, and S.S. Murray, *Doxorubicin inhibits differentiation and enhances expression of the helix-loop-helix genes Id and mTwi in mouse osteoblastic cells.* Biochem Int, 1992. **28**(1): p. 67-75.

185. Murray, S.S., et al., *Expression of helix-loop-helix regulatory genes during differentiation of mouse osteoblastic cells.* J Bone Miner Res, 1992. **7**(10): p. 1131-8.

186. Connerney, J., et al., *Twist1 homodimers enhance FGF responsiveness of the cranial sutures and promote suture closure.* Dev Biol, 2008. **318**(2): p. 323-34.

187. Connerney, J., et al., *Twist1 dimer selection regulates cranial suture patterning and fusion.* Dev Dyn, 2006. **235**(5): p. 1345-57.

188. Behr, B., M.T. Longaker, and N. Quarto, *Craniosynostosis of coronal suture in twist1 mice occurs through endochondral ossification recapitulating the physiological closure of posterior frontal suture.* Front Physiol, 2011. **2**: p. 37.

189. Carver, E.A., K.F. Oram, and T. Gridley, *Craniosynostosis in Twist heterozygous mice: a model for Saethre-Chotzen syndrome.* Anat Rec, 2002. **268**(2): p. 90-2.

190. Yoshida, T., et al., *Twist is required for establishment of the mouse coronal suture.* J Anat, 2005. **206**(5): p. 437-44.

191. el Ghouzzi, V., et al., *Mutations of the TWIST gene in the Saethre-Chotzen syndrome.* Nat Genet, 1997. **15**(1): p. 42-6.

192. Howard, T.D., et al., *Mutations in TWIST, a basic helix-loop-helix transcription factor, in Saethre-Chotzen syndrome.* Nat Genet, 1997. **15**(1): p. 36-41.

193. Yousfi, M., et al., *Twist haploinsufficiency in Saethre-Chotzen syndrome induces calvarial osteoblast apoptosis due to increased TNFalpha expression and caspase-2 activation.* Hum Mol Genet, 2002. **11**(4): p. 359-69.

194. Dong, Y.F., et al., *Transforming growth factor-beta and Wnt signals regulate chondrocyte differentiation through Twist1 in a stage-specific manner.* Mol Endocrinol, 2007. **21**(11): p. 2805-20.

195. Guzzo, R.M., et al., *Persistent expression of Twist1 in chondrocytes causes growth plate abnormalities and dwarfism in mice.* Int J Dev Biol, 2011. **55**(6): p. 641-7.

196. Hemming, S., et al., *EZH2 and KDM6A act as an epigenetic switch to regulate mesenchymal stem cell lineage specification.* Stem Cells, 2014. **32**(3): p. 802-15.

197. Gronthos, S. and A.C. Zannettino, *A method to isolate and purify human bone marrow stromal stem cells.* Methods Mol Biol, 2008. **449**: p. 45-57.

198. Coussens, A.K., et al., *In vitro differentiation of human calvarial suture derived cells with and without dexamethasone does not induce in vivo-like expression.* J Cell Physiol, 2009. **218**(1): p. 183-91.

199. De Pollack, C., et al., *Increased bone formation and osteoblastic cell phenotype in premature cranial suture ossification (craniosynostosis).* J Bone Miner Res, 1996. **11**(3): p. 401-7.

200. Andrews, S., *FastQC A Quality Control tool for High Throughput Sequence Data*. 2014.

201. Ward, C.M., To, H. & Pederson, S. M., *ngsReports: An R Package for managing FastQC reports and other NGS related log files.* bioRxiv, 2018.

202. Schubert, M., S. Lindgreen, and L. Orlando, *AdapterRemoval v2: rapid adapter trimming, identification, and read merging.* BMC Res Notes, 2016. **9**: p. 88.

203. Dobin, A., et al., *STAR: ultrafast universal RNA-seq aligner.* Bioinformatics, 2012. **29**(1): p. 15-21.

204. Liao, Y., G.K. Smyth, and W. Shi, *featureCounts: an efficient general purpose program for assigning sequence reads to genomic features.* Bioinformatics, 2013. **30**(7): p. 923-930.

205. McCarthy, D.J., Y. Chen, and G.K. Smyth, *Differential expression analysis of multifactor RNA-Seq experiments with respect to biological variation.* Nucleic Acids Res, 2012. **40**.

206. Robinson, M., D. McCarthy, and G. Smyth, *edgeR: a Bioconductor package for differential expression analysis of digital gene expression data.* Bioinformatics, 2010. **26**.

207. Ritchie, M.E., et al., *limma powers differential expression analyses for RNA-sequencing and microarray studies.* Nucleic Acids Res, 2015. **43**(7): p. e47.

208. Robinson, M.D. and A. Oshlack, *A scaling normalization method for differential expression analysis of RNA-seq data.* Genome Biology, 2010. **11**(3): p. R25.

209. Law, C.W., et al., *voom: precision weights unlock linear model analysis tools for RNA-seq read counts.* Genome Biology, 2014. **15**(2): p. R29.

210. Durinck, S., et al., *Mapping identifiers for the integration of genomic datasets with the R/Bioconductor package biomaRt.* Nature Protocols, 2009. **4**: p. 1184.

211. R., K. *pheatmap: Pretty Heatmaps*. 2019; R package version 1.0.12:[Available from: https://CRAN.R-project.org/package=pheatmap

212. Alborzi, A., et al., *Endochondral and intramembranous fetal bone development: osteoblastic cell proliferation, and expression of alkaline phosphatase, m-twist, and histone H4.* J Craniofac Genet Dev Biol, 1996. **16**(2): p. 94-106.

213. Rice, D.P., et al., *Integration of FGF and TWIST in calvarial bone and suture development.* Development, 2000. **127**(9): p. 1845-55.

214. Norton, J.D. and G.T. Atherton, *Coupling of cell growth control and apoptosis functions of Id proteins.* Mol Cell Biol, 1998. **18**(4): p. 2371-81.

215. Geoffroy, V., et al., *High bone resorption in adult aging transgenic mice overexpressing cbfa1/runx2 in cells of the osteoblastic lineage.* Mol Cell Biol, 2002. **22**(17): p. 6222-33.

216. Komori, T., *Regulation of osteoblast differentiation by transcription factors.* J Cell Biochem, 2006. **99**(5): p. 1233-9.

217. Liu, W., et al., *Overexpression of Cbfa1 in osteoblasts inhibits osteoblast maturation and causes osteopenia with multiple fractures.* J Cell Biol, 2001. **155**(1): p. 157-66.

218. Inaoka, T., et al., *Molecular cloning of human cDNA for cathepsin K: novel cysteine proteinase predominantly expressed in bone.* Biochem Biophys Res Commun, 1995. **206**(1): p. 89-96.

219. Li, J., H. Xie, and Y. Jiang, *Mucopolysaccharidosis IIIB and mild skeletal anomalies: coexistence of NAGLU and CYP26B1 missense variations in the same patient in a Chinese family.* BMC Med Genet, 2018. **19**(1): p. 51.

220. Lind, T., et al., *Excessive dietary intake of vitamin A reduces skull bone thickness in mice.* PLoS One, 2017. **12**(4): p. e0176217.

221. Lind, T., et al., *Bones in human CYP26B1 deficiency and rats with hypervitaminosis A phenocopy Vegfa overexpression.* Bone Rep, 2018. **9**: p. 27-36.

222. Chen, F., et al., *Hop is an unusual homeobox gene that modulates cardiac development.* Cell, 2002. **110**(6): p. 713-23.

223. Jain, R., et al., *HEART DEVELOPMENT. Integration of Bmp and Wnt signaling by Hopx specifies commitment of cardiomyoblasts.* Science, 2015. **348**(6242): p. aaa6071.

224. Hemming, S., et al., *Identification of Novel EZH2 Targets Regulating Osteogenic Differentiation in Mesenchymal Stem Cells.* Stem Cells Dev, 2016. **25**(12): p. 909-21.

225. Kuzmichev, A., et al., *Different EZH2-containing complexes target methylation of histone H1 or nucleosomal histone H3.* Mol Cell, 2004. **14**(2): p. 183-93.

226. Damsky, C.H. and D. Ilic, *Integrin signaling: it's where the action is.* Curr Opin Cell Biol, 2002. **14**(5): p. 594-602.

227. Hynes, R.O., *Integrins: bidirectional, allosteric signaling machines.* Cell, 2002. **110**(6): p. 673-87.

228. Humphries, J.D., A. Byron, and M.J. Humphries, *Integrin ligands at a glance.* J Cell Sci, 2006. **119**(Pt 19): p. 3901-3.

229. Ruoslahti, E. and J.C. Reed, *Anchorage dependence, integrins, and apoptosis.* Cell, 1994. **77**(4): p. 477-8.

230. Zhang, Z., et al., *The alpha 5 beta 1 integrin supports survival of cells on fibronectin and up-regulates Bcl-2 expression.* Proc Natl Acad Sci U S A, 1995. **92**(13): p. 6161-5.

231. Hamidouche, Z., et al., *Priming integrin alpha5 promotes human mesenchymal stromal cell osteoblast differentiation and osteogenesis.* Proc Natl Acad Sci U S A, 2009. **106**(44): p. 18587-91.

232. Hamidouche, Z., et al., *Crosstalks between integrin alpha 5 and IGF2/IGFBP2 signalling trigger human bone marrow-derived mesenchymal stromal osteogenic differentiation.* BMC Cell Biol, 2010. **11**: p. 44.

233. Cha, B.H., et al., *Administration of tauroursodeoxycholic acid enhances osteogenic differentiation of bone marrow-derived mesenchymal stem cells and bone regeneration.* Bone, 2016. **83**: p. 73-81.

234. Han, H.J., T. Tokino, and Y. Nakamura, *CSR, a scavenger receptor-like protein with a protective role against cellular damage causedby UV irradiation and oxidative stress.* Hum Mol Genet, 1998. **7**(6): p. 1039-46.

235. Peiser, L. and S. Gordon, *The function of scavenger receptors expressed by macrophages and their role in the regulation of inflammation.* Microbes Infect, 2001. **3**(2): p. 149-59.

236. Peiser, L., S. Mukhopadhyay, and S. Gordon, *Scavenger receptors in innate immunity.* Curr Opin Immunol, 2002. **14**(1): p. 123-8.

237. Pluddemann, A., C. Neyen, and S. Gordon, *Macrophage scavenger receptors and host-derived ligands.* Methods, 2007. **43**(3): p. 207-17.

238. Balla, B., et al., *Transcriptional profiling of immune system-related genes in postmenopausal osteoporotic versus non-osteoporotic human bone tissue.* Clin Immunol, 2009. **131**(2): p. 354-9.

239. Zhu, Z.H., et al., *CSR1 induces cell death through inactivation of CPSF3.* Oncogene, 2009. **28**(1): p. 41-51.

240. Hong, D., et al., *Morphological and proteomic analysis of early stage of osteoblast differentiation in osteoblastic progenitor cells.* Exp Cell Res, 2010. **316**(14): p. 2291-300.

241. Jin, C., et al., *Regulation of EGF receptor signaling by the MARVEL domain-containing protein CKLFSF8.* FEBS Lett, 2005. **579**(28): p. 6375-82.

242. Zhu, J., et al., *EGFR signaling suppresses osteoblast differentiation and inhibits expression of master osteoblastic transcription factors Runx2 and Osterix.* J Cell Biochem, 2011. **112**(7): p. 1749-60.

243. Both, J., et al., *Focal chromosomal copy number aberrations identify CMTM8 and GPR177 as new candidate driver genes in osteosarcoma.* PLoS One, 2014. **9**(12): p. e115835.

244. Salvi, A., et al., *In vitro c-met inhibition by antisense RNA and plasmid-based RNAi down-modulates migration and invasion of hepatocellular carcinoma cells.* Int J Oncol, 2007. **31**(2): p. 451-60.

245. Zhang, W., et al., *Down-regulation of CMTM8 induces epithelial-to-mesenchymal transition-like changes via c-MET/extracellular signal-regulated kinase (ERK) signaling.* J Biol Chem, 2012. **287**(15): p. 11850-8.

246. Bhattacharjee, A., et al., *Slick (Slo2.1), a rapidly-gating sodium-activated potassium channel inhibited by ATP.* J Neurosci, 2003. **23**(37): p. 11681-91.

247. Joiner, W.J., et al., *Formation of intermediate-conductance calcium-activated potassium channels by interaction of Slack and Slo subunits.* Nat Neurosci, 1998. **1**(6): p. 462-9.

248. Yuan, A., et al., *The sodium-activated potassium channel is encoded by a member of the Slo gene family.* Neuron, 2003. **37**(5): p. 765-73.

249. Laue, K., et al., *Craniosynostosis and multiple skeletal anomalies in humans and zebrafish result from a defect in the localized degradation of retinoic acid.* Am J Hum Genet, 2011. **89**(5): p. 595-606.

250. Shin, C.H., et al., *Modulation of cardiac growth and development by HOP, an unusual homeodomain protein.* Cell, 2002. **110**(6): p. 725-35.

251. Hamamori, Y., et al., *The basic domain of myogenic basic helix-loop-helix (bHLH) proteins is the novel target for direct inhibition by another bHLH protein, Twist.* Mol Cell Biol, 1997. **17**(11): p. 6563-73.

252. Massari, M.E. and C. Murre, *Helix-loop-helix proteins: regulators of transcription in eucaryotic organisms.* Mol Cell Biol, 2000. **20**(2): p. 429-40.

253. Yevshin, I., et al., *GTRD: a database on gene transcription regulation-2019 update.* Nucleic Acids Res, 2019. **47**(D1): p. D100-D105.

254. Ooki, A., et al., *Potential utility of HOP homeobox gene promoter methylation as a marker of tumor aggressiveness in gastric cancer.* Oncogene, 2010. **29**(22): p. 3263-75.

255. Trivedi, C.M., et al., *Hopx and Hdac2 interact to modulate Gata4 acetylation and embryonic cardiac myocyte proliferation.* Dev Cell, 2010. **19**(3): p. 450-9.

256. Kook, H., et al., *Cardiac hypertrophy and histone deacetylase-dependent transcriptional repression mediated by the atypical homeodomain protein Hop.* J Clin Invest, 2003. **112**(6): p. 863-71.

257. Kee, H.J., et al., *Enhancer of polycomb1, a novel homeodomain only protein-binding partner, induces skeletal muscle differentiation.* J Biol Chem, 2007. **282**(10): p. 7700-9.

258. Yamashita, K., H. Katoh, and M. Watanabe, *The homeobox only protein homeobox (HOPX) and colorectal cancer.* Int J Mol Sci, 2013. **14**(12): p. 23231-43.

259. Asanoma, K., et al., *HOP/NECC1, a novel regulator of mouse trophoblast differentiation.* J Biol Chem, 2007. **282**(33): p. 24065-74.

260. Asanoma, K., et al., *NECC1, a candidate choriocarcinoma suppressor gene that encodes a homeodomain consensus motif.* Genomics, 2003. **81**(1): p. 15-25.

261. Chen, Y., et al., *Homeobox gene HOP has a potential tumor suppressive activity in human lung cancer.* Int J Cancer, 2007. **121**(5): p. 1021-7.

262. Chen, Y., et al., *Identification of a novel homeobox-containing gene, LAGY, which is downregulated in lung cancer.* Oncology, 2003. **64**(4): p. 450-8.

263. Cheung, W.K., et al., *Control of alveolar differentiation by the lineage transcription factors GATA6 and HOPX inhibits lung adenocarcinoma metastasis.* Cancer Cell, 2013. **23**(6): p. 725-38.

264. Lemaire, F., et al., *Loss of HOP tumour suppressor expression in head and neck squamous cell carcinoma.* Br J Cancer, 2004. **91**(2): p. 258-61.

265. Waraya, M., et al., *Cancer specific promoter CpG Islands hypermethylation of HOP homeobox (HOPX) gene and its potential tumor suppressive role in pancreatic carcinogenesis.* BMC Cancer, 2012. **12**: p. 397.

266. Yamaguchi, S., et al., *Homeobox gene HOPX is epigenetically silenced in human uterine endometrial cancer and suppresses estrogen-stimulated proliferation of cancer cells by inhibiting serum response factor.* Int J Cancer, 2009. **124**(11): p. 2577-88.

267. Yamashita, K., et al., *HOP/OB1/NECC1 promoter DNA is frequently hypermethylated and involved in tumorigenic ability in esophageal squamous cell carcinoma.* Mol Cancer Res, 2008. **6**(1): p. 31-41.

268. Takeda, N., et al., *Hopx expression defines a subset of multipotent hair follicle stem cells and a progenitor population primed to give rise to K6+ niche cells.* Development, 2013. **140**(8): p. 1655-64.

269. Yang, J.M., et al., *Expression of the homeobox gene, HOPX, is modulated by cell differentiation in human keratinocytes and is involved in the expression of differentiation markers.* Eur J Cell Biol, 2010. **89**(7): p. 537-46.

270. Mariotto, A., et al., *HOPX: The Unusual Homeodomain-Containing Protein.* J Invest Dermatol, 2016. **136**(5): p. 905-911.

271. Chen, C.Y. and R.J. Schwartz, *Recruitment of the tinman homolog Nkx-2.5 by serum response factor activates cardiac alpha-actin gene transcription.* Mol Cell Biol, 1996. **16**(11): p. 6372-84.

272. Durocher, D., et al., *The cardiac transcription factors Nkx2-5 and GATA-4 are mutual cofactors.* EMBO J, 1997. **16**(18): p. 5687-96.

273. Sepulveda, J.L., et al., *Combinatorial expression of GATA4, Nkx2-5, and serum response factor directs early cardiac gene activity.* J Biol Chem, 2002. **277**(28): p. 25775-82.

274. Liu, F., et al., *Histone-deacetylase inhibition reverses atrial arrhythmia inducibility and fibrosis in cardiac hypertrophy independent of angiotensin.* J Mol Cell Cardiol, 2008. **45**(6): p. 715-23.

275. Pu, Y., et al., *Adiponectin Promotes Human Jaw Bone Marrow Stem Cell Osteogenesis.* J Dent Res, 2016. **95**(7): p. 769-75.

276. Yamauchi, T., et al., *Cloning of adiponectin receptors that mediate antidiabetic metabolic effects.* Nature, 2003. **423**(6941): p. 762-9.

277. Shinoda, Y., et al., *Regulation of bone formation by adiponectin through autocrine/paracrine and endocrine pathways.* J Cell Biochem, 2006. **99**(1): p. 196-208.

278. Ceddia, R.B., et al., *Globular adiponectin increases GLUT4 translocation and glucose uptake but reduces glycogen synthesis in rat skeletal muscle cells.* Diabetologia, 2005. **48**(1): p. 132-9.

279. Fu, Y., et al., *Adiponectin promotes adipocyte differentiation, insulin sensitivity, and lipid accumulation.* J Lipid Res, 2005. **46**(7): p. 1369-79.

280. Thorn, S.L., et al., *Chronic AMPK activity dysregulation produces myocardial insulin resistance in the human Arg302Gln-PRKAG2 glycogen storage disease mouse model.* EJNMMI Res, 2013. **3**(1): p. 48.

281. Lin, Y.Y., et al., *Adiponectin receptor 1 regulates bone formation and osteoblast differentiation by GSK-3beta/beta-catenin signaling in mice.* Bone, 2014. **64**: p. 147-54.

282. China, S.P., et al., *Globular adiponectin reverses osteo-sarcopenia and altered body composition in ovariectomized rats.* Bone, 2017. **105**: p. 75-86.

283. Takahashi, K., K. Hiwada, and T. Kokubu, *Isolation and characterization of a 34,000-dalton calmodulin- and F-actin-binding protein from chicken gizzard smooth muscle.* Biochem Biophys Res Commun, 1986. **141**(1): p. 20-6.

284. Yoshikawa, H., et al., *Mice lacking smooth muscle calponin display increased bone formation that is associated with enhancement of bone morphogenetic protein responses.* Genes Cells, 1998. **3**(10): p. 685-95.

285. Wu, K.C. and J.P. Jin, *Calponin in non-muscle cells.* Cell Biochem Biophys, 2008. **52**(3): p. 139-48.

286. Su, N., et al., *Overexpression of H1 calponin in osteoblast lineage cells leads to a decrease in bone mass by disrupting osteoblast function and promoting osteoclast formation.* J Bone Miner Res, 2013. **28**(3): p. 660-71.

287. Xu, H., et al., *Actin cytoskeleton mediates BMP2-Smad signaling via calponin 1 in preosteoblast under simulated microgravity.* Biochimie, 2017. **138**: p. 184-193.

288. Han, W., et al., *Molecular cloning and characterization of chemokine-like factor 1 (CKLF1), a novel human cytokine with unique structure and potential chemotactic activity.* Biochem J, 2001. **357**(Pt 1): p. 127-35.

289. Han, W., et al., *Identification of eight genes encoding chemokine-like factor superfamily members 1-8 (CKLFSF1-8) by in silico cloning and experimental validation.* Genomics, 2003. **81**(6): p. 609-17.

290. Berditchevski, F., *Complexes of tetraspanins with integrins: more than meets the eye.* J Cell Sci, 2001. **114**(Pt 23): p. 4143-51.

291. Sanchez-Pulido, L., et al., *MARVEL: a conserved domain involved in membrane apposition events.* Trends Biochem Sci, 2002. **27**(12): p. 599-601.

292. Pearse, B.M., C.J. Smith, and D.J. Owen, *Clathrin coat construction in endocytosis.* Curr Opin Struct Biol, 2000. **10**(2): p. 220-8.

293. Jin, C., et al., *CMTM8 induces caspase-dependent and -independent apoptosis through a mitochondria-mediated pathway.* J Cell Physiol, 2007. **211**(1): p. 112-20.

294. Lu, J., et al., *Cancer Research Advance in CKLF-like MARVEL Transmembrane Domain Containing Member Family (Review).* Asian Pac J Cancer Prev, 2016. **17**(6): p. 2741-4.

295. Gronthos, S. and P.J. Simmons, *The growth factor requirements of STRO-1-positive human bone marrow stromal precursors under serum-deprived conditions in vitro.* Blood, 1995. **85**(4): p. 929-40.

296. Hamacher, M., et al., *Plasmolipin: genomic structure, chromosomal localization, protein expression pattern, and putative association with Bardet-Biedl syndrome.* Mamm Genome, 2001. **12**(12): p. 933-7.

297. Bienstock, R.J. and J.C. Barrett, *KAI1, a prostate metastasis suppressor: prediction of solvated structure and interactions with binding partners; integrins, cadherins, and cell-surface receptor proteins.* Mol Carcinog, 2001. **32**(3): p. 139-53.

298. Wang, Y., et al., *Internalization of inactive EGF receptor into endosomes and the subsequent activation of endosome-associated EGF receptors. Epidermal growth factor.* Sci STKE, 2002. **2002**(161): p. pl17.

299. Burke, P., K. Schooler, and H.S. Wiley, *Regulation of epidermal growth factor receptor signaling by endocytosis and intracellular trafficking.* Mol Biol Cell, 2001. **12**(6): p. 1897-910.

300. Lai, W.H., et al., *Ligand-mediated autophosphorylation activity of the epidermal growth factor receptor during internalization.* J Cell Biol, 1989. **109**(6 Pt 1): p. 2751-60.

301. Schlessinger, J., *New roles for Src kinases in control of cell survival and angiogenesis.* Cell, 2000. **100**(3): p. 293-6.

302. Tsukada, Y., K. Miyazawa, and N. Kitamura, *High intensity ERK signal mediates hepatocyte growth factor-induced proliferation inhibition of the human hepatocellular carcinoma cell line HepG2.* J Biol Chem, 2001. **276**(44): p. 40968-76.

303. Kondo, A., et al., *Coupling of Grb2 to Gab1 mediates hepatocyte growth factor-induced high intensity ERK signal required for inhibition of HepG2 hepatoma cell proliferation.* J Biol Chem, 2008. **283**(3): p. 1428-36.

304. Zhang, W., et al., *CMTM8 is Frequently Downregulated in Multiple Solid Tumors.* Appl Immunohistochem Mol Morphol, 2017. **25**(2): p. 122-128.

305. Li, D., et al., *An alternative splice form of CMTM8 induces apoptosis.* Int J Biochem Cell Biol, 2007. **39**(11): p. 2107-19.

306. Su, Y., et al., *CMTM3 inhibits cell migration and invasion and correlates with favorable prognosis in gastric cancer.* Cancer Sci, 2014. **105**(1): p. 26-34.

307. Chen, S.Q., et al., *[Effects of novel human chemokine-like factor superfamily 8 on proliferation and EGFR expression of HL-60 cells]*. Zhongguo Shi Yan Xue Ye Xue Za Zhi, 2007. **15**(3): p. 458-61.

308. Gao, D., et al., *CMTM8 inhibits the carcinogenesis and progression of bladder cancer.* Oncol Rep, 2015. **34**(6): p. 2853-63.

309. Zhang, S., et al., *Functional characterization of the tumor suppressor CMTM8 and its association with prognosis in bladder cancer.* Tumour Biol, 2016. **37**(5): p. 6217-25.

310. Gronthos, S., et al., *Bone marrow stromal stem cells for tissue engineering.* Periodontol 2000, 2006. **41**: p. 188-95.

311. Isenmann, S., et al., *hTERT transcription is repressed by Cbfa1 in human mesenchymal stem cell populations.* J Bone Miner Res, 2007. **22**(6): p. 897-906.

312. Shi, S., et al., *Bone formation by human postnatal bone marrow stromal stem cells is enhanced by telomerase expression.* Nat Biotechnol, 2002. **20**(6): p. 587-91.

313. Chang, J., et al., *Noncanonical Wnt-4 signaling enhances bone regeneration of mesenchymal stem cells in craniofacial defects through activation of p38 MAPK.* J Biol Chem, 2007. **282**(42): p. 30938-48.

314. de Boer, J., et al., *Wnt signaling inhibits osteogenic differentiation of human mesenchymal stem cells.* Bone, 2004. **34**(5): p. 818-26.

315. Gregory, C.A., et al., *How Wnt signaling affects bone repair by mesenchymal stem cells from the bone marrow.* Ann N Y Acad Sci, 2005. **1049**: p. 97-106.

316. Lin, G.L. and K.D. Hankenson, *Integration of BMP, Wnt, and notch signaling pathways in osteoblast differentiation.* J Cell Biochem, 2011. **112**(12): p. 3491-501.

317. Liu, N., et al., *High levels of beta-catenin signaling reduce osteogenic differentiation of stem cells in inflammatory microenvironments through inhibition of the noncanonical Wnt pathway.* J Bone Miner Res, 2011. **26**(9): p. 2082-95.

318. Psaltis, P.J., et al., *Concise review: mesenchymal stromal cells: potential for cardiovascular repair.* Stem Cells, 2008. **26**(9): p. 2201-10.

319. Zhou, S., *TGF-beta regulates beta-catenin signaling and osteoblast differentiation in human mesenchymal stem cells.* J Cell Biochem, 2011. **112**(6): p. 1651-60.

320. Balla, B., et al., *Different gene expression patterns in the bone tissue of aging postmenopausal osteoporotic and non-osteoporotic women.* Calcif Tissue Int, 2008. **82**(1): p. 12-26.

321. Hwang, J.Y., et al., *Association of TWIST1 gene polymorphisms with bone mineral density in postmenopausal women.* Osteoporos Int, 2010. **21**(5): p. 757-64.

322. Bourgeois, P., et al., *The variable expressivity and incomplete penetrance of the twist-null heterozygous mouse phenotype resemble those of human Saethre-Chotzen syndrome.* Hum Mol Genet, 1998. **7**(6): p. 945-57.

323. Brennan, F.R., et al., *Safety and immunotoxicity assessment of immunomodulatory monoclonal antibodies.* MAbs, 2010. **2**(3): p. 233-55.

324. Soo, K., et al., *Twist function is required for the morphogenesis of the cephalic neural tube and the differentiation of the cranial neural crest cells in the mouse embryo.* Dev Biol, 2002. **247**(2): p. 251-70.

325. Abdelrahman, A.E., S.A. Arafa, and R.A. Ahmed, *Prognostic Value of Twist-1, E-cadherin and EZH2 in Prostate Cancer: An Immunohistochemical Study.* Turk Patoloji Derg, 2017.

326. Gurumurthy, C.B., et al., *Reproducibility of CRISPR-Cas9 methods for generation of conditional mouse alleles: a multi-center evaluation.* Genome Biol, 2019. **20**(1): p. 171.

327. Noiman, T. and C. Kahana, *A Simple Combined Use of CRISPR-Cas9 and Cre-LoxP Technologies for Generating Conditional Gene Knockouts in Mammalian Cells.* CRISPR J, 2018. **1**: p. 278-285.

328. Hemming, S., et al., *EZH2 deletion in early mesenchyme compromises postnatal bone microarchitecture and structural integrity and accelerates remodeling.* FASEB J, 2017. **31**(3): p. 1011-1027.

329. Cakouros, D., et al., *Specific functions of TET1 and TET2 in regulating mesenchymal cell lineage determination.* Epigenetics Chromatin, 2019. **12**(1): p. 3.